

## Preface to the special issue on biohydrology dedicated to the memory of Dr. Louis W. Dekker

Paul D. Hallett<sup>1\*</sup>, Tammo S. Steenhuis<sup>2,3</sup>, Coen Ritsema<sup>4</sup>, Ľubomír Lichner<sup>5</sup>

<sup>1</sup> School of Biological Sciences, University of Aberdeen, Aberdeen, AB24 3UU, UK.

<sup>2</sup> Department of Biological and Environmental Engineering, 206 Riley Robb Hall, Cornell University, Ithaca, NY, 14853 USA.

<sup>3</sup> Faculty of Civil and Water Resources Engineering, Bahir Dar University, Bahir Dar, Ethiopia.

<sup>4</sup> Soil Physics and Land Management Group, Wageningen University, the Netherlands.

<sup>5</sup> Institute of Hydrology, Slovak Academy of Sciences, Dúbravská cesta 9, 84104 Bratislava, Slovak Republic.

\* Corresponding author. E-mail: paul.hallett@abdun.ac.uk

Over a scientific career spanning an amazing 63 years, Dr. Louis W. Dekker advanced our understanding of soil and hydrological processes greatly. He sadly passed away in November 2019 at the age of 80, while still actively involved in research. He left behind a scientific legacy that will continue to influence research in the years to come. This special issue on Biohydrology is dedicated to the memory of Dr. Louis Dekker. His impact is reflected not only in the citations to his work by the 14 papers in this special issue that covers topics ranging from water use by plants to soil water repellency, but more importantly by the many scientists that had the privilege to work with him. They are carrying forward his excitement for soil science and its many unique aspects.

It is fitting to pay tribute to Dr. Louis Dekker in this Biohydrology Special Issue, as he was a founder of the Biohydrology conferences that emerged from a meeting at the European Geosciences Union in 2005. Due to his international prominence, he was selected as chairman of the 1st Biohydrology conference in Prague in 2006 and was guest-editor of the 1st Special issue on biohydrology published in *Biologia* in 2006. A legacy of these conferences was a network of multidisciplinary researchers who last met at the 5<sup>th</sup> Biohydrology conference in Valencia, Spain in 2019. Earlier, in 1998, along with his very close colleague Prof. Coen Ritsema, he hosted a workshop at his home institution (DLO Winand Staring Centre for Integrated Land, Soil and Water Research in Wageningen) that was the beginning of the soil water repellency research community. This workshop produced a special issue of the *Journal of Hydrology* with an impressive 32 articles that have so far been cited about 3700 times (Ritsema and Dekker, 2000).

Dr. Louis Dekker started his career in 1956 as a soil surveyor for Stiboka. He became fascinated by the patterns of soils in the landscape while making the soil maps (Dekker and Dewerd, 1973). After all Dutch soils were surveyed in the 1970s, he immersed himself in finding the origins of the patterns he noticed earlier while discovering new ones at the same time by taking thousands of field samples not only in the Netherlands but in other countries that he happened to visit. Based on this fieldwork, he was the first to claim the phrase that preferential flow was the rule rather than the exception. He also discovered the widespread occurrence of water repellency in temperate climates and questioned the common assumption that soil water repellency was a rare property limited to a few soils in extreme environments (Dekker and Ritsema, 1996; Dekker et al., 2001). Based on his seminal research work, he was awarded a doctorate on the same day as his colleague and friend Coen Ritsema in 1998. He is one of the very few people

that earned this honour without a formal university education. His research was just that outstanding.

One of his major contributions was identifying and quantifying the temporal nature of soil water repellency, which he found was often, but not always linked to fluctuations in water content and temperature (Dekker et al., 1998). He co-authored one of the early seminal articles describing the physics of water repellent soil (Bauters et al., 2000) and provided some of the earliest evidence linking water repellency to preferential flow path development (Dekker and Ritsema, 1996; Ritsema and Dekker, 1996). Dr. Louis Dekker's pioneering soil water repellency research has led to a surge in interest starting in the 1990s (Dekker et al., 2005b). This special issue that reports on the biohydrology workshop is built on the achievements of Dr. Louis Dekker.

Dr. Louis Dekker developed robust techniques to characterise soil water repellency in the field (Dekker et al., 2009) and applied them to a range of challenges such as water repellency induced by forest fires (Stoof et al., 2011) and vegetation (Oostindie et al., 2017). He sought approaches to combat water repellency that provided a large contribution to the development of surfactants used in agriculture and the turfgrass industry (Dekker et al., 2005a, 2019). The review article by Fidanza et al. (2020) reviews water repellency development in intensively managed amenity turf, including a focus on the use of surfactants. The 20 citations to Dr Louis Dekker's work in this article reflect his impact and high esteem. Fidanza et al. (2020) found that both scientific and trade literature on water repellency in turf has grown dramatically in recent years, accompanied by the development of about 200 surfactant formulations in the USA alone. They highlighted research on dune systems by Dekker et al. (2001) as a key study that has guided turfgrass scientists and practitioners.

Desert systems share similar properties to coastal dunes, including continual burial of surfaces by newly deposited sand. Jia et al. (2020) found that sand burial caused a marked decrease in water repellency, but unless burial depth was greater than 0.5 mm, water repellency rapidly re-emerged and reached levels worse than before burial. Soil water repellency can also be a major challenge in forested land, as investigated by Piyaruwan et al. (2020). They showed that nonindigenous eucalyptus and pine trees exacerbated soil water repellency, which was reflected in decreased groundwater levels that the authors argued arose from depleted recharge through the soil from precipitation. This interdisciplinary study modelled groundwater levels over the past 40 years from remote sensing data and assessed the social impact by questionnaires to the surrounding

communities on well water availability. Eucalyptus and pine trees in this region should be replaced by species that have less impact on soil water repellency and groundwater recharge.

Nonindigenous tree species can also be difficult to manage during periods of drought when they may be susceptible to water deficit and high temperatures. Leštianska et al. (2020) assessed drought and temperature impacts from measurements of stem water deficit and maximum daily shrinkage for a number of tree species in 2018 when it was extremely hot and dry, and in 2017 when temperature and precipitation were close to average. They found that *Larix decidua* and *Picea abies*, which are not native to central Slovakia where the study was conducted, were affected more by heat and drought than *Abies alba* and *Pinus sylvestris*. This study is highly significant in identifying economically important tree species that can cope with erratic weather that is occurring more frequently. The spatial impact of groundwater availability on forest decline was examined with geostatistics and multi-criteria analysis by Jokačević et al. (2020). This approach allowed for areas in danger of forest decline to be identified so that they could be protected.

Wild olive trees are highly adapted to extremely dry soil conditions, which Corona and Montaldo (2020) demonstrated was due to their ability to access water through fractures in the underlying bedrock. They argued that ecohydrology often ignores this source of water that provided 97% of evapotranspiration in a dry summer. Although current precipitation in Sardinia, where the study was conducted, is sufficient to recharge deep water each year, future climate predictions suggest that wild olive trees will be at risk.

In commercial olive tree and vegetable production, intensive tillage often occurs that can mineralise carbon and structurally destabilise soils. Bogunovic et al. (2020) found that adding grass cover and removing tillage in olive tree management resulted in marked improvements to nutrient retention, soil loss, structural stability, and run-off. A new technology that could alleviate the use of tillage in weed control and also help to conserve water in soils is the application of hydromulches. Verdú et al. (2020) observed that under very dry conditions that almost completely dried soils, hydromulches resulted in only a 67% loss in water. Moreover, the mechanical strength of the hydromulch was sufficient to suppress the emergence of weed seedlings.

As freshwater resources are depleted and under increasing pressure for a range of uses, treated wastewater is increasingly used for irrigation. This presents a potential risk of antibiotics contaminating the environment, which could have negative impacts on soil microbial communities. In a laboratory study, Fér et al. (2020) measured that increasing the concentration of the antibiotic sulfamethoxazole resulted in an exponential increase in carbon dioxide efflux. In the field, this could result in increased greenhouse gas emissions and harm the capacity of the soil microbial community to perform functions such as nutrient cycling. Another soil management approach that may conserve water and have added benefits to carbon sequestration and greenhouse gas emissions is tillage. There is a paucity of field based data on how tillage influences emissions, so the study by Horák et al. (2020) provided valuable new insight. They found that tillage caused negligible difference in CO<sub>2</sub> and N<sub>2</sub>O emissions over the growing season, with the best predictors of emissions being temperature in the early season and water-filled pore space later in the growing season.

Other papers in this special issue provide new evidence that challenges common perceptions. It is commonly thought that dew provides a major water source for desert lichens. However, using climate data and published data on the photosynthetic

activity of lichen, Kidron and Kronenfeld (2020) predicted that most of the water used by lichens in the Tabernas desert comes from rain. Lichen is a rock dwelling organism that tends to inhabit north facing slopes in the Negev Highlands where this research was conducted, whereas cyanobacteria inhabit south facing slopes. Kidron and Starinsky (2020) found that different mineral weathering between these organisms drove aspect dependent ion enrichment of run-off water. Whilst some ions (Ca<sup>2+</sup> and HCO<sub>3</sub><sup>-</sup>) could be explained by the parent material, K<sup>+</sup> was associated with cyanobacteria and Mg<sup>2+</sup> was associated with lichen.

Addisie et al. (2020) provide new data and modelling of hillslope hydrology from the Ethiopian highlands that was the first to incorporate subsurface flow through a perched water table. Unlike temperate climates where soils tend to be moist at crop sowing and then dry out progressively, in tropical regions soils tend to be dry at the beginning of cropping and then get progressively wetter into the rainy season. By combining subsurface flow through the perched water table and overland flow, Addisie et al. (2020) quantified the dominant sources of stream water. Model predictions of water table height and discharge from the watershed fit fairly well to experimental data. Improving predictions further requires far more field investigations using more sophisticated measurement approaches across the complex Ethiopian highlands.

A modified laboratory measurement approach for assessing soil water infiltration and repellency was developed by Sepehria et al. (2020). They adapted a microinfiltrometer developed by Leeds-Harrison et al. (1994) to enhance the tension range and conductance of the tip in contact with soil, and to decrease measurement error from tube deformation and evaporation. This new device allowed for measurements at tensions up to -40 cm and for readings over several days, so that water repellency breakdown and a broad range of conducting pore sizes could be explored. Advancing approaches to measure soil water repellency in the laboratory and field were major outcomes of Dr. Louis Dekker's research too (Dekker et al., 2009), as evident from the 8 citations to his research by Sepehria et al. (2020).

The diverse nature of papers in this special issue, all dealing with various hydrological processes and challenges, reflect the breadth of Dr. Louis Dekker's research. He actively promoted his discipline by editing special issues, so we hope this special issue goes some way to continue this tradition. Soil and hydrological sciences lost a great investigator, but the citations to so many of Dr. Louis Dekker's papers in this special issue are evidence that his memory and impact on research will continue for many years to come.

## REFERENCES

- Addisie, M.B., Ayele, G.K., Hailu, N., Langendoen, E.J., Tilahun, S.A., Schmitter, P., Parlange, J.-Y., Steenhuis, T.S., 2020. Connecting hillslope and runoff generation processes in the Ethiopian Highlands: The Ene-Chilala watershed. *J. Hydrol. Hydromech.*, 68, 4, 313–327.
- Bauters, T.W.J., Steenhuis, T.S., DiCarlo, D.A., Nieber, J.L., Dekker, L.W., Ritsema, C.J., Parlange, J.-Y., Haverkamp, R., 2000. Physics of water repellent soils. *J. Hydrol.*, 231–232, 233–243.
- Bogunovic, I., Telak, L.J., Pereira, P., Filipovic, V., Filipovic, L., Percin, A., Durdevic, B., Birkás, M., Dekemati, I., Rodrigo-Comino, J., 2020. Land management impacts on soil properties and initial soil erosion processes in olives and vegetable crops. *J. Hydrol. Hydromech.*, 68, 4, 328–337.

- Corona, R., Montaldo, N., 2020. On the transpiration of wild olives under water-limited conditions in a heterogeneous ecosystem with shallow soil over fractured rock. *J. Hydrol. Hydromech.*, 68, 4, 338–350.
- Dekker, L.W., Deweerdt, M.D., 1973. Value of soil survey for archeology. *Geoderma*, 10, 169–178.
- Dekker, L.W., Ritsema, C.J., 1996. Uneven moisture patterns in water repellent soils. *Geoderma*, 70, 87–99.
- Dekker, L.W., Ritsema, C.J., Oostindie, K., Boersma, O.H., 1998. Effect of drying temperature on the severity of soil water repellency. *Soil Sci.*, 163, 780–796.
- Dekker, L.W., Doerr, S.H., Oostindie, K., Ziogas, A.K., Ritsema, C.J., 2001. Water repellency and critical soil water content in a dune sand. *Soil Sci. Soc. Am. J.*, 65, 1667–1674.
- Dekker, L.W., Oostindie, K., Kostka, S.J., Ritsema, C.J., 2005a. Effects of surfactant treatments on the wettability of a water repellent grass-covered dune sand. *Aust. J. Soil Res.*, 43, 383–395.
- Dekker, L.W., Oostindie, K., Ritsema, C.J., 2005b. Exponential increase of publications related to soil water repellency. *Aust. J. Soil Res.*, 43, 403–441.
- Dekker, L.W., Ritsema, C.J., Oostindie, K., Moore, D., Wesseling, J.G., 2009. Methods for determining soil water repellency on field-moist samples. *Water Resour. Res.*, 45, 4, W00D33. DOI:10.1029/2008WR007070.
- Dekker, L.W., Ritsema, C.J., Oostindie, K., Wesseling, J.G., Geissen, V., 2019. Effects of a soil surfactant on grass performance and soil wetting of a fairway prone to water repellency. *Geoderma*, 338, 481–492.
- Fér, M., Kodešová, R., Kalkušová, B., Klement, A., Nikodem, A., 2020. An empirical model for describing the influence of water content and concentration of sulfamethoxazole (antibiotic) in soil on the total net CO<sub>2</sub> efflux. *J. Hydrol. Hydromech.*, 68, 4, 351–358.
- Fidanza, M., Kostka, S., Bigelow, C., 2020. Communication of soil water repellency causes, problems, and solutions of intensively managed amenity turf from 2000 to 2020. *J. Hydrol. Hydromech.*, 68, 4, 306–312.
- Horák, J., Igaz, D., Aydın, E., Šimanský, V., Buchkina, N., Balashov, E., 2020. Changes in direct CO<sub>2</sub> and N<sub>2</sub>O emissions from a loam Haplic Luvisol under conventional moldboard and reduced tillage during growing season and post-harvest period of red clover. *J. Hydrol. Hydromech.*, 68, 3, 271–278.
- Jia, R.L., Gao, Y.H., Liu, L.C., Yang, H.T., Zhao, Y., 2020. Effect of sand burial on the subcritical water repellency of a dominant moss crust in a revegetated area of the Tengger Desert, Northern China. *J. Hydrol. Hydromech.*, 68, 3, 279–284.
- Jokanović, V.N., Vulević, T., Lazarević, K., 2020. Risk assessment of forest decline by application of geostatistics and multi-criteria analysis. *J. Hydrol. Hydromech.*, 68, 3, 285–292.
- Kidron, G.J., Kronenfeld, R., 2020. Atmospheric humidity is unlikely to serve as an important water source for crustose soil lichens in the Tabernas Desert. *J. Hydrol. Hydromech.*, 68, 4, 359–367.
- Kidron, G.J., Starinsky, A., 2020. Lithobiont-dependent ionic composition in runoff water. *J. Hydrol. Hydromech.*, 68, 3, 293–301.
- Leeds-Harrison, P.B., Youngs, E.G., Uddin, B., 1994. A device for determining the sorptivity of soil aggregates. *Eur. J. Soil Sci.*, 45, 269–272.
- Leštianska, A., Fleischer, P. Jr., Fleischer, P., Merganičová, K., Štelcová, K., 2020. Interspecific variation in growth and tree water status of conifers under water-limited conditions. *J. Hydrol. Hydromech.*, 68, 4, 368–381.
- Oostindie, K., Dekker, L.W., Wesseling, J.G., Geissen, V., Ritsema, C.J., 2017. Impacts of grass removal on wetting and actual water repellency in a sandy soil. *J. Hydrol. Hydromech.*, 65, 88–98.
- Piyaruwan, H.I.G.S., Jayasinghe, P.K.S.C., Leelamanie, D.A.L., 2020. Water repellency in eucalyptus and pine plantation forest soils and its relation to groundwater levels estimated with multi-temporal modeling. *J. Hydrol. Hydromech.*, 68, 4, 382–391.
- Ritsema, C.J., Dekker, L.W., 1996. Water repellency and its role in forming preferred flow paths in soils. *Aust. J. Soil Res.*, 34, 475–487.
- Ritsema, C.J., Dekker, L.W., 2000. Special issue: Water repellency in soils - Preface. *J. Hydrol.*, 231, 1–3.
- Sepehrnia, N., Woche, S.K., Goebel, M.-O., Bachmann, J., 2020. Development of a universal microinfiltrometer to estimate extent and persistence of soil water repellency as a function of capillary pressure and interface chemical composition. *J. Hydrol. Hydromech.*, 68, 4, 392–403.
- Stoof, C.R., Moore, D., Ritsema, C.J., Dekker, L.W., 2011. Natural and fire-induced soil water repellency in a portuguese shrubland. *Soil Sci. Soc. Am. J.*, 75, 2283–2295.
- Verdú, A.M.C., Mas, M.T., Josa, R., Ginovart, M., 2020. The effect of a prototype hydromulch on soil water evaporation under controlled laboratory conditions. *J. Hydrol. Hydromech.*, 68, 4, 404–410.

# Communication of soil water repellency causes, problems, and solutions of intensively managed amenity turf from 2000 to 2020

Michael Fidanza<sup>1\*</sup>, Stanley Kostka<sup>1</sup>, Cale Bigelow<sup>2</sup>

<sup>1</sup> Division of Science, Berks Campus, Pennsylvania State University, 111 Luerksen Building, Reading, PA 19610 USA.

<sup>2</sup> Department of Horticulture and Landscape Architecture, Purdue University, West Lafayette, IN 47907 USA.

\* Corresponding author. E-mail: maf100@psu.edu

**Abstract:** Research and investigations of soil water repellency in turfgrass science is a relatively recent endeavor, with most notable progress beginning in the late 1990s and early 2000s and continuing into the present. The objectives of this review were to determine the extent of publications from 2000 to the present on the topic of soil water repellency in turfgrass science, and to assemble a list of soil surfactant product formulations currently available for the amenity turf industry in the USA and United Kingdom/Republic of Ireland in 2019. From 1 January 2000 through 1 June 2020, cumulative number of referred or peer-reviewed research journal articles was 64, the number of abstracts, reports, and proceedings was 87, and the number of professional and trade journal articles was 86. Published works in all categories represented a linear increase over time, and is indicative of increased research activity into this critical area of study. Soil surfactant products and formulations in the USA totaled 192, with 65 in UK/Ireland. The nonionic soil surfactant chemical category is the largest, representing 74% of products in the USA, and 66% of products in UK/Ireland. With formulation category, block copolymers and formulations that contain block copolymers or structurally modified block copolymers as a formulation component comprise the largest group with 58% of products in the USA, and 49% of products in UK/Ireland. Also by formulation category, 25% of USA products and 23% of UK/Ireland products are comprised of anionic and anionic blends and other formulations. Of note, 17% of products in the USA and 28% of products in UK/Ireland do not disclose their formulation.

Dr. Louis Dekker's pioneering insight and advances in soil water repellency has provided turfgrass scientists with a firm foundation and guidance with which to pursue research into the causes, problems, and amelioration of soil water repellency in turfgrass ecosystems. The global amenity turf industry remains the segment where Dr. Dekker's research has had the most influence and impact to both scientists and turf practitioners.

**Keywords:** Soil hydrophobicity; Soil surfactants; Turfgrass science; Golf courses; Sports pitches; Localized dry patch; Rootzone.

## INTRODUCTION

Within the discipline of soil science, the concept and associated causes, characteristics, and consequences of soil water repellency has been extensively studied in agriculture and natural ecosystems (DeBano, 2000; DeBano and Dekker, 2000; Dekker and Ritsema, 1994; Doerr et al., 2000; Hallett, 2008; Wallis and Horne, 1992) and research continues to expand our understanding of this important topic (Dekker et al., 2005), which also includes investigations on methods for remediation and management (Müller and Deurer, 2011). The study of soil water repellency in turfgrass science is a relatively recent endeavor.

Water repellent soils in turfgrass culture was first mentioned in reports by Letey et al. (1963, 1969) and DeBano and Letey (1969). The first extensive observations of soil water repellency associated with managed turf, as related to localized dry spots or dry patches on golf course putting greens, was published by Snyder (1969) and subsequently by Miller and Wilkinson (1977) and Wilkinson and Miller (1978). After more than a decade gap in this research area, Wallis et al. (1990) investigated soil water repellency in sand in New Zealand, which was extrapolated to include sands used in turf culture, and Tucker et al. (1990) documented soil water repellency issues on sand rootzones of golf course turf in Georgia (USA). Shortly after, Cisar and Williams (1994) reported on the phenomenon occur-

ring in south Florida (USA). Cisar et al. (1997) and Kostka et al. (1997), however, published some of the first refereed journal articles specifically addressing soil water repellency management in turf.

Dr. Louis Dekker was instrumental in advancing our understanding of soil water repellency in turfgrass rootzones (Dekker et al., 2001b; Kostka and Fidanza, 2019a; Kostka et al., 2002). An international workshop on soil water repellency, organized by Ritsema and Dekker (2003), brought together researchers from multiple disciplines but all with an interest in this phenomenon. That three-day meeting provided a unique opportunity for collaboration and interdisciplinary cooperation among scientists to conduct global research on soil water repellency. Where there had once been considerable insularity within soil science sub-disciplines, there were now cross-disciplinary collaboration. By 2000, more research was published on the phenomenon and issues of soil water repellency in turf by York and Canaway (2000) and Dekker et al. (2001a), followed by others (Kostka et al., 2005; McMillan et al., 2013; Moody et al., 2009; Schlossberg et al., 2005), as well as methods to alleviate soil water repellency problems in managed turfgrass swards (Cisar et al., 2000; Dekker et al., 2003; Kostka, 2000; Kostka et al., 2007a; Park et al., 2004).

Since the early 2000s, and beginning with that international workshop on soil water repellency, there has been a continuous and consistent record of research published on the topic of soil

water repellency within the discipline of turfgrass science, soil physics, ecology, and biohydrology. Also since the early 2000s, there has been a steady effort with publishing research-based methods to ameliorate soil water repellency in turf with the use of soil surfactants (Kostka, 2000). Soil surfactants are frequently referred to as “wetting agents” by practitioners in the turfgrass industry (Zontek and Kostka, 2012). The proper label of “soil surfactant”, however, is a more appropriate term to use from a soil science perspective (Fidanza et al., 2019; Kostka et al., 2008). Surfactants are compounds that lower the surface tension (or interfacial tension) between two liquids, between a gas and a liquid, or between a liquid and a solid. Soil surfactants are employed for many useful purposes and benefits in turfgrass management (Kostka and Fidanza, 2019b). For example, soil surfactants are used by turfgrass managers (i.e., golf course superintendents, greenkeepers, course managers, sports pitch managers) for a variety of purposes, strategies, and benefits, including the improvement with wettability of rootzone soil, alleviation and mitigation of soil water repellency, treatment for localized dry spots or dry patches, for irrigation water use efficiency and optimization, to improve the application, distribution, and efficacy of plant protection products, to improve plant nutrition and fertility programs, to support turf resiliency and recovery during abiotic and biotic stress periods, and as a component of an overall plant and soil health strategy (Moore et al., 2010; Zontek and Kostka, 2012). A survey of golf course superintendents in the USA revealed that soil surfactants are the number one water conservation practice employed on their golf courses (Gelernter et al., 2015). Today, an extensive number of soil surfactant products are available in the marketplace, which has resulted in a great deal of confusion and misinformation for the end-user (Kostka and Fidanza, 2018).

Therefore, the first objective of this review was to determine what research and other supportive literature was published from 2000 to the present on the topic of soil water repellency in turfgrass science. The second objective was to assemble a comprehensive list of soil surfactant products and/or product formulations currently available in the turf industry marketplace in the USA and the UK and Republic of Ireland.

## MATERIALS AND METHODS

### Soil water repellency literature in turfgrass science

The Turfgrass Information Center (<https://tic.msu.edu>) located at Michigan State University (East Lansing, MI, USA), was used to access the on-line database, Turfgrass Information File (TGIF). To date, the TGIF database contains over a quarter million records, with 60% of those records linked directly to full-text item. TGIF enabled a search for all publications utilizing the keywords search of “soil water repellency” within the discipline of turfgrass science and management. A search parameter timeline was designated as publications from 1 Jan 2000 through 1 Jun 2020, and included three specific categories: (1) refereed journal articles (i.e., peer-reviewed articles published in scientific journals), (2) abstracts, reports, and proceedings, and (3) professional and trade journal articles.

### Soil surfactant products in the turf marketplace

The largest global markets for soil surfactants are the two countries with the largest number of golf courses, the United States and the United Kingdom. To determine the diversity of commercially available products in these markets, we utilized Google and its associated search options (i.e., Google Scholar).

Keywords included: Soil wetting agent, soil surfactant, and manufacturer names and brands. We supplemented online searches with extensive reviews of trade journals and press releases. Other sources included social media, specifically product marketing posts and testimonials via Twitter, as well as tradeshow to obtain further product information and speak directly to company representatives. Formulation compositions were derived from product labels, Safety Data Sheets (SDSs), Chemical Abstracting Service Number databases, and archival online information searches, with all findings further assessed through database analysis of compound synonyms. Separately, searches were conducted via the databases accessible via ESPACE, the USPTO, and Google Patents.

## RESULTS AND DISCUSSION

### Soil water repellency literature in turf: Refereed journal articles

From 1 Jan 2000 to 1 Jun 2020, refereed or peer-reviewed articles published in scientific journals ranged from one to eight per year, with three years of no articles, and an overall average of 3.4 articles published per year (Figure 1). The total cumulative number of articles published was 64, which revealed a linear progression over time (Figure 2), with a slight lag in 2003–2004 and again in 2019, and a noticeable increasing trend during 2010–2018 attributed to more scientists investigating this topic in amenity turf.

### Soil water repellency literature in turf: Published abstracts, reports, and proceedings

From 1 Jan 2000 to 1 Jun 2020, published abstracts, reports, and proceedings ranged from one to fifteen per year, with three years of none produced, with an overall average of 4.6 published works per year (Figure 3). The total cumulative number of publications was 87, which also revealed a linear progression over time (Figure 4). An increasing trend was noticeable at the annual international tri-society meeting of the American Society of Agronomy, Crop Science Society of America, and the Soil Science Society of America, where several abstracts have been presented each year in 2017, 2018, and 2019, on the specific topic of soil surfactant research in turf. Of note, those abstracts

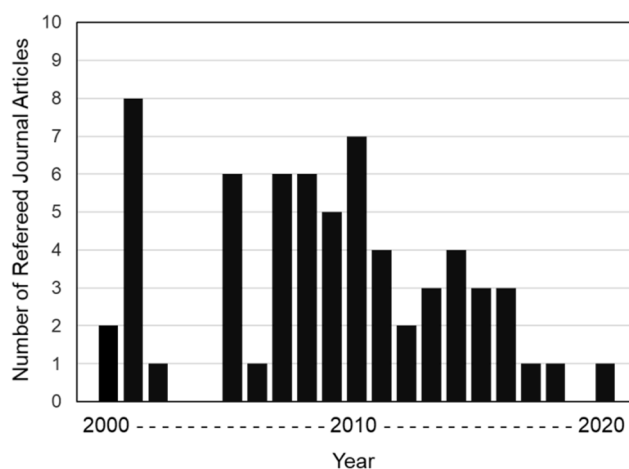


**Fig. 1.** Number of refereed journal articles (i.e., peer-reviewed articles published in scientific journals) that focuses or includes the topic of soil water repellency in turfgrass science and management, from 1 Jan 2000 to 1 Jun 2020.

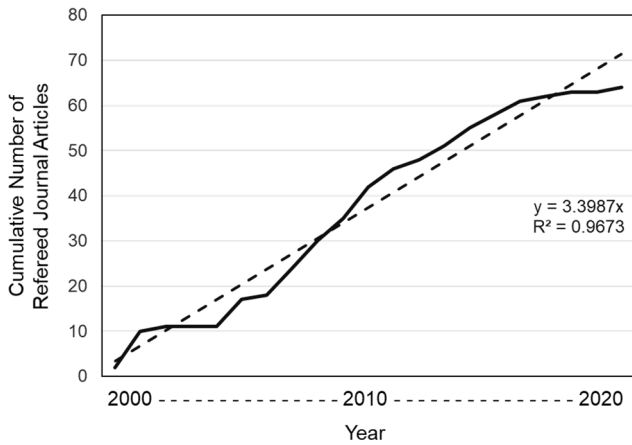


**Fig. 2.** Cumulative number of refereed journal articles (i.e., peer-reviewed articles published in scientific journals) that focuses or includes the topic of soil water repellency in turfgrass science and management, from 1 Jan 2000 to 1 Jun 2020; actual articles (—) trendline (---).

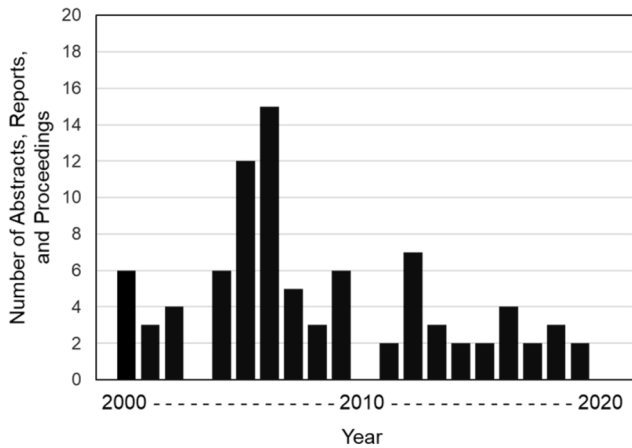


**Fig. 3.** Number of published abstracts, reports, and proceedings that focuses or includes the topic of soil water repellency in turfgrass science and management, from 1 Jan 2000 to 1 Jun 2020.

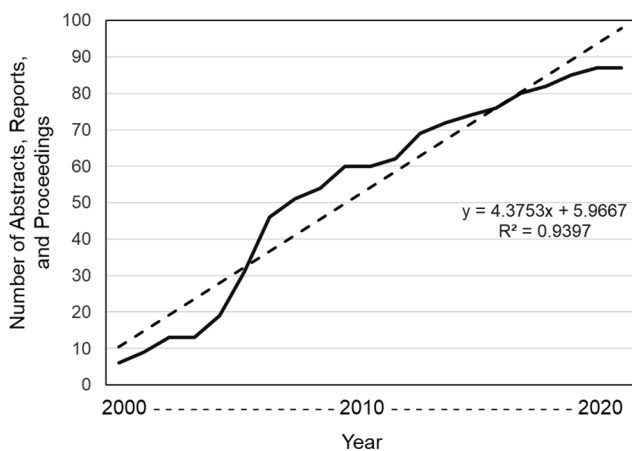


**Fig. 4.** Cumulative number of published abstracts, reports, and proceedings that focuses or includes the topic of soil water repellency in turfgrass science and management, from 1 Jan 2000 to 1 Jun 2020; actual articles (—) and trendline (---).

were not counted in Figures 3 and 4, since the keywords “soil water repellency” were not included in those abstracts. Based on the number of recent research abstracts presented, it is anticipated that more refereed journal articles will be published in the near future on the topic of soil surfactant evaluations and soil water repellency issues in turf.

**Soil water repellency literature in turf: Professional and trade journal articles**

From 1 Jan 2000 to 1 Jun 2020, published professional and trade journal articles primarily written for the practitioner audience ranged from one to eighteen per year, with an overall average of 4.5 articles per year (Figure 5). The total cumulative number of publications was 86, which resembled a linear progression over time (Figure 6). Of note, 18 articles were produced in 2005, which was attributed to research being conducted and presented at international conferences in the early 2000s on those topics of understanding soil water repellency, and the amelioration of soil water repellency using soil surfactants, in turfgrass ecosystems.

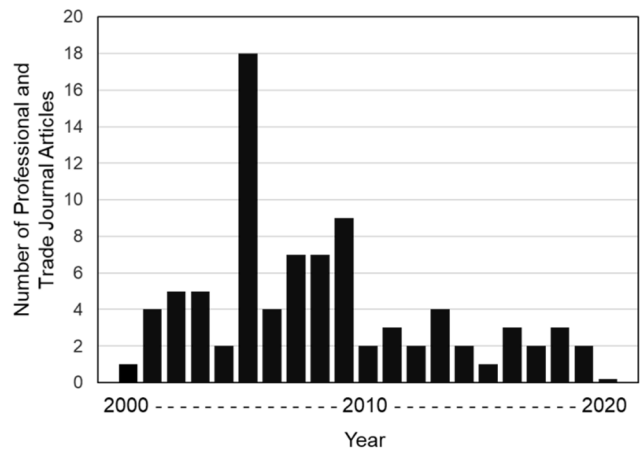


**Fig. 5.** Number of professional and trade journal articles that focuses or includes the topic of soil water repellency in turfgrass science and management, from 1 Jan 2000 to 1 Jun 2020.

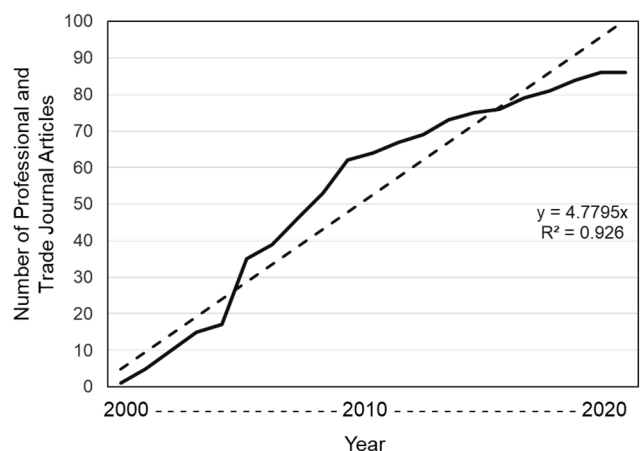


**Fig. 6.** Cumulative number of professional and trade journal articles that focuses or includes the topic of soil water repellency in turfgrass science and management, from 1 Jan 2000 to 1 Jun 2020; actual articles (—) and trendline (---).

**Soil surfactant products in USA, 2019**

In the early 1990’s, the USA soil surfactant products for turf was composed of a handful of predominately national brands. By 2019, that number swelled to 192 branded soil surfactant formulations being offered by 43 companies in a market with an estimated retail value of \$50–75 million USD (Table 1). The products were classified into chemical class, chemical category, and ultimately into 20 formulation categories based on composition. Evaluating soil surfactant products in the marketplace based on chemical class, most were nonionic surfactants with 142 of 192 (or 74%), 18 (or 9%) were anionic surfactants or blends of anionic and nonionic surfactants, and the remaining

32 (or 17%) were undisclosed (i.e., no information on composition could be elucidated based on publicly available information). Examining soil surfactants based on formulation category revealed the largest single formulation consisted of the 94 (or 49%) products composed of block copolymer surfactants. When considering other formulations that also contained block copolymers or structurally modified block copolymers as formulation components, that number reached a total of 112 (or 58%). The remaining formulation categories within the nonionic chemical class consisted of 30 (or 16%) surfactants of polyoxyethylene and polyalkylenes blends, alkylpolyglucosides, alcohol ethoxylates, a botanical, and an organosilicate.

**Table 1.** Soil surfactant products for the turf industry in the USA market in 2019.

Chemical Class	<i>n</i>	Chemical Category	<i>n</i>	Formulation Category	<i>n</i>
Nonionic	142	Block Copolymer	112	Block Copolymer	94
				Block Copolymer - Alcohol Ethoxylate Blends	3
				Block Copolymer + Alkylpolyglycoside	5
				Block Copolymer - Maleic Acid Blends	3
				Block Copolymer - Solvent Blends	2
				Modified Methyl Capped Block Copolymer	1
				Oleic Acid Esters of Block Copolymer	1
				Other Block Copolymer Blends	3
		Alcohol	2	Alcohol Ethoxylates	2
		Alkylpolyglucoside	4	Alkylpolyglucoside	4
		Botanical	1	Yucca plant extract	1
		Organosilicone	1	Organosilicone	1
		Polyalkylene	5	Hexahydroxy Polyalkylene Polymers	1
Octahydroxy Polyalkylene Polymers	4				
Polyoxyethylene	17	Polyoxyethylene - Alkylpolyglucoside Blends	2		
		Polyoxyethylene - Block Copolymer Blends	2		
		Polysorbate Polyoxyethylene Copolymer	13		
Anionic	18	Anionic and Blends with Anionics	18	Anionic Blends	11
				Blends of Anionic and Nonionic	7
Unknown	32	Not Disclosed	32	Not Disclosed	32

*Total Products in the Marketplace:* 192

**Table 2.** Soil surfactant products for the turf industry in the UK and Republic of Ireland markets in 2019.

Chemical Class	<i>n</i>	Chemical Category	<i>n</i>	Formulation Category	<i>n</i>
Nonionic	43	Block Copolymer	32	Block Copolymer	19
				Block Copolymer + Alkylpolyglycoside	3
				Block Copolymer + Fatty Amine + Organosilicone + Acetic Acid	1
				Block Copolymer + Glycol	1
				Block Copolymer + Organosilicone	1
				Block Copolymer + Succinate	1
				Block Copolymer + Terpene-derived Surfactant	1
				Block Copolymer + Not disclosed	2
				Alkyl-terminated Block Copolymer	1
				Alkyl-terminated Block Copolymer + Block Copolymer	1
		Oleic Acid Esters of Block Copolymer	1		
		Alcohol	1	Ethoxylated Fatty Alcohols	1
		Botanical	2	Yucca plant extract	2
Organosilicone	3	Organosilicone	3		
Other / Not Categorized	2	Aqueous Hydrophobic Polymer	1		
		Ducosate Sodium Sulfate	1		
Polyalkylene	2	Hexahydroxy Polyalkylene Polymers	1		
		Octahydroxy Polyalkylene Polymers	1		
Polyoxyethylene	1	Polysorbate Polyoxyethylene Copolymer	1		
Anionic	4	Anionic and Blends with Anionics	4	Anionic + Alcohol Ethoxylate	1
				Anionic + Block Copolymer	1
				Anionic - Not disclosed	2
Unknown	18	Not Disclosed	18	Not Disclosed	18

*Total Products in the Marketplace:* 65

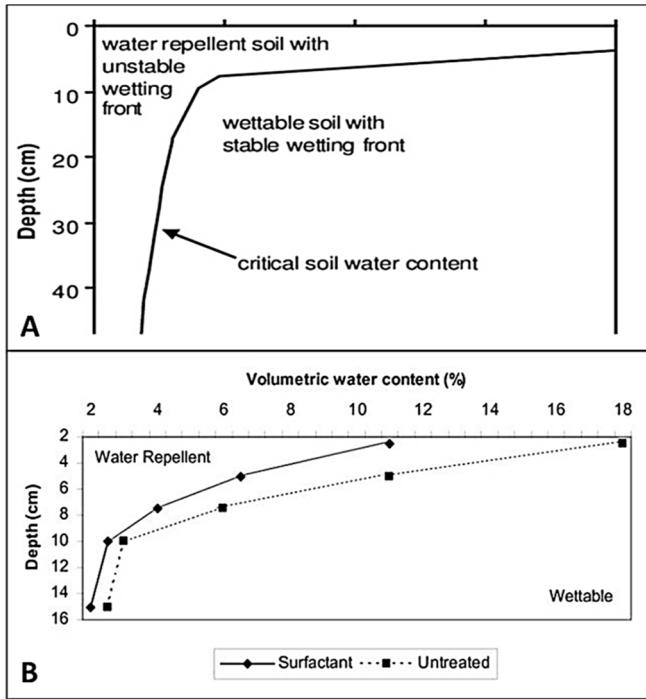


**Fig. 7.** A: Concept of critical water content derived from investigations on dune sand (from Dekker et al., 2001b), indicating that a rootzone becomes water repellent when the volumetric water content drops below a critical threshold, and this condition can be influenced by rootzone depth. B: Concept of critical water content applied to sand rootzones of a golf course putting green (from Kostka et al., 2007b), which was derived from the original concept of Dekker et al. (2001b), indicating that on golf course putting greens with constructed sand rootzones the soil can “flip” or change very quickly from wettable to water repellent, but the use of a soil surfactant can help lower that critical water content threshold. Thus, where soil wettability is less than optimal, soil surfactants in combination with appropriate irrigation and soil cultivation practices can improve soil hydrological behavior resulting in improved irrigation efficiency and water conservation.

### Soil surfactant products in United Kingdom and Republic of Ireland, 2019.

While the US is the world’s largest golf turf market with over 15,000 golf courses, the United Kingdom and the Republic of Ireland support nearly 3,000 golf courses. In the UK and Ireland, a total of 65 branded soil surfactant formulations are being sold by 18 companies (Table 2), with a retail value not determined. The proportional listing of products based on chemical class is similar to the USA market, with 43 of 65 (or 66%) based exclusively on nonionics, 4 of 65 (or 6%) as anionics, and 18 of 65 (or 28%) as unknown. A review of soil surfactants based on formulation category indicated the largest single formulation was the 19 (or 29%) products composed of block copolymer surfactants. When including other formulations that also contained block copolymers or structurally modified block copolymers as formulation components, that number climbed to a total of 32 (or 49%). The remaining formulation categories within the nonionic chemical class consisted of 11 (or 17%) surfactants of alcohol, botanical, organosilicone, polyalkylene, polyoxyethylene, and two products not categorized to formulation but are listed within the nonionic chemical category.

There are evident parallels between the formulations, with nonionic block copolymer surfactants being well represented in the United States, the United Kingdom, and the Republic of Ireland. A notable difference in the markets is the presence of more organosilicone soil surfactant products in the UK and Ireland, and more alkylpolyglucoside and polyoxyethylene soil surfactant products in the USA. Nonetheless, the dominant presence of nonionic block copolymer surfactants as soil water management products in amenity turf is evident. While chemical analysis of soil surfactants in the non-disclosed formulation category could not be conducted, it is likely that nonionic block copolymer formulations were well represented within that non-disclosed group as well.

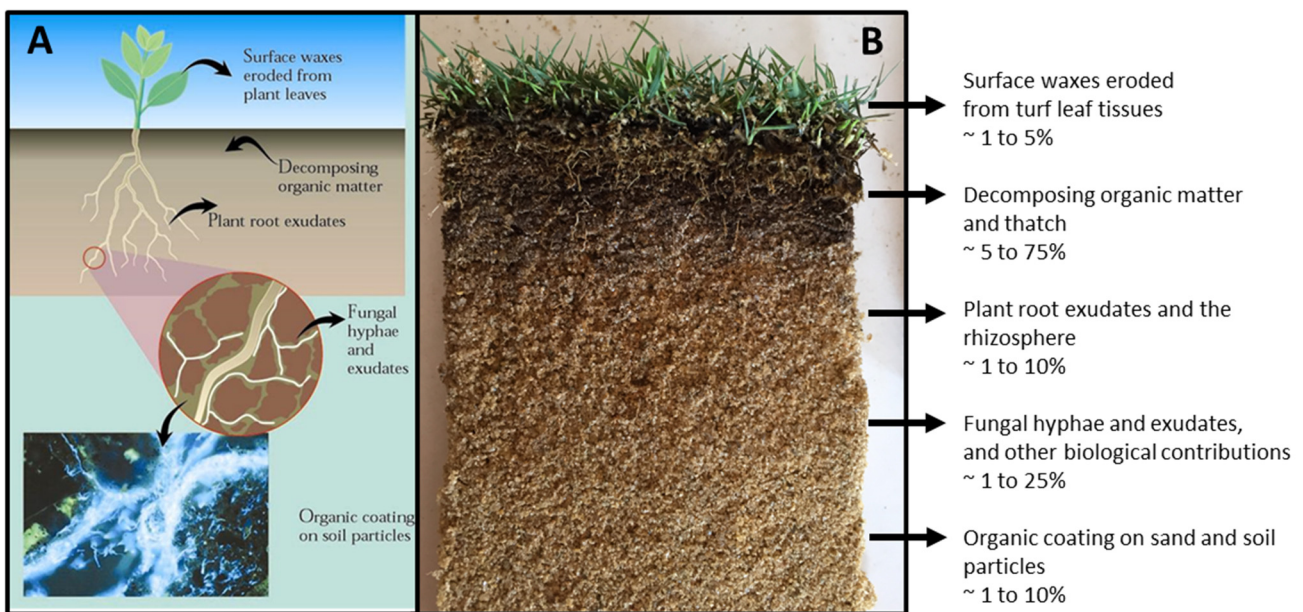


**Fig. 8.** A: The origin of water repellency from microbiota and decomposing organic matter in the soil, as adapted from Hallett (2007). B: Profile of creeping bentgrass (*Agrostis stolonifera*) from a golf course fairway, with speculation as to the contribution of various components toward the development of water repellency in the rootzone.

## CONCLUSION

Dr. Louis Dekker's pioneering research in soil water repellency has enabled turfgrass scientists to understand a diversity of implications with not only water but overall plant and soil health, mobilization of organically bound nitrogen, modification of rootzone and surface moisture heterogeneity, impacts on leaching, and is now leading us to further explore the rhizosphere in turfgrass ecosystems. Of one particular publication in the scientific literature worthy of further insight, the contribution of Dekker et al. (2001b) has led turfgrass scientists as well as practitioners on a journey to a better understanding of not just soil water repellency (Hallett, 2008; Kostka and Fidanza, 2019a), but impacts on flow and rootzone water distribution in the rootzone (Bigelow et al., 2001; Gross, 2016; Kvalbein and Aamlid, 2014). The basic principles Dr. Dekker explored studying those old dunes had direct applicability to issues impacting soils and turf productivity globally (Figure 7), and his research enabled transformative change in how turfgrass scientists investigated soil water repellency in managed amenity turf, and how they looked further into what a soil surfactant could do (Kostka et al., 2007b). To this day, turfgrass scientists are still developing new research-based findings (Figure 8) as guided by Dr. Dekker's early observations (Fidanza, 2007; Fidanza et al., 2007; Hallett et al., 2006; Kostka and Fidanza, 2019a; Kostka et al., 2005, 2008; McMillan et al., 2013; Moore et al., 2010). Moreover, the global turf industry remains the segment where Dr. Dekker's research has had the most influence.

Research on soil surfactant use in the turf industry has expanded dramatically over the past 25–30 years from a single spot treatment to a critical component and commonly accepted practice for water management in amenity turf. What originated as a tool to mitigate dry patch (localized dry spots) has expanded broadly into large scale management of soil water repellency, infiltration and flow phenomena to modify critical rootzone water content as a parameter to be managed for turf health and playability, reducing heterogeneity of rootzone volumetric water content, improving rootzone reservoir recharge and irrigation efficiency, reduced overland flow and leaching, particularly of nutrients and pesticides, improve turf quality, as a component of an overall program to manage abiotic and biotic stresses, and as a component of an overall plant and soil/rhizosphere health program (Kostka and Fidanza, 2019a).

*Acknowledgements.* Dr. Louis W. Dekker was always welcoming to those of us pursuing research in turfgrass science, and he always insisted that we were included and had the opportunity to participate in the various conferences and symposiums on the topic of soil water repellency. His research in soil physics provided a science-based foundation needed to broaden our understanding of those concepts and critical areas of research for turfgrass science. We are grateful that he shared his enthusiasm and knowledge with us, provided guidance and insights, and more importantly that he was our colleague and friend. Most importantly, he was a mentor.

## REFERENCES

- Bigelow, C.A., Bowman, D.C., Cassel, D.K., 2001. Water retention of sand-based putting green mixtures as affected by the presence of gravel sub-layers. *International Turfgrass Society Research Journal*, 9, 479–486.
- Cisar, J.L., Williams, K.E., 1994. Wetting agent effects on turf soil-water repellency. *HortScience*, 29, 5, 552.
- Cisar, J.L., Snyder, R.H., Snyder, G.H., 1997. Alleviating soil-water repellency. *International Turfgrass Society Research Journal*, 8, 139–145.
- Cisar, J.L., Williams, K.E., Vivas, H.E., Haydu, J.J., 2000. The occurrence and alleviation by surfactants of soil-water repellency on sand-based turfgrass systems. *Journal of Hydrology*, 231–232, 352–358.
- DeBano, L.F., 2000. Water repellency in soils: a historical overview. *Journal of Hydrology*, 231–232, 4–32.
- DeBano, L.F., Letey, J. (Eds.), 1969. *Proceedings of the Symposium on Water Repellent Soils*. University of California, Riverside, 6–10 May 1968, 354 p.
- DeBano, L.F., Dekker, L.W., 2000. Water repellency bibliography. *Journal of Hydrology*, 231–232, 409–432.
- Dekker, L.W., Ritsema, C.J., 1994. How water moves in a water repellent sandy soil: 1. Potential and actual water repellency. *Water Resource Research*, 30:2507–2517.
- Dekker, L.W., Oostindie, K., Ziogas, A.K., Ritsema, C.J., 2001a. The impact of water repellency on soil moisture variability and preferential flow. *International Turfgrass Society Research Journal*, 9, 498–505.
- Dekker, L.W., Doerr, S.H., Oostindie, K., Ziogas, A.K., Ritsema, C.J., 2001b. Water repellency and critical soil water content in a dune sand. *Soil Science Society of America Journal*, 65, 1667–1674.
- Dekker, L.W., Oostindie, K., Kostka, S.J., Ritsema, C.J., 2003. Treating water repellent surface layer with surfactant. In: Ritsema, C.J., Dekker, L.W. (Eds.): *Soil Water Repellency: Occurrence, Consequences, and Amelioration*, Elsevier, Amsterdam, pp. 313–345.
- Dekker, L.W., Oostindie, K., Ritsema, C.J., 2005. Exponential increase of publications related to soil water repellency. *Soil Res.*, 43, 403–441.
- Doerr, S.H., Shakesby, R.A., Walsh, R.P.D., 2000. Soil water repellency: Its causes, characteristics and hydrogeomorphological significance. *Earth Sci. Rev.*, 51, 33–65.
- Fidanza, M.A., 2007. Characterization of soil properties associated with type-I fairy ring symptoms in turfgrass. *Biologia*, 62, 533–536.
- Fidanza, M.A., Cisar, J.L., Kostka, S.J., Gregos, J.S., Schlossberg, M.J., Franklin, M., 2007. Preliminary investigation of soil chemical and physical properties associated with type-I fairy ring symptoms in turfgrass. *Hydrological Processes*, 21, 17, 2285–2290.
- Fidanza, M., Kostka, S., Ervin, E., Bigelow, C., 2019. The European Union's view on biostimulants: What may be coming our way. *Golf Course Management*, 87, 9, 58–62.
- Gelernter, W.D., Stowell, L.J., Johnson, M.E., Brown, C.D., Beditz, J.F., 2015. Documenting trends in water use and conservation practices on U.S. golf courses. *Crop, Forage and Turfgrass Management*, 1, 1, 1–10.
- Gross, P., 2016. Five things to know about water management during summer. USGA Green Section. Source: <https://www.usga.org/course-care/regional-updates/west-region/five-things-to-know-about-water-management-on-greens-during-summ.html>.
- Hallett, P.D., 2007. An introduction to soil water repellency. In: *Proceedings of the 8<sup>th</sup> International Symposium on Adjuvants for Agrochemicals (ISAA 2007)*, 13 p.
- Hallett, P.D., 2008. A brief overview of the causes, impacts and amelioration of soil water repellency - a review. *Soil and Water Research*, 3, S21–S29.
- Hallett, P.D., White, N.A., Ritz, K., 2006. Impact of basidiomycete fungi on the wettability of soil contaminated with a hydrophobic polycyclic aromatic hydrocarbon. *Biologia*, 61, Suppl. 19, S334–S338.

- Kostka, S.J., 2000. Amelioration of water repellency in highly managed soils and the enhancement of turfgrass performance through the systematic application of surfactants. *Journal of Hydrology*, 231–232, 359–368.
- Kostka, S.J., Fidanza, M., 2018. The quagmire that is soil surfactants in golf and sports turf management. ASA, CSSA and SSSA International Annual Meetings. *Agronomy Abstracts*, p. 113267.
- Kostka, S.J., Fidanza, M., 2019a. Revisiting concepts on the development of soil water repellency. ASA, CSSA and SSSA International Annual Meetings. *Agronomy Abstracts*, p. 122260.
- Kostka, S., Fidanza, M., 2019b. Soil surfactant usage based on solid science. *Golf Course Industry*, online. <https://www.golfcourseindustry.com/article/soil-surfactant-research-guidance/>
- Kostka, S.J., Cisar, J.L., Short, J.R., Mane, S., 1997. Evaluation of soil surfactants for the management of soil water repellency in turfgrass. *International Turfgrass Society Research Journal*, 8, 485–494.
- Kostka, S.J., Dekker, L.W., Oostindie, K., Ritsema, C.J., Miller, C.M., Karcher, D.E., 2002. Advances in understanding and managing water repellent soils. In: *Irrigation Show 2002: Technical Session Proceedings*. Irrigation Association, Falls Church, VA, pp. 1–8.
- Kostka, S.J., Cisar, J.L., Ritsema, C.J., Dekker, L.W., Franklin, M.A., Mitra, S., McCann, S.E., 2005. Surfactants and soil water repellency in golf course soils - water use and environmental implications. In: *Proceedings of the 25th Irrigation Association Conference*, pp. 235–246.
- Kostka, S.J., Cisar, J.L., Mitra, S., Park, D.M., Ritsema, C.J., Dekker, L.W., Franklin, M.A., 2007a. Irrigation efficiency - Surfactants can save water and help maintain turfgrass quality. *Golf Course Industry*, 19, 4, 91–95.
- Kostka, S.J., Dekker, L., Ritsema, C., Cisar, J.L., Franklin, M.K., 2007b. Surfactants as management tools for ameliorating soil water repellency in turfgrass systems. In: *Proceedings of the 8<sup>th</sup> International Symposium on Adjuvants for Agrochemicals (ISAA 2007)*, 7 p.
- Kostka, S.J., Dekker, L.W., Oostindie, K., Mauser, K., Franklin, M.A., 2008. May surfactants affect more than wetting in water repellent soils? 1st European Turfgrass Society Conference Proceedings. Pisa, Italy, 1 May 2008, pp. 109–110.
- Kvalbein, A., Aamlid, T.S., 2014. *Irrigation of turf on golf courses - a greenkeeper guide to understanding the theory and practice*. Publication of the Scandinavian Turfgrass and Environment Research Foundation; Stockholm, Sweden.
- Letey, J., Osborn, J.F., Valoris, N., 1969. Wetting agents and water repellent soils. Southern Regional Turf Research Committee Report, 1968–69. 8 p.
- Letey, J., Welch, N., Pelishek, R.E., Osborn, J., 1963. Effect of wetting agents on irrigation of water repellent soils. *California Turfgrass Culture*, 13, 1, 1–2.
- McMillan, M.F., Kostka, S., Boerth, T., Fidanza, M., Bigelow, C., Cisar, J., Soldat, D., Karas, I., Williams, K., 2013. Monitoring seasonal soil water repellency in USA golf course putting greens. *International Turfgrass Society Research Journal*, 12, 815–818.
- Miller, R.H., Wilkinson, J.F., 1977. Nature of the organic coating on sand grains of non-wettable golf greens. *Soil Sci. Soc. Am. J.*, 41, 1203–1204.
- Moody, D.R., Schlossberg, M.J., Archibald, D.D., McNitt, A.S., Fidanza, M.A., 2009. Soil water repellency development in amended sand rootzones. *Crop Science*, 49, 5, 1885–1892.
- Moore, D., Kostka, S.J., Boerth, T.J., Franklin, M., Ritsema, C.J., Dekker, L.W., Oostindie, K., Stoof, C., Wesseling, J., 2010. The effect of soil surfactants on soil hydrological behavior, the plant growth environment, irrigation efficiency and water conservation. *J. Hydrol. Hydromech.*, 58, 3, 142–148.
- Müller, K., Deurer, M., 2011. Review of the remediation strategies for soil water repellency. *Agr. Ecosyst. Environ.*, 144, 208–221.
- Park, D.M., Cisar, J.L., Williams, K.E., Snyder, G.H., 2004. Alleviation of soil water repellency in sand based bermudagrass in South Florida. *Acta Horticulturae*, 661, 111–115.
- Ritsema, C.J., Dekker, L.W. (Eds.), 2003. *Soil Water Repellency*. Elsevier Science, Amsterdam.
- Schlossberg, M.J., McNitt, A.S., Fidanza, M.A., 2005. Development of water repellency in sand-based root zones. *International Turfgrass Society Research Journals*, 10, 1123–1130.
- Snyder, G.H., 1969. Soil water repellency. In: *Proceedings of the Florida Turf-Grass Management Conference*. 23–25 September 1969. Florida Turfgrass Association, Orlando, FL, pp. 105–106.
- Tucker, K.A., Karnok, K.J., Radcliffe, D.E., Landry, Jr., G., Roncadori, R.W., Tan, K.H., 1990. Localized dry spots as caused by hydrophobic sands on bentgrass greens. *Agronomy Journal*, 82, 549–555.
- Wallis, M.G., Horne, D.J., 1992. Soil water repellency. *Advances in Soil Science*, 20, 91–146.
- Wallis, M.G., Horne, D.J., McAuliffe, K.W., 1990. A study of water repellency and its amelioration in a yellow-brown sand: 1. Severity of water repellency and the effects of wetting and abrasion. *New Zealand Journal of Agricultural Research*, 33, 1, 139–144.
- Wilkinson, J.F., Miller, R.H., 1978. Investigation and treatment of localized dry spots on sand golf greens. *Agronomy Journal*, 70, 299–304.
- York, C.A., Canaway, P.M., 2000. Water repellent soils as they occur on UK golf greens. *Journal of Hydrology*, 231–232, 126–133.
- Zontek, S.J., Kostka, S.J., 2012. Understanding the different wetting agent chemistries: A surfactant is a wetting agent but a wetting agent may not be a surfactant. Surprised? USGA Green Section Record, 50, 15, 1–6.

Received 23 June 2020

Accepted 17 July 2020

# Connecting hillslope and runoff generation processes in the Ethiopian Highlands: The Ene-Chilala watershed

Meseret B. Addisie<sup>1,2</sup>, Getaneh K. Ayele<sup>1</sup>, Nigus Hailu<sup>1</sup>, Eddy J. Langendoen<sup>3</sup>, Seifu A. Tilahun<sup>1</sup>, Petra Schmitter<sup>4</sup>, J.-Yves Parlange<sup>5</sup>, Tammo S. Steenhuis<sup>1,5\*</sup>

<sup>1</sup> Faculty of Civil and Water Resources Engineering, Bahir Dar University, Bahir Dar, Ethiopia.

<sup>2</sup> Guna Tana Integrated Field Research and Development Center, Debre Tabor University, Ethiopia.

<sup>3</sup> US Department of Agriculture, Agricultural Research Service, National Sedimentation Laboratory, Oxford, MS, USA.

<sup>4</sup> International Water Management Institute (IWMI) East Africa Office, Addis Ababa, Ethiopia.

<sup>5</sup> Department of Biological and Environmental Engineering, 206 Riley Robb Hall, Cornell University, Ithaca, NY, 14853 USA.

\* Corresponding author. E-mail: tammo@cornell.edu

**Abstract:** Effective watershed planning requires an understanding of the hydrology. In the humid tropical monsoon climates and especially in volcanic highland regions such as the Ethiopian Highlands, the understanding of watershed processes is incomplete. The objective is to better understand the hydrology of the volcanic regions in the humid highlands by linking the hillslope processes with the discharge at the outlet. The Ene-Chilala watershed was selected for this study. The infiltration rate, piezometric water levels and discharge from two nested sub watersheds and at the watershed outlet were measured during a four-year period. Infiltration rates on the hillsides exceeded the rainfall intensity most of the time. The excess rain recharged a perched hillside aquifer. Water flowed through the perched aquifer as interflow to rivers and outlet. In addition, saturation excess overland flow was generated in the valley bottoms. Perched water table heights were predicted by summing up the recharge over the travel time from the watershed divide. Travel times ranged from a few days for piezometers close to the divide to 40 days near the outlet. River discharge was simulated by adding the interflow from the upland to overland flow from the saturated valley bottom lands. Overland flow accounted only for one-fourth of the total flow. There was good agreement between predicted and observed discharge during the rain phase therefore the hillslope hydrologically processes were successfully linked with the discharge at the outlet.

**Keywords:** Hillslope hydrology; Saturation; Rainfall intensity; Perched groundwater; Ethiopian Highlands.

## 1 INTRODUCTION

Understanding the hydrological processes in watersheds is vital for sustainable utilization of water resources, and to reduce flooding downstream (Agnew et al., 2006; Fox et al., 2016; Nyssen et al., 2005; Steenhuis et al., 2009; Tebebu et al., 2015). While watershed hydrology is well researched in temperate regions, knowledge is still lacking in developing countries with a humid monsoon climate, especially in the volcanic African highlands.

One of the main differences between temperate and tropical climates is that precipitation during the rain phase can be three to six times that of temperate climates (Rosenzweig and Liverman, 1992). Another difference between the two climates is that in the temperate climate the soils are at field capacity at the beginning of the growing season, and then become drier with time, while for a tropical monsoon climate moisture conditions are low at planting and the soils become wetter with progress of the rainy season (Liu et al., 2008). In addition, in volcanic highlands the water mass balance of a watershed does not close (Adem et al., in preparation). In the uplands water is lost through faults that appear as springs at lower elevations. Finally, the hydrology is changing rapidly in most developing countries because of soil degradation and hardpan formation with the loss of organic matter due to continuous tillage (García-Orenes et al., 2012; Sop and Oldeland, 2013; Tebebu et al., 2017; Zimale et al., 2017). Thus, although the physical laws of water movement are the same, knowledge from the developed countries that are located in temperate climates

cannot be used without modifications for sustainable water management in developing countries situated in the tropics with monsoon climates.

In the Ethiopian Highlands, most findings of hydrological studies are limited to surface runoff. The studies show that both saturated excess and infiltration excess (Hortonian) overland flow occur to various extent (Tilahun et al., 2013; Zenebe et al., 2013). In the semi-arid northern Ethiopia highlands in Tigray, the Hortonian overland flow occurs especially in the beginning of the rain phase (Descheemaeker et al., 2009; Nyssen et al., 2005; Walraevens et al., 2009; Zenebe et al., 2013). In the sub-humid and humid Ethiopian Highlands, Tilahun et al. (2014) and Bayabil et al. (2010) found that the median infiltration rates for the volcanic surface soils are greater than the rainfall intensity and surface runoff, therefore, only can take place when the soils become saturated (Bayabil et al., 2010, 2016, 2017; Dunne and Black, 1970; Lyon et al., 2006; Steenhuis et al., 2009; Tilahun et al., 2013, 2015). Soil saturation in these soils occurs mainly in the valley bottoms (Güntner et al., 2004; Tebebu et al., 2010; Tilahun et al., 2013).

In addition to surface runoff, interflow is a major component of the discharge at the watershed outlet in humid highlands (Gurtz et al., 2003; Jackson et al., 2014; Setegn et al., 2010; Whipkey, 1965). Interflow occurs when the soil at the hillside is above field capacity and a saturated layer develops above the hardpan (Alemie et al., 2019; Tilahun et al., 2014, 2019). The water table depth above the hardpan increases from the divide to the saturated area (Bayabil et al., 2010; Betson, 1964; Guzman et al., 2017a, b).

To predict surface runoff, watershed models have been applied in the Ethiopia highlands such as Soil and Water Assessment Tool (SWAT) (Betrie et al., 2011; Kaleab and Manoj, 2013; Moges et al., 2016; Setegn et al., 2010), Agricultural Non-Point Source Pollution (AGNEPS) (Haregeweyn and Yohannes, 2003) and Water Erosion Prediction Project (WEPP) (Zelege, 2000). These models assume that runoff is generated by infiltration excess and cannot simulate both the variable saturated source area runoff from sloping perched water tables and the valley bottoms (Moges et al., 2016). Models that are capable of simulating the saturated areas are the Hydrologiska Byrans Vattenbalansavdelning (HBV), modified versions of SWAT such as SWAT-HS (Hoang et al., 2017, 2018) and Parameter Efficient Distributed model (PED) (Guzman et al., 2017a; Moges et al., 2016; Steenhuis et al., 2009; Tesemma et al., 2010; Tilahun et al., 2015). The PED was developed initially for the humid and sub humid highlands of Ethiopian to simulate river discharge. PED, HBV and SWAT simulated the discharge at the outlet with the same accuracy, but PED only could predict the location of the observed source areas of surface runoff (Moges et al., 2016).

Relatively few groundwater modeling studies were carried out in the Ethiopian Highlands. In the Rift Valley, Ayenew (2001), Ayenew and Tilahun (2008) and Ayenew et al. (2008a, b) used MODFLOW to simulate regional groundwater tables. In the Awash basin, Berehanu et al. (2017) simulated large basin scale groundwater. Chebud and Melesse (2009) performed groundwater simulations in the Fogera plain in the Lake Tana basin. The only other groundwater studies were conducted by MSc students and have not been published (theses are listed in Berehanu et al., 2017).

Despite that the subsurface flow makes up the major portion of the river flow in the Ethiopian Highlands (Ayele et al., 2016; Tilahun et al., 2019), none of the watershed or groundwater models mentioned above have modeled the perched groundwater on the hillside and validated the predictions with actual observation of groundwater levels on the hillside. One of the reasons for the lack of validation is that the hillside groundwater levels are not routinely available. Only recently, a few studies have measured perched water tables (Alemie et al., 2019; Bayabil et al., 2010; Guzman et al., 2017a; Tilahun et al., 2019).

To overcome this knowledge gap, the objective of this paper is to better understand the hydrology of the volcanic regions in the (sub) humid tropics by making observation of the perched water tables on the hillsides and river discharge. Specifically, the aim is to predict the river discharge as the sum of the surface runoff generated from the saturated areas and the interflow from the hillside with a model that is validated with the level of the perched water table observations. The Ene-Chilala watershed in Ethiopia was selected. The watershed is a typical representation of the volcanic landscape in the sub-humid highlands of Ethiopia with gully prone, periodically saturated bottom lands and steep to moderately sloping uplands. We measured groundwater levels and observed river flows for two nested sub watersheds and at the watershed outlet. For the Ethiopian Highlands, this study links for the first time measured water tables on the hillside and valley bottom with river discharge.

To explore the interaction between upland runoff and river flow we used the analytical solutions developed by Alemie et al. (2019) for predicting discharge and water tables for perched hillslope aquifers that are currently incorporated in the PED model. We decided against using MODFLOW because the input data for this complex landscape in the Ethiopian Highlands is not available. We used therefore analytical solutions because they require a minimum in input data while providing

insights in the hydrologic processes. The Thornthwaite Mather procedure was selected to predict the recharge on the hillside and the saturation excess runoff for the saturated areas.

## 2 MATERIALS AND METHODS

### 2.1 Study site

The study was conducted in the 4.14 km<sup>2</sup> Ene-Chilala watershed in the headwaters of the Birr River, which is located in upper Blue Nile basin, Ethiopia. The topography ranges from 2001 m a.s.l. near the watershed outlet to 2414 m a.s.l. in the headwaters. The long-term average annual rainfall is 1200 mm a<sup>-1</sup> of which more than 80% falls between July and August. The watershed is characterized by rugged topography. Hillside slopes are on average 35%. The valley bottom has a 5% slope. Sixty five percent of the watershed is cultivated land, 23% has bushes/shrubs on the basaltic rocks, and 12% is grazing land in the periodically saturated bottom lands (Figure 1a). In the northeastern part of the watershed basaltic rocks are exposed. The soil was lost after conversion of the forests to agricultural lands in the 1980's. The valley bottoms are affected by severe gully erosion.

Three small watersheds were selected within the larger 414-ha watershed (Figure 1b). They are named according to their location: NE, NW and SW watersheds. In the 83-ha NE and 149-ha NW watersheds the stream discharge was monitored. In the SW watershed six gully heads were stabilized in 2014 and 2015 (Addisie et al., 2017, 2018; Ayele et al., 2016) and water tables were monitored in 2014.

### 2.2 Data collection and analysis

Precipitation and stream discharge at the outlet of the NE and NW sub watersheds and of the entire watershed were measured during the monsoon rain phase from June to September for a four-year period from 2013 to 2016. The perched groundwater table levels in the piezometers were determined from July to November in 2014. Twelve infiltration tests were carried out in 2014 with a single ring infiltrometer in the SW watershed with four tests at three different slope positions. Steady state values are reported.

#### 2.2.1 Rainfall measurements

The 5-minute rainfall depths were recorded using an automatic tipping bucket rain gage instrumented in the center of the watershed during the four-year period of the monsoon phase from June to September (Figure 1b). In addition, one manual rain gage was installed at the center of the watershed to record daily rainfall in case the automatic gauge stopped recording.

#### 2.2.2 Infiltration measurements

The infiltration capacity of the soil was determined at 12 locations. The measurements were performed at three slope positions consisting of valley bottoms with slopes ranging from 0–6%, mid slopes with slopes between 7–15%, and upslope with inclination above 15% (Figure 1b and Table S1). Measurements were carried out for the principal land uses at each slope position. A single ring infiltrometer was driven an average of 10 cm into the ground. The steady-state infiltration capacity was measured when the water depth changes with time remained constant. The water depth was read with a plastic ruler. Simple descriptive statistics were used to calculate the median infiltration capacity. The infiltration capacity of the soil

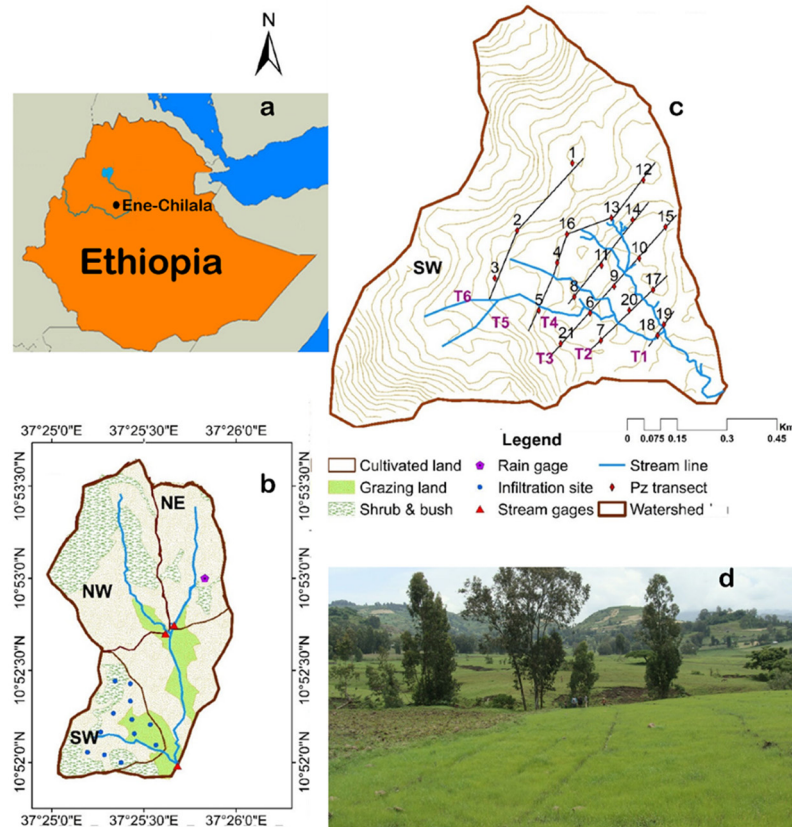


**Fig. 1.** Overview of the Ene-Chilala watershed, Ethiopia. (a) Location of the Ene-Chilala watershed relative to Lake Tana and the Blue Nile River. (b) The Ene-Chilala watershed with NE, NW and the SW sub-watersheds detailing land use and the location of infiltration test sites. (c) Elevation map of the SW watershed with the location of piezometers along six transects; the contour lines are spaced 10 m apart. (d) The Ene-Chilala watershed with tef crop in the foreground and the periodically saturated bottom lands used for grazing animals and the mountains in the NE part of the watershed in the background.

was compared with the five-minute rainfall intensity exceedance probability for the period from 2013 to 2016.

### 2.2.3 Water table measurements

The dynamics of the perched water table was studied in a 76-ha watershed in the southwestern part of Ene-Chilala (called SW watershed, Figure 1c) with a developing gully system. About 2% of the watershed area was incised by gullies. The average length of the gullies was about 174 m with a maximum length of 318 m (Figure S2). The depth of gullies varied from 1.3 to 5.7 m and their width varied from 4 to 14 m. The land use of the SW watershed is similar to that of the main watershed with 64% cultivated land, 20% bush/shrub, and 16% grazing land. The valley bottom grazing land was saturated from July to September (Figure 1b). The soil texture for the upper slope was sandy loam, loam in the mid slopes, and clay in the valley bottom.

Twenty-one piezometers (P) were installed by hand to the restrictive layer with a maximum depth of 4.23 m. The piezometers were located along 6 transects perpendicular to the gullies (Figure 1c): *Down Slope Transects* consisting of transect T1 with piezometers P18 and P19 and transect T2 with piezometers P7, P17 and P20; *Mid Slope Transects* comprising transect T3 with piezometers P6, P9, P10, P15, and 21, and transect T4 with piezometers P8, P11 and P14; and *Upslope Transects* entailing transect T5 with piezometers P4, P5, P12, P13, and P16, and transect T6 with piezometers P1, P2, and P3. The depth of instrumented piezometers varied from 1.2 m from the top of the SW watershed where the bedrock of basalt is at

shallow soil depth to 4.23 m in the valley bottom where a sapolite layer is located at 4 to 6 m depth (Table S2).

The piezometers consisted of 5-cm diameter PVC pipes. The pipes were capped at their bottom end to avoid the intrusion of sediment and at the upper end to avoid rain falling in. The water level in the piezometers was measured in the morning and late afternoon. The average of the two measurements was used as the daily water table depth. The average monthly water table was interpolated in ArcGIS using ordinary kriging interpolation with a spherical semi variogram, which is the best method according to Nikroo et al. (2010). Before the interpolation, the piezometers at the greatest distance from the gully system were used as boundary for the ArcGIS tool.

### 2.2.4 Streamflow measurement

The streamflow depth and velocity were measured with a stepwise rectangular masonry weir at three locations in the 414-ha watershed: at the bridge located at the main watershed outlet, and at the outlets of the 83-ha NE and the 149-ha NW watersheds (Figure 1b). The water level was recorded manually every 15 minutes following the start of a precipitation event. In addition, the flow velocity was measured at the water surface with a float that was dropped 7 m upstream of the weir. The average stream velocity was determined by multiplying the surface velocity by two-third. The discharge was computed as the product of the average velocity and the cross-sectional area of the flow. Frequent adjustments were needed for the zero depth after large rainstorms. The best-fit rating curve was employed to develop the relationship between the flow depth and storm discharge.

### 2.2.5 Statistical analysis

The one-way analysis of variance (ANOVA) statistical test was conducted to investigate if there was a statistically significant difference between the mean values of infiltration rate at three landscape positions (upper, middle and lower slopes) using IBM SPSS 20 (Statistical Package for Social Sciences) software. In addition, post hoc multiple comparisons were made between slope and infiltration at each slope. The performance of the hydrology model was evaluated using the Nash-Sutcliff Efficiency, NSE (Nash and Sutcliffe, 1970), Root Mean Square Error, RMSE (Golmohammadi et al., 2014), and Relative Volume Error, RVE (Wale et al., 2009). They are defined as: Nash-Sutcliff Efficiency, NSE (Nash and Sutcliffe, 1970):

$$NSE = 1 - \frac{\sum_{i=1}^n (Q_{pred(i)} - Q_{obs(i)})^2}{\sum_i (Q_{obs(i)} - \overline{Q_{obs}})^2} \quad (1)$$

Root Mean Square Error, RMSE (Golmohammadi et al., 2014):

$$RMSE = \sqrt{\frac{\sum_{i=1}^n (Q_{pred(i)} - Q_{obs(i)})^2}{n}} \quad (2)$$

and Relative Volume Error, RVE (Wale et al., 2009):

$$RVE = \left( \frac{\sum_{i=1}^n (Q_{pred(i)} - Q_{obs(i)})}{\sum_{i=1}^n Q_{obs}} \right) \times 100 \quad (3)$$

where  $\overline{Q_{obs}}$  is the mean of observed stream flow,  $Q_{pred}$  and  $Q_{obs}$  are predicted and observed flow respectively,  $n$  is the number of observations.

### 2.3 Predicting shallow water tables and discharge

Each watershed was divided into two regions consisting of (i) the permeable hillside area where rainwater infiltrates to a perched aquifer and flows as interflow to the outlet ( $q_i$ ) and (ii) the periodically saturated area in the valley bottom producing surface runoff ( $q_s$ ). In the following sections, we will discuss the analytical solutions for water table level and discharge of the hillslope first, followed by the surface runoff of saturated areas. The sum of the interflow from the permeable hillside and the surface runoff from the valley bottom is the flow at the watershed outlet.

#### 2.3.1 Hillside

Excess rainfall creates a perched hillside aquifer. Water flows as interflow through this aquifer to the valley bottom. An analytical solution for subsurface flow in the hillside aquifer with daily varying recharge was developed by Alemie et al. (2019). The solution was obtained by identifying a characteristic travel time for water to flow from the groundwater divide to the river or well. This travel time is independent of the amount of rainfall since the driving force for the water is the slope of the hardpan, and the difference in water table height along the slope is much smaller than the difference in elevation.

Using the method of characteristics, the outflow of the hill slope at day  $t$  can be predicted as the average recharge over the characteristic time prior to day  $t$  (details are provided in Alemie et al., 2019);

$$Q_i[x, t] = x \sum_{\tau=t-t_x}^t \frac{R[\tau]}{t_x} \quad \text{for } t \geq t - t_x \quad (4)$$

where the square brackets are used to indicate the independent variables,  $Q_i[x, t]$  is the interflow per unit width of hillslope ( $L^2 T^{-1}$ ) at the river channel at distance  $x$  from the groundwater divide (L) on day  $t$  (T),  $t_x$  is the travel time (T) of the groundwater from the divide to a point  $x$ ,  $R[t]$  is the recharge per unit area and day  $t$  (L) to the groundwater on day  $t$  that is summed over a period of  $t_x$  days prior to day  $t$ . The sum of all recharge over the travel time and divided by the travel time is the average recharge over the characteristic travel time period.

The water table height above the bedrock using the same method of characteristics can be expressed as the total recharge over the characteristic travel time divided by the drainable porosity (for details see Alemie et al., 2019):

$$h[x, t] = \sum_{\tau=t-t_x}^t \frac{R[\tau]}{\mu} \quad \text{for } t \geq t - t_x \quad (5)$$

where  $h[x, t]$  is the water table height above the bedrock (L), and  $\mu$  is the drainable porosity  $L^3 L^{-3}$ .

For piezometers that are located in the vicinity of stream channels, a portion of the interflow from upslope is transported by the stream to the outlet and thus only a portion of the recharge water flowing downhill will determine the water table height in the well. In this case, a factor  $f$  between 0 and 1 is introduced for the portion that flows downhill

$$h[x, t] = \frac{f}{\mu} \sum_{\tau=t-t_x}^t R[\tau] \quad \text{for } t \geq t - t_x \quad (6)$$

Since both  $f$  and  $\mu$  are constants and cumbersome to measure separately, we introduce an apparent drainable porosity  $\mu^* = \frac{\mu}{f}$  and Eq. (6) can be written as

$$h[x, t] = \frac{1}{\mu^*} \sum_{\tau=t-t_x}^t R[\tau] \quad \text{for } t \geq t - t_x \quad (7)$$

The water table height is limited by the soil surface and a minimum water level above the bedrock, which is usually zero, but in case of a regional groundwater or blockage of the interflow by volcanic dikes there is a minimum static water level in the well. With these two conditions, the water level of the sloping aquifer can be written as (Alemie et al., 2019).

$$h[x, t] = \min \left( h_{\min}[x] + \frac{1}{\mu^*} \sum_{\tau=t-t_x}^t R[\tau], h_{\max}[x] \right) \quad \text{for } t \geq t - t_x \quad (8)$$

where  $h_{\min}[x]$  is the minimum groundwater depth (L) and  $h_{\max}[x]$  is the height (L) of the soil surface above the bedrock.

#### 2.3.2 Groundwater recharge

The recharge to the aquifer was estimated by Thornthwaite Mather (TM) procedure (Steenhuis and van der Molen, 1986; Thornthwaite and Mather, 1955). The TM procedure keeps a water balance of the root zone and assumes that all water above field capacity drains to the groundwater instantaneously. Evaporation is equal to the potential rate when the soil is above field capacity and decreases linearly with the moisture content from

field capacity to wilting point (Herceg et al., 2016) from potential rate at field capacity to zero at wilting point. The Thornthwaite Mather procedure is formally presented in Appendix A for a daily time step.

### 2.3.3 Valley bottom: surface runoff:

A portion of the watershed is saturated during the rain phase. Rain falling on this part will become surface runoff after the soil becomes saturated. Evaporation rate is at the potential rate. Thus, by keeping a simple water balance with evaporation and rainfall as input parameters, the surface runoff,  $q_s$ , ( $L T^{-1}$ ) can be calculated as:

$$q_s[t] = \max(W[t-1] + P[t] - E[t], 0) \quad (9)$$

$$W[t] = \max(W[t-1] + P[t] - E[t], W_s) \quad (10)$$

where  $W[t]$  is the water content of the valley bottom per unit area ( $L^3 L^{-2}$ ),  $W_s$  is the water content of the soil at saturation per unit area ( $L^3 L^{-2}$ ),  $P[t]$  is the precipitation on day  $t$  (L) at time  $t$ , and  $E[t]$  is the evapotranspiration (L) at time  $t$  predicted with the Thornthwaite Mather procedure.

### 2.3.4 Watershed discharge at the outlet

The discharge at the outlet consists of the interflow plus the surface runoff. The discharge in the river per unit area  $q_t[t]$  ( $L T^{-1}$ ) can then predicted by the sum of the flows of the two areas

$$q_t[t] = \frac{A_h}{x} Q_i[x, t] + A_v q_s[t] \quad (11)$$

where  $A_h$  is the fraction of the hillside area and  $A_v$  is the fraction of the valley bottom in the watershed that contribute to the outlet. Note that in Ethiopian Highlands only part of the hillslopes of the watershed drains to the outlet. The remaining area drains through faults or natural pipes and will appear as springs at lower elevations.

## 3 RESULTS

The observed rainfall, infiltration rates, water levels in the piezometers are presented first followed by a comparison of the predicted and observed water table heights in the SW watershed. The outflow of the NW, NE and the entire Ene-Chilala watershed is presented with the predicted results.

### 3.1 Rainfall

The total rainfall amount for the four-year period during the four monsoon months was 1046 mm in 2013, 530 mm in 2014, 832 mm in 2015 and 732 mm in 2016 (Table 1). From the total 5237 events, about 34% of the events occurred in August and 27% in July (Table 1). The maximum daily rainfall was 68 mm on 8 August 2015. The largest 5-min rainfall intensity was  $119 \text{ mm hr}^{-1}$  on 20 August 2013. Five-minute rainfall intensities greater than  $15 \text{ mm hr}^{-1}$  occurred 9% of the time and greater than  $30 \text{ mm hr}^{-1}$  occurred 3% of the time (Table 1).

### 3.2 Infiltration capacity

The steady state infiltration rate,  $I_f$ , ranged from  $7 \text{ mm hr}^{-1}$  in the saturated valley bottoms to  $275 \text{ mm hr}^{-1}$  in the unsaturated hillsides (Table S1), and were related with slope of the land surface (Figure S1)

$$I_f = 0.256 S^{1.81} \quad (r^2 = 0.75) \quad (12)$$

where  $I_f$  is steady state infiltration capacity ( $\text{mm hr}^{-1}$ ) and  $S$  is slope (%). The differences in infiltration rate between lowest and other slope positions was significant ( $p < 0.01$ ). Studies in Thailand similarly found a power relationship between slope and infiltration rate (Janeau et al., 2003).

### 3.3 Shallow groundwater table observations in the SE watershed

The water table heights are restricted either by the surface of the soil or the bedrock. Thus, we plotted in Figure 2 the water levels in the piezometer with respect to the soil surface (left) and the height above the bedrock (right side) in five groups that behaved similarly with respect to either the surface or bedrock boundaries (Table 2).

The water levels in the Group A (piezometers P5, P6, P13, P18 and P19, see Figure 1c and Table 2) were located close to the gully. The water levels in these piezometers during the rain phase remained nearly at the same height at various depths from the surface (Figure 2a), but in all cases close to the bedrock (Figure 2b). Slight increases in water level occurred during periods of heavy rainfall. Minor increases in water level could not be explained by the rainfall such as the rise of the water table in piezometer 19 around July 21 (Figure 2a, b), which was caused by other external factors such as perhaps slipping of the banks.

**Table 1.** Monthly 5-minute rainfall intensity distribution from 2013 to 2016. The total number of 5-minute rainfall events the number of events (# Exceeding) and the percentage in each month (percentage) greater than 15 and 30  $\text{mm hr}^{-1}$ .

Year	Number of 5 min rainfall events	Intensities greater than 15 $\text{mm hr}^{-1}$				Intensities greater than 30 $\text{mm hr}^{-1}$				
		Jun	Jul	Aug	Sep	Jun	Jul	Aug	Sep	
2013	2114	Total events	190	405	783	736	190	405	783	736
		# Exceeding	45	24	46	69	15	7	15	26
		Percentage	24	6	6	9	8	2	2	4
2014	1165	Total events	105	393	497	170	105	393	497	170
		# Exceeding	10	6	36	10	3	0	4	0
		Percentage	10	2	7	4	3	0	1	0
2015	511	Total events	197	217	170	8	197	217	170	8
		# Exceeding	7	23	25	0	4	12	9	0
		Percentage	6	11	15	0	3	6	5	0
2016	1366	Total events	275	388	410	293	275	388	410	293
		# Exceeding	27	27	35	37	12	9	12	19
		Percentage	10	7	9	13	4	2	3	6

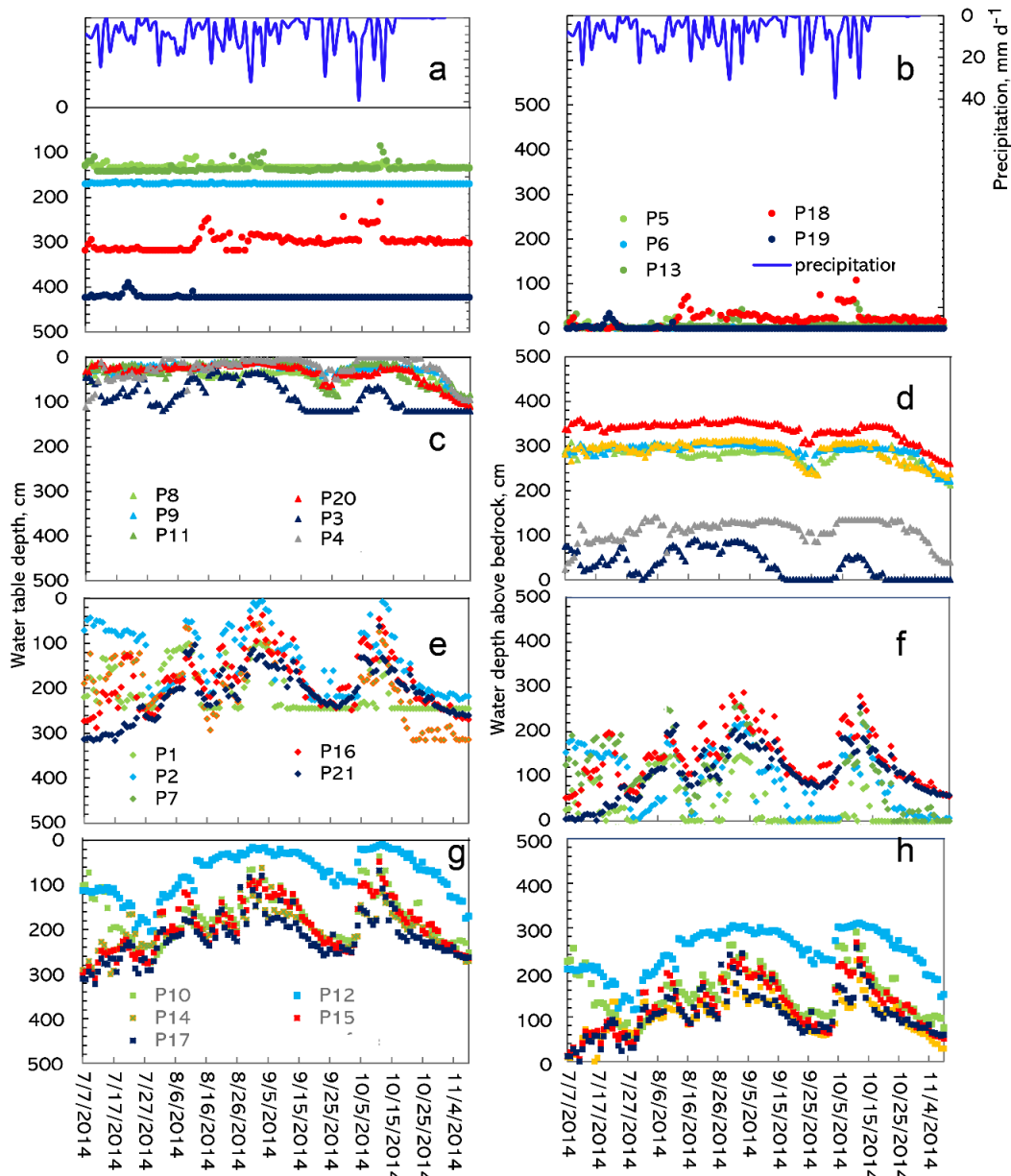


**Fig. 2.** Piezometer water levels for the southwest Ene-Chilala watershed. (a, c, e, g): Observed water table heights from the surface. (b, d, f, h): Observed water table height from the bedrock. Groups of piezometers with the same trend are depicted together: (a, b) group A (piezometers P5, P6, P13, P18, P19) found close to the gullies; (c, d) group B (piezometers P8, P9, P11, P20, P3, P4) located between the gullies with the water table close to the surface; (e, f) Group C (piezometers P1, P2, P16) north of gully and Group E (piezometers P7, P21) west of the gullies; and (g, h) group D (piezometers P10, P12, P14, P15, P17) east of the gully.

**Table 2.** Piezometer groups and model input values for water table prediction.

Group	Piezometers	General location	Model parameters value			
			Travel time (days)	Drainable porosity	Well depth (m)	Minimum water table (m)
Group A	5, 6, 13, 19	All piezometers close to gully	na	na	na	0
	18	Downslope close to gully	11	0.3	3	0
Group B	3	Upslope, between gullies	20	0.15	1.5	0
	4	Upslope, between gullies	30	0.15	1.4	0
	8, 9, 11	Middle slope, between gullies	40	0.15	3	1.95
	20	Downslope, between gullies	30	0.15	3.5	2.6
Group C	1	Upslope above gullies	5	0.045	1.5	0
	2,16	Upslope	10	0.045	2.5	0.2
Group D	10, 14, 15, 17	Middle and down-slope, right of gullies	12	0.045	3	0
	12	Upslope, right of gullies	26	0.09	3	1.1
Group E	7, 21	Down and middle slope, left of gullies	11	0.045	3	0

The piezometers in Group B (P3, P4, P8, P9, P11 and P20) were located between the gullies (Figure 1c, Table 2). The water levels remained relatively constant as well (Figures 2c, d). The groundwater levels for piezometers P4, P8, P9, P11 and P20 were at the surface during the observation period from July to October, and started to decrease in November after the rain had stopped (Figure 2c). Unlike the piezometers in Group A where the depth of the water table was dependent on the depth of the impermeable layer, here the levels were dependent on the ground surface. Hence, the height of the water table above the bedrock in Figure 2d was the difference between the land surface and the bedrock. Only in piezometer P3 the water table was slightly below the surface during some time when the rainfall is small.

The groundwater level for the remaining piezometers (i.e., Groups C, D and E that were not close to or between the gullies, Figure 1c) were varying during the rain phase with a pattern (Figure 2e-h) that was between the two extremes of Group A (close to bedrock, Figure 2a, b) and Group B (close to surface, Figure 2c, d).

The water tables for Group C (piezometers P1, P2, P16) uphill of the gullies and Group E (P7, P21) on the left bank are plotted as the depth from the surface (Figure 2e) and above the bedrock (Figure 2f). Before July 27, there is great variability in water table depth (Figure 2e) and height (Figure 2f). This is likely related to the amount of water needed uphill to bring the soil to field capacity after the dry phase before the groundwater is recharged and flow downhill flow commences. Thus, piezometer P2 has shallower soil uphill than Piezometer 21. After the end of July, the water table behavior observed in all piezometers for Group C and D is similar with increasing water levels during periods of high rain and decreasing levels when the rainfall is less. We hypothesize that all soils are at field

capacity or above from the middle to end of July (Liu et al., 2008; Tilahun et al., 2013), and the whole watershed is contributing. Hence, the dependence on rainfall is the same for all piezometers independent of soil depth. The piezometers P1 and P2 fall dry during periods with little rain (Figure 2f), while piezometer 16 has the same height pattern above the bedrock (Figure 2f), but since the soil is shallower (Table 2) the water table is closer to the surface (Figure 2e). In November after the rains have stopped, the water tables separate again with water tables in Piezometers 2 and 21 dropping faster than the other piezometers. This is consistent with the fast rise in the beginning of the rain phase because the shallow soils dry out faster than the deep soils due to evaporation, and therefore the quantity of water flowing towards the piezometer is decreasing faster for the shallowest soils compared with the deep soil.

The monthly average kriged water table depth for the area near the gullies in the SW watershed from July through November 2014 are shown in Figure 3. Water tables are not extrapolated uphill of the piezometer locations. In general, the water table started to rise in the beginning of the rain phase in July (Figure 3a), was closest to the surface in August (Figure 3b), and then declined slightly as the rainfall decreased in early September (Figure 3c). In addition, the water table decrease in October was small because there was a significant but unusual rain in the beginning of October (Figure 3d). In November when all rainfall had ceased, the water table went down sharply (Figure 3e). The depth of the gully and the water table depth were closely related. Thus, with a gully depth of 1 to 2 m in the upstream (Figure 3), the water depth in piezometers 5, 6 and 13 was 1 to 2 m. More downslope, the gullies were 3 to 4 m deep and the water table depth in piezometers 18 and 19 was nearly the same depth.

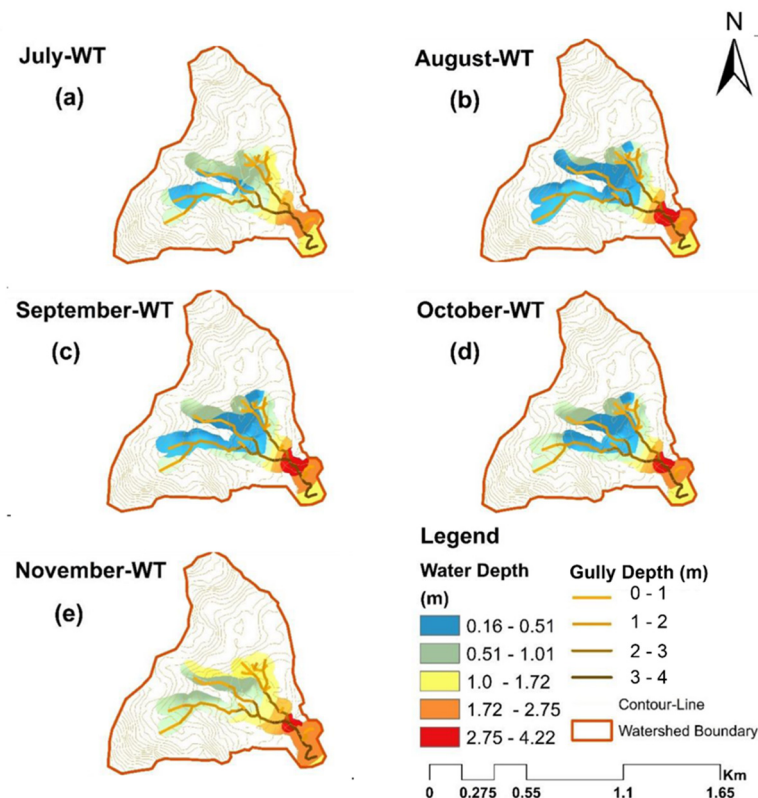


**Fig. 3.** The map showing the average monthly water table depth in the Ene-Chilala watershed for the months of July to November 2014. Gullies are shown as dark yellow lines with their depth indicated with different color intensity (light color represent shallow depths and dark represents deeper depth).

## 4 CONNECTING THE HILLSLOPE AND STREAMFLOW: A DISCUSSION

In this section, we combine the infiltration measurements with the rainfall intensities to justify that all excess rainfall on the hillside will recharge the groundwater. Then, the calculated recharge values are used to predict the hillslope water levels and interflow, and finally the sum of the predicted hillslope outflow and the runoff of the saturated area is compared with the observed discharge at the three gauging stations.

### 4.1 Rainfall intensity, infiltration rate and water table interaction

In order to understand where the runoff originates in the watershed, we plotted in Figure 4 the 5-minute rainfall intensities (Table 1) versus the median infiltration rate for each slope position. We choose the median infiltration rate since any runoff for locations with infiltration rates less than the median will infiltrate further downhill (Stomph et al., 2002).

The median infiltration rate of  $7 \text{ mm h}^{-1}$  downslope is 20 to 40% of the time equal or less than to the five-minute rainfall intensity (Table S1; Figure 4). Thus, the downslope area that was saturated at the time of the infiltration measurement is the source of the runoff. At the midslope area, very little overland flow is produced because less than 3% of the 5-minute rainfall intensities exceeded the median infiltration rate of  $48 \text{ mm h}^{-1}$ . The median upslope infiltration rate of  $160 \text{ mm h}^{-1}$  was never exceeded. Thus, the runoff is produced mainly from the grazing land area in the bottom part of watershed (Figure 1d). Outside the saturated area all rainfall infiltrates and the soil water that does not evaporate will recharge the groundwater. Our infiltration measurements corroborate the assumptions made to obtain the analytical solutions in section 2.3.

To confirm that our understanding of the rainfall-runoff processes was correct, a field walk along the channel was organized with the farmers. The farmers confirmed that the saturated bottomland used for animal grazing was the source of the surface runoff. The saturated area identified by the farmers was plotted using hand-held Garmin GPS tracking (identified by the light blue line in Figure S2) and was indeed identical to the saturated area measured with the piezometers.

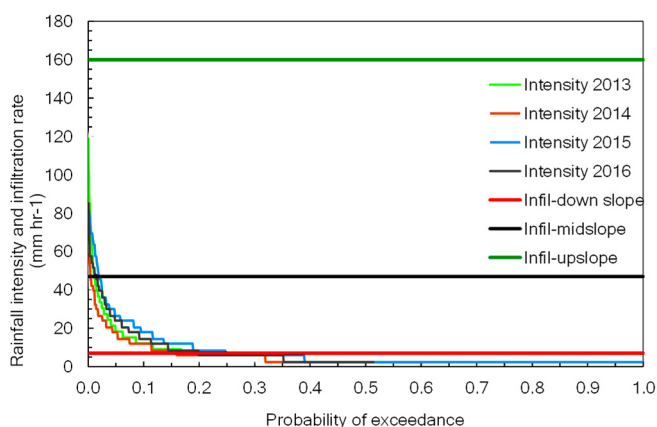


**Fig. 4.** Comparison of the median infiltration (infil) rate for downslope, midslope and upslope positions (horizontal lines) and exceedance probability of 5-minute rainfall intensities for the period 2013 to 2016.

### 4.2 Predicting the groundwater table

The perched water table height prediction has only three fitting parameters. These are the maximum root zone water content in the Thornthwaite Mather Procedure (Appendix A), the characteristic travel time of the water from the uphill boundary, and the effective porosity (Eq. 8). The maximum water content determines how much water can be stored in the root zone and indirectly the actual evaporation rate. However, during most of the rain phase the soil is at or near field capacity and evaporation is at the potential rate. The travel time depends on the hydraulic gradient (assumed to equal the slope of the bedrock), the saturated conductivity and the distance to the groundwater divide. We expect that the velocity of the interflow is decreasing downslope, because the slope decreases going from the top of the watershed to the river (Figure 1c). The effective porosity is made up of the effective drainable porosity and a factor that determines the amount of flow lost to the open channel. Thus, it should be constant uphill and then increase downhill after the head of the first gully.

The landscape is extremely complex, and it cannot be expected that an exact fit can be obtained with these three parameters. Consequently, in evaluating the model results, we should only expect to match the general pattern.

The model was fitted to the water table height above the bedrock between mid-July and mid-September for each group of piezometers, see Figure 5. The individual piezometers in a group are listed in Table 2. Predicted versus observed water table heights for all piezometers are plotted for the period between mid-July and mid-September in Figure 6. When the behavior of water tables within a piezometer group was very similar, a single fit for that group was performed. For example, for Group D with 5 piezometers (Figure 5d), one simulation encompassed the observed water tables for four piezometers P10, P14, P15 and P17; though with an additional simulation for piezometer P12 that had a greater water depth above the bedrock. For Groups B and C, each piezometer was fitted separately (Figures 5b, c and Table 2).

The fitted subsurface parameters are listed in Table 2. For the Group C and Group E piezometers in the upslope area the water tables are predicted using short retention times (ranging from 4 to 11 days, Table 2 and Figure 5c, e), whereas longer travel times of up to 40 days were used for piezometers in the midslope and downslope areas (Group B, Figure 5b and Table 2). The water table in piezometers P5, P6, P13 and P19 in Group A (Figure 5a) were close to bedrock and controlled by the gully, and therefore could not be predicted by the theory that assumed the hydraulic gradient was equal to the slope of the watershed. Piezometer P18 in Group A (Figure 5a) has, as expected, a large effective porosity because most of the water was likely diverted to the creek before it would reach the piezometer. It was also close to the watershed boundary. Left bank (Group E, Figure 5e and Table 2) behaved like an upslope area with a relatively short characteristic travel time of 11 days and small effective porosity that was equal to other studies (Tilahun et al., 2019). The Group C piezometers P1, P2 and P16 (Figure 5c and Table 2) were upslope as well and had short characteristic travel times of 4 to 10 days and a small effective porosity. This is in accordance with Figure 1c where the distance to watershed boundary for the two piezometers on the west side of the gullies (P7 and P21, Group E) is the same order as for piezometer P2 and P16 (Group C). As expected, we also find a short travel time for Group D (P10, P12, P14, P15, P17) that were close to the right border. Only piezometer P12 had a

long travel time of 26 days because, according to the topography shown in Figure 1c, water originated from the upper boundary that was much farther away than the right boundary; P12 was also downhill of piezometer P1 in group C.

Looking in detail to the fit of the water tables over the period of observation, the model reasonably well predicts the water table in the piezometers from the middle of July to the middle of September (Figures 5, 6), but some deviations occur before and after this period (Figure 5). For example, in Group B (piezometers between the gullies, Figure 5b), the rise of the water table in piezometers 8, 9, 11, and 20 is under predicted

and the decline is not fast enough. The rise and fall of the piezometers 3 and 4 in Figure 5b are well predicted. For Group C (piezometer 16, Figure 5c), Group D (piezometer 10, Figure 5d) and Group E (piezometer 16 and 21, Figure 5d) the under prediction of the rise of the water table in the beginning of the rain phase is followed by an under prediction of the decrease in water table after the rain phase ends. This indicates that the storage upslope of the piezometers is underestimated by the model. More rainfall is needed to fill up the reservoir than assumed in the model and more water is subsequently released after the rain ends.

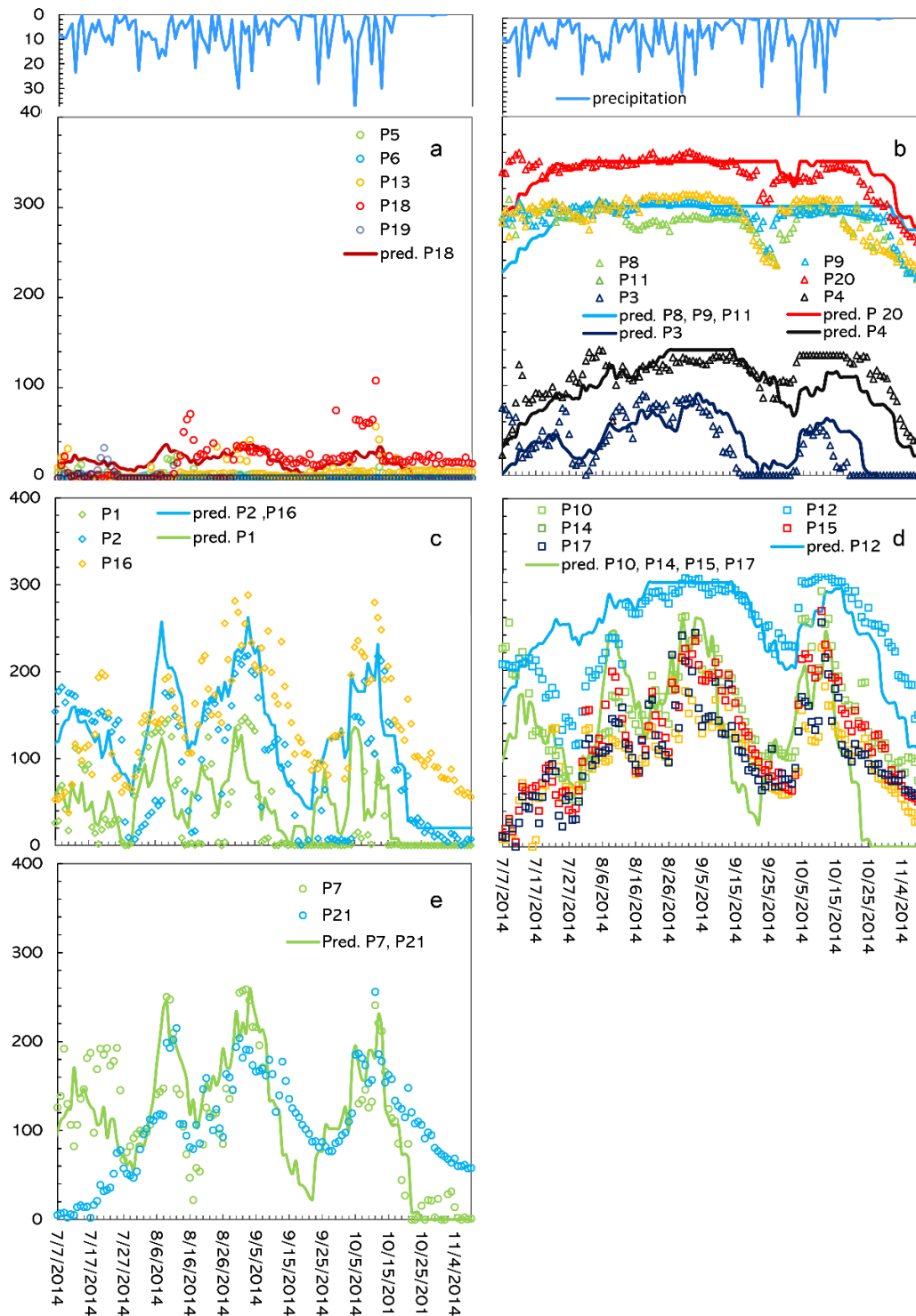


**Fig. 5.** Comparison of predicted and observed water table depth relative to the impermeable layer at different locations in the Ene-Chilala watershed: (a) Group A piezometers, (b) Group B piezometers, (c) Group C piezometers, (d) Group D piezometers, and (e) Group E piezometers.

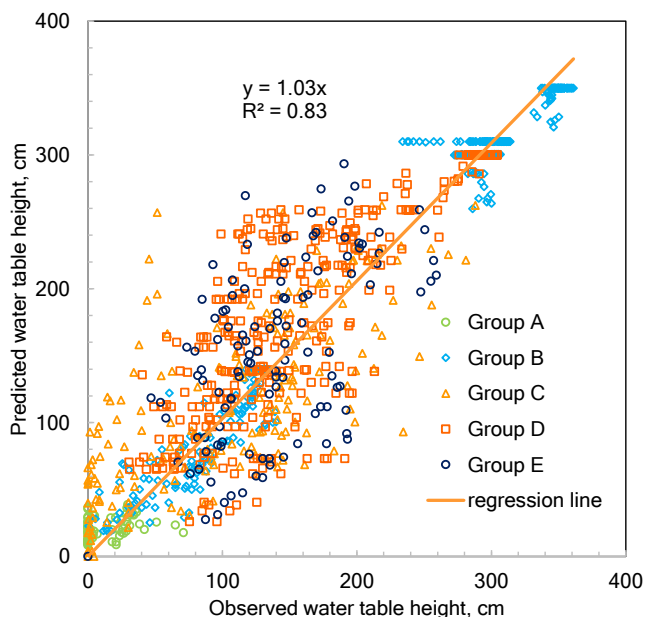


**Fig. 6.** Comparison of observed and predicted daily water table depth above the bedrock for the period from July 15 to September 15 for the Ene-Chilala watershed. The colors and symbols indicate the different groups of piezometers listed in Table 2.

4.2.1 Fitting the discharge in the three watersheds

The discharge was measured at the outlet weirs of the NE, NW and whole watershed from June to September for the four years from 2013–2016. We do not have separate measurements for the SW watershed, so we cannot use the fitted parameters for the interflow model directly. The first step in the calibration was carrying out an annual water mass balance by comparing the amount discharged from the watershed and the amount that was contributed from the rainfall and lost by evaporation. We found that in the NE watershed only 50% of the watershed reached the outlet (Table 3). All the rainfall (after subtracting the evaporation) was accounted for in the NW watershed. In the entire watershed 90% of rainfall reached the outlet. The contributing area to the outlet was divided in unsaturated hillside where the water infiltrated (called hillside) and a saturated area.

**Table 3.** Calibrated model input parameters and values for the surface runoff prediction for the NE, NW and whole watershed.

	NE watershed	NW watershed	Whole watershed
Saturated area proportion	0.15	0.2	0.2
Hillside area proportion	0.35	0.8	0.7
Saturated area maximum storage, mm	10	10	10
Hillside maximum storage, mm	50	50	50
Characteristic travel time, $t_r$ days	40	40	40
<b>Model performance</b>			
NSE	0.77	0.56	0.82
RMSE	0.48	0.67	0.43
RVE (%)	6.57	16.30	5.76

We assumed that the maximum storage for the three watersheds was 50 mm for the hillside and 10 mm for the saturated area (Table 3). This is the same as used for the interflow predictions presented in the previous section. To predict the interflow, a travel time of 40 days was used (Table 2). This is the same as

the fitted travel time data for the downslope piezometers in Group B in the SW watershed. Finally, we needed to separate the portion of streamflow into interflow and saturation excess overland flow. Based on visual observations we assumed that 15% of the NE watershed and 20% of the remaining watersheds were saturated (Table 3). These values are of the same order as that observed in the SW watershed. However, early in the rain phase the selected values overestimate the saturated area. The predicted discharge for the NE, NW and the entire watershed over the period 2013–2016 fitted the observed daily data well with Nash Sutcliffe Efficiency values of 0.77, 0.56, and 0.82, and RMSE of 0.48, 0.67 and 0.43, respectively (Table 3 and Figure 7). The RVE result for the NE, NW and SW watershed was 6.6%, 16.3% and 5.7%. The result shows a satisfactory value that the model reasonably predicts the observed discharge well (smaller than  $\pm 10\%$ , Wale et al., 2009) except the NW watershed (Table 3). As expected the model predicted runoff in the early rain phase which was not observed. This is due to a too large saturated area.

In summary, despite that the geology, land use and cropping pattern were highly complex, we found that both the trend of the water table and the discharge from the watershed could be predicted with six fitted parameters. These are: effective drainable porosity, subsurface flow travel time for both the hillside and saturated areas, fractional areas for the saturated bottomlands and hillslopes and maximum root zone storage. This clearly indicates that the many individual parts in the landscape interact with each other and produce watershed flow patterns on a scale that is much larger than the individual parts (Beven, 2018; Schweitzer, 1997). This is called self-organization of complexity and occurs in many fields. Sidle et al. (2001) contributed the self-organization to preferential flow paths, which is in accordance with our findings in the 4.1-km<sup>2</sup> Ene-Chilala watershed where subsurface travel times of 40 days in silty and clay soils can only be achieved when water flows preferentially.

5 CONCLUSION

To understand the hydrology of the Ene-Chilala watershed, a field study was conducted from in which we measured streamflow for three years and water table heights for one year. The interactions between the rainfall, infiltration and groundwater were analyzed. Like other watersheds in the sub humid highlands, the Ene-Chilala watershed is characterized by interflow on the hillsides and saturation excess overland flow near the rivers. The infiltration rate of the soil was greater on the hillslope than the flatter and saturated bottomlands. Flow from the hillslope was as interflow, through a perched water. The pattern of the groundwater table heights was predicted well especially after the soils were at field capacity. The streamflow response at the outlet is a combination of overland flow and interflow from the hillslope and prediction were good provided that only five calibration parameters were used in this complex watershed for both discharge and water table prediction. Since the interflow and water table predictions were based on the same theory and interflow was the major portion of the discharge we were able to directly link the hillslope processes the discharge at the watershed outlet. Although this study was the first in linking hillslope processes with the discharge at the outlet in the Ethiopian Highlands, the study was hampered by shifting channel configurations that affected the streamflow predictions. Further studies are needed to validate the theory on the interaction of hillslope hydrology and the watershed outflow in other parts of the Ethiopian Highlands using other and more sophisticated methods to characterize the flows.

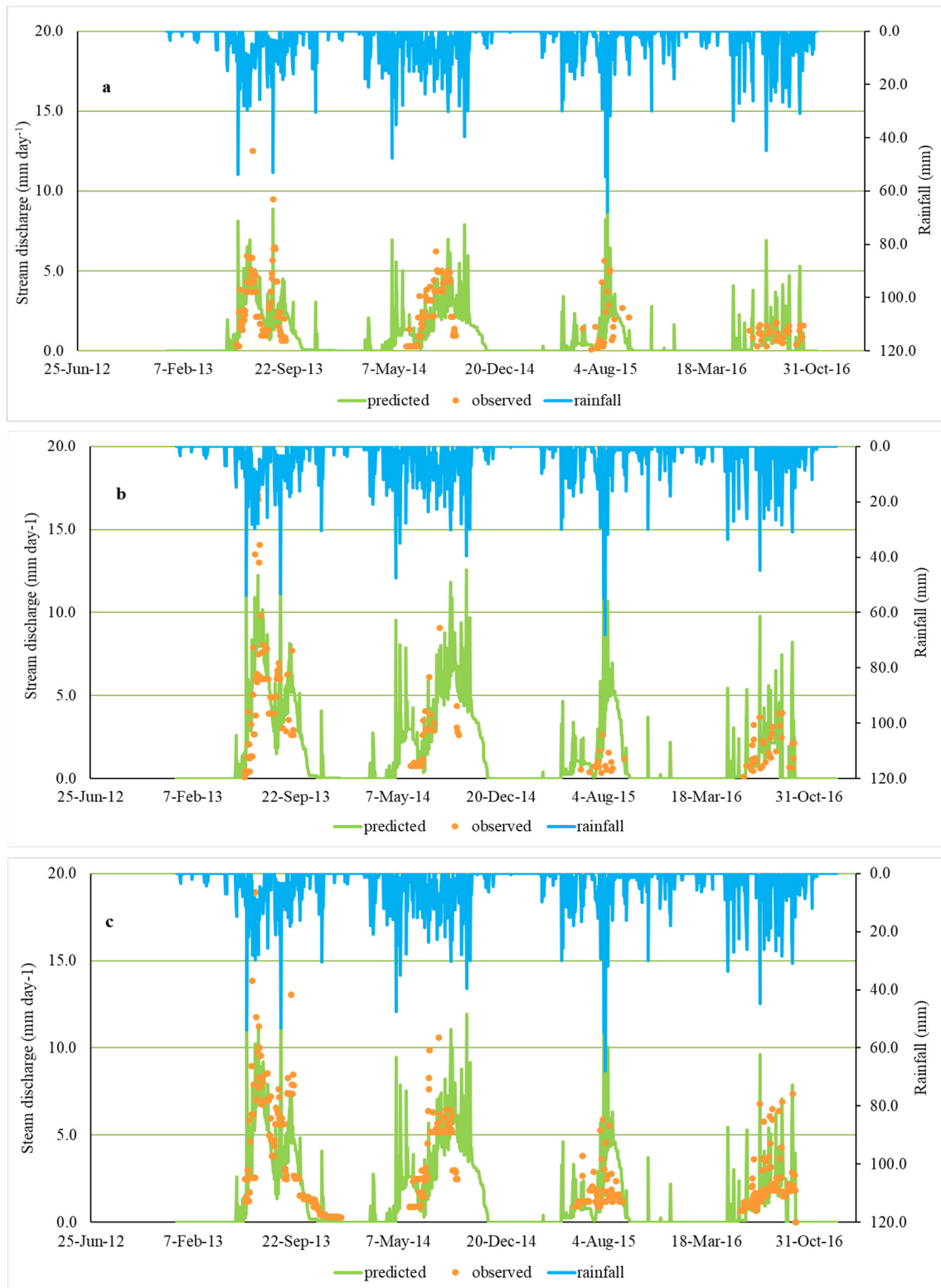


**Fig. 7.** Comparison of the observed and predicted stream flow from the Ene-Chilala watershed from 2013 to 2016. a) Watershed NE, b) watershed NW, and c) the whole watershed.

*Acknowledgements.* This research was sponsored in part by the following organizations: USAID-PEER project (AID-OAA-A-11-00012); International Foundation for Science (W/5844-1); Norman E. Borlaug Leadership Enhancement in Agriculture Program Borlaug (LEAP-016258-82); the Innovation Laboratory for Small Scale Irrigation project funded by Feed the Future through the U.S. Agency for International Development (USAID); the International Water Management Institute

through the CGIAR Research Program on Water, Land and Ecosystems (WLE) in the Nile Basin and East Africa region to bolster opportunities for increased agricultural productivity through key ecosystem services; First Presbyterian Church in Ithaca, New York; Blue Nile Water Institute, Bahir Dar, Ethiopia; Quarit District Office of Agriculture; and the Ethiopian Road Authority.

## REFERENCES

- Addisie, M.B., Ayele, G.K., Gessess, A.A., Tilahun, S.A., Zegeye, A.D., Moges, M.M., Schmitter, P., Langendoen, E.J., Steenhuis, T.S., 2017. Gully head retreat in the sub-humid Ethiopian Highlands: The Ene-Chilala catchment. *Land Degradation & Development*, 28, 1579–1588. DOI: 10.1002/ldr.2688
- Addisie, M.B., Langendoen, E.J., Aynalem, D.W., Ayele, G.K., Tilahun, S.A., Schmitter, P., Mekuria, W., Moges, M.M., Steenhuis, T.S., 2018. Assessment of practices for controlling shallow valley-bottom gullies in the sub-humid Ethiopian highlands. *Water*, 10, 389. DOI: 10.3390/w10040389
- Agnew, L.J., Lyon, S.W., Gérard-Marchant, P., Collins, V.B., Lembo, A.J., Steenhuis, T.S., Walter, M.T., 2006. Identifying hydrologically sensitive areas: bridging the gap between science and application. *Journal of Environmental Management*, 78, 63–76.
- Alemie, T.C., Tilahun, S.A., Ochoa-Tocachi, B.F., Schmitter, P., Buytaert, W., Parlange, J.Y., Steenhuis, T.S., 2019. Predicting (observed) shallow groundwater tables for sloping highland aquifers. *Water Resources Research*, 55, 11088–11100. DOI:10.1029/2019WR025050
- Ayele, G.K., Gessess, A.A., Addisie, M.B., Tilahun, S.A., Tebebu, T.Y., Tenessa, D.B., Langendoen, E.J., Nicholson, C.F., Steenhuis, T.S., 2016. A biophysical and economic assessment of a community-based rehabilitated gully in the Ethiopian highlands. *Land Degradation & Development*, 27, 270–280.
- Aynew, T., 2001. Numerical groundwater flow modeling of the Central Main Ethiopian rift lakes basin. *SINET: Ethiopian Journal of Science*, 24, 167–184. <https://doi.org/10.4314/sinet.v24i2.18184>
- Aynew, T., Tilahun, N., 2008. Assessment of lake-groundwater interactions and anthropogenic stresses, using numerical groundwater flow model, for a rift lake catchment in Central Ethiopia. *Lakes & Reservoirs: Research & Management*, 13, 325–343. <https://doi.org/10.1111/j.1440-1770.2008.00383.x>
- Aynew, T., Demille, M., Wohnillich, S., 2008a. Hydrogeological framework and occurrence of groundwater in the Ethiopian aquifers. *Journal of African Earth Sciences*, 52, 97–113. <https://doi.org/10.1016/j.jafrearsci.2008.06.006>
- Aynew, T., Demlie, M., Stefan, W.S., 2008b. Application of numerical modeling for groundwater flow system analysis in the Akaki Catchment, Central Ethiopia. *Mathematical Geosciences*, 40, 887–906.
- Bayabil, H.K., Tilahun, S.A., Collick, A.S., Yitafaru, B., Steenhuis, T.S., 2010. Are runoff processes ecologically or topographically driven in the (sub) humid Ethiopian highlands? The case of the Maybar watershed. *Ecohydrology*, 3, 457–466.
- Bayabil, H.K., Tebebu, T.Y., Stoof, C.R., Steenhuis, T.S., 2016. Effects of a deep-rooted crop and soil amended with charcoal on spatial and temporal runoff patterns in a degrading tropical highland watershed. *Hydrology and Earth System Sciences*, 20, 875–885.
- Bayabil, H.K., Yiftaru, B., Steenhuis, T.S., 2017. Shift from transport limited to supply limited sediment concentrations with the progression of monsoon rains in the Upper Blue Nile Basin. *Earth Surface Processes and Landforms*, 42, 1317–1328.
- Berehanu, B., Aynew, T., Azagegn, T., 2017. Challenges of groundwater flow model calibration using MODFLOW in Ethiopia: With particular emphasis to the Upper Awash River Basin. *Journal of Geoscience and Environment Protection*, 5, 50–66. DOI: 10.4236/gep.2017.53005
- Betrie, G.D., Mohamed, Y.A., Griensven, A.V., Srinivasan, R., 2011. Sediment management modelling in the Blue Nile Basin using SWAT model. *Hydrology and Earth System Sciences*, 15, 807–818.
- Betson, R.P., 1964. What is watershed runoff? *Journal of Geophysical Research*, 69, 1541–1552.
- Beven, K., 2018. A century of denial: Preferential and nonequilibrium water flow in soils, 1864–1984. *Vadose Zone Journal*, 17, 180153. DOI: 10.2136/vzj2018.08.0153
- Chebud, Y.A., Melesse, A.M., 2009. Numerical modeling of the groundwater flow system of the Gumera sub-basin in Lake Tana basin, Ethiopia. *Hydrological Processes*, 23, 3694–3704.
- Descheemaeker, K., Raes, D., Nyssen, J., Poesen, J., Haile, M., Deckers, J., 2009. Changes in water flows and water productivity upon vegetation regeneration on degraded hillslopes in northern Ethiopia: a water balance modelling exercise. *The Rangeland Journal*, 31, 237–249.
- Dunne, T., Black, R.D., 1970. Partial area contributions to storm runoff in a small New England watershed. *Water Resources Research*, 6, 1296–1311.
- Enku, T., Melesse, A.M., 2014. A simple temperature method for the estimation of evapotranspiration. *Hydrological Processes*, 28, 2945–2960.
- Fox, G.A., Sheshukov, A., Cruse, R., Kolar, R.L., Guertault, L., Gesch, K.R., Dutnell, R.C., 2016. Reservoir sedimentation and upstream sediment sources: perspectives and future research needs on streambank and gully erosion. *Environmental Management*, 57, 945–955.
- García-Orenes, F., Roldán, A., Mataix-Solera, J., Cerdà, A., Campoy, M., Arcenegui, V., Caravaca, F., 2012. Soil structural stability and erosion rates influenced by agricultural management practices in a semi-arid Mediterranean agroecosystem. *Soil Use and Management*, 28, 571–579.
- Golmohammadi, G., Prasher, S., Madani, A., Rudra, R., 2014. Evaluating three hydrological distributed watershed models: MIKE-SHE, APEX, SWAT. *Hydrology*, 1, 20–39.
- Güntner, A., Seibert, J., Uhlenbrook, S., 2004. Modeling spatial patterns of saturated areas: An evaluation of different terrain indices. *Water Resources Research*, 40, W05114.
- Gurtz, J., Zappa, M., Jasper, K., Lang, H., Verbunt, M., Badoux, A., Vitvar, T., 2003. A comparative study in modeling runoff and its components in two mountainous catchments. *Hydrological Processes*, 17, 297–311.
- Guzman, C.D., Zimale, F.A., Tebebu, T.Y., Bayabil, H.K., Tilahun, S.A., Yitafaru, B., Rientjes, T.H., Steenhuis, T.S., 2017a. Modeling discharge and sediment concentrations after landscape interventions in a humid monsoon climate: The Anjeni watershed in the highlands of Ethiopia. *Hydrological Processes*, 31, 1239–1257.
- Guzman, C.D., Tilahun, S.A., Dagne, D.C., Zegeye, A.D., Tebebu, T.Y., Yitafaru, B., Steenhuis, T.S., 2017b. Modeling sediment concentration and discharge variations in a small Ethiopian watershed with contributions from an unpaved road. *Journal of Hydrology and Hydromechanics*, 65, 1–17.
- Haregeweyn, N., Yohannes, F., 2003. Testing and evaluation of the agricultural non-point source pollution model (AGNPS) on Augucho catchment, western Hararge, Ethiopia. *Agriculture, Ecosystems & Environment*, 99, 201–212.
- Herceg, A., Kalicz, P., Kisfaludi, B., Gribovszki, Z., 2016. A monthly-step water balance model to evaluate the hydrological effects of climate change on a regional scale for irrigation design. *Slovak Journal of Civil Engineering*, 24, 27–35.

- Hoang, L., Schneiderman, E.M., Moore, K.E., Mukundan, R., Owens, E.M., Steenhuis, T.S., 2017. Predicting saturation-excess runoff distribution with a lumped hillslope model: SWAT-HS. *Hydrological Processes*, 31, 2226–2243.
- Hoang, L., Mukundan, R., Moore, K.E., Owens, E.M., Steenhuis, T.S., 2018. The effect of input data resolution and complexity on the uncertainty of hydrological predictions in a humid, vegetated watershed. *Hydrology and Earth System Sciences*, 22, 5947–5965. <https://doi.org/10.5194/hess-22-5947-2018>
- Jackson, C.R., Bitew, M., Du, E., 2014. When interflow also percolates: downslope travel distances and hillslope process zones. *Hydrological Processes*, 28, 3195–3200. <https://doi.org/10.1002/hyp.10158>
- Janeau, J.L., Bricquet, J.P., Planchon, O., Valentin, C., 2003. Soil crusting and infiltration on steep slopes in northern Thailand. *European Journal of Soil Science*, 54, 543–554.
- Kaleab, M.M., Manoj, K.J., 2013. Runoff and sediment modeling using SWAT in Gumera Catchment, Ethiopia. *Open Journal of Modern Hydrology*, 3, 196–206. DOI: 10.4236/ojmh.2013.34024
- Liu, B.M., Collick, A.S., Zeleke, G., Adgo, E., Easton, Z.M., Steenhuis, T.S., 2008. Rainfall-discharge relationships for a monsoonal climate in the Ethiopian highlands. *Hydrological Processes*, 22, 1059–1067.
- Lyon, S.W., Lembo Jr, A.J., Walter, M.T., Steenhuis, T.S., 2006. Defining probability of saturation with indicator kriging on hard and soft data. *Advances in Water Resources*, 29, 181–193.
- Moges, M.A., Schmitter, P., Tilahun, S.A., Langan, S., Dagnew, D.C., Akale, A.T., Steenhuis, T.S., 2016. Suitability of watershed models to predict distributed hydrologic response in the Awramba watershed in Lake Tana basin. *Land Degradation & Development*, 28, 1386–1397.
- Nash, J., Sutcliffe, J., 1970. River flow forecasting through conceptual models part IA discussion of principles. *Journal of Hydrology*, 10, 282–290. DOI: 10.1016/00221694(70)90255-6
- Nikroo, L., Kompani-Zare, M., Sepaskhah, A.R., Shamsi, S.R., 2010. Groundwater depth and elevation interpolation by kriging methods in Mohr Basin of Fars province in Iran. *Environmental Monitoring and Assessment*, 166, 387–407.
- Nyssen, J., Vandenreyken, H., Poesen, J., Moeyersons, J., Deckers, J., Haile, M., Salles, C., Govers, G., 2005. Rainfall erosivity and variability in the Northern Ethiopian Highlands. *Journal of Hydrology*, 311, 172–187.
- Poesen, J., Nachtergaele, J., Verstraeten, G., Valentin, C., 2003. Gully erosion and environmental change: importance and research needs. *Catena*, 50, 91–133.
- Rosenzweig, C., Liverman, D., 1992. Predicted effects of climate change on agriculture: A comparison of temperate and tropical regions. In: Majumdar, S.K., Kalkstein, L.S., Yarnal, B., Miller, E.W., Rosenfeld, L.M. (Eds.): *Global Climate Change: Implications, Challenges and Mitigation Measures*. The Pennsylvania Academy of Sciences, Easton, Pennsylvania, pp. 342–361.
- Schweitzer, F., 1997. Self-organization of complex structures: from individual to collective dynamics. Some introductory remarks. In: Schweitzer, F. (Eds.): *Self-organization of Complex Structures: from Individual to Collective Dynamics*. CRC Press, Baton Rouge.
- Setegn, S.G., Srinivasan, R., Melesse, A.M., Dargahi, B., 2010. SWAT model application and prediction uncertainty analysis in the Lake Tana Basin, Ethiopia. *Hydrological Processes*, 24, 357–367.
- Side, R.C., Noguchi, S., Tsuboyama, Y., Laursen, K., 2001. A conceptual model of preferential flow systems in forested hillslopes: evidence of self-organization. *Hydrological Processes*, 15, 1675–1692.
- Sop, T.K., Oldeland, J., 2013. Local perceptions of woody vegetation dynamics in the context of a ‘greening Sahel’: a case study from Burkina Faso. *Land Degradation & Development*, 24, 511–527.
- Steenhuis, T.S., van der Molen, W.H., 1986. The Thornthwaite-Mather procedure as a simple engineering method to predict recharge. *J. Hydrol.*, 84, 221–229.
- Steenhuis, T.S., Collick, A.S., Easton, Z.M., Leggesse, E.S., Bayabil, H.K., White, E.D., Awulachew, S.B., Adgo, E., Ahmed, A.A., 2009. Predicting discharge and sediment for the Abay (Blue Nile) with a simple model. *Hydrological Processes*, 23, 3728–3737. <https://doi.org/10.1002/hyp.7513>
- Stomph, T.J., De Ridder, N., Steenhuis, T.S., Van de Giesen, N.C., 2002. Scale effects of Hortonian overland flow and rainfall-runoff dynamics: Laboratory validation of a process-based model. *Earth Surface Processes and Landforms*, 27, 847–855.
- Tebebu, T.Y., Abi, A.Z., Zegeye, A.D., Dahlke, H.E., Easton, Z.M., Tilahun, S.A., Collick, A.S., Kidnau, S., Moges, S., Dadgari, F., 2010. Surface and subsurface flow effect on permanent gully formation and upland erosion near Lake Tana in the northern highlands of Ethiopia. *Hydrology and Earth System Sciences*, 14, 2207–2217.
- Tebebu, T.Y., Steenhuis, T.S., Dagnew, D.C., Guzman, C.D., Bayabil, H.K., Zegeye, A.D., Collick, A.S., Langan, S., Macalister, C., Langendoen, E.J., 2015. Improving efficacy of landscape interventions in the (sub) humid Ethiopian highlands by improved understanding of runoff processes. *Frontiers in Earth Science*, 3, 49. DOI: 10.3389/feart.2015.00049
- Tebebu, T.Y., Bayabil, H.K., Stoof, C.R., Giri, S.K., Gessess, A.A., Tilahun, S.A., Steenhuis, T.S., 2017. Characterization of degraded soils in the humid Ethiopian highlands. *Land Degradation & Development*, 28, 1891–1901.
- Tesemma, Z.K., Mohamed, Y.A., Steenhuis, T.S., 2010. Trends in rainfall and runoff in the Blue Nile basin: 1964–2003. *Hydrological Processes*, 24, 3747–3758.
- Thornthwaite, C.W., Mather, J.R., 1955. The water balance. *Publ. Climatol.*, 8, 1.
- Tilahun, S., Guzman, C., Zegeye, A., Engda, T., Collick, A., Rimmer, A., Steenhuis, T., 2013. An efficient semi-distributed hillslope erosion model for the subhumid Ethiopian Highlands. *Hydrology and Earth System Sciences*, 17, 1051–1063.
- Tilahun, S.A., Guzman, C.D., Zegeye, A.D., Ayana, E.K., Collick, A.S., Yitaferu, B., Steenhuis, T.S., 2014. Spatial and temporal patterns of soil erosion in the semi-humid Ethiopian highlands: a case study of Debre Mawi watershed. In: Melesse, A.M., Abteu, W., Setegn, S.M. (Eds.): *Nile River Basin*. Springer.
- Tilahun, S.A., Guzman, C.D., Zegeye, A.D., Dagnew, D.C., Collick, A.S., Yitaferu, B., Steenhuis, T.S., 2015. Distributed discharge and sediment concentration predictions in the sub-humid Ethiopian highlands: the Debre Mawi watershed. *Hydrological Processes*, 29, 1817–1828.
- Tilahun, S.A., Yilak, D.L., Schmitter P., Zimale, F.A., Langan S., Barron, J., Parlange, J.-Y., Steenhuis, T.S., 2019. Establishing irrigation potential of a hillslope aquifer in the African highlands. *Hydrological Processes*, 34, 8, 1741–1753. <https://doi.org/10.1002/hyp.13659>
- Wale, A.T., Rientjes, H.M., Gieske, A.S., Getachew, H.A.,

2009. Ungauged catchment contributions to Lake Tana's water balance. *Hydrological Processes*, 23, 3682–3693.

Walraevens, K., Vandecasteele, I., Martens, K., Nyssen, J., Moeyersons, J., Gebreyohannes, T., De Smedt, F., Poesen, J., Deckers, J., Van Camp, M., 2009. Groundwater recharge and flow in a small mountain catchment in northern Ethiopia. *Hydrological Sciences Journal*, 54, 739–753.

Whipkey, R.Z., 1965. Subsurface storm flow from forested slopes. *Hydrological Sciences Journal*, 10, 74–85.

Yenehun, A., Kristine, W.O., Batelaan., 2017. Spatial and temporal variability of groundwater recharge in Geba basin, Northern Ethiopia. *Journal of African Earth Sciences*, 134, 198–212. <https://doi.org/10.1016/j.jafrearsci.2017.06.006>

Zelege, G., 2000. Landscape dynamics and soil erosion process modelling in the north-western Ethiopian highlands. University of Berne, Institute of Geography. <https://www.cabdirect.org/cabdirect/abstract/20016786872>

Zenebe, A., Vanmaercke, M., Poesen, J., Verstraeten, G., Haregeweyn, N., Haile, M., Amare, K., Deckers, J., Nyssen, J., 2013. Spatial and temporal variability of river flows in the degraded semi-arid tropical mountains of northern Ethiopia. *Zeitschrift für Geomorphologie*, 57, 143–169.

Zimale, F.A., Tilahun, S.A., Tebebu, T.Y., Guzman, C.D., Hoang, L., Schneiderman, E.M., Langendoen, E.J., Steenhuis, T.S., 2017. Improving watershed management practices in humid regions. *Hydrological Processes*, 31, 3294–301.

Received 26 February 2020  
Accepted 22 April 2020

**APPENDIX A**

**The Thornthwaite Mather procedure**

The evaporation is equal to the potential rate when it is exceeded by the rainfall, otherwise depends on the moisture content in the soil

$$P[t] \geq E_p[t] \quad E_a[t] = E_p[t] \quad (A1)$$

$$P[t] < E_p[t]$$

$$E_a[t] = P[t] + \frac{W[t-1]}{\Delta t} \left( 1 - \exp\left( \frac{P[t] - E_p[t]}{W_{fc}} \right) \right) \quad (A2)$$

where  $P[t]$  is the precipitation (L) on day  $t$  (T),  $E_p[t]$  is the potential evaporation (L) on day  $t$ ,  $E_a[t]$  is the actual evaporation on day  $t$ ,  $W[t - \Delta t]$  is the available water in the root zone (L) on the previous day, and  $W_{fc}$  is the amount of water that can be stored at field capacity in the root zone (L). The potential evaporation,  $E_p$ , was estimated using Enku and Melesse, (2014).

The available soil moisture content in the root zone is either equal to the maximum amount of water that can be stored at field capacity in the root zone,  $W_{fc}$ , when sum of rain and the previous moisture content is greater than field capacity, or otherwise it is simply the sum of the fluxes and the previous day moisture content. Formally this can then be written as:

$$W[t] = \min((W[t-1] + P[t] - E_a[t]), W_{fc}) \quad (A3)$$

The excess above field capacity becomes the recharge, i.e.,

$$R[t] = \max((W[t-1] + P[t] - E_a[t] - W_{fc}), 0) \quad (A4)$$

where  $R[t]$  is the excess rain water that percolates daily downwards on day  $t$  and  $W[t]$  is related to the moisture content as  $W[t] = d(\theta - \theta_{wp})$  where  $\theta$  is the average moisture content of the rootzone,  $\theta_{wp}$  is the moisture content at wilting point, and  $d$  is the rooting depth (L).

**SUPPLEMENTARY MATERIAL**

**Table S1.** Infiltration test sites for the various land uses and slope positions in the Ene-Chilala watershed.

Test ID	Infiltration rate (mm hr <sup>-1</sup> )	Land use type	Landscape position
1	7	Homestead	Downslope
2	8	Grazing land	
3	7	Grazing land	
4	11	Grazing land	
5	40	Cultivated	Middle slope
6	70	Cultivated	
7	55	Cultivated	
8	23	Cultivated	
9	50	Bush/grazing	Upper slope
10	200	Bushland	
11	275	Cultivated	
12	120	Cultivated	

**Table S2.** Depth, surface elevation, average, median, standard deviation (Sdv.), minimum (Min) and maximum (Max) of water table (WT) depth for the 21 piezometers in the Ene-Chilala watershed. Location of the piezometers is shown in Figure 1b.

Pz Id	Depth of piezometer (m)	Elevation a.s.l. (m)	Average WT depth (m)	Median WT depth (m)	AWT elevation from the surface (m)	Min	Max	Sdv.
P_1	2.45	2055	2.09	2.42	2053	0.98	2.45	0.49
P_2	2.50	2056	1.34	1.36	2055	0.07	2.27	0.70
P_3	1.20	2052	0.86	0.90	2051	0.30	1.20	0.31
P_4	3.23	2030	0.45	0.48	2030	0.00	1.15	0.33
P_5	1.34	2038	1.31	1.33	2037	0.55	1.34	0.08
P_6	1.70	2039	1.69	1.70	2037	1.65	1.70	0.01
P_7	3.15	2018	1.99	1.81	2016	0.38	3.15	0.71
P_8	3.20	2023	0.40	0.34	2023	0.12	1.08	0.19
P_9	3.17	2024	0.27	0.23	2024	0.11	0.97	0.18
P_10	3.26	2026	1.73	1.78	2024	0.36	2.82	0.55
P_11	3.21	2029	0.32	0.24	2029	0.01	0.91	0.24
P_12	3.20	2023	0.77	0.67	2022	0.01	2.05	0.53
P_13	1.42	2037	1.35	1.37	2036	0.85	1.42	0.09
P_14	3.00	2024	1.98	1.99	2022	0.62	3.00	0.46
P_15	3.15	2014	1.92	1.95	2012	0.48	3.10	0.59
P_16	3.25	2016	1.83	1.87	2014	0.37	2.88	0.61
P_17	3.22	2012	2.16	2.18	2010	0.68	3.22	0.51
P_18	3.18	2009	2.97	3.00	2006	1.23	3.18	0.23
P_19	4.23	2008	4.22	4.23	2004	3.90	4.23	0.04
P_20	3.70	2011	0.34	0.26	2011	0.09	1.10	0.23
P_21	3.18	2022	2.12	2.12	2020	0.62	3.16	0.56

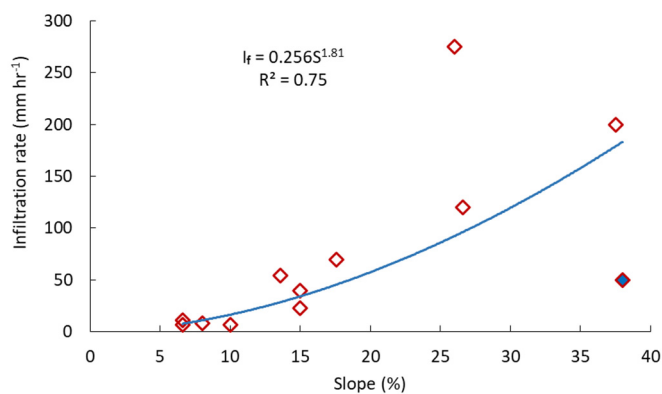


**Fig. S1.** The relationship between infiltration rate and slope. The blue filled diamond indicates a location where the infiltration decreases with an increase in slope, which may be due to the presence of shallow soil depth near the top of the watershed.

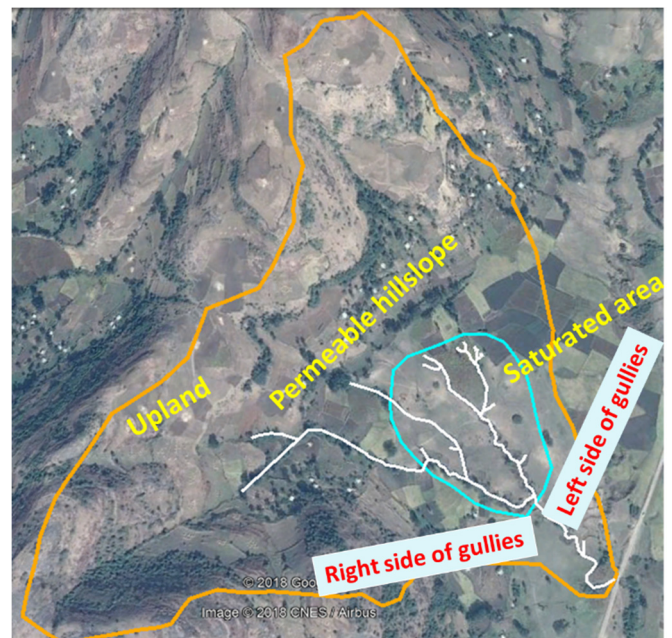


**Fig. S2.** Saturated area delineation from farmers observation displayed over the satellite image (the blue line) following areas where water stays longer and grazing area with grasses; the white lines are active gully networks.

# Land management impacts on soil properties and initial soil erosion processes in olives and vegetable crops

Igor Bogunovic<sup>1\*</sup>, Leon Josip Telak<sup>1</sup>, Paulo Pereira<sup>2</sup>, Vilim Filipovic<sup>1</sup>, Lana Filipovic<sup>1</sup>, Aleksandra Percin<sup>1</sup>, Boris Durdevic<sup>3</sup>, Márta Birkás<sup>4</sup>, Igor Dekemati<sup>4</sup>, Jesus Rodrigo Comino<sup>5,6</sup>

<sup>1</sup> Faculty of Agriculture, University of Zagreb, Svetosimunska 25, HR-10000, Zagreb, Croatia.

<sup>2</sup> Environmental Management Laboratory, Mykolas Romeris University, LT-08303 Vilnius, Lithuania.

<sup>3</sup> Faculty of Agrobiotechnical Sciences Osijek, Josip Juraj Strossmayer University of Osijek, Vladimira Preloga 1, HR-31000, Osijek, Croatia.

<sup>4</sup> Szent Istvan University, Faculty of Agricultural and Environmental Sciences, Gödöllő, Páter K. u. 1, H-2103, Gödöllő, Hungary.

<sup>5</sup> Department of Physical Geography, University of Trier, Germany.

<sup>6</sup> Soil Erosion and Degradation Research Group, Department of Geography, Valencia University, Blasco Ibáñez, 28, 46010 Valencia, Spain.

\* Corresponding author. Tel.: +385-1-2393815. E-mail: ibogunovic@agr.hr

**Abstract:** This research aims to assess the impacts of soil use management on runoff, soil losses, and their main soil controls in vegetable cropland (CROP), tilled olives (OT), and grass-covered olive orchards (OGC) on Leptosol in Croatia. Soil analysis and rainfall simulation experiments were conducted to quantify runoff (Run), soil, and nutrient losses. Bulk density (BD) was significantly higher at OT plots, in addition to the CROP plots. Water-stable aggregates (WSA), mean weight diameter (MWD), and soil organic matter (OM) were significantly higher in OGC plots compared to the other land uses. Run and soil loss (SL) were significantly higher in CROP and OT plots compared to the OGC plots. The CROP plots showed soil management that can be considered as unsustainable with 52, 68- and 146-times higher losses of phosphorus (P loss), nitrogen (N loss), and carbon (C loss) compared to the OGC plots. The principal component analysis showed that MWD was associated with vegetation cover (VC), water-holding capacity (WHC), WSA, OM, total nitrogen (TN), time to ponding (TP), and time to runoff (TR). These variables were negatively related to P<sub>2</sub>O<sub>5</sub>, Run, SL, and P, N, and C loss. Results indicate the need for the adoption of conservation strategies in croplands and olive orchards.

**Keywords:** Soil erosion; Tillage; Rainfall simulation; Agriculture land management; Mediterranean.

## INTRODUCTION

Essential for life on the Earth, soils directly or indirectly sustaining 95% of the produced food over the world (FAO, 2015). Thus, the conservation of soils for natural ecosystems and human health is vital (Steffan et al., 2018). Along with functions such as supplying a medium for plants to take the nutrients, water, and support the roots, soils provide other necessary ecosystem services such as nutrient cycling, water quality regulation, water supply regulation, air quality regulation, climate regulation, and food, fiber, and fuel supply (Pereira et al., 2018a). Soils are also crucial for the stability and resilience of the Earth's surface environment (Ludwig et al., 2018). However, several soil functions are affected by land degradation processes, such as nutrient depletion and soil erosion (García-Ruiz et al., 2017). In order to feed an increasing human population and animals, agricultural soils are being affected by non-sustainable land management uses, which are characterized by an intensive production or the use of heavy machinery with negative impacts on soil nutrients and biodiversity (Ebabu et al., 2020; Sanaullah et al., 2020). Previous studies recognized a high variation in runoff (Run) and soil erosion by water due to land-use changes, wildfires, and grazing (Biddoccu et al., 2017; Dalla Rosa et al., 2017; Pereira et al., 2018b). However, along the Mediterranean area, millennia agricultural practices, vulnerable environment, extreme climate conditions characterized by extreme and irregular rainfall events, long dry periods on bare soils are recognized as drivers for higher soil and water losses (Covelli et al., 2020; Kosmas et al., 2015; Salvia et al., 2019).

In agricultural ecosystems, soil losses are high on bare lands. Several authors demonstrated that the intensive tillage practices such as plowing, rotatory-type tillage or herbicides application, increase soil losses above the tolerable levels (Abidela Hussein et al., 2019; Gómez et al., 2018; Ryken et al., 2018). Tillage and crop protection managements require a high number of machinery passes. This increases soil organic matter (OM) depletion (Ebabu et al., 2020), the occurrence of crust (Birkas et al., 2014), and soil compaction (Biddoccu et al., 2017), meanwhile the pore system is unfavorably modified, and infiltration is reduced (Novara et al., 2020). Therefore, land use and management are key factors controlling the intensity and the frequency of overland flow and soil loss (Baiamonte et al., 2019; Kosmas et al., 1997).

Olive orchards and vegetables are typical crops of traditional production spread in the rural areas of Mediterranean Croatia. Olive orchards are established mainly on sloped and low quality and productivity soils (Beaufoy and Pienkowski, 2000), while vegetables require higher labor inputs and intensive high-productivity agricultural practices (Ebert et al., 2019). Therefore, each land use has a high susceptibility to soil degradation if no correct land management plans are designed and applied.

In the Mediterranean, several works indicate that soil erosion is the major problem associated with olive orchards (e.g., Gómez et al., 2018; Martínez et al., 2006; Taguas et al., 2015). Naturally, reported soil losses much depend on scale and methodology, as is previously highlighted (Fleskens and Stroosnijder, 2007; Gómez et al., 2008). Nevertheless, soil disturbance and bare soil in olive orchards produce soil loss

more than  $25 \text{ t ha}^{-1} \text{ year}^{-1}$  if rills and gullies occur (Taguas et al., 2015). However, other research even demonstrated increased erosion rates of  $47 \text{ t ha}^{-1} \text{ year}^{-1}$  (Vanwalleghem et al., 2011). In cropland vegetable fields, soils also exceed very often tolerable soil loss (Montgomery, 2007), reaching  $12 \text{ t ha}^{-1} \text{ year}^{-1}$  (Bagarello et al., 2018; O'Rourke and Petersen, 2016; Pournader et al., 2018; Preiti et al., 2017). In this context, the preservation management strategies developed in the shape of no-tillage (croplands), grass cover (orchards), or mulching (croplands and orchards) (Triplett and Dick, 2008) are key to conserve the soils. Such practices decrease sediment, nutrient and water losses for several magnitudes in addition to conventional tillage (Bogunovic et al., 2018; Gómez et al., 2009; Kosmas et al., 1997).

Despite the generally high erosion rates in olive orchards and in areas where vegetable production is dominant, the majority of cropland cultivation in the Mediterranean area is still under unsustainable management, as is the case for Croatia and no updated information with *in situ* measurements exists for Croatia (Bogunovic et al., 2020). Several scientists studied different land management impacts on specific soil properties and hydrological responses during the last two decades. However, combining different point of views such as *in situ* experiments, conservative and traditional land uses such as olives and vegetables and their respective response to the activation of the initial soil erosion processes is missing (e.g., Arhonditsis et al., 2000; Blavet et al., 2009; Dunjó et al., 2004; Gilley et al., 1997; Mohammad and Adam, 2010; Návár and Synnott, 2000; Qiang et al., 2016). This work aims to compare the impact of different land management on soil properties and hydrological response in olive orchards and vegetable croplands. To achieve this goal, soil analysis, and rainfall simulation experiments were used for the first time in Dalmatia, Croatia.

## MATERIALS AND METHODS

### Study area

To compare three different treatments in olive orchards and vegetable croplands, a representative study area in Polaca (Dalmatia, Croatia) was selected (WGS coordinates:  $44^{\circ}00' \text{ N}$ ;  $15^{\circ}29' \text{ E}$ ) at 71 m a.s.l. (Figure 1). The climate is Mediterranean with an average annual rainfall of 838 mm and an average annual temperature of  $15.2^{\circ}\text{C}$  (Vrana meteorological station  $43^{\circ}57' \text{ N}$ ,  $15^{\circ}28' \text{ E}$ , 14 m a.s.l., 4.9 km from study area). The highest monthly rainfall occurs during September and October (109 and 102 mm) and the lowest during July and August (28 and 52 mm). The rainfall intensity of 60 mm per hour has a returning period of about 13 months (Zaninovic et al., 2008). The investigated area is a part of Ravni Kotari - lowland areas up to 200 m altitude, with the alternating limestone-dolomite hills and flysch valleys of the Dinaric lie (Fritz, 1978). Most of the Ravni Kotari area comprises water-permeable Cretaceous limestone and limestone breccia, and partially permeable dolomites and marl limestone. A small part is composed of water-tight clastite (Fritz, 1978).

The soils in this area are classified as Calcaric Leptosol (IUSS-WRB, 2015). It is characterized by a clay-soil texture with  $\sim 35\%$  sand,  $\sim 22\%$  silt, and  $\sim 43\%$  clay, with rock fragments cover  $< 3\%$ . Some general properties register 1.93% of OM,  $35.9 \text{ mg kg}^{-1}$  available phosphorus ( $\text{P}_2\text{O}_5$ ), and  $59.9 \text{ mg kg}^{-1}$  available potassium ( $\text{K}_2\text{O}$ ). The region has a long tradition of production of olive, vines, and vegetables.

### Field experiments and laboratory analyses

Three types of land use management were studied: vegetable croplands (CROP), grass-covered olive orchard (OGC), and tilled olive orchard (OT). The fields extend to cover an area of

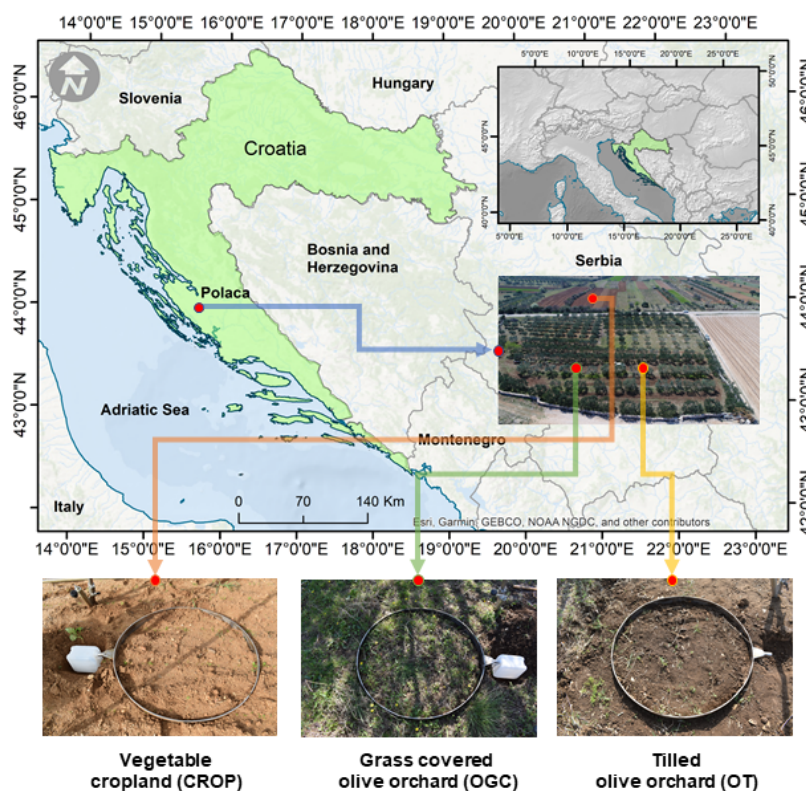


Fig. 1. Study area and plots of the selected rainfall simulation experimental plots.

2.05 ha, all with medium-deep soil of similar properties. The vegetable cropland (CROP) was cultivated using the most common farming techniques in the region, which include moldboard plowing (up to 30 cm depth) in late autumn, followed by the rotation cultivator (up to 15 cm). After each vegetable harvest, the soil is tilled by rotation cultivator before planting another culture. In CROP treatment, the usual number of cultures in the rotation was three per year. Fertilizer was applied to the treatment (before planting) in the form of 15-15-15 NPK at a nominal rate of 800 kg ha<sup>-1</sup> and urea 150 kg ha<sup>-1</sup>, rates typical of local cultivation practices. At the time of measurements, the spinach (*Spinacia oleraceae* L.) planted 15 days before covering a small portion of soil (< 5% soil area). At the time of measurement, the CROP and OT treatment were tilled 15 and 60 days ago, respectively. Olives were managed with grass cover (OGC) between the trees. The grass is mowed and kept on the surface as a mulch. No herbicides were used here to suppress the weeds. Every several years the inter-row and row positions were fertilized using the 15-15-15 NPK in autumn at the nominal rate of 1000 kg ha<sup>-1</sup> and calcium ammonium nitrate 200 kg ha<sup>-1</sup> (in late spring during the flowering stage). The OT is conventionally tilled in each inter-row position by disking to a depth of 10 cm. During the season, these tillage operations were repeated 3–4 times to keep the soil bare. During the field campaign, vegetation cover reached an average of about 11%.

At CROP, OGC, and OT treatments, eight sampling points (separated by six meters) following a transect were selected to conduct the rainfall simulation experiments and soil sampling. Rainfall simulation experiments were performed during April 2019 under wet soil conditions (> 20% soil water content) with a rainfall simulator (UGT Rainmaker, Müncheberg, Germany). The device was calibrated to reproduce rainstorms of 58 mm h<sup>-1</sup> rainfall intensity, during 30 minutes on a circular plot of 0.785 m<sup>2</sup> (metal ring 100 cm in diameter). Rainfall intensity was adjusted by the time that the nozzle (VeeJet 80/100 nozzle, the pressure at 0.5 bar, at the height of 200 cm) remains at the reversal points and nozzle turning speed (Schindewolf and Schmidt, 2012). Plastic collectors (n = 144) were placed under the rainfall simulator to collect the drops. After 30 minutes of the experiment at an intensity of 58 mm h<sup>-1</sup>, the rainfall distribution coefficient of variation is 4.66. The mean drop size was 0.7 mm, and the mean falling velocity was 6.263 m s<sup>-1</sup>.

After establishing each ring plot, undisturbed soil samples and soil core samples were taken from 10 cm downslope of each metal ring. Before the simulation, each plot was photographed to obtain vegetation cover (VC) percentage. To estimate the final VC, we used ArcGIS 10.2 software (ESRI, USA) to compare the relation on pixels to the vegetation in addition to the plot area. The slope was measured inside the ring area using a Bosch GLM 80 Professional instrument. Finally, when each simulation started, time to ponding (TP) and time to runoff generation (TR) were measured with a digital chronometer (Keesstra et al., 2019).

Undisturbed samples (8 per treatment, 24 in total) were collected at the 0–10 cm soil depth using 100 cm<sup>3</sup> cylinders. The soil cores were wetted for determination of water holding capacity (WHC) and dried in an oven at 105°C for 24 h to obtain the bulk density (BD) according to Black (1965). Undisturbed samples (8 per treatment, 24 in total) were collected at the 0–10 cm depth, stored into rectangular boxes, and used for determination of the mean weight diameter (MWD) and the water-stable aggregates (WSA). During the procedure, the bulk soil was very carefully broken into small pieces by hands (Diaz-Zorita et al., 2002). After drying, the distribution of par-

ticular aggregate size fractions (<0.25, 0.25–0.5, 0.5–1.0, 1.0–2.0, 2.0–4.0, 0.4–0.5, and 0.5–0.8 mm) was determined by dry sieving for 30 seconds (Kemper and Rosenau, 1986). MWD was calculated after weighting each aggregate size using the following equation (Eq. (1)):

$$\text{MWD} = \sum_{i=1}^n xi \cdot wi, \quad (1)$$

where  $xi$  is the mean diameter of any particular size range of aggregates separated by sieving, and  $wi$  is the weight of aggregates in that size range as a fraction of the total dry weight of soil used. WSA was determined by wet sieving apparatus (similar to Kemper and Rosenau, 1986) by soaking 4 g of aggregates (diameter 0.4–0.5 mm) in distilled water for 3 min. After replacing cans with a dispersing solution (2 g L<sup>-1</sup> sodium hydroxide), sieving continued until only the sand particles were left on the sieves. Both sets of cans were dried at 105°C and weighted. Percentage of WSA was obtained using the equation:

$$\text{WSA} = \frac{Wds}{Wds + Wdw}, \quad (2)$$

where WSA is the percentage of water-stable aggregates,  $Wds$  is the weight of aggregates dispersed in dispersing solution (g), and  $Wdw$  is the weight of aggregate dispersed in distilled water (g). Remains of the aggregate sizes were milled and sieved through a 2 mm mesh to determine soil chemical properties. OM content was calculated according to the digestion method (Walkly and Black, 1934). Also, P<sub>2</sub>O<sub>5</sub> concentration in soils and sediments (P loss) was determined after the samples were subjected to extraction with AL method (Egner et al., 1960) and using a spectrophotometer (Hach, Germany, model DR/2000). Finally, total nitrogen (TN) concentration in soils, as well as the carbon (C loss) and nitrogen (N loss) concentrations in sediments, were obtained by a dry-combustion method using Vario MACRO CHNS analyzer.

During each rainfall simulation, the water and soil loss in the form of overland flow and suspended sediment was stored in a plastic container and then transported to the laboratory. The collected surface flow was weighed and filtered to obtain Run and soil loss (SL) after drying a filter paper. Sediment concentration (SC) was calculated, dividing the mass of SL by the mass of the Run in the samples. Dried sediments were milled and passed through 2 mm mesh as a preparation to analyze the C, N, and P<sub>2</sub>O<sub>5</sub> as it was above-mentioned.

### Statistical analysis

Before performing a statistical comparison of each result obtained for every treatment, data were checked for normality and heteroscedasticity using the Kolmogorov–Smirnov and Levene's tests. Data normality and homogeneity of the variances were considered at  $p > 0.05$ . The majority of the variables showed a normal distribution. VC, C loss, and P<sub>2</sub>O<sub>5</sub> showed normality after a logarithmic transformation. A one-way ANOVA was used to identify significant differences among plots (VC, C loss and P<sub>2</sub>O<sub>5</sub> with logarithmic transformation). If significant differences were found (at  $p < 0.05$ ), the Tukey HSD *post-hoc* test was applied. Data presented in the graphs were untransformed. A Principal Component Analysis (PCA) based on the correlation matrix was applied (using the log-transformed data) to identify association among the variables. Statistical analyses were carried out using Statistica 12.0 for windows. Graphics were depicted using Plotly (<https://chart-studio.plot.ly>).

## RESULTS

### Environmental plot conditions and soil properties

Slope, VC, and soil properties for the different treatments are summarized in Table 1. Our results showed that there were no significant differences in slope among the treatments. VC in CROP (4.5%) and OT (10.9%) was significantly lower than VC in OGC (83.6%). WSA and BD were also significantly different among all treatments. WHC values in CROP (37.3%) were significantly lower than OGC (40.8%). A similar situation was observed in BD. BD was as follows: CROP (1.30 g cm<sup>-3</sup>) < OGC (1.32 g cm<sup>-3</sup>) < OT (1.42 g cm<sup>-3</sup>). Also, no significant differences were identified in SWC which varied from 22.5% in the OT to 24.5% in the CROP treatment. MWD and WSA values ranged from 2.74 mm (CROP) to 3.72 mm (OGC) and from 46.7% (CROP) to 65.8% (OGC), respectively. Both parameters were significantly higher in OGC than to OT and CROP treatments. OM and TN were significantly different among treatments as follows: OGC (2.53% OM; 0.14% TN) > OT (1.88% OM; 0.10% TN) > CROP (0.86% OM; 0.05% TN). Soil P<sub>2</sub>O<sub>5</sub> ranged from 11.11 at OT to 92.08 mg kg<sup>-1</sup> in the CROP treatment. P<sub>2</sub>O<sub>5</sub> values were also significantly different among the treatments: CROP > OGC > OT.

### Initial soil erosion processes using rainfall simulation experiments

The effects of soil management on hydrological response are shown in Figures 2 and 3. The TP ranged from 90 to 180 s (mean 123.7 s) in the CROP plots, from 240 to 480 s (mean 307.5 s) in the OT plots and from 300 to 540 s (mean 412.5 sec) in the OGC plots. The TR ranged from 180 to 300 s (mean 225.6 s) in the CROP plots, from 420 to 1020 s (mean 652.5 sec) in the OT plots and from 660 to 1140 s (mean 840 s) in the OGC plots. In both cases, the CROP TP and TR values were significantly lower than in other plots. The Run values ranged from 10.4 to 15.6 L m<sup>-2</sup> (mean 12.3 L m<sup>-2</sup>) in the CROP plots, from 0.78 to 3.06 L m<sup>-2</sup> (mean 1.85 L m<sup>-2</sup>) in the OT plots and from 0.02 to 0.69 L m<sup>-2</sup> (mean 0.26 g L<sup>-2</sup>) in the OGC plots. The SL values ranged from 85.5 to 246.1 g m<sup>-2</sup> (mean 143.1 g m<sup>-2</sup>) in the CROP plots, from 10.5 to 64.8 g m<sup>-2</sup> (mean 31.5 g m<sup>-2</sup>) in the OT plots and from 0.06 to 4.5 g m<sup>-2</sup> (mean 1.8 g m<sup>-2</sup>) in the OGC plots. Significant differences were observed in the Run and SL among all treatments. On average, Run and SL were significantly higher in CROP than in OT and OGC. SC values ranged from 9.23 g L<sup>-1</sup> to 30.05 g L<sup>-1</sup> at OT plots, from 7.97 g L<sup>-1</sup> to 15.81 g L<sup>-1</sup> at CROP plots and from 3.31 g L<sup>-1</sup> to 8.19 g L<sup>-1</sup> at OGC plots. SC showed different

behavior, exhibiting significantly high differences in OT plots (17.08 g L<sup>-1</sup>), followed by the CROP plots (11.30 g L<sup>-1</sup>), and OGC plots (6.16 g L<sup>-1</sup>). The P loss, N loss, and C loss values at CROP, OT, and OGC plots ranged from 0.0003 g m<sup>-2</sup> (OGC) to 0.1574 g m<sup>-2</sup> (CROP), from 0.003 g m<sup>-2</sup> (OGC) to 0.204 g m<sup>-2</sup> (CROP) and from 0.07 g ha<sup>-1</sup> (OGC) to 9.87 g m<sup>-2</sup> (CROP), respectively. P, N, and C loss were significantly higher at CROP plots than in OT and OGC plots.

### Principal component analysis

The first three factors explained 77.1% of the total variance. Factor 1 explained 58.6%, and Factors 2 and 3 explained 11.2% and 7.3%, respectively, of all variances. Factor 1 had high positive loadings in VC, WHC, MWD, WSA, OM, TN, TP, and TR, and high negative for P<sub>2</sub>O<sub>5</sub>, Run, SL, C loss, P loss and N loss (Table 2). Factor 2 had high positive loadings for BD and high negative loadings for SWC. Finally, factor 3 had high positive loadings in slope and SC. The intersection between Factor 1 and Factor 2 shows that Run, SL, P<sub>2</sub>O<sub>5</sub>, N loss, P loss, and C loss are inversely related to the majority of the other variables, especially to the slope, VC, TP, TR, OM and TN (Figure 4A). The land management practices had different impacts on soil properties and hydrological response for all treatments. The impact is notably different between the CROP and the other treatments. The variability is much higher in the CROP in addition to OGC and OT (Figure 4B).

## DISCUSSION

The results revealed that different land management changed some soil properties whereby the soil was more compacted at OT than at OGC and CROP plots. This is in agreement with the observations of previous studies. Tilled plots showed higher compaction than to the grassed ones in Mediterranean olive orchards (Gucci et al., 2012; López-Vicente and Álvarez, 2018). High BD at OT can be attributed to soil consolidation and tractor traffic, while a lower BD at CROP treatment can be related to the type of the tillage performance 15 days before conducting the measurements. Moreover, the experiments were conducted in a period without any traffic impact in this treatment. WHC was significantly higher in the OGC than the CROP plot, which was attributed to the vegetation cover on OGC plots. VC can improve the hydraulic properties of soils after several years and enhance the existence of medium-size pores to retain more water (Çerçioğlu et al., 2019). Moreover, higher root density of cover crops increases porosity and OM, with a notable improvement in soil structure (Jarvis et al., 2017;

**Table 1.** Results of one-way ANOVA analysis considering soil properties and plot conditions. Different letters after mean values in the columns represent significant difference at  $p < 0.05$ ; ns, not significant at a  $p < 0.05$ . Abbreviations: CROP, vegetable cropland; OGC, olive orchard grass-covered, OT, olive orchard tilled; VC, vegetation cover; BD, bulk density; WHC, water holding capacity; SWC, soil water content; MWD, mean weight diameter; WSA, water-stable aggregates; OM, organic matter; P<sub>2</sub>O<sub>5</sub>, available phosphorous and TN, total nitrogen.

Land use	Slope (°)	VC (%)	WHC (%)	SWC (%)	BD (g cm <sup>-3</sup> )	MWD (mm)	WSA (%)	OM (%)	P <sub>2</sub> O <sub>5</sub> (mg kg <sup>-1</sup> )	TN (%)
CROP	6.5 a	4.5 b	37.3 b	24.5 a	1.30 b	2.74 b	46.7 b	0.86 c	92.08 a	0.05 c
OGC	8.5 a	83.6 a	40.8 a	23.5 a	1.32 ab	3.72 a	65.8 a	2.53 a	20.49 b	0.14 a
OT	7.9 a	10.9 b	38.3 ab	22.5 a	1.42 a	2.98 b	48.4 b	1.88 b	11.11 c	0.10 b
P value	n.s.	***	**	n.s.	*	***	**	***	***	***

\*\*\* Statistical significance at  $p < 0.001$ . \*\* Statistical significance at  $p < 0.01$ . \*Statistical significance at  $p < 0.05$ .

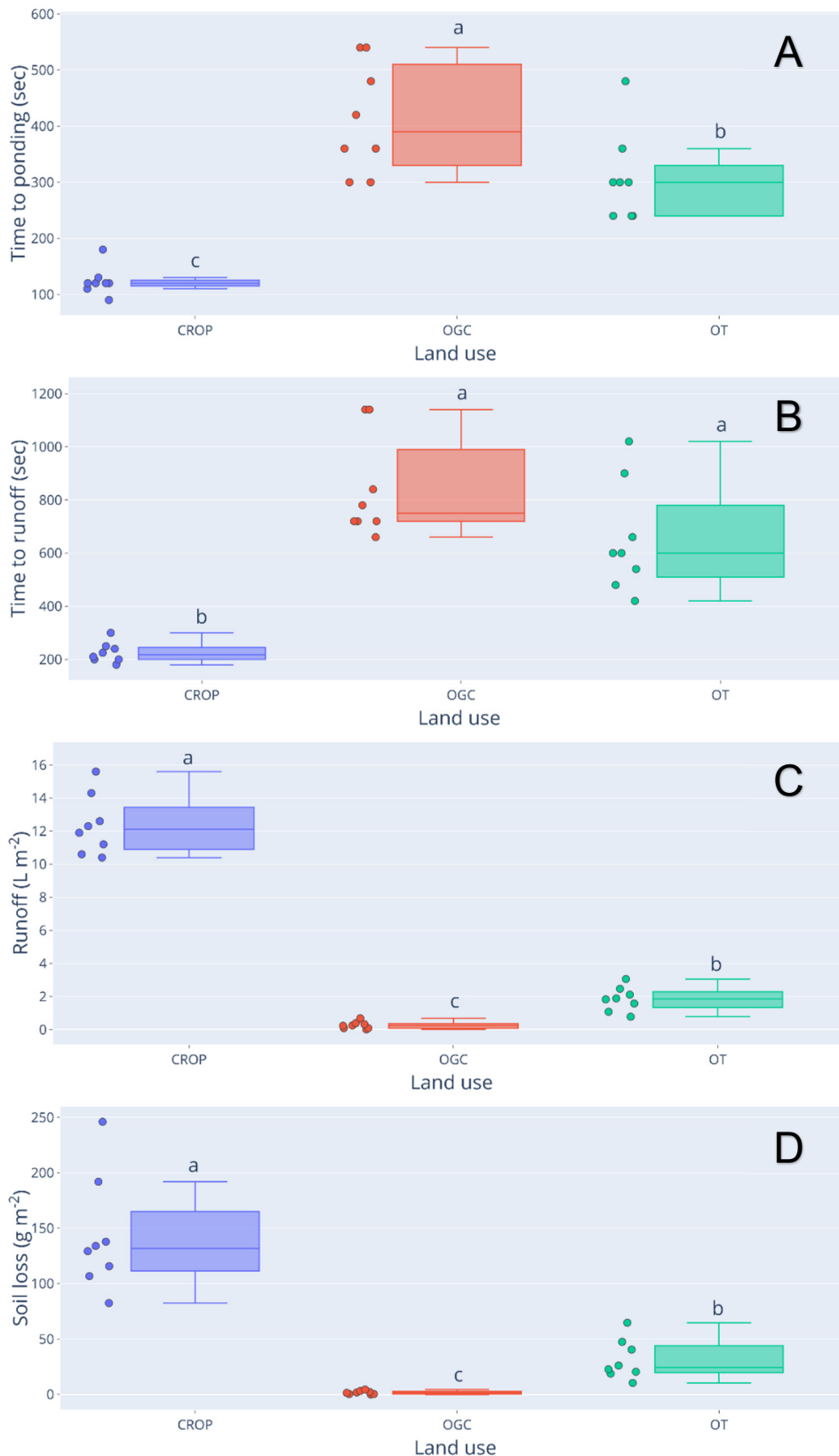


**Fig. 2.** Box plots and results of one-way ANOVA analysis for the effects of land use on A) time to ponding, B) time to runoff generation, C) runoff, and D) soil loss. Different letters represent a significant difference at  $p < 0.05$ . Abbreviations: CROP, vegetable cropland, OGC, grass-covered olive orchard, OT, olive orchard tilled.

Zaibon et al., 2016). Our study also confirmed this behavior. Frequent tillage at OGC and OT plots expose soil aggregates to wet-dry cycles and disruptive raindrop impact, enhancing aggregates to disruption (Six et al., 2000). Tilled soil from subsoil was exposed to air, increasing the OM mineralization

and decreasing their content compared to OGC. However, rotation type tillage performed several times a year at CROP plots created smaller aggregates and more considerable disturbance in addition to disking (Birkas et al., 2014) at the OT plot. It could be a reason for low OM occurring with this land use.

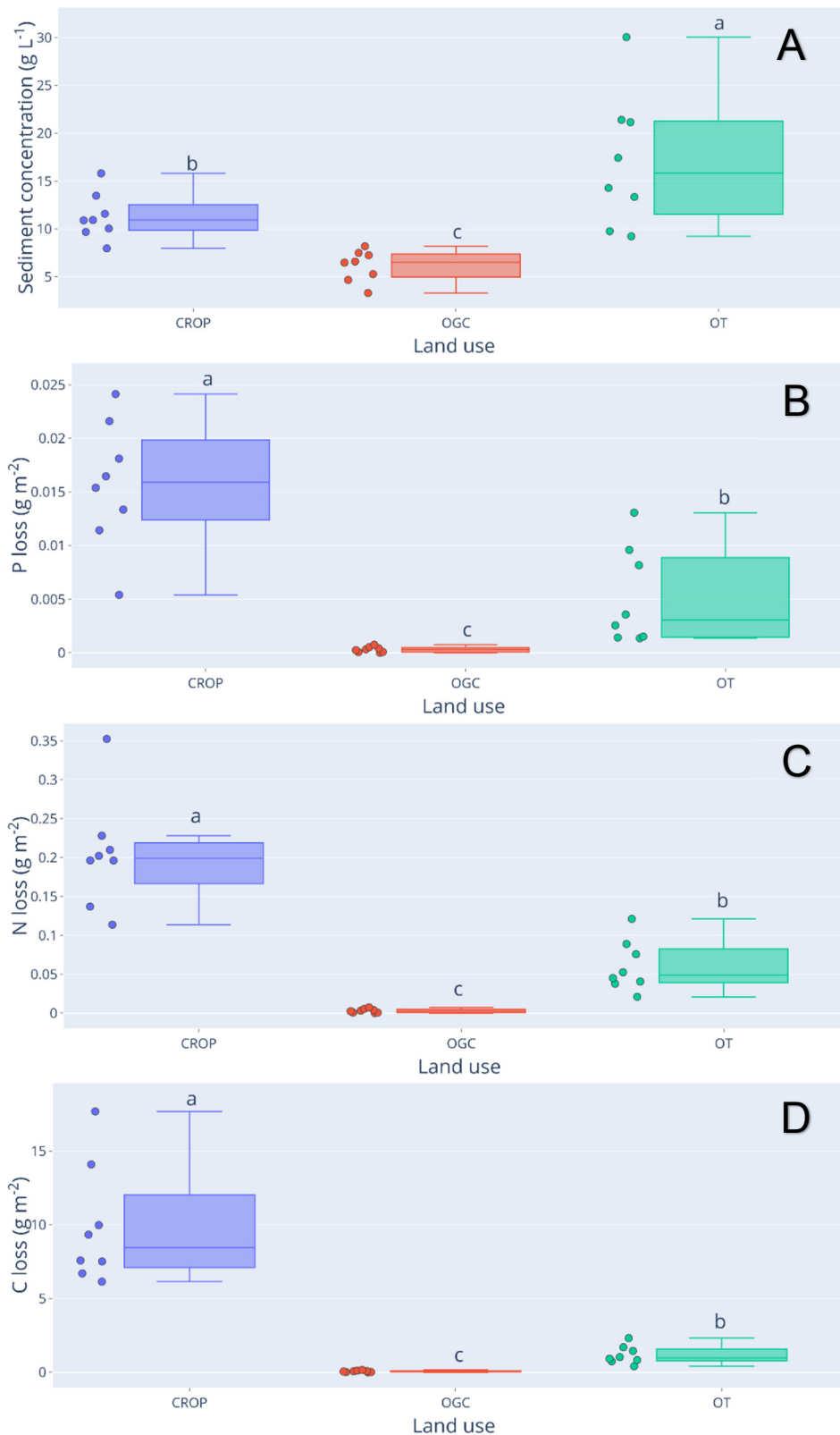


**Fig. 3.** Box plots and results of one-way ANOVA analysis for the effects of land use on A) sediment concentration, B) phosphorus loss (P loss), C) nitrogen loss (N loss), and D) carbon loss (C loss). Different letters represent a significant difference at  $p < 0.05$ . Abbreviations: CROP, vegetable cropland, OGC, olive orchard grass-covered, OT, olive orchard tilled.

MWD and WSA were significantly higher at the OGC, compared to the OT and CROP treatment. Usually, aggregate stability is higher in grass-covered or no-tilled soils than the tilled ones (e.g., Blavet et al., 2009; Kay, 2018). This is attributed to the low OM concentration at CROP and OT plots, which cause soil structure degradation. Moreover, high MWD at the OGC plots

formed a higher percentage of macro and medium-size pores. The lowest MWD at CROP plots enhanced higher micro-pores percentage in the soil. Such structure behavior directly affects WHC since it is known that soil water retention characteristic is highly related to the soil structure (Rabot et al., 2018). Significantly high P<sub>2</sub>O<sub>5</sub> at CROP plots could be attributed to the intensive

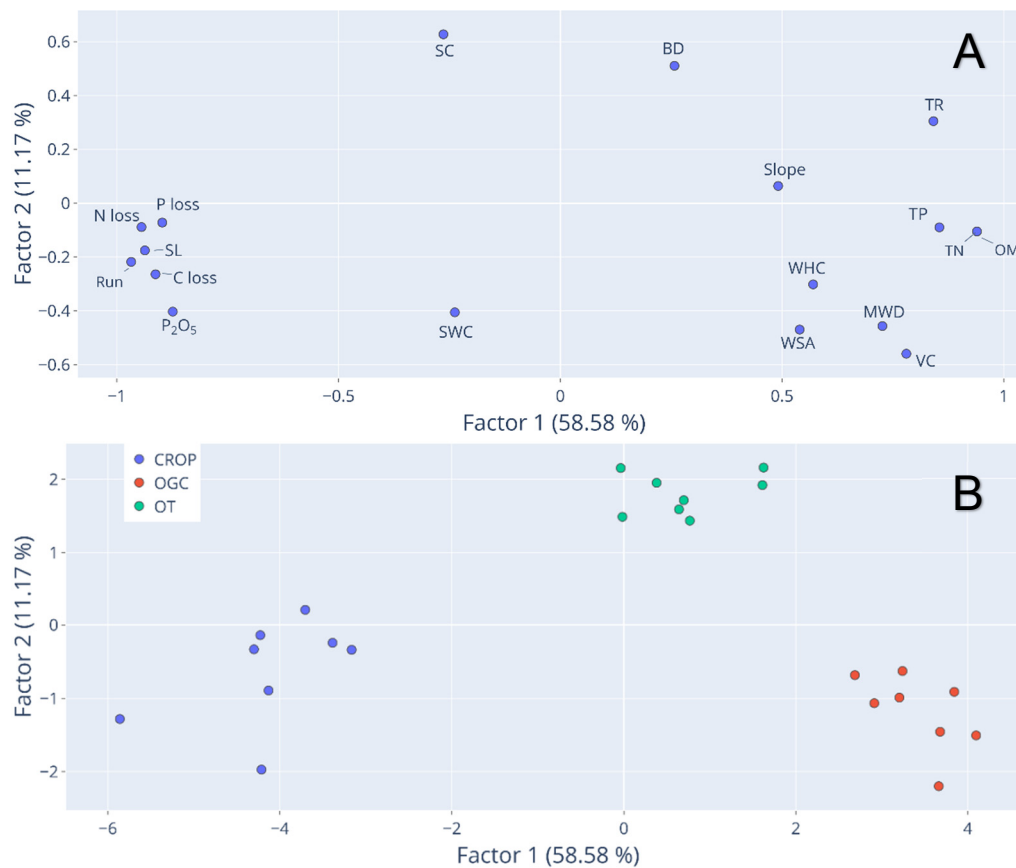


**Fig. 4.** Interaction among Factors 1 and 2, (A) Variables and (B) Cases considering different land-use management. Abbreviations: CROP, vegetable cropland; OGC, olive orchard grass-covered, OT, olive orchard tilled; VC, vegetation cover; BD, bulk density; WHC, water holding capacity; SWC, soil water content; MWD, mean weight diameter; WSA, water-stable aggregates; OM, organic matter; P<sub>2</sub>O<sub>5</sub>, available phosphorous; TN, total nitrogen; TP, time to ponding; TR, time to runoff; Run, runoff; SC, sediment concentration; SL, soil loss; N loss, nitrogen loss; C loss; carbon loss and P loss; phosphorous loss.

**Table 2.** Loadings matrix considering the first three factors extracted from the Principal Component Analysis. Eigenvalues retained in each factor are in bold. VC, Vegetation cover; BD, bulk density; WHC, water holding capacity; SWC, soil water content; MWD, mean weight diameter; WSA, water-stable aggregates; OM, organic matter; P<sub>2</sub>O<sub>5</sub>, available phosphorous; TN, Total nitrogen; TP, time to ponding; TR, time to runoff; Run, runoff; SC, sediment concentration; SL, soil loss; N loss, nitrogen loss; C loss, carbon loss and P loss, phosphorous loss.

Variable	Factor 1	Factor 2	Factor 3
Slope	0.47492	0.092375	<b>0.720672</b>
VC	<b>0.79197</b>	-0.537184	0.040386
WHC	<b>0.58085</b>	-0.290380	0.029580
SWC	-0.23316	<b>-0.433243</b>	0.294177
BD	0.24896	<b>0.487314</b>	-0.303622
MWD	<b>0.73001</b>	-0.453207	0.053658
WSA	<b>0.54848</b>	-0.466899	0.090782
OM	<b>0.93929</b>	-0.078403	0.185447
P <sub>2</sub> O <sub>5</sub>	<b>-0.86250</b>	-0.417675	-0.063128
TN	<b>0.93929</b>	-0.078403	0.185447
TP	<b>0.86025</b>	-0.083010	0.045993
TR	<b>0.86559</b>	0.033234	-0.276317
Run	<b>-0.96014</b>	-0.243496	-0.059710
SL	<b>-0.93384</b>	-0.213232	0.085730
SC	-0.29574	0.602604	<b>0.621059</b>
P loss	<b>-0.90143</b>	-0.109361	0.229045
N loss	<b>-0.94360</b>	-0.124460	0.096008
C loss	<b>-0.90681</b>	-0.301916	0.039662

fertilization performed for each of several cultures per year on this treatment. However, TN concentrations in treatments are highly related to OM since it is a dominant source. Meanwhile, mineral N is known as susceptible to leaching, denitrification, and runoff (Robertson, 1997).

This study demonstrates that the use of frequent tillage for different land uses increases Run and erosion rates. We have to consider the small plot size used for the rainfall simulation experiments, which allow detecting the initial soil erosion activation and soil responses, therefore more research must be conducted using more repetitions or erosion plots for larger scales (Iserloh et al., 2013). Differences in soil loss between treatments occur due to following: CROP plots registered the lowest OM content, WSA and MWD, and VC, which contributes to a higher Run and SL when compared to OT. This is a consequence of intense tillage practices. Although all these variables were the lowest in CROP plot, which contributed to high overland flow and erosion rates, the highest BD was observed in OT. This was attributed to the fact that soil in CROP plots were more frequently tilled, decreasing OM and the stability of the aggregates. In addition, in crop plots soils were tilled with a rotation cultivator that is very destructive to soil aggregates (Birkas et al., 2014). This increases the vulnerability to sediment detachment. Our study agrees with others, e.g., in Spain, where tillage seems to be responsible for 3.6 times higher erosion rates and cover crop plots (Gómez et al., 2009). In clay-sandy soil in Italy, Fleskens and Stroosnijder (2007) reported 357% higher erosion rates on tilled olive orchard plots in addition to grass-covered plots. Vegetation protects the splash

and delay Run due to stable macropores, which enhance the infiltration (de Almeida et al., 2018; Çerçioğlu et al., 2019).

Moreover, grass cover act as a natural barrier for overland flow minimizes the sediment movement, and decreases the SC. Nutrient losses were significantly high in CROP and OT and follow a similar pattern as soil loss. The 52, 68, and 146 times higher losses of phosphorus, nitrogen, and carbon at CROP plots, in addition to OGC plots indicate the unsustainability of frequently tilled management. Also, a similar degradation dynamic is visible at OT plots with 17, 20, and 17 times higher phosphorus, nitrogen, and carbon loss in addition to OGC. Similar results were noted elsewhere (Bogunovic et al., 2020; Gómez et al., 2011).

PCA analysis supports the above-described results. Factor 1 revealed that the VC, WHC, MWD, WSA, OM, TN, TP, and TR are positively associated. This is in agreement with other findings identified in the literature since high VC increases the rooting system, which secretes cementing agents and acts as an attractant for soil fauna as a source of food. This increases a high MWD and WSA, by secretion products as cementing agents for soil structure (Bogunovic et al., 2019b; Kay, 2018). Parallel with TP and TR, a high VC increases OM, which is beneficial to soil structure (Franzuebbers, 2002; Keesstra et al., 2019). Subsequently, it enhances the capacity of soils to retain water. The mentioned soil properties are inversely related to Run, SL, and C, N, and P loss. This dynamic was observed at CROP and OT plots (Figures 2 and 3) and confirms the idea that tillage practices trigger soil erosion and nutrient losses. Poor soil structure exacerbates soil hydrological response. Factor 2 inversely relates BD and SWC, while factor 3 relates slope and SC. High BD decreases and modifies the pore system and decreases the medium-sized pores, which retain soil water. The high SC in soils with high slope may be attributed to the higher overland flow energy, which detaches soil particles and increases their concentration in the Run. Overall, the type of soil management is a crucial factor in controlling erosion.

Our results also showed that specific land use management can influence soil ecosystems and, consequently, affect essential soil functions (Blavet et al., 2009; Mohammad and Adam, 2010; Qiang et al., 2016). In agricultural areas, soil erosion depends on natural soil properties, tillage methods, herbicides application, vegetation cover, and organic matter properties. Agricultural soils in Croatia are often bare soils because of the intense tillage or use of herbicides (Bogunovic et al., 2020). Thus, non-planned soil management considering these variations will enhance soil erosion rates. We claim the need for the adoption of more environmental and conservative soil erosion control measures. This current study demonstrates that tilled land uses (CROP and OT) have deteriorated structure, lower soil cover, and less resistance to sediment detachment and soil loss. Those findings demonstrate that conservation management and strategies for bare soils in olive orchards and vegetable croplands in Dalmatia need to be developed. The plantation of grass on the olive orchard or the reduction of tillage frequency on cropland vegetables could be a solution to increase VC. Also, there are important differences between OT and CROP, especially in soil structure, OM, and hydrological response. This shows that land-use management plays a crucial role in land sustainability. The high degradation among two tillage managements in different land uses very likely reflect the long-term impact of tillage intensity and vegetable cropland frequency. The current research contributes to a better understanding of the land-use management conducted in traditional agricultural sectors in Dalmatia. However, this is a first approach which uses rainfall simulation, obviously having serious limitation for

an extrapolation for the whole cultivated area. Future research should be focused on the temporal variability and identification of runoff and erosion at different scales of catchments, considering the identification of critical geomorphological, pedological, and soil management practices.

## CONCLUSION

Land use management substantially affected soil properties and soil hydrological response after simulated high-intensity rains. Tillage practices conducted in the Mediterranean decreased OM and soil structural quality, while grass coverage increased soil quality. In the vegetable cropland, soil WHC, MWD, WSA, OM, and TN were lower than in the grass-covered olive orchard. On the other hand, tilled olive orchard recorded lower MWD, WSA, OM, and TN than the OGC. High soil and nutrient losses were recorded at vegetable cropland and tilled olive orchard. Such results indicate that the application of frequent intensive tillage interventions at vegetable cropland very likely intensified soil degradation, overland flow, and soil and nutrient losses. WSA and MWD were probably affected by tillage-induced deterioration and mineralization of OM in long-time management in the vegetable cropland and tilled olive orchard. Soil and water losses in tilled olive plantations and vegetable croplands compared to grass-covered land olives in Dalmatia are not sustainable when using traditional tillage management. However, in grass-covered olive plantations, runoff and SL are low, indicating that soil structural stability and soil cover are vital factors to increase land-use sustainability.

*Acknowledgements.* This work was supported by the Croatian Science Foundation through the project "Soil erosion and degradation in Croatia" (UIP-2017-05-7834) (SEDCRO). The authors are grateful for the support of Family farm Bobanović from Polača.

## REFERENCES

- Abidela Hussein, M., Muche, H., Schmitter, P., Nakawuka, P., Tilahun, S.A., Langan, S., Barron, J., Steenhuis, T.S., 2019. Deep tillage improves degraded soils in the (sub)humid Ethiopian Highlands. *Land*, 8, 11, 159.
- Arhonditsis, G., Giourga, C., Loumou, A., 2000. Ecological patterns and comparative nutrient dynamics of natural and agricultural Mediterranean-type ecosystems. *Environ. Manage.*, 26, 5, 527–537.
- Bagarello, V., Ferro, V., Pampalano, V., Porto, P., Todisco, F., Vergni, L., 2018. Predicting soil loss in central and south Italy with a single USLE-MM model. *J. Soil. Sediment.* 18, 12, 3365–3377.
- Baiamonte, G., Minacapilli, M., Novara, A., Gristina, L., 2019. Time scale effects and interactions of rainfall erosivity and cover management factors on vineyard soil loss erosion in the semi-arid area of Southern Sicily. *Water*, 11, 978.
- Beaufoy, G., Pienkowski, M., 2000. The environmental impact of olive oil production in the European Union: Practical options for improving the environmental impact. European Forum on Nature Conservation and Pastoralism. Available at: <https://ec.europa.eu/environment/agriculture/pdf/oliveoil.pdf>
- Biddoccu, M., Ferraris, S., Pitacco, A., Cavallo, E., 2017. Temporal variability of soil management effects on soil hydrological properties, runoff and erosion at the field scale in a hillslope vineyard, North-West Italy. *Soil Till. Res.*, 165, 46–58.
- Birkas, M., Jug, D., Kiscic, I., 2014. Book of Soil Tillage. Szent Istvan University, Godollo, Hungary, 322 p.
- Black, C.A., 1965. Method of Soil Analysis. Part 2. Chemical and

- Microbiological Properties. American Society of Agronomy, Inc., Madison, 1159 p.
- Blavet, D., De Noni, G., Le Bissonnais, Y., Leonard, M., Maillo, L., Laurent, J.Y., Asseline, J., Leprun, J.C., Arshad, M.A., Roose, E., 2009. Effect of land use and management on the early stages of soil water erosion in French Mediterranean vineyards. *Soil Till. Res.*, 106, 1, 124–136.
- Bogunovic, I., Pereira, P., Kusic, I., Sajko, K., Sraka, M., 2018. Tillage management impacts on soil compaction, erosion and crop yield in Stagnosols (Croatia). *Catena*, 160, 376–384.
- Bogunovic, I., Fernández, M.P., Kusic, I., Marimón, M.B., 2019b. Agriculture and grazing environments. In: Pereira, P. (Ed.): *Soil Degradation, Restoration and Management in a Global Change Context*. 1st ed. Elsevier, London, UK, Volume 4, pp. 23–70.
- Bogunovic, I., Telak, L.J., Pereira, P., 2020. Agriculture management impacts on soil properties and hydrological response in Istria (Croatia). *Agronomy*, 10, 2, 282.
- Çerçioğlu, M., Anderson, S.H., Udawatta, R. P., Alagele, S., 2019. Effect of cover crop management on soil hydraulic properties. *Geoderma*, 343, 247–253.
- Covelli, C., Cimorelli, L., Pagliuca, D.N., Molino, B., Pianese, D., 2020. Assessment of erosion in river basins: A distributed model to estimate the sediment production over watersheds by a 3-Dimensional LS Factor in RUSLE Model. *Hydrology*, 7, 1, 13.
- Dalla Rosa, J., Cooper, M., Darboux, F., Medeiros, J.C., Campanaro, C., Martins Pinto, L.R., 2017. Influence of crust formation on soil porosity under tillage systems and simulated rainfall. *Hydrology*, 4, 1, 3.
- de Almeida, W.S., Panachuki, E., de Oliveira, P.T.S., da Silva Menezes, R., Sobrinho, T.A., de Carvalho, D.F., 2018. Effect of soil tillage and vegetal cover on soil water infiltration. *Soil Till. Res.*, 175, 130–138.
- Diaz-Zorita, M., Perfect, E., Grove, J.H., 2002. Disruptive methods for assessing soil structure. *Soil Till. Res.*, 64, 1–2, 3–22.
- Dunjó, G., Pardini, G., Gispert, M., 2004. The role of land use-land cover on runoff generation and sediment yield at a microplot scale, in a small Mediterranean catchment. *J. Arid Environ.*, 57, 2, 239–256.
- Ebabu, K., Tsunekawa, A., Haregeweyn, N., Adgo, E., Meshesha, D.T., Aklog, D., Masunaga, T., Tsubo, M., Sultan, D., Fenta, A.A., Yibeltal, M., 2020. Exploring the variability of soil properties as influenced by land use and management practices: A case study in the Upper Blue Nile basin, Ethiopia. *Soil Till. Res.*, 200, 104614.
- Ebert, A.W., Dubois, T., Tenkouano, A., Mavlyanova, R., Wang, J.F., HanumanthaRao, B., Ramasamy, S., Kumar, S., Beed, F.D., Pottorff, M., Chen, W.Y., Nair, R.M., Nayyar, H., Chen, W.Y., 2019. Sustainable vegetable production to sustain food security under climate change at global level (No. RESEARCH). In: Yadav, S.S., Redden, R.J., Hatfield, J.L., Ebert, A.W., Hunter, D. (Eds): *Food Security and Climate Change*. 1<sup>st</sup> Edition. John Wiley & Sons Ltd, pp. 319–358.
- Egnér, H.A.N.S., Riehm, H., Domingo, W.R., 1960. Untersuchungen über die chemische Bodenanalyse als Grundlage für die Beurteilung des Nährsto zustandes der Böden. II. Chemische Extraktionsmethoden zur Phosphor-und Kaliumbestimmung. *Lantbrukshögskolans Ann.*, 26, 199–215.
- Espadas-Aldana, G., Vialle, C., Belaud, J.-P., Vaca-Garcia, C., Sablayrolles, C., 2019. Analysis and trends for Life Cycle Assessment of olive oil production. *Sustainable Production and Consumption*, 19, 216–230.
- FAO, 2015. Healthy soils are the basis for healthy food production. Food and Agriculture Organization of the United Nations. Available at: <http://www.fao.org/3/a-i4405e.pdf>
- Fleskens, L., Stroosnijder, L., 2007. Is soil erosion in olive groves as bad as often claimed? *Geoderma*, 141, 3–4, 260–271.
- Franzluebbers, A.J., 2002. Water infiltration and soil structure related to organic matter and its stratification with depth. *Soil Till. Res.*, 66, 197–205.
- Fritz, F., 1978. Hydrogeology of Ravni Kotari and Bukovica. *Carsus lugoslaviae* 10/1, JAZU Zagreb, 43 p.
- García-Ruiz, J.M., Beguería, S., Lana-Renault, N., Nadal-Romero, E., Cerdà, A., 2017. Ongoing and emerging questions in water erosion studies. *Land Degrad. Dev.*, 28, 5–21.
- Gilley, J.E., Doran, J.W., Karlen, D.L., Kaspar, T.C., 1997. Runoff, erosion, and soil quality characteristics of a former Conservation Reserve Program site. *J. Soil Water Conserv.* 52, 3, 189–193.
- Gómez, J.A., Sobrinho, T.A., Giráldez, J.V., Fereres, E., 2009. Soil management effects on runoff, erosion and soil properties in an olive grove of Southern Spain. *Soil Till. Res.*, 102, 1, 5–13.
- Gómez, J.A., Giráldez, J.V., Vanwallegem, T., 2008. Comments on “Is soil erosion in olive groves as bad as often claimed?” by L. Fleskens and L. Stroosnijder. *Geoderma*, 147, 93–95.
- Gómez, J.A., Llewellyn, C., Basch, G., Sutton, P.B., Dyson, J.S., Jones, C.A., 2011. The effects of cover crops and conventional tillage on soil and runoff loss in vineyards and olive groves in several Mediterranean countries. *Soil Use Manage.*, 27, 4, 502–514.
- Gómez, J.A., Campos, M., Guzmán, G., Castillo-Llanque, F., Vanwallegem, T., Lora, Á., Giráldez, J.V., 2018. Soil erosion control, plant diversity, and arthropod communities under heterogeneous cover crops in an olive orchard. *Environ. Sci. Pollut. Res.*, 25, 2, 977–989.
- Gucci, R., Caruso, G., Bertolla, C., Urbani, S., Taticchi, A., Esposto, S., Servili, M., Sifola, M.I., Pellegrini, S., Pagliai, M., Vignozzi, N., 2012. Changes of soil properties and tree performance induced by soil management in a high-density olive orchard. *Eur. J. Agron.*, 41, 18–27.
- Iserloh, T., Ries, J. B., Arnáez, J., Boix-Fayos, C., Butzen, V., Cerdà, A., Echeverría, M.T., Fernández-Gálvez, J., Fister, W., Geißler, C., Gómez, J.A., Gómez-Macpherson, H., Kuhn, N.J., Lázaro, R., León, F.J., Martínez-Mena, M., Martínez-Murillo, J.F., Marzen, M., Mingorance, M.D., Ortigosa, L., Peters, P., Regüés, D., Ruiz-Sinoga, J.D., Scholten, T., Seegera, M., Solé-Benet, A., Wengel, R., Wirtz, S., 2013. European small portable rainfall simulators: A comparison of rainfall characteristics. *Catena*, 110, 100–112.
- IUSS-WRB, 2015. World Reference Base for Soil Resources 2014, Update 2015: International Soil Classification System for Naming Soils and Creating Legends for Soil Maps. World Soil Resources Reports No. 106; FAO, Rome, Italy, 192 p.
- Jarvis, N., Forkman, J., Koestel, J., Kätterer, T., Larsbo, M., Taylor, A., 2017. Long-term effects of grass-clover leys on the structure of a silt loam soil in a cold climate. *Agric. Ecosyst. Environ.*, 247, 319–328.
- Kay, B.D., 2018. Soil structure and organic carbon: a review, in: Lal, R., Kimble, J.M., Follett, R.F., Stewart B.A. (Eds.): *Soil Processes and the Carbon Cycle*. 1st edition, CRC Press: Boca Raton, Florida USA, pp. 169–197.
- Kemper, W.D., Rosenau, R.C., 1986. Aggregate stability and size distribution. In: Klute, A. (Ed.): *Methods of Soil Analysis*. American Society of Agronomy, Inc., Madison, pp. 425–442.
- Keesstra, S.D., Rodrigo-Comino, J., Novara, A., Giménez-Morera, A., Pulido, M., Di Prima, S., Cerdà, A., 2019. Straw mulch as a sustainable solution to decrease runoff and erosion in glyphosate-treated clementine plantations in Eastern Spain. An assessment using rainfall simulation experiments. *Catena*, 174, 95–103.
- Kosmas, C., Danalatos, N., Cammeraat, L.H., Chabart, M., Diamantopoulos, J., Farand, R., Gutierrez, L., Jacob, A., Marques, H., Martínez-Fernandez, J., Mizara, A., Moustakas, N., Nicolau, J.M. Oliveros, C., Pinna, G., Puddu, R., Puigdefabregas, J., Roxo, M., Simao, A., Stamou, G., Tomasi, N., Usai, D., Vacca, A., 1997. The effect of land use on runoff and soil erosion rates under Mediterranean conditions. *Catena*, 29, 1, 45–59.
- Kosmas, C., Detsis, V., Karamesouti, M., Kounalaki, K., Vassiliou, P., Salvati, L., 2015. Exploring long-term impact of grazing

- management on land degradation in the socio-ecological system of Asteroussia Mountains, Greece. *Land*, 4, 3, 541–559.
- López-Vicente, M., Álvarez, S., 2018. Stability and patterns of topsoil water content in rainfed vineyards, olive groves, and cereal fields under different soil and tillage conditions. *Agric. Water Manage.*, 201, 167–176.
- Ludwig, M., Wilmes, P., Schrader, S., 2018. Measuring soil sustainability via soil resilience. *Sci. Total Environ.*, 626, 1484–1493.
- Martínez, J.R.F., Zuazo, V.H.D., Raya, A.M., 2006. Environmental impact from mountainous olive orchards under different soil-management systems (SE Spain). *Sci. Total Environ.*, 358, 1–3, 46–60.
- Mohammad, A.G., Adam, M.A., 2010. The impact of vegetative cover type on runoff and soil erosion under different land uses. *Catena*, 81, 2, 97–103.
- Montgomery, D.R., 2007. Soil erosion and agricultural sustainability. *Proc. Natl. Acad. Sci. U.S.A.*, 104, 33, 13268–13272.
- Návar, J., Synnott, T.J., 2000. Surface runoff, soil erosion, and land use in Northeastern Mexico. *Terra Latinoam.*, 18, 3, 247–253.
- Novara, A., Favara, V., Novara, Amelia, Francesca, N., Santangelo, T., Columba, P., Chironi, S., Ingrassia, M., Gristina, L., 2020. Soil Carbon Budget Account for the Sustainability Improvement of a Mediterranean Vineyard Area. *Agronomy*, 10, 336.
- O'Rourke, M.E., Petersen, J., 2016. Reduced tillage impacts on pumpkin yield, weed pressure, soil moisture, and soil erosion. *HortScience*, 51, 12, 1524–1528.
- Pereira, P., Bogunovic, I., Muñoz-Rojas, M., Brevik, E.C., 2018a. Soil ecosystem services, sustainability, valuation and management. *Curr. Opin. Environ. Sci. Health*, 5, 7–13.
- Pereira, P., Francos, M., Brevik, E.C., Ubeda, X., Bogunovic, I., 2018b. Post-fire soil management. *Curr. Opin. Environ. Sci. Health*, 5, 26–32.
- Plotly. Available online: <https://chart-studio.plot.ly/> (accessed on 09 March 2020).
- Pournader, M., Ahmadi, H., Feiznia, S., Karimi, H., Peirovan, H.R., 2018. Spatial prediction of soil erosion susceptibility: an evaluation of the maximum entropy model. *Earth Sci. Inform.*, 11, 3, 389–401.
- Preiti, G., Romeo, M., Bacchi, M., Monti, M., 2017. Soil loss measure from Mediterranean arable cropping systems: Effects of rotation and tillage system on C-factor. *Soil Till. Res.*, 170, 85–93.
- Qiang, F.E.N.G., Wenwu, Z.H.A.O., Jun, W.A.N.G., Zhang, X., Mingyue, Z.H.A.O., Zhong, L., Yuanxin, L.I.U., Xuening, F.A.N.G., 2016. Effects of different land-use types on soil erosion under natural rainfall in the Loess Plateau, China. *Pedosphere*, 26, 2, 243–256.
- Rabot, E., Wiesmeier, M., Schlüter, S., Vogel, H.J., 2018. Soil structure as an indicator of soil functions: a review. *Geoderma*, 314, 122–137.
- Ryken, N., Nest, T.V., Al-Barri, B., Blake, W., Taylor, A., Bodé, S., Ruyschaert, G., Boeckx, P., Verdoort, A., 2018. Soil erosion rates under different tillage practices in central Belgium: New perspectives from a combined approach of rainfall simulations and <sup>7</sup>Be measurements. *Soil Till. Res.*, 179, 29–37.
- Robertson, G.P., 1997. Nitrogen use efficiency in row-crop agriculture: crop nitrogen use and soil nitrogen loss. In: Jackson, L.E. (Ed.): *Ecology in Agriculture*. Academic Press, San Diego, USA, pp. 347–365.
- Salvia, R., Egidi, G., Vinci, S., Salvati, L., 2019. Desertification risk and rural development in Southern Europe: Permanent assessment and implications for sustainable land management and mitigation policies. *Land*, 8, 12, 191.
- Sanaullah, M., Usman, M., Wakeel, A., Cheema, S.A., Ashraf, I., Farooq, M., 2020. Terrestrial ecosystem functioning affected by agricultural management systems: A review. *Soil Till. Res.*, 196, 104464.
- Schindewolf, M., Schmidt, J., 2012. Parameterization of the EROSION 2D/3D soil erosion model using a small-scale rainfall simulator and upstream runoff simulation. *Catena*, 91, 47–55.
- Six, J., Paustian, K., Elliott, E.T., Combrink, C., 2000. Soil structure and organic matter. I. Distribution of aggregate-size classes and aggregate-associated carbon. *Soil Sci. Soc. Am. J.*, 64, 2, 681–689.
- Steffan, J.J., Brevik, E.C., Burgess, L.C., Cerdà, A., 2018. The effect of soil on human health: an overview. *Eur. J. Soil Sci.*, 69, 1, 159–171.
- Taguas, E.V., Guzmán, E., Guzmán, G., Vanwalleghem, T., Gómez, J.A., 2015. Characteristics and importance of rill and gully erosion: a case study in a small catchment of a marginal olive grove. *Cuad. de Investig. Geogr.*, 41, 107–126.
- Triplett Jr, G. B., Dick, W.A., 2008. No-tillage crop production: A revolution in agriculture! *Agronomy J.*, 100, S-153.
- Vanwalleghem, T., Amate, J.I., de Molina, M.G., Fernández, D.S., Gómez, J.A., 2011. Quantifying the effect of historical soil management on soil erosion rates in Mediterranean olive orchards. *Agric. Ecosyst. Environ.*, 142, 3–4, 341–351.
- Walkly, A., Black, I.A., 1934. An examination of digestion methods for determining soil organic matter and a proposed modification of the chromic and titration. *Soil Sci. Soc. Am. J.*, 37, 29–38.
- Zaibon, S., Anderson, S.H., Kitchen, N.R., Haruna, S.I., 2016. Hydraulic properties affected by topsoil thickness in switchgrass and corn-soybean cropping systems. *Soil Sci. Soc. Am. J.*, 80, 5, 1365–1376.
- Zaninović, K., Gajić-Čapka, M., Perčec Tadić, M., Vučetić, M., Milković, J., Bajić, A., Cindrić, K., Cvitan, L., Katushin, Z., Kaučić, D., Likso, T., Lončar, E., Lončar, Z., Mihajlović, D., Pandžić, K., Patarčić, M., Srnec, L., Vučetić, V., 2000. *Climate Atlas of Croatia: 1961–1990:1971–2000*. Meteorological and Hydrological Service, Zagreb.

Received 8 June 2020  
Accepted 29 July 2020

# On the transpiration of wild olives under water-limited conditions in a heterogeneous ecosystem with shallow soil over fractured rock

Roberto Corona<sup>\*</sup>, Nicola Montaldo

Dipartimento di Ingegneria Civile Ambientale e Architettura, Università di Cagliari, Via Marengo, 3, I-09123 Cagliari, Italy.

<sup>\*</sup> Corresponding author. Tel.: +39-070-675-5318. E-mail: roberto.corona@unica.it

**Abstract:** Mediterranean ecosystems are typically heterogeneous and savanna-like, with trees and grass competing for water use. By measuring sap flow, we estimated high transpiration of wild olive, a common Mediterranean tree, in Sardinia despite dry conditions. This estimate agrees with independent estimates of tree transpiration based on energy balance, highlighting the wild olive's strong tolerance of dry conditions. The wild olive can develop an adaptation strategy to tolerate dry conditions. In this Sardinian case study, the wild olive grew in shallow soil, and the tree roots expanded into the underlying fractured basalt. The trees survived in dry periods using water infiltrated during wet seasons into fractured rocks and held in soil pockets. We estimated a high upward vertical flux through the bottom soil layer from the underlying substrate, which reached 97% evapotranspiration in August 2011. The water taken up by tree roots from bedrock hollows is usually neglected in ecohydrological modeling.

**Keywords:** Evapotranspiration; Rock moisture; Water uptake; Sap flow; Energy balance.

## INTRODUCTION

In the Mediterranean regions there is a persistent declining trend in precipitation and decreasing runoff (Altin and Barak, 2014; Martinez-Fernandez et al., 2013; Montaldo and Sarigu, 2017; Vicente-Serrano et al., 2011), with consequences for the sustainability of agricultural and water resources. Mediterranean ecosystems are typically heterogeneous and savanna-like, with contrasting plant functional types (e.g., trees and grass) competing for water use (Breshears, 2006; Detto et al., 2006; Montaldo et al., 2008; Sankaran et al., 2005; Scholes and Archer 1997; Villegas et al., 2014). In these ecosystems, evapotranspiration ( $ET$ ) is a leading loss term of the root-zone water budget (Rana and Katerji, 2000), which may reach a yearly magnitude roughly equal to precipitation in semi-arid conditions (Baldocchi et al., 2004; Kurc and Small, 2004; Maselli et al., 2004; Reynolds et al., 2000; Rodriguez-Iturbe, 2000). Despite the attention these ecosystems have received (Breshears, 2006; Holdo and Brocato, 2015; Yu and D'Odorico, 2015), a general lack of knowledge persists about how to partition  $ET$  into its components (Eliades et al., 2018; Williams et al., 2004; Zhou et al., 2016), and about the relationship between  $ET$  and plant survival strategies under water stress.

Detto et al. (2006) investigated a typical heterogeneous Mediterranean ecosystem in water-limited conditions located at Orroli in Sardinia (Italy), a site with a patchy mixture of Mediterranean vegetation types: trees (mainly wild olive, *Olea sylvestris*) and grass on thin soil (~17 cm depth) above fractured basalt (Montaldo et al., 2008; Montaldo et al., 2013). Using an eddy covariance tower to estimate  $ET$  ( $ET_{EC}$ ), Detto et al. (2006) highlighted a strong tolerance to prolonged drought of the wild olive, a common Mediterranean species (Lumaret and Ouazzani, 2001; Terral et al., 2004), which still, even during the extreme dry conditions of summer 2003, transpired at rates close to potential.

Nowadays,  $ET$  is widely estimated using eddy covariance towers (Detto et al., 2006; Jung et al., 2010; Williams et al., 2012), but direct measurements are required for estimating the tree transpiration component ( $T_t$ ) in heterogeneous ecosystems

and dry conditions. Indeed, as soil dries, the mean ecosystem  $ET$  becomes low and the  $T_t$  component becomes predominant, especially with low tree cover (e.g., < 40% of the mosaic), as is typical in these ecosystems (Baldocchi et al., 2004; Detto et al., 2006; Kurc and Small, 2004; Montaldo et al., 2008). In this sense, the use of sap flow sensors to estimate tree transpiration (Oren et al., 1998) is very attractive (Bovard et al., 2005; Cammalleri et al., 2013; Hassler et al., 2018; Liu et al., 2015; Montaldo et al., 2020; Oishi et al., 2008; Paço et al., 2009; Williams et al., 2004). At the same time, sap flux measurements may themselves be affected by errors associated with calibration (Köstner et al., 1998; Steppe et al., 2015). Estimating  $T_t$  reliability is essential for identifying the likely source of water during the dry season, and so independent verification of this value would decrease the uncertainty. We propose to make such verification using an approach based on energy balance (Detto et al., 2006; Fritschen and Simpson, 1989; Garratt, 1992). We recognize that the energy balance approach is also somewhat uncertain (Foken, 2008), but if two very different approaches produce a similar estimate of  $T_t$ , then results from subsequent analyses become more reliable.

Sap flow sensors are already used for estimating  $T_t$  in cultivated (both rainfed and irrigated) olive trees (*Olea europaea*) (Chebbi et al., 2018; Karray et al., 2008; Rallo and Provenzano, 2013; Tognetti et al., 2004). As expected,  $T_t$  decreased drastically as soil dried in rainfed cultivated olive trees, reaching very low values (Ennajeh et al., 2008; Sofo et al., 2008); this is also commonly represented in ecohydrologic models (Karray et al., 2008; Kutilek and Nielsen, 1994; Laio et al., 2001; Nadezhdina et al., 2015; Rallo and Provenzano, 2013; Verhoef and Egea, 2014). We used sap flow sensors for  $T_t$  measurements of the Sardinian wild olive trees (Montaldo et al., 2020), and investigated its relationship with soil moisture; this relationship should be almost invariant according to Detto et al. (2006), in contrast with the observations in rainfed cultivated olives noted above.

According to field experiments in the Mediterranean region for other tree species, such as holm oaks in Portugal (Balugani et al., 2017; David et al., 2007; Paço et al., 2009), Spain (Perez-

Priego et al., 2017), and southern France (Limousin et al., 2009), trees also transpired at relatively high rates during dry summers. However, these sites were characterized by deep soils or shallow groundwater (Balugani et al., 2017), while the Sardinian trees that Detto et al. (2006) investigated grew in shallow soil. Generally, the behavior of *ET* components during periods of water stress depends on soil depth. In deep soils, transpiration and evaporation are theoretically expected to draw from distinct water sources, with evaporation decreasing as surface water decreases; tree transpiration remains high because roots uptake water from deep soil layers. In thin soils with shallow-rooted plants, evaporation and tree transpiration are theoretically expected to utilize the same surface water source, both becoming negligible when the soil dries entirely (Berkelhammer et al., 2016). Although the Sardinian field site should be an example of the second case, the thin soil in Sardinia sits above fractured bedrock (Detto et al., 2006), which is quite common in semi-arid and arid climates (Schwinning, 2010). For instance, in Mediterranean regions, upstream watersheds are often characterized by trees growing on such shallow soils above fractured bedrock or cemented horizons (Witty et al., 2003). In these conditions, roots may penetrate below the thin soil through cracks, fractures, and dissolution features, and trees can survive dry seasons using water infiltrated during previous wet seasons into fractured rocks and held in soil pockets (Cannon, 1911; Eliades et al., 2018; Estrada-Medina et al., 2013). This water becomes a sort of “rock moisture” (Rempe and Dietrich, 2018). Water uptake by roots in the rocks may be predominant for *ET*, up to 70–90% in semi-arid and arid climates (Breshears et al., 2009; Eliades et al., 2018; McCole and Stern, 2007; Schwinning, 2010). This is a significant water source of *ET* that ecohydrologists usually neglect (Schwinning, 2010). The water uptake of roots in the rocks may be the actual source of the wild olive’s transpiration under dry conditions in the Sardinian field.

We thus had the following objectives: 1) to quantify wild olive transpiration and its relationship with soil moisture, evaluating tree resistance to dry conditions; and 2) to quantify the eventual water uptake of the tree roots from the rocks and its role in sustaining the survival of wild olive during dry periods.

## METHODS

### The Orroli site

The Orroli field site is located in east-central Sardinia (39°41'12.57" N, 9°16'30.34" E, 500 m a.s.l.; see details in Detto et al., 2006; Detto et al., 2008; Montaldo et al., 2008; Montaldo et al., 2013). The landscape is a patchy mixture of tree clumps forming canopy cover over ~33% of the footprint area, ~1.5 km<sup>2</sup> on a gently sloping (~3° from northwest to southeast) plateau, and inter-clump zones are covered by herbaceous and grass species during periods of high moisture. The dominant tree species is wild olive, in patches ranging in height from 3.5–4.5 m, and C3 herbaceous (grass) species (*Asphodelus microcarpus*, *Ferula comunis*, *Bellium bellidioides*, *Scolymus hispanicum*, *Sonchus arvensis*, *Vicia sativa*, *Euphorbia characias*, *Daucus carota*, *Bellis perennis*; monocotyledons: *Avena fatua*, *Hordeum murinum*) grow only during wet seasons, reaching approximate heights of 0.5 m (Montaldo et al., 2008; Montaldo et al., 2013).

The climate at the flux site is maritime Mediterranean, with a mean annual precipitation (1922–2007) of 643 mm; mean monthly precipitation varies from 93 mm in December to 11 mm in July. The mean annual air temperature is 14.6°C, with mean monthly values ranging between 23.7°C in July and

7.1°C in January. The soil ranges in depth from 0–50 cm, averaging 17 cm ± 6 cm (standard deviation, SD) above fractured basalt; quickly plunging into water-limited conditions during the rainless summer (Detto et al., 2006; Montaldo et al., 2008). The soil is silt loam (19% sand, 76% silt, 5% clay) with a bulk density of 1.38 g/cm<sup>3</sup> and porosity of 53%. In May 2017 electrical resistivity tomography (ERT) was used to detect singularities such as cracks, fractures and soil pockets in the rocks, and their relative water content (Muchingami et al., 2012; Nijland et al., 2010; Rodriguez-Robles et al., 2017; Travelletti et al., 2012). The 23.5 m long images (unit electrode spacing of 0.50 m) were collected along three transects at 2 m, 5 m and 8 m from a tree clump. Rocks, cracks, soil pockets and water content were qualitatively estimated from the observed electrical resistivity map of each transect. Tree roots penetrating vertically into the fractured basalt were also noted when digging root trenches and other excavations for a separate study.

### Micrometeorological and soil measurements

Three-dimensional time series data for wind velocity, air temperature, and CO<sub>2</sub> and water vapor gas concentration at 10 Hz, were averaged over 30-minute intervals (Montaldo et al., 2008; Montaldo et al., 2013; Montaldo and Oren, 2016). This data was used to estimate *ET* and sensible heat flux based on the standard eddy covariance method (Baldocchi, 2003). The measurements were made with a Campbell Scientific CSAT-3 tri-axial sonic anemometer (Campbell Scientific Inc., Logan, Utah, USA) and a Licor-7500 CO<sub>2</sub>/H<sub>2</sub>O infrared gas analyzer (Licor Inc., Lincoln, NE, USA) positioned adjacent to each other at the top of a 10 m tall tower, operating from April 2003 at the Orroli site (Detto et al., 2006). The effect of the gentle slope of the plateau was removed by utilizing the conventional planar fit method, and the Webb-Pearman-Leuning adjustment was applied (Detto et al., 2006; Detto et al., 2008).

A Vaisala HMP45 (Vaisala, Helsinki, Finland) sensor was used to measure air temperature ( $\xi_a$ ) and relative humidity (*RH*). Vapor pressure deficit, *VPD*, was calculated as  $VPD = e^*(\xi_a) (1 - RH)$ , where the saturation vapor pressure  $e^*$  is related to  $\xi_a$  through the Clausius-Clayperon equation (Stull, 1988).

Three infrared transducers, IRTS-P (Apogee Instrument Inc., Logan, Utah, USA) (accuracy of 0.3°C), were used to measure the surface temperature ( $\xi_s$ ) of the different land cover components. One IRTS-P was positioned to monitor the leaf surface temperature of a wild olive canopy clump at 3.5 m height above the ground with a canopy view zenith angle of ~70°, a second sensor was positioned to monitor either bare soil or grass (depending on the season) at 1.6 m above the ground with a view zenith angle of ~50°, and a third sensor was placed at a greater height (10 m above the ground, view zenith angle of ~40°) to observe a mixture of trees and bare soil or grass. To derive net radiation, the incoming and outgoing shortwave and longwave radiation components were measured with a CNR-1 (Kipp and Zonen, Delft, The Netherlands) integral radiometer positioned at 10 m with a hemispherical field of view. Photosynthetically active radiation (*PAR*) was measured with a LI-190 Quantum Sensor (Licor Inc., Lincoln, NE, USA). Soil heat flux was measured at two locations close to the tower with thermopile plates, HFT3 (REBS), placed 8 cm below the surface, and two thermocouples (per plate) were placed at 2 and 6 cm to estimate soil temperature.

Seven frequency domain reflectometer probes (FDR, Model CS-616, Campbell Scientific Inc., Logan, Utah, USA) were inserted in the soil close to the tower (3.3–5.5 m away) to

estimate mean soil moisture ( $\theta$ ) within the soil layer. FDR calibration ( $\theta = 2.456 - 7.135 \tau + 6.701 \tau^2 - 1.884 \tau^3$ , where  $\tau$  is the output period in milliseconds) was made using 15 periodic gravimetric water content samples taken over a wide range of  $\theta$  (0.08–0.52) near the probes.

Precipitation was measured using a PMB2 rain gauge (CAE, San Lazzaro di Savena, Italy). To estimate the fraction of land cover components at the site, a multispectral, high-spatial-resolution (2.8 m) Quickbird satellite image (DigitalGlobe Inc.) was acquired (3 August 2003) (Detto et al., 2006), and we applied a supervised classification scheme based on the parallel piped algorithm (Montaldo et al., 2008). This classification was verified using more recent Google Earth images (12 December 2010 and 17 March 2017).

### Sap flow measurements

We used four sap flow sensors of the SFS2 M type (UP GmbH, Ibbenbüren, Germany), which comprise two needles with copper-constantan thermocouples and a heating wire. The top needle was heated using a constant power source of 120 mA. Both thermocouples were interconnected and provided a signal that corresponds directly with the temperature difference of both sensor elements. The temperature difference was influenced by the sap flow density (Granier, 1987), and the mean value of xylem water flux ( $j_s$ ) along the radius is expressed as (Granier, 1985):

$$j_s = 0.714 [(\Delta T_{\text{night}} / \Delta T_{\text{actual}}) - 1]^{1.231} \quad (1)$$

where  $\Delta T_{\text{night}}$  is the temperature difference at night (i.e., when sap flow is zero), and  $\Delta T_{\text{actual}}$  is the actual temperature difference.

The sensors (length of 2 cm) were inserted into the trunks of four wild olive trees at a height of 40 cm. The diameters of the wild olive trees ranged from 6.8 cm to 8.3 cm, and the monitored trees were in a clump (at 3 m from the tower) that was also monitored by one infrared transducer. Measurements were taken from the sensors at 1 s intervals, averaged over 30 min, and stored on a CR3000 datalogger (Campbell Scientific, Logan, UT, USA). Sap flux was measured from August 30, 2011, to December 30, 2011, hereinafter called the ‘‘SF-period’’ (DOY = 243–364, 2011). We also used the recent (from August 22, 2014 to July 9, 2017) sap flux measurements of Montaldo et al. (2020) to increase the data extension.

### Transpiration estimate at tree scale

Tree transpiration was first estimated using the sap flow sensors. The mean value of tree sap flows,  $\overline{J_s}$ , was scaled to tree transpiration,  $T_t^{SF}$ , using  $A_{sw}/A_g$  ( $A_{sw}$  is the tree sapwood area, and  $A_g$  is the ground area of the clump canopy projection) as (Oren et al., 1998):

$$T_t^{SF} = \overline{J_s} \frac{A_{sw}}{A_g} \quad (2)$$

$A_{sw}$  was estimated at an average 41.3 cm<sup>2</sup> from sapwood depth measurements made in the cores of three trees in the clump, and  $A_{sw}/A_g$  averaged 0.0031.

For the energy balance–based tree transpiration estimate,  $T_t^{EB}$ , we followed the approach of Detto et al. (2006), using their Equations (7)–(14), which use tree canopy  $\xi_s$ , wind velocity, air temperature, and radiometer measurements.

We also estimated the tree  $\beta$ -function (Detto et al., 2006; Verhoef and Egea, 2014):

$$\beta = \frac{T_t}{PE} \quad (3)$$

where  $T_t$  is the tree transpiration, and  $PE$  is the potential evaporation which was estimated using the Priestley–Taylor equation [e.g., Brutsaert (1992), Equation (10.23)], with the  $\alpha_e$  Priestley–Taylor coefficient assumed to be equal to 1.26.

### Evapotranspiration estimate at the scale of the eddy covariance footprint

Evapotranspiration was estimated using the eddy-covariance method ( $ET_{EC}$ ), which provides an  $ET$  estimate related to the flux footprint of the micrometeorological tower.

Upscaling the sap-flux measurements to the eddy covariance footprint was accomplished by multiplying  $T_t^{SF}$  by the fraction of tree cover in the footprint,  $F_{fp,t}$ , thereby assuming that the monitored wild olives and their transpiration were representative of the trees in the eddy covariance footprint.  $F_{fp,t}$  was estimated using the high-resolution satellite image and applying the two-dimensional footprint model of Detto et al. (2006) (Equation (4)).

A total evapotranspiration at the eddy-covariance footprint scale ( $ET_{fp}$ ) was also estimated as:

$$ET_{fp} = F_{fp,t} T_t + F_{fp,g} T_g + F_{fp,bs} E_{bs} + E_w \quad (4)$$

where  $E_{bs}$  is the soil evaporation,  $T_g$  is the grass transpiration, and  $F_{fp,g}$  and  $F_{fp,bs}$  are the fractions of grass cover and bare soil in the flux footprint respectively, estimated using Equation (4) of Detto et al. (2006), with  $F_{fp,t} + F_{fp,g} + F_{fp,bs} = 1$ . We estimated  $T_g$  and  $E_{bs}$  using the energy balance method, Equations (7)–(14) of Detto et al. (2006), which takes surface temperatures ( $\xi_s$ ), wind velocity, air temperature, and radiometer measurements. The  $ET_{fp}$  estimate can be compared with the eddy covariance–based estimate of  $ET$  ( $ET_{EC}$ ).

### Soil water balance to estimate the water uptake of the tree roots in the rock

The soil water balance at the scale of the eddy covariance footprint can be estimated as:

$$P - Q - ET - f_d = \Delta S \quad (5)$$

where  $P$  is the precipitation,  $\Delta S$  is the variation of water in the soil layer,  $f_d$  is the vertical flux through the bottom of the soil layer from the underlying rocky substrate, and  $Q$  is runoff.  $Q$  is typically a large loss term during wet periods (Corona et al., 2018; Montaldo and Sarigu, 2017), and decreases in the dry season. During wet periods dominated by drainage,  $f_d$  is commonly downward (positive), but it may become upward (negative) during dry periods, when root water uptake may sustain wild olive transpiration. Soil water budget terms were computed on a monthly time scale, which is appropriate for deep soil water dynamics (e.g., Miller et al., 2010; Orellana et al., 2012).

In order to estimate  $f_d$  from the soil water balance Equation (5),  $f_d$  was evaluated as:

$$f_d = P - Q - ET - \Delta S \quad (6)$$

Rain gauge observations were used for  $P$ , eddy covariance observations were used for  $ET$ , and soil moisture observations were used for the variation of water in the soil layer [ $\Delta S = \Delta \theta (1 - rc) d_s$ , with soil depth  $d_s$  equal to 0.17 m and rock content  $rc$  equal to 10%]. Surface runoff  $Q$  was estimated using the widely known Soil Conservation Service (SCS) method

(Chow et al., 1988; Ponce, 1989; Soil Conservation Service, 1972, 1986). We estimated the key parameter for the SCS method, the  $CN$  curve number, using the results of the rainfall simulator experiments by Wilson et al. (2014), which were carried out at the same Orroli field site. To simulate the runoff coefficient of 0.8 observed in the rainfall simulator experiments of Wilson et al. (2014) (with rainfall intensity of 61.6 mm/h and wet antecedent moisture conditions [AMC]), a  $CN$  value of 89 (for AMC II; Ponce, 1989) was calibrated and used here to estimate  $Q$ . Runoff  $Q$  was first estimated on a daily time scale, which is appropriate for the SCS method, and then aggregated to the monthly time scale to compute soil water balance. Hence, knowing  $P$ ,  $Q$ ,  $ET$ , and  $\Delta S$ ,  $f_d$  can be estimated from Equation (6).

## RESULTS

Meteorological forcing variables are shown in Figure 1, where  $PAR$ ,  $VPD$ ,  $\xi_a$ , and precipitation daily time series are reported. The observation period covered part of summer (from August 31 to September 23), all of fall, and part of winter, which involved a wide range of meteorological conditions. Indeed,  $PAR$  reached  $10 \text{ mmol m}^{-2} \text{ d}^{-1}$  in summer and decreased to  $3\text{--}4 \text{ mmol m}^{-2} \text{ d}^{-1}$  in winter (Figure 1a), and  $VPD$ , which was close to 3 kPa during the summer, decreased to values lower than 0.5 kPa during fall and winter (Figure 1b). A similar negative trend was observed for  $\xi_a$ , which decreased from  $\sim 27^\circ \text{C}$  in summer to  $\sim 5^\circ \text{C}$  in winter (Figure 1c). In contrast, soil moisture started drying out in summer and, after several rain events, increased to reach saturated conditions in late fall (Figure 1d).

## Transpiration at tree scale

A general decrease in tree transpiration as estimated using sap flux sensors was observed from the end of summer to winter (Figure 2a) due to energy and atmospheric constraints, as was clearly shown in the decrease of  $PAR$ ,  $VPD$ , and  $\xi_a$  (Figure 1).  $T_i^{SF}$  was high in the summer (up to 2.5 mm/d), slightly lower in the fall (average 1.8 mm/d), and reached its lowest values ( $< 1 \text{ mm/d}$ ) at the end of the year.  $T_i^{SF}$  was then compared with the energy balance estimate of transpiration ( $T_i^{EB}$ ) (Figure 2a). The two independent daily estimates of tree transpiration closely agreed (root mean square difference of 0.45 mm/d,  $T_i^{SF} = 0.74 T_i^{EB} + 0.33$ ,  $R^2 = 0.68$ ,  $p < 0.001$ , forcing the relationship through zero resulted in a slope of 0.89 with similar statistics), with similar means and standard deviations (mean  $T_i^{SF}$  of 1.50 mm/d [SD = 0.7 mm/d] and mean  $T_i^{EB}$  of 1.64 mm/d [SD = 0.8 mm/d]). Hence, considering the reasonable agreement between the two estimates, we can conclude that tree transpiration was accurately estimated.

Soil moisture content was very low at the beginning of the observation period, but two intense storms on DOY = 247 and 268 of 2011 led to an increase of  $\theta$  up to 0.35 (Figure 1d). Rainfall events in November 2011 (from 18 to 22 November) then brought the soil close to saturation. However,  $T_i^{SF}$  of the wild olive tree was almost insensitive to the low soil moisture in the first half of the observation period (Figures 2). Indeed, high rates of transpiration were still observed during a long dry period (from 10 October to 4 November; Figure 1d), with a

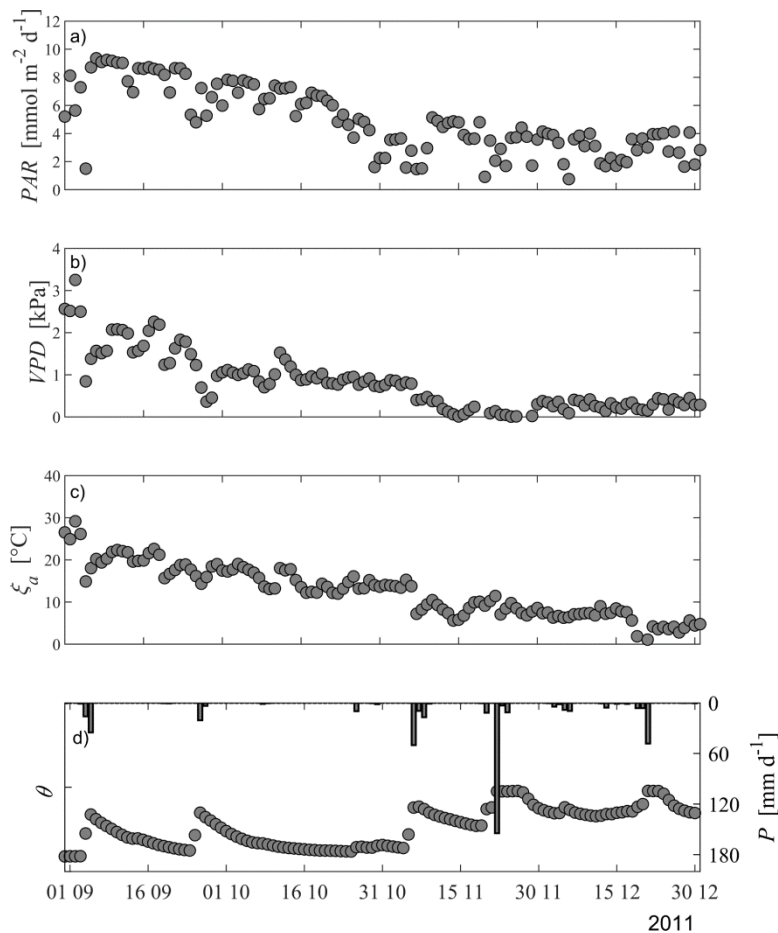


**Fig. 1.** Environmental conditions at the Orroli site: daily data for (a) photosynthetically active radiation ( $PAR$ ); (b) vapor pressure deficit ( $VPD$ ); (c) air temperature ( $\xi_a$ ); (d) soil moisture ( $\theta$ ) and precipitation ( $P$ ).

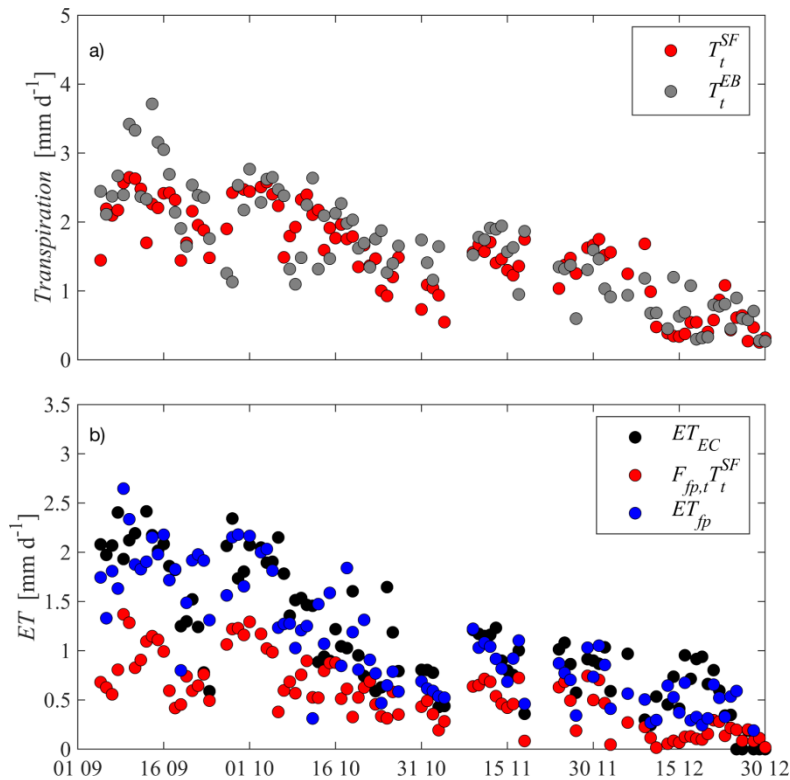


**Fig. 2.** (a) Daily estimates of tree transpiration using sap flow sensor measurements ( $T_t^{SF}$ ) and the energy balance approach ( $T_t^{EB}$ ); (b) Evapotranspiration ( $ET$ ) at the eddy covariance footprint scale: daily time series of eddy covariance-based evapotranspiration ( $ET_{EC}$ ), sap flux-based transpiration ( $F_{fp,t} T_t^{SF}$ ), and ecosystem  $ET$  ( $ET_{fp}$ ) given by Equation (4).

mean value of transpiration equal to  $\sim 1.5$  mm/d and a mean value of  $\theta$  equal to  $\sim 0.15$ . The effect of low soil moisture on tree transpiration is well depicted in Figure 3, which shows the  $\beta$ -function computed across a wide range of  $\theta$  during a dry period (from 26 September to 25 October), with  $VPD$  and  $PAR$  not limiting (Figure 1 and Figure 2a). The values of  $\beta$  were almost insensitive to changes in surface soil moisture, and the  $\beta$ -function never fell below 0.6, with the lowest point reached when the soil moisture content also reached its lowest value (Figure 3). We compared these results with observations in cultivated rainfed olive trees in Tunisia (Ennajeh et al., 2008) and Italy (Sofa et al., 2008), where instead, as expected,  $\beta$  proportionally decreased with soil moisture below a limiting soil moisture ( $\theta$ ) reaching almost zero values (Figure 3). We then further compared  $\beta$  estimates with the recent observations of Montaldo et al. (2020) at the same site in a dry period during 2015 (from 18 June to 19 July).  $\beta$  values were similar to those observed in 2011 (the minimum value of  $\beta$  was a little lower, equal to 0.52, although soil reached drier conditions), confirming the low sensitivity of  $\beta$  to  $\theta$  (Figure 3).

Although wild olives are tolerant to water stress (Lo Gullo and Salleo, 1988), they cannot transpire at rates close to potential without a water source, so that in our field, an additional water resource supported the wild olive survival. This resource may be the water in the underlying fractured basalt, taken up by the wild olive roots in the rock. We will estimate this water flux, computing  $f_a$  using Equation (6).

### Evapotranspiration at the eddy-covariance footprint scale

To compute  $f_a$  from Equation (6), we needed to estimate  $ET$ . First, we estimated  $ET$  using the eddy-covariance method.  $ET_{EC}$  decreased from 2–2.5 mm/d at the end of summer (due to a few rain events, Figure 1d) to less than 1 mm/d in late fall and win-

ter (Figure 2b). Sap flux measurements were scaled to the eddy-covariance footprint ( $F_{fp,t} T_t^{SF}$ ), exhibiting lower values than  $ET_{EC}$ . Neither soil evaporation nor grass transpiration were included in ( $F_{fp,t} T_t^{SF}$ ), so large differences were observed between  $F_{fp,t} T_t^{SF}$ , and  $ET_{EC}$  in general (mean  $F_{fp,t} T_t^{SF} = 0.54$  mm/d [SD = 0.35 mm/d], mean  $ET_{EC} = 1.13$  mm/d [SD = 0.64 mm/d], root mean square difference of 0.2 mm/d, and  $R^2 = 0.6$  with  $p < 0.001$ ; Figure 2b). Using Equation (4), we added  $E_{bs}$  and  $T_g$  and estimated  $ET_{fp}$ ; the estimate of  $ET_{fp}$  agreed well with the estimated  $ET_{EC}$  (mean  $ET_{fp} = 1.1$  mm/d [SD = 0.6 mm/d]; root mean square difference of 0.38 mm/d,  $ET_{fp} = 0.8 ET_{EC} + 0.14$ ,  $R^2 = 0.64$  with  $p < 0.0001$ ). The intercept of the relationship between  $ET_{fp}$  and  $ET_{EC}$  was not significantly different from zero ( $p = 0.155$ ); forcing the relationship through zero resulted in a slope of 0.90 with similar statistics, confirming the reliability of the  $ET_{EC}$  estimate. Large differences between  $F_{fp,t} T_t^{SF}$  and  $ET_{EC}$  were observed during periods with higher  $\theta$  (e.g., in September and from 9 November to 30 December of 2011), when soil evaporation was high, and during late fall and winter, when  $T_g$  also increased.

We compared the differences between  $F_{fp,t} T_t^{SF}$  and  $ET_{EC}$  in the wet September 2011 with those of the dry September 2014 reported in Montaldo et al. (2020). The potential evaporation was similar (mean PE = 3.75 mm/d in September 2011, and mean PE = 3.78 mm/d in September 2014), while the differences in precipitation ( $P = 79$  mm in September 2011 and  $P = 8$  mm in September 2014) impacted  $ET_{EC}$ , which was almost five times greater in the wet September 2011 (mean  $ET_{EC} = 1.8$  mm/d) than in the dry September 2014 (mean  $ET_{EC} = 0.4$  mm/d) (Figure 4). Instead tree transpiration was almost insensitive to the monthly precipitation, with similar values (mean  $F_{fp,t} T_t^{SF} = 0.5$  mm/d in September 2011 and mean  $F_{fp,t} T_t^{SF} = 0.4$  mm/d in September 2014) in the two contrasting

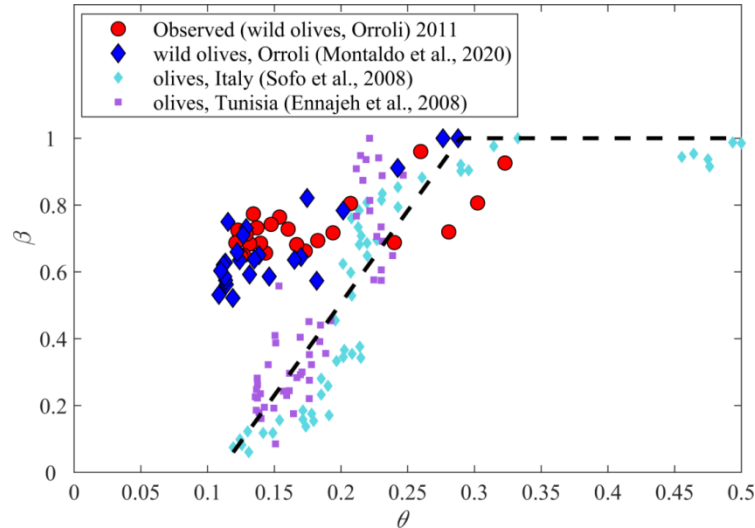


**Fig. 3.**  $\beta$ -function (ratio between tree transpiration and potential evaporation) estimates based on sap flux measurements in the wild olives of the Orroli site (red circles) versus soil moisture ( $\theta$ ). For comparison,  $\beta$ -function estimated using Montaldo et al. (2020) data at the Orroli site, and the experimental data of Sofa et al. (2008) and Ennajeh et al. (2008) in cultivated olives, with their fitted  $\beta$ -function (black dashed line; note that we estimated the fitted line), which increases linearly with  $\theta$  below a limiting soil moisture of  $\approx 0.3$ , and equal to 1 for higher values.

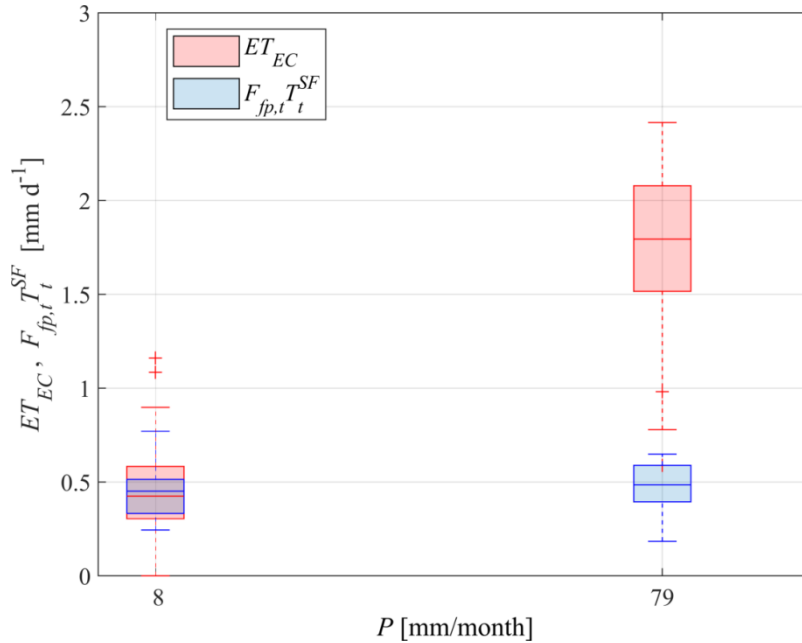


**Fig. 4.** The evapotranspiration ( $ET_{EC}$ ) and the transpiration at the footprint scale ( $F_{fp,t}^{SF}$ ) of the wet September 2011 (with precipitation,  $P$ , of 79 mm/month) and the dry September 2014 ( $P = 8$  mm/month) of Montaldo et al. (2020). The box and whiskers represent quartiles, outliers are depicted individually, and lines indicate means.

September (Figure 4). This suggested that an additional water resource supported wild olive survival in the dry September 2014, and, again, this water resource may be in the underlying fractured basalt (i.e.,  $f_a$ ).

#### Soil water balance

We estimated the soil water budget terms of Equation (6) on a monthly scale. We derived the vertical flux through the bottom of the soil layer from the underlying substrate ( $f_a$ ) using the eddy covariance estimate of  $ET$ , the observed water content variation in the soil layer ( $\Delta S$ ), the observed  $P$  from the rain gauge, and the estimates of  $Q$  (Figure 5). Across the SF-period,  $f_a$  was downward (i.e., positive) in November and December 2011, meaning that drainage was recharging the reservoirs in

the fractured rocky layer, while  $f_a$  was negative during the previous dry months of September and October 2011. In the two dry months, the trees absorbed water (a total of 37 mm) from the rocky substratum to sustain their transpiration (34% of  $ET$  in September 2011 and 42% of  $ET$  in October 2011).

Because the SF-period started just before September, which was a dry month, and is also the start of the Sardinian hydrologic year, we extended the estimate of soil water balance to the previous hydrologic year (September 2010–August 2011). This verified that the water recharge of the fractured rock reservoir during the wet seasons of the previous 2010/11 hydrologic year was sufficient to sustain the root water uptake from the rocky substratum in September–October 2011 (Figure 6). In October 2010, rain increased soil water content (positive

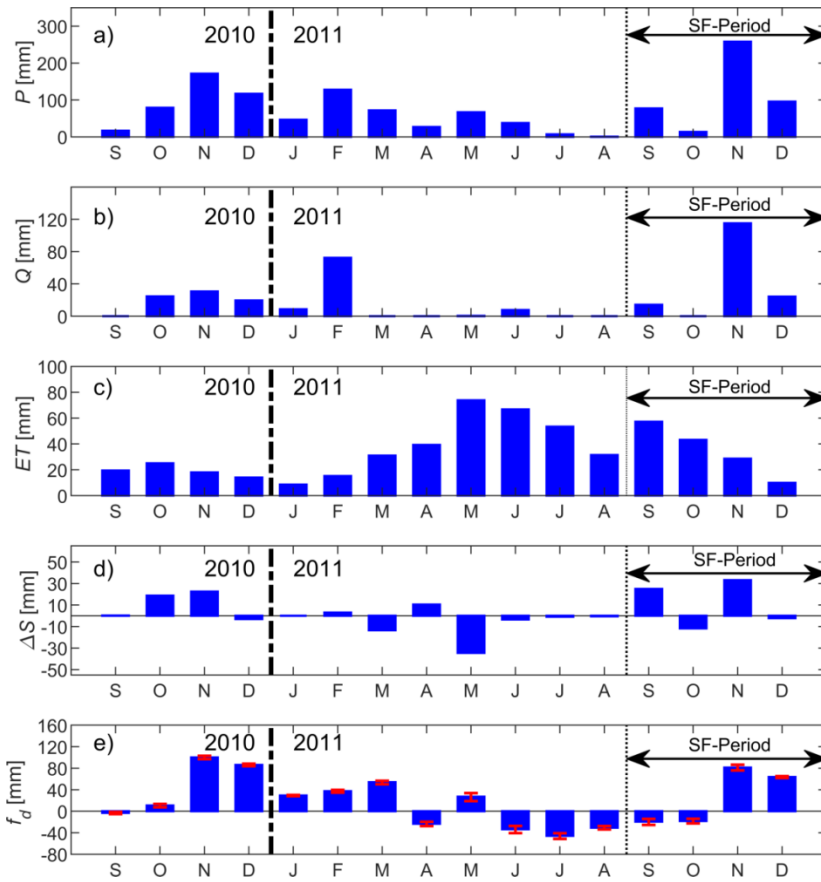


**Fig. 5.** Monthly soil water balance components (in mm/month) for the sap flux observation period (“SF-period”, August–December 2011) and the previous hydrologic year (2010/11) at the Orroli site: (a) precipitation ( $P$ ); (b) runoff ( $Q$ ), (c) evapotranspiration ( $ET$ ); (d) variation in soil water content ( $\Delta S$ ); and (e) vertical flux through the bottom of the soil layer ( $f_d$ ) (the 5<sup>th</sup> and 95<sup>th</sup> percentiles of the 2000 runs of the  $f_d$  sensitivity analysis are also reported).

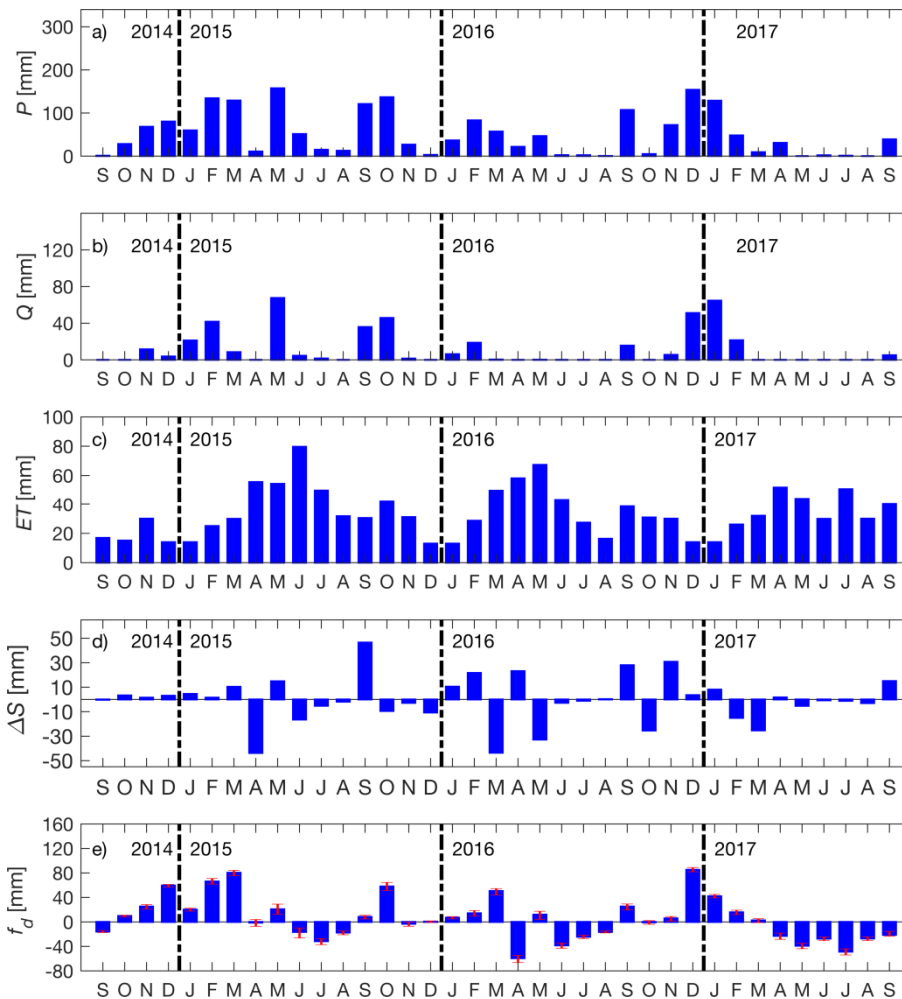


**Fig. 6.** Monthly soil water balance components (in mm/month) for the 2014/2015, 2015/2016 and 2016/2017 hydrologic years at the Orroli site: (a) precipitation ( $P$ ); (b) runoff ( $Q$ ); (c) evapotranspiration ( $ET$ ); (d) variation in soil water content ( $\Delta S$ ); and (e) vertical flux through the bottom of the soil layer ( $f_d$ ) (the 5<sup>th</sup> and 95<sup>th</sup> percentiles of the 2000 runs of the  $f_d$  sensitivity analysis are also reported).

$\Delta S$  of 19 mm), so from November 2010,  $P$  produced drainage (positive  $f_d$  of 90 mm).  $ET$  was low during fall 2010 ( $\sim 30$  mm/month) before rising in spring 2011, reaching its highest value in May ( $= 74$  mm, Figure 5b). The variation in soil water content ( $\Delta S$ ) was positive in the first months of fall, negative at the end of spring, and mostly negligible in winter and summer (Figure 5c). In summer 2011, large negative values of  $f_d$  were evaluated (a total of  $-110$  mm), and  $f_d$  reached a maximum value of 97% of  $ET$  in August 2011. When computing the annual water budget of the 2010/11 hydrologic year ( $P = 767.4$  mm,  $Q = 164$  mm,  $ET = 520$  mm, and  $\Delta S \sim 0$  mm), we estimated a positive total  $f_d$  of 85 mm (that is, by summing all the monthly values of  $f_d$ ), which was greater than 37 mm (the negative total  $f_d$  of September–October 2011). The water uptake of the roots in the rocks during the dry months (September and October 2011) of the SF-period was thus made possible by the large recharge from the rocky reservoir during the fall and winter of the previous 2010/11 hydrologic year.

We further extended the analysis using Montaldo et al.'s (2020) database for the same site, which included the hydrologic years 2014/2015, 2015/2016 and 2016/2017 (Figure 6). Values of  $f_d$  were generally positive in autumn and winter except in the 2015/16 hydrologic year, because the last two months of 2015 and January 2016 were unusually dry, and  $f_d$  was negligible due to the equilibrium between rain and  $ET$ , both small. The highest negative value of  $f_d$  was reached in April 2016 ( $f_d = -60$  mm). An unusually long dry period started in March 2017, producing negative  $f_d$  in spring and summer 2017 (Figure 6), balanced by the earlier large drainage in autumn 2016 and winter 2017. Generally we note water uptake of the roots in the rocks during dry months (when the surface soil moisture was not enough for supporting evapotranspiration needs), and a recharge of the rocky reservoir during fall and winter (Figures 5 and 7).

From the ERT information we note fractures, cracks, solid rocks (characterized by electrical resistivity values higher than 350 Ohm m), and low electrical resistivity ( $< 50$  Ohm m) parts, which suggest wet soils (Figure 7). The ERT images confirmed qualitatively that trees can uptake water from the roots in fractured rocks for transpiration, even if surface soil is dry.

Because positive  $f_d$  values recharged the rocky reservoir and balanced the negative  $f_d$  of dry months, we can expect that the sum of monthly  $f_d$  will be positive for ecosystem sustainability on a yearly time scale. Using the entire database from 2003 (Detto et al., 2006; Montaldo et al., 2008), we computed the sum of monthly  $f_d$  for the hydrologic years, which were characterized by strong annual precipitation variability in Sardinia (Figure 8). The sum of monthly  $f_d$  was positive for all years, increasing with annual precipitation ( $P_y$ ) up to 200–240 mm for  $P_y > 750$  mm. In contrast the sum of monthly  $f_d$  approached 0 for  $P_y < 550$  mm (Figure 8), which resulted in a threshold for the water budget that ensured the survival of the trees in the ecosystem. Instead, as expected, annual  $ET$  was not sensitive to  $P_y$ , ranging from 390–460 mm (Figure 8), in agreement with Montaldo and Oren (2018), because evapotranspiration variability in this Sardinian area is mainly controlled by the seasonal variability in precipitation (Montaldo and Oren, 2018). Finally, we also performed a sensitivity analysis of  $f_d$  to uncertainties in the measured flux of Equation (6). Using a Monte Carlo simulation framework, we generated 2000 simulations varying the measured terms of Equation (6) simultaneously and independently through the inclusion of uncertainties in each term [2% for  $P$  (instrument accuracy), 20% for  $ET$  (Mauder et al., 2013; Wang et al., 2015), 5% for  $\Delta S$  (instrument accuracy), and 10% for  $CN$ , which is the key parameter for the  $Q$  estimation]. The 5<sup>th</sup> and 95<sup>th</sup> percentiles of the ensembles of  $f_d$  predictions are plotted in the Figures 6 and 7e. The low sensitivity of  $f_d$  predictions for all the four hydrologic years confirmed the robustness of the results.

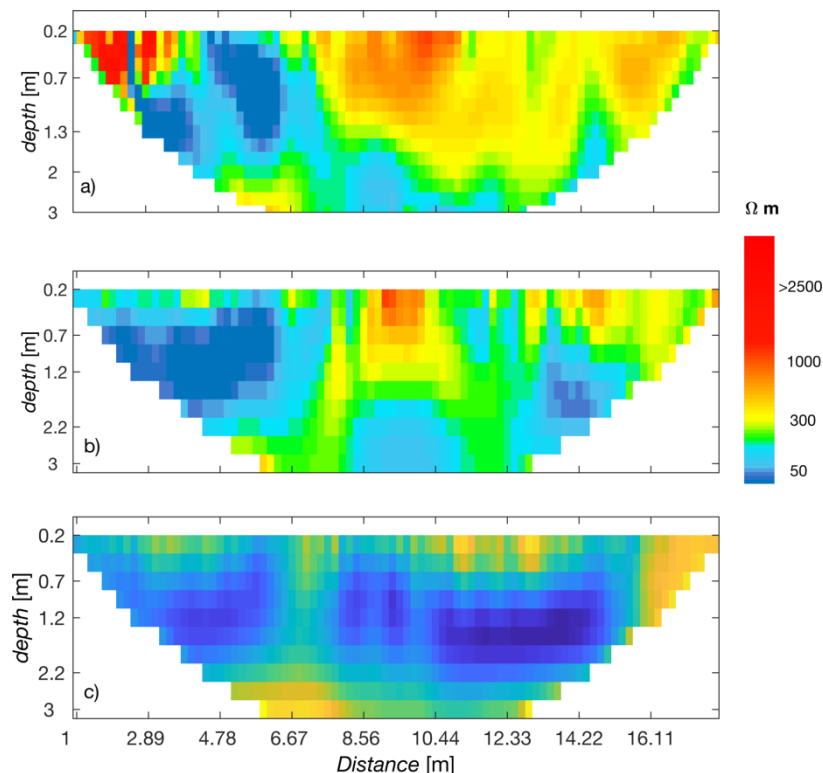


**Fig. 7.** Inverse model electrical resistivity (in Ohm m) tomography (ERT, unite electrode spacing of 0.50 m) images of 3 transects at the distance of 2, 5 and 8 m from a tree clump (panels a, b, and c respectively). Fractured rock and solid rock are associated with electrical resistivity higher than 350 and 1000 Ohm m respectively, while low values indicate the presence of wet soils.

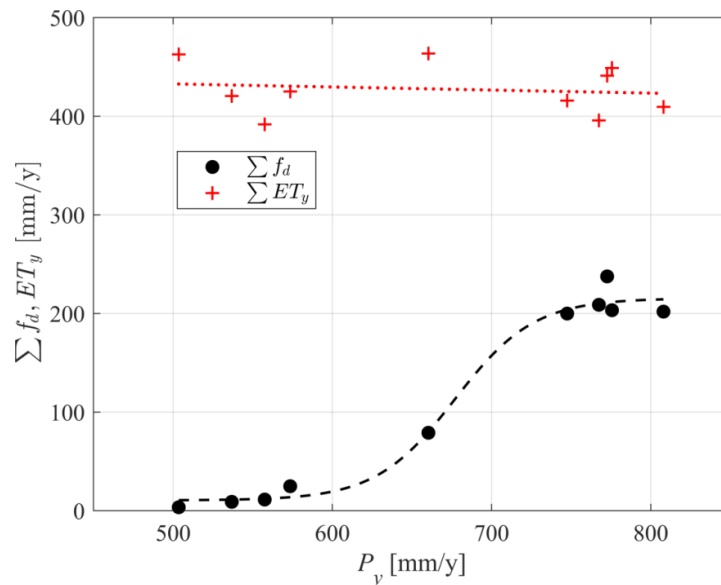


**Fig. 8.** The annual evapotranspiration ( $ET_y$ ) and the annual sum of  $f_d$  ( $\Sigma f_d$ ) versus annual precipitation ( $P_y$ ) at the Orroli site. Data from 2003 (note: incomplete years were excluded). The dotted red line is the regression line between  $ET_y$  and  $P_y$  ( $ET_y = 447.6 - 0.1 P_y$ ;  $R^2 = 0.02$ ,  $p = 0.7$ ), and the dashed black line is the regression line between  $\Sigma f_d$  and  $P_y$  ( $\Sigma f_d = 7.5 + 208.2 / (1 + e^{-(P_y - 676.2) / 25.5})$ ;  $R^2 = 0.99$ ,  $p < 0.0001$ ).

## DISCUSSION AND CONCLUSIONS

Although wild olive trees are common in Mediterranean regions (Lumaret and Ouazzani, 2001; Terral et al., 2004), their transpiration and their sensitivity to soil moisture have rarely been investigated (Lo Gullo and Salleo, 1988; Fernández et al., 1997). Using sap flow sensor measurements, we measured a high transpiration of wild olive trees in Sardinia at the end of a dry summer in 2011 (Figure 2a). This agrees with independent estimates of tree transpiration based on energy balance (Figure 2a), and with Montaldo et al.'s (2020) recent results at the Orroli site during the dry September 2014 (Figure 4). The values of the  $\beta$ -function still exceeded 0.6 when soil moisture content was at its lowest (Figure 3), in agreement with the results of Detto et al. (2006), who estimated the  $\beta$ -functions for wild olive during another summer period at the Orroli site (summer 2003) using a different approach, and consistent with the  $\beta$ -function that we estimated using the recent Montaldo et al. (2020) transpiration observations (Figure 3). Instead, our results are in contrast with observations of cultivated rainfed olives in the Mediterranean region (Ennajeh et al., 2008; Sofu et al., 2008), and the common rule (Karray et al., 2008; Kutilek and Nielsen, 1994; Laio et al., 2001; Larcher, 1995; Nadezhdina et al., 2015; Rallo and Provenzano, 2013; Verhoef and Egea, 2014) of  $\beta$  decreasing with soil moisture below a limiting soil moisture. Generally, it is not unusual that wild genotypes are more tolerant to environmental stresses than other genotypes of the same plant species (Lipshitz et al., 1991; Saykhul et al., 2016). Actually, wild olive can develop an adaptation strategy to rely on a range of avoidance and tolerance mechanisms which maintain internal water status and metabolic activity during dry periods (Connor et al., 2005; Fernandez et al., 1997; Lo Gullo and Salleo, 1988; Ramos and Santos, 2009). This strategy consists of the control of transpiration and water uptake of roots developed in deep soil layers (Nadezhdina et al., 2015). In the Sardinian case study, however, the wild olive grew in shallow soil that was dry for a long period, and the only way for the trees to survive was for their roots to expand into the underlying fractured basalt. In this way, trees can survive dry periods using water infiltrated into fractured rock during previous wet seasons and held in soil pockets (Cannon, 1911;

Estrada-Medina et al., 2013). We observed tree roots penetrating vertically into the fractured basalt and, using ERT, we detected fractures, cracks, water, and soil pockets in the underlying basalt (Figure 7).

We proposed to compute tree root uptake from the fractured rock using the monthly soil water balance, estimating the vertical flux from the underlying rock substrate ( $f_d$ ) as the residual term (Equation (6)), knowing  $ET$ ,  $P$ ,  $\Delta S$  and  $Q$ .  $ET$  was the key term of (6), and after demonstrating the reliability of the eddy covariance method for  $ET$  estimates, we used these estimates of  $ET$  in Equation (6). We estimated high positive values for  $f_d$  (up to 90 mm/month in November 2010; Figure 4) during wet months. In wet periods, water infiltrated downward in the fractured rock, producing an essential “water reservoir”. Indeed, tree roots used the water reservoir from the rock to sustain tree transpiration during dry periods (negative  $f_d$ ). We estimated the highest negative  $f_d$  in July 2011 (−45 mm/month), and we obtained an  $f_d$  value of −30 mm/month in August 2011 when  $f_d$  was 97% of  $ET$ . Considering the 2014–2017 period observed by Montaldo et al. (2020), the negative value of  $f_d$  was even higher (= −59 mm/month) in April 2016, when  $f_d$  almost reached the 100% of  $ET$ , consistent with previous estimates (Breshears et al., 2009; Eliades et al., 2018; McCole and Stern, 2007; Schwinning, 2010).

The wild olive tolerated dry conditions in the Sardinia case study and still transpired at high rates thanks to water uptake by roots in fractured rock. As do other tree species in Mediterranean regions, wild olive trees continue physiological activity and maintain transpiration even during drought, when the moisture of the thin soil layer is at a minimum. Trees in arid and semiarid regions often grow on thin soils overlaying fractured bedrock or cemented horizons (Allen, 2009; Barbata et al., 2015; Bornyasz et al., 2005; Breshears et al., 2009; Lewis and Burgy, 1964), with roots penetrating the rocky substratum through cracks, fractures, and dissolution features (Cannon, 1911). The water uptake of roots in rock has been observed in coast live oak in California (Bornyasz et al., 2005), oak in Pennsylvania (Hasenmueller et al., 2017); chaparral shrub in south California (Graham et al., 1997; Graham et al., 2010; Sternberg et al., 1996); holm oak in Spain (Barbata et al., 2015); pine in New Mexico (Breshears et al., 2009), California (Hubbert et al.,

2001; Rose et al., 2003; Witty et al., 2003), Cyprus (Eliades et al., 2018), and Oregon (with *Arctostaphylos viscida*, Zwieniecki and Newton, 1995); juniper in Texas (Kukowski et al., 2013; McCole and Stern, 2007; Schwinning, 2008); and *Gymnopodium floribundum* in Mexico (Estrada-Medina et al., 2013). The potentially large source of water represented by rock fractures is usually neglected by ecohydrologists (Rempe and Dietrich, 2018), and our findings support Schwinning's (2010) challenge to elucidate the "ecohydrology of roots in rocks". We developed a method for its computation and demonstrated that the contribution of water uptake from roots in fractured rock during drought can be vital in sustaining tree transpiration under dry conditions. Such uptake must thus be considered in the ecohydrological modeling of semi-arid and arid basins.

The Sardinian site is characterized by a strong interannual variability of annual precipitation, as typical of the Mediterranean region (Giorgi et al., 2004; Montaldo et al., 2008; Ramos, 2001), and using all the data collected at the Sardinian site from 2003, we estimated a lower limit for annual precipitation (~500 mm/y; Figure 8) below which the recharge of rock reservoir during wet months could no longer sustain the tree's water needs during the dry months, jeopardizing the tree's survival in the ecosystem. At present, the developed woody cover percentage (~33%) of the Sardinian site is sustainable with the historical mean annual precipitation (MAP) (~650 mm/y), according to Yang et al. (2016) and Axelsson and Hanan (2017), who estimated sustainable woody cover percentages for a large range of MAP in Africa and Texas dry ecosystems. We demonstrated that drier conditions, such as those predicted by future climate change projections in the Mediterranean area (Cayan et al., 2008; Mariotti et al., 2008; Mastrandrea and Luers, 2012; May, 2008; Ozturk et al., 2015), with a reduction of MAP up to ~15% in Sardinia (Montaldo and Oren, 2018), could impact the existing tree-grass ecosystem equilibrium, decreasing the woody cover spatial distribution.

**Acknowledgements.** This research was funded by MIUR through the SWATCH European project of PRIMA MED program, the ALTOS European project of PRIMA MED program, and the FLUXMED European project of WATER JPI program. We acknowledge Giulio Vignoli, Gian Piero Deidda, Luca Piroddi, Luigi Michele Noli, and Mario Sitzia, for ERT measurements. We thank two anonymous reviewers for their useful comments and suggestions.

## REFERENCES

- Allen, M.F., 2009. Bidirectional water flows through the soil-fungal-plant mycorrhizal continuum. *New Phytologist*, 182, 290–293. DOI: 10.1111/j.1469-8137.2009.02815.x
- Altın, T.B., Barak, B., 2014. Changes and trends in total yearly precipitation of the Antalya district, Turkey. *Procedia - Social and Behavioral Sciences*, 120, 586–599.
- Axelsson, C.R., Hanan, N.P., 2017. Patterns in woody vegetation structure across African savannas. *Biogeosciences*, 14, 3239–3252. <https://doi.org/10.5194/bg-14-3239-2017>
- Baldocchi, D.D., 2003. Assessing the eddy covariance technique for evaluating carbon dioxide exchange rates of ecosystems: past, present and future. *Global Change Biology*, 9, 479–492. DOI: 10.1046/j.1365-2486.2003.00629.x
- Baldocchi, D.D., Xu, L.K., Kiang, N., 2004. How plant functional-type, weather, seasonal drought, and soil physical properties alter water and energy fluxes of an oak-grass savanna and an annual grassland. *Agricultural and Forest Meteorology*, 123, 13–39. DOI: 10.1016/j.agrformet.2003.11.006
- Balugani, E., Lubczynski, W., Reyes-Acosta, L., van der Tol, C., Francés, A.P., Metselaar, K., 2017. Groundwater and unsaturated zone evaporation and transpiration in a semi-arid open woodland. *Journal of Hydrology*, 547, 54–66. DOI: 10.1016/j.jhydrol.2017.01.042
- Barbeta, A., Mejía-Chang, M., Ogaya, R., Voltas, J., Dawson, T.E., Peñuelas, J., 2015. The combined effects of a long-term experimental drought and an extreme drought on the use of plant-water sources in a Mediterranean forest. *Global Change Biology*, 21, 1213–1225. DOI: 10.1111/gcb.12785
- Berkelhammer, M., Noone, D.C., Wong, T.E., Burns, S.P., Knowles, J.F., Kaushik, A., Blanken, P.D., Williams, M.W., 2016. Convergent approaches to determine an ecosystem's transpiration fraction. *Global Biogeochemical Cycles*, 30, 933–951. DOI: 10.1002/2016gb005392
- Bornyas, M.A., Graham, R.C., Allen, M.F., 2005. Ectomycorrhizae in a soil-weathered granitic bedrock regolith: Linking matrix resources to plants. *Geoderma*, 126, 141–160. DOI: 10.1016/j.geoderma.2004.11.023
- Bovard, B.D., Curtis, P.S., Vogel, C.S., Su, H.B., Schmid, H.P., 2005. Environmental controls on sap flow in a northern hardwood forest. *Tree Physiology*, 25, 31–38.
- Breshears, D.D., 2006. The grassland–forest continuum: trends in ecosystem properties for woody plant mosaics? *Frontiers in Ecology and the Environment*, 4, 96–104. DOI: 10.1890/1540-9295004[0096:TGCTIE]2.0.CO;2
- Breshears, D.D., Myers, O.B., Barnes, F.J., 2009. Horizontal heterogeneity in the frequency of plant-available water with woodland intercanopy-canopy vegetation patch type rivals that occurring vertically by soil depth. *Ecohydrology*, 2, 503–519. DOI: 10.1002/eco.75
- Brutsaert, W., 1982. *Evaporation into the Atmosphere: Theory, History, and Applications*. Kluwer Academic Publishers, 299 p.
- Cammalleri, C., Rallo, G., Agnese, C., Ciralo, G., Minacapilli, M., Provenzano, G., 2013. Combined use of eddy covariance and sap flow techniques for partition of ET fluxes and water stress assessment in an irrigated olive orchard. *Agricultural Water Management*, 120, 89–97. DOI: 10.1016/j.agwat.2012.10.003
- Cannon, W.A., 1911. *The Root Habits of Desert Plants*. Published by the Carnegie Institution of Washington.
- Cayan, D.R., Maurer, E., Dettinger, M.D., Hayhoe, K., 2008. Climate change scenarios for the California region. *Climatic Change*, 87, 21–42. <https://doi.org/10.1007/s10584-007-9377-6>
- Chebbi, W., Boulet, G., Le Dantec, V., Lili Chabaane, Z., Fanise, P., Mougnot, B., Ayari, H., 2018. Analysis of evapotranspiration components of a rainfed olive orchard during three contrasting years in a semi-arid climate. *Agricultural and Forest Meteorology*, 256, 159–178.
- Chow, V., Maidment, D., Mays, L., 1988. *Applied Hydrology*. 2nd Ed. McGraw-Hill, New York, USA.
- Connor, D.J., 2005. Adaptation of olive (*Olea europaea* L.) to water-limited environments. *Australian Journal of Agricultural Research*, 56, 1181–1189. DOI: 10.1071/ar05169
- Corona, R., Montaldo, N., Albertson, J.D., 2018. On the role of NAO-driven interannual variability in rainfall seasonality on water resources and hydrologic design in a typical Mediterranean basin. *Journal of Hydrometeorology*, 19, 485–498. DOI: 10.1175/jhm-d-17-0078.1

- David, T.S., Henriques, M.O., Kurz-Besson, C., et al, 2007. Water-use strategies in two co-occurring Mediterranean evergreen oaks: surviving the summer drought. *Tree Physiology*, 27, 793–803. DOI: 10.1093/treephys/27.6.793
- Detto, M., Katul, G., Mancini, M., Montaldo, N., Albertson, J.D., 2008. Surface heterogeneity and its signature in higher-order scalar similarity relationships. *Agricultural and Forest Meteorology*, 148, 902–916. DOI: 10.1016/j.agrformet.2007.12.008
- Detto, M., Montaldo, N., Albertson, J.D., Mancini, M., Katul, G., 2006. Soil moisture and vegetation controls on evapotranspiration in a heterogeneous Mediterranean ecosystem on Sardinia, Italy. *Water Resources Research*, 42, 16. DOI: 10.1029/2005wr004693
- Eliades, M., Bruggeman, A., Lubczynski, M.W., Christou, A., Camera, C., Djuma, H., 2018. The water balance components of Mediterranean pine trees on a steep mountain slope during two hydrologically contrasting years. *Journal of Hydrology*, 562, 712–724. DOI: 10.1016/j.jhydrol.2018.05.048
- Ennajeh, M., Tounekti, T., Vadel, A.M., Khemira, H., Cochard, H., 2008. Water relations and drought-induced embolism in olive (*Olea europaea*) varieties 'Meski' and 'Chemlali' during severe drought. *Tree Physiology*, 28, 6, 971–976. DOI: 10.1093/treephys/28.6.971
- Estrada-Medina, H., Graham, R.C., Allen, M.F., Jimenez-Osornio, J.J., Robles-Casolco, S., 2013. The importance of limestone bedrock and dissolution karst features on tree root distribution in northern Yucatan, Mexico. *Plant and Soil*, 362, 37–50. DOI: 10.1007/s11104-012-1175-x
- Fernandez, J.E., Moreno, F., Giron, I.F., Blozquez, O.M., 1997. Stomatal control of water use in olive tree leaves. *Plant and Soil*, 190, 179–192. DOI: 10.1023/a:1004293026973
- Finnigan, J., 2004. The footprint concept in complex terrain. *Agricultural and Forest Meteorology*, 127, 117–129. DOI: 10.1016/j.agrformet.2004.07.008
- Foken, T., 2008. The energy balance closure problem: An overview. *Ecological Applications*, 18, 1351–1367. DOI: 10.1890/06-0922.1
- Fritschen, L.J., Simpson, J.R., 1989. Surface energy and radiation balance system: General description and improvements. *Journal of Applied Meteorology*, 28, 680–689.
- Garratt, J.R., 1992. *The Atmospheric Boundary Layer*. Cambridge Univ. Press, New York.
- Giorgi, F., Bi, X., Pal, J.S., 2004. Mean interannual variability and trends in a regional climate change experiment over Europe. I. Present-day climate (1961–1990). *Climate Dynamics*, 22, 733–756.
- Graham, R.C., Rossi, A.M., Hubbert, K.R., 2010. Rock to regolith conversion: Producing hospitable substrates for terrestrial ecosystems. *GSA Today*, 20, 2, 4–9.
- Graham, R.C., Anderson, M.A., Stemberg, P.D., Tice, K.R., Schoeneberger, P.J., et al., 1997. Morphology, porosity, and hydraulic conductivity of weathered granitic bedrock and overlying soils. *Soil Science Society of America Journal*, 61, 516–522. DOI: 10.2136/sssaj1997.03615995006100020021x
- Granier, A., 1985. Une nouvelle méthode pour la mesure du flux de sève brute dans le tronc des 440 arbres. *Ann. Sci. Forest.* 42, 193–200.
- Granier, A., 1987. Evaluation of transpiration in a Douglas-fir stand by means of sap flow measurements. *Tree Physiology*, 3, 309–320.
- Hasenmueller, E.A., Gu, X., Weitzman, J.N., et al., 2017. Weathering of rock to regolith: The activity of deep roots in bedrock fractures. *Geoderma*, 300, 11–31. DOI: 10.1016/j.geoderma.2017.03.020
- Hassler, S.K., Weiler, M., Blume, T., 2018. Tree-, stand- and site-specific controls on landscape-scale patterns of transpiration. *Hydrology and Earth System Sciences*, 22, 13–30. DOI: 10.5194/hess-22-13-2018
- Holdo, R.M., Brocato, E.R., 2015. Tree-grass competition varies across select savanna tree species: a potential role for rooting depth. *Plant Ecology*, 216, 577–588. DOI: 10.1007/s11258-015-0460-1
- Hubbert, K.R., Graham, R.C., Anderson, M.A., 2001. Soil and weathered bedrock: Components of a Jeffrey pine plantation substrate. *Soil Science Society of America Journal*, 65, 1255–1262. DOI: 10.2136/sssaj2001.6541255x
- Jung, M., Reichstein, M., Ciais, P., et al., 2010. Recent decline in the global land evapotranspiration trend due to limited moisture supply. *Nature*, 467, 951–954. DOI: 10.1038/nature09396
- Karray, J.A., Lhomme, J.P., Masmoudi, M.M., Mechlia N.B., 2008. Water balance of the olive tree-annual crop association: A modeling approach. *Agricultural Water Management*, 95, 5, 575–586. DOI: 10.1016/j.agwat.2007.12.006
- Köstner, B., Granier, A., Cermak, J., 1998. Sapflow measurements in forest stands: methods and uncertainties. *Annales Des Sciences Forestieres*, 55, 13–27. DOI: 10.1051/forest:19980102
- Kukowski, K.R., Schwinning, S., Schwartz, B.F., 2013. Hydraulic responses to extreme drought conditions in three co-dominant tree species in shallow soil over bedrock. *Oecologia*, 171, 819–830. DOI: 10.1007/s00442-012-2466-x
- Kurc, S.A., Small, E.E., 2004. Dynamics of evapotranspiration in semiarid grassland and shrubland ecosystems during the summer monsoon season, central New Mexico. *Water Resources Research*, 40. DOI: 10.1029/2004wr003068
- Kutilek, M., Nielsen, D.R., 1994. *Soil Hydrology*. Catena Verlag.
- Laio, F., Porporato, A., Ridolfi, L., Rodriguez-Iturbe, I., 2001. Plants in water-controlled ecosystems: active role in hydrologic processes and response to water stress - II. Probabilistic soil moisture dynamics. *Advances in Water Resources*, 24, 7, 707–723. DOI: 10.1016/s0309-1708(01)00005-7
- Larcher, W., 1995. *Physiological plant ecology*. 3rd Ed. Springer, 506 p.
- Lewis, D.C., Burgy, R.H., 1964. The relationship between oak tree roots and ground water in fractured rock as determined by tritium tracing. *Journal of Geophysical Research*, 69, 2579–2588.
- Limousin, J.M., Rambal, S., Ourcival, J.M., Rocheteau A., Joffre, R., Rodriguez-Cortina, R., 2009. Long-term transpiration change with rainfall decline in a Mediterranean *Quercus ilex* forest. *Global Change Biology*, 15, 2163–2175. DOI: 10.1111/j.1365-2486.2009.01852.x
- Lipshitz, N., Gophna, R., Hartman, M., Biger, G., 1991. The beginning of olive (*olea europaea*) cultivation in the old-world - a reassessment. *Journal of Archaeological Science*, 18, 4, 441–453. DOI: 10.1016/0305-4403(91)90037-p
- Liu, X.D., Li, Y., Chen, X., Zhou, G., Cheng, J., Zhang, D., Meng, Z., Zhang, Q., 2015. Partitioning evapotranspiration in an intact forested watershed in southern China. *Ecology*, 8, 1037–1047. DOI: 10.1002/eco.1561
- Lo Gullo, M.A., Salleo, S., 1988. Different strategies of drought resistance in three Mediterranean sclerophyllous trees growing in the same environmental conditions. *New Phytologist*, 108, 267–276.

- Lumaret, R., Ouazzani, N., 2001. Brief communications. *Nature*, 413.
- Mariotti, A., Zeng, N., Yoon, J.H., Artale, V., Navarra, A., Alpert, P., Li, L.Z.X., 2008. Mediterranean water cycle changes: Transition to drier 21st century conditions in observations and CMIP3 simulations. *Environmental Research Letters*, 3, 4, 1–8. <https://doi.org/10.1088/1748-9326/3/4/044001>
- Martínez-Fernández, J., Sánchez, N., Herrero-Jiménez, C.M., 2013. Recent trends in rivers with near-natural flow regime: The case of the river headwaters in Spain. *Progress Physical Geography*, 37, 685–700. <https://doi.org/10.1177/0309133313496834>
- Maselli, F., Chiesi, M., Bindi, M., 2004. Multi-year simulation of Mediterranean forest transpiration by the integration of NOAA-AVHRR and ancillary data. *International Journal of Remote Sensing*, 25, 3929–3941. DOI: 10.1080/01431160310001653546
- May, W., 2008. Potential future changes in the characteristics of daily precipitation in Europe simulated by the HIRHAM regional climate model. *Climate Dynamics*, 30, 581–603. <https://doi.org/10.1007/s00382-007-0309-y>
- Mastrandrea, M.D., Luers, A.L., 2012. Climate change in California: Scenarios and approaches for adaptation. *Climatic Change*, 111, 5–16. <https://doi.org/10.1007/s10584-011-0240-4>
- Mauder, M., Cuntz, M., Drüe, C., Graf, A., Rebmann, C., Schmid, H.P., Schmidt, M., Steinbrecher, R., 2013. A strategy for quality and uncertainty assessment of long-term eddy-covariance measurements. *Agricultural and Forest Meteorology*, 169, 122–135.
- McCole, A.A., Stern, L.A., 2007. Seasonal water use patterns of *Juniperus ashei* on the Edwards Plateau, Texas, based on stable isotopes in water. *Journal of Hydrology*, 342, 238–248. DOI: 10.1016/j.jhydrol.2007.05.024
- Miller, G.R., Chen, X., Rubin, Y., Ma, S., Baldocchi, D.D., 2010. Groundwater uptake by woody vegetation in a semiarid oak savanna. *Water Resources Research*, 46, 10. DOI: 10.1029/2009wr008902
- Montaldo, N., Albertson, J.D., Mancini, M., 2008. Vegetation dynamics and soil water balance in a water-limited Mediterranean ecosystem on Sardinia, Italy. *Hydrology and Earth System Sciences*, 12, 1257–1271. DOI: 10.5194/hess-12-1257-2008
- Montaldo, N., Corona, R., Albertson, J.D., 2013. On the separate effects of soil and land cover on Mediterranean ecohydrology: Two contrasting case studies in Sardinia, Italy. *Water Resources Research*, 49, 1123–1136. DOI: 10.1029/2012wr012171
- Montaldo, N., Oren, R., 2016. The way the wind blows matters to ecosystem water use efficiency. *Agricultural and Forest Meteorology*, 217, 1–9.
- Montaldo, N., Sarigu, A., 2017. Potential links between the North Atlantic Oscillation and decreasing precipitation and runoff on a Mediterranean area. *Journal of Hydrology*, 553, 419–437. DOI: 10.1016/j.jhydrol.2017.08.018
- Montaldo, N., Oren, R., 2018. Changing seasonal rainfall distribution with climate directs contrasting impacts at evapotranspiration and water yield in the Western Mediterranean Region. *Earth's Future*, 6. <https://doi.org/10.1029/2018EF000843>
- Montaldo, N., Curreli, M., Corona, R., Oren, R., 2020. Fixed and variable components of evapotranspiration in a Mediterranean wild-olive - grass landscape mosaic. *Agricultural and Forest Meteorology*, 280, [doi.org/10.1016/j.agrformet.2019.107769](https://doi.org/10.1016/j.agrformet.2019.107769).
- Muchingami, I., Hlatywayo, D.J., Nel, J.M., Chuma, C., 2012. Electrical resistivity survey for groundwater investigations and shallow subsurface evaluation of the basaltic-greenstone formation of the urban Bulawayo aquifer. *Physics and Chemistry of the Earth*, 50–52, 44–51.
- Nadezhdina, N., Ferreira, M.I., Conceicao, N., Pacheco, C.A., Hausler, M., David, T.S., 2015. Water uptake and hydraulic redistribution under a seasonal climate: long-term study in a rainfed olive orchard. *Ecohydrology*, 8, 387–397. DOI: 10.1002/eco.1545
- Nijland, W., van der Meijde, M., Addink, E.A., de Jong, S.M., 2010. Detection of soil moisture and vegetation water abstraction in a Mediterranean natural area using electrical resistivity tomography. *Catena*, 81, 3, 209–216.
- Oishi, A.C., Oren, R., Stoy, P.C., 2008. Estimating components of forest evapotranspiration: A footprint approach for scaling sap flux measurements. *Agricultural and Forest Meteorology*, 148, 1719–1732. DOI: 10.1016/j.agrformet.2008.06.013
- Orellana, F., Verma, P., Loheide II, S.P.E., 2012. Monitoring and modeling water-vegetation interactions in groundwater-dependent ecosystems. *Reviews of Geophysics*, 50. DOI: 10.1029/2011rg000383
- Oren, R., Phillips, N., Katul, G., Ewers, B.E., Pataki, D.E., 1998. Scaling xylem sap flux and soil water balance and calculating variance: a method for partitioning water flux in forests. *Annales Des Sciences Forestieres*, 55, 191–216. DOI: 10.1051/forest:19980112
- Ozturk, T., Ceber, Z.P., Türkeş, M., Kurnaz, M.L., 2015. Projections of climate change in the Mediterranean Basin by using downscaled global climate model outputs. *International Journal of Climatology*, 35, 14, 4276–4292.
- Paço, T.A., David, T.S., Henriques, M.O., Pereira, J.S., Valente, F., Banza, J., Pereira, F.L., Pinto, C., David, J.S., 2009. Evapotranspiration from a Mediterranean evergreen oak savannah: The role of trees and pasture. *Journal of Hydrology*, 369, 98–106. DOI: 10.1016/j.jhydrol.2009.02.011
- Perez-Priego, O., El-Madany, T.S., Migliavacca, M., Kowalski, A.S., Jung, M., Carrara, A., Kolle, O., Martín, M.P., Pacheco-Labrador, J., Moreno, G., Reichstein, M., 2017. Evaluation of eddy covariance latent heat fluxes with independent lysimeter and sapflow estimates in a Mediterranean savannah ecosystem. *Agricultural and Forest Meteorology*, 236, 87–99. DOI: 10.1016/j.agrformet.2017.01.009
- Ponce, V.M., 1989. *Engineering Hydrology: Principles and Practices*. Prentice-Hall, Englewood Cliffs, New Jersey, USA.
- Rallo, G., Provenzano, G., 2013. Modelling eco-physiological response of table olive trees (*Olea europaea* L.) to soil water deficit conditions. *Agricultural Water Management*, 120, 79–88. DOI: 10.1016/j.agwat.2012.10.005
- Ramos, A.F., Santos, F.L., 2009. Water use, transpiration, and crop coefficients for olives (cv. Cordovil), grown in orchards in Southern Portugal. *Biosystems Engineering*, 102, 321–333. DOI: 10.1016/j.biosystemseng.2008.12.006
- Ramos, M.C., 2001. Rainfall distribution patterns and their change over time in a Mediterranean area. *Theoretical and Applied Climatology*, 69, 3–4, 163–170.
- Rana, G., Katerji, N., 2000. Measurement and estimation of actual evapotranspiration in the field under Mediterranean climate: a review. *European Journal of Agronomy*, 13, 125–153.
- Rempe, D.M., Dietrich, W.E., 2018. Direct observations of rock moisture, a hidden component of the hydrologic cycle. *Proceedings of the National Academy of Sciences of the*

- United States of America, 115, 2664–2669. DOI: 10.1073/pnas.1800141115
- Reynolds, J., Kemp, P., Tenhunen, J., 2000. Effects of long-term rainfall variability on evapotranspiration and soil water distribution in the Chihuahuan Desert: A modeling analysis. *Plant Ecology*, 150, 145–159.
- Rodriguez-Iturbe, I., 2000. Ecohydrology: A hydrologic perspective of climate-soil-vegetation dynamics. *Water Resources Research*, 36, 3–9.
- Rodriguez-Robles, U., Arredondo, T., Huber-Sannwald, E., Ramos-Leal, A., Yépez, E.A., 2017. Technical note: Application of geophysical tools for tree root studies in forest ecosystems in complex soils. *Biogeosciences*, 14, 5343–5357. DOI: 10.5194/bg-14-5343-2017
- Rose, K.L., Graham, R.C., Parker, D.R., 2003. Water source utilization by *Pinus jeffreyi* and *Arctostaphylos patula* on thin soils over bedrock. *Oecologia*, 134, 46–54. DOI: 10.1007/s00442-002-1084-4
- Sankaran, M., et al., 2005. Determinants of woody cover in African savannas. *Nature*, 438, 846–849. DOI: 10.1038/nature04070
- Saykhul, A., Chatzistathis, T., Chatzissavvidis, C., Therios, I., Menexes, G., 2016. Root growth of cultivated and "wild" olive in response to potassium mineral nutrition. *Journal of Plant Nutrition*, 39, 11, 1513–1523. DOI: 10.1080/01904167.2016.1143503
- Scholes, R.J., Archer, S.R., 1997. Tree-grass interactions in savannas. *Annual Review of Ecology and Systematics*, 28, 517–544.
- Schwinning, S., 2008. The water relations of two evergreen tree species in a karst savanna. *Oecologia*, 158, 373–383. DOI: 10.1007/s00442-008-1147-2
- Schwinning, S., 2010. The ecohydrology of roots in rocks. *Ecohydrology*, 3, 238–245. DOI: 10.1002/eco.134
- Sofa, A., Manfreda, S., Fiorentino, M., Dichio, B., Xiloyannis, C., 2008. The olive tree: a paradigm for drought tolerance in Mediterranean climates. *Hydrology and Earth System Sciences*, 12, 1, 293–301. DOI: 10.5194/hess-12-293-2008
- Soil Conservation Service, 1972. *National Engineering Handbook, Hydrology*. Section 4. US Department of Agriculture: Washington, DC.
- Soil Conservation Service, 1986. *National Engineering Handbook*. Section 4: Hydrology, Soil Conservation Service, USDA, Washington, D.C.
- Steppe, K., Vandegehuchte, M.W., Tognetti, R., Mencuccini, M., 2015. Sap flow as a key trait in the understanding of plant hydraulic functioning. *Tree Physiology*, 35, 341–345. DOI: 10.1093/treephys/tpv033
- Sternberg, P.D., Anderson, M.A., Graham, R.C., Beyers, J.L., Tice, K.R., 1996. Root distribution and seasonal water status in weathered granitic bedrock under chaparral. *Geoderma*, 72, 89–98. DOI: 10.1016/0016-7061(96)00019-5
- Stull, R.B., 1988. *An Introduction to Boundary Layer Meteorology*. Kluwer Academic Publishers.
- Terral, J.F., Badal, E., Heinz, C., Roiron, P., Thiebault, S., Figueiral, I., 2004. A hydraulic conductivity model points to post-Neogene survival of the Mediterranean olive. *Ecology*, 85, 3158–3165. DOI: 10.1890/03-3081
- Tognetti, R., Costagli, G., Minnocci, A., Gucci, R., 2004. Irrigation effects on daily and seasonal variations of trunk sap flow and leaf water relations in olive trees. *Plant and Soil*, 263, 1–2, 249–264. DOI: 10.1023/b:plso.0000047738.96931.91
- Travalletti, J., Malet, J.-P., 2012. Hydrological response of weathered clay-shale slopes: water infiltration monitoring with time-lapse electrical resistivity tomography. *Hydrological Processes*, 26, 2106–2119. DOI: 10.1002/hyp.7983
- UP Sap Flow System User Manual Version 2.6. UP Umweltanalytische Produkte GmbH.
- Verhoef, A., Egea, G., 2014. Modeling plant transpiration under limited soil water: Comparison of different plant and soil hydraulic parameterizations and preliminary implications for their use in land surface models. *Agricultural and Forest Meteorology*, 191, 22–32.
- Vicente-Serrano, S.M., Saz-Sánchez, M.A., Cuadrat, J.M., 2011. Effects of the North Atlantic Oscillation (NAO) on combined temperature and precipitation winter modes in the Mediterranean mountains: Observed relationships and projections for the 21st century. *Global and Planetary Change*, 77, 62–76.
- Villegas, J.C., Espeleta, J.E., Morrison, C.T., Breshears, D.D., Huxman, T.E., 2014. Factoring in canopy cover heterogeneity on evapotranspiration partitioning: Beyond big-leaf surface homogeneity assumptions. *Journal of Soil and Water Conservation*, 69, 78A–83A. DOI: 10.2489/jswc.69.3.78A
- Wang, J.M., Zhuang, J.X., Wang, W.Z., Liu, S.M., Xu, Z.W., 2015. Assessment of uncertainties in eddy covariance flux measurement based on intensive flux matrix of HiWATER-MUSOEXE. *IEEE Geoscience and Remote Sensing Letters*, 12, 2, 259–263. DOI: 10.1109/lgrs.2014.2334703
- Williams, C.A., et al., 2012. Climate and vegetation controls on the surface water balance: Synthesis of evapotranspiration measured across a global network of flux towers. *Water Resources Research*, 48. DOI: 10.1029/2011wr011586
- Williams, D.G., Cable, W., Hultine, K., Hoedjes, J.C.B., Yépez E.A., Simonneaux, V., Er-Raki, S., Boulet, G., de Bruin, H.A.R., Chehbouni, A., Hartogensis, O.K., Timouk, F., 2004. Evapotranspiration components determined by stable isotope, sap flow and eddy covariance techniques. *Agricultural and Forest Meteorology*, 125, 241–258. DOI: 10.1016/j.agrformet.2004.04.008
- Wilson, T.G., Cortis, C., Montaldo, N., Albertson, J.D., 2014. Development and testing of a large, transportable rainfall simulator for plot-scale runoff and parameter estimation. *Hydrology and Earth System Sciences*, 18, 4169–4183. DOI: 10.5194/hess-18-4169-2014
- Witty, J.H., Graham, R.C., Hubbert, K.R., Doolittle, J.A., Wald, J.A., 2003. Contributions of water supply from the weathered bedrock zone to forest soil quality. *Geoderma*, 114, 389–400. DOI: 10.1016/s0016-7601(03)00051-x
- Yang, X., Crews, K.A., Yan, B., 2016. Analysis of the pattern of potential woody cover in Texas savanna. *International Journal of Applied Earth Observation and Geoinformation*, 52, 527–531.
- Yu, K.L., D'Odorico, P., 2015. Hydraulic lift as a determinant of tree-grass coexistence on savannas. *New Phytologist*, 207, 1038–1051. DOI: 10.1111/nph.13431
- Zhou, S., Yu, B.F., Zhang, Y., Huang, Y.F., Wang, G.Q., 2016. Partitioning evapotranspiration based on the concept of underlying water use efficiency. *Water Resources Research*, 52, 1160–1175. DOI: 10.1002/2015wr017766
- Zwieniecki, M.A., Newton, M., 1995. Roots growing in rock fissures: Their morphological adaptation. *Plant and Soil*, 172, 181–187. DOI: 10.1007/bf00011320

Received 17 December 2019

Accepted 6 June 2020

# An empirical model for describing the influence of water content and concentration of sulfamethoxazole (antibiotic) in soil on the total net CO<sub>2</sub> efflux

Miroslav Fér\*, Radka Kodešová, Barbora Kalkušová, Aleš Klement, Antonín Nikodem

Czech University of Life Sciences Prague, Faculty of Agrobiolgy, Food and Natural Resources, Dept. of Soil Science and Soil Protection, Kamýcká 129, CZ-16500 Prague 6, Czech Republic.

\* Corresponding author. Tel.: +420 2 24 38 27 57. E-mail: mfer@af.czu.cz

**Abstract:** The aim of the study was to describe the impact of the soil water content and sulfamethoxazole, SUL, (antibiotic) concentration in soil on the net CO<sub>2</sub> efflux. Soil samples were taken from topsoils of a Haplic Fluvisol and Haplic Chernozem. Soil samples were packed into the steel cylinders. The net CO<sub>2</sub> efflux was measured from these soil columns after application of fresh water or SUL solution at different soil water contents. The experiments were carried out in dark at 20°C. The trends in the net CO<sub>2</sub> efflux varied for different treatments. While initially high values for water treatment exponentially decreased in time, values for solution treatment increased during the first 250–650 minutes and then decreased. The total net CO<sub>2</sub> effluxes measured for 20 hours related to the soil water content followed the second order polynomial functions. The maximal values were measured for the soil water content of 0.15 cm<sup>3</sup> cm<sup>-3</sup> (Haplic Fluvisol with water or solution, Haplic Chernozem with solution) and 0.11 cm<sup>3</sup> cm<sup>-3</sup> (Haplic Chernozem with water). The ratios between values measured for solution and water at the same soil water contents exponentially increased with increasing SUL concentration in soils. This proved the increasing stimulative influence of SUL on soil microbial activity.

**Keywords:** Repacked soil columns; Antibiotics; Soil respiration; CO<sub>2</sub> emission; Birch effect; CO<sub>2</sub> efflux stimulation.

## INTRODUCTION

Emission of CO<sub>2</sub> from various sources into the atmosphere is one of the factors affecting the climate change. Vegetation and soils are important carbon pools. Soil can store a large amount of carbon. However, due to management practices soil can become also a significant source of CO<sub>2</sub> in the atmosphere (Bahn et al., 2010; Kuzyakov, 2006). A CO<sub>2</sub> efflux from the soil surface is influenced by many abiotic and biotic factors including soil temperature, soil water content, organic carbon content, composition and activity of microbial community, etc. (Balogh et al., 2011; Buchmann, 2000; Davidson and Janssens, 2006; Davidson et al., 1998; Fér et al., 2014, 2018a; Zhong et al., 2016). The microbial activity and consequently CO<sub>2</sub> emission can be influenced by many amendments including contaminants that can occur in the soils environment. Recently, treated wastewater is used for irrigation due to a water scarcity. Sewage sludge or farm biosolids are used as fertilizers. Nowadays, with the development of instruments and measurement accuracy, it has been found that these sources include variety of micropollutants including the human and veterinary pharmaceuticals that can contaminate soils and plants (Charuaud et al., 2019; Golovko et al., 2016; Ivanová et al., 2018; Klement et al., 2020; Kodešová et al., 2019a, b; Velicchi and Zambello, 2015). Depending on compounds and soil properties, pharmaceuticals can be strongly sorbed in the soils environment or can be highly mobile and can contaminate ground water (e.g., Fér et al., 2018b; Klement et al., 2018; Kočárek et al., 2016; Kodešová et al., 2015; Schaffer and Licha, 2015; Schmidtová et al., 2020). On one hand, their dissipation from soils is mostly driven by microbial conditions (e.g., Al-Khazray et al., 2018; Biel-Maeso et al., 2019; Hurtado et al., 2017; Kodešová et al., 2016, 2020; Shen et al., 2018; Srinivasan and Sarmah, 2014; Zhang et al., 2017). On the other hand, pharmaceuticals and particularly

antibiotics can strongly affect a microbial structure and activity (i.e., also CO<sub>2</sub> efflux). Antibiotics can either inhibit the activity of microorganisms and consequently reduce degradation of compounds or the activity and degradation of compounds can be enhanced due to an interaction among compounds in soil solution (Caraccilo et al., 2015; Chen and Xie, 2018; Frková et al., 2020; Grenni et al., 2018; Thelusmond et al., 2019; Zhi et al., 2019).

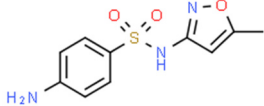
To assess microbial conditions a basal respiration (i.e., CO<sub>2</sub> accumulation rates) (Molaei et al., 2017) or substrate induce respiration can be measured using a small amount of a disturbed soil sample (Anderson and Domsch, 1985). CO<sub>2</sub> accumulation rates can be also measured during the degradation experiment (OECD, 2002). However, information about an actual influence of a certain antibiotic on a CO<sub>2</sub> emission from the surface of a larger soil samples is limited. To our knowledge, there is no study evaluating the coupled impact of antibiotic (in our case SUL) concentration in soil and soil water content on the net efflux of CO<sub>2</sub> from the soil. Therefore, the goals of our study were a) to evaluate the effect of increasing soil water contents on the soil CO<sub>2</sub> efflux from approximately one-kilogram soil samples packed in steel cylinders; b) to evaluate the impact of the increasing soil water content and concentration of SUL in soils on the soil CO<sub>2</sub> efflux; and c) to propose an empirical model how to describe the influence of water content and concentration of SUL in soil on CO<sub>2</sub> efflux.

## MATERIALS AND METHODS

### Sulfamethoxazole

The pharmaceutically active ingredient SUL (Table 1), which is very often used in human and in veterinary medicine, was chosen for this study. SUL is a sulfonamide bacteriostatic antibiotic that is mostly used in combination with trimethoprim,

**Table 1.** Sulfamethoxazole properties (<https://www.drugbank.ca/>) and the average parameters  $K_F$  and  $n$  of the Freundlich sorption isotherm ( $s = K_F c^{1/n}$ , where  $s$  is the concentration sorbed onto the soil particles and  $c$  is the concentration in soil water) and average dissipation half-life  $DT_{50}$  measured on 11 topsoils by Kodešová et al. (2015, 2016).

CAS	Molecular structure	MW (g mol <sup>-1</sup> )	Solubility (mg L <sup>-1</sup> )	Log Kow
723-46-6		253.28	610	0.89
pKa	$K_F$ (cm <sup>3/n</sup> μg <sup>1-1/n</sup> g <sup>-1</sup> )	n	DT <sub>50</sub> (days)	
pKa <sub>1</sub> = 1.7 (basic) pKa <sub>2</sub> = 5.6 (acidic)	2.22±1.68	1.65	7.84±3.2	

**Table 2.** Basic soil properties: the average values and standard deviation of electric conductivity measured in water ( $EC_{H_2O}$ ) and ethanol ( $EC_{ET}$ ), active soil reaction ( $pH_{H_2O}$ ), potential soil reaction ( $pH_{KCl}$ ), oxidizable organic carbon content ( $C_{OX}$ ), particle density ( $\rho_s$ ), bulk density ( $\rho_D$ ), total soil porosity ( $P$ ) and sand, silt and clay content (%) for the Haplic Fluvisol (A) and the Haplic Chernozem (B).

	$EC_{H_2O}$ (μS cm <sup>-1</sup> )	$EC_{ET}$ (μS cm <sup>-1</sup> )	$pH_{H_2O}$ (-)	$pH_{KCl}$ (-)	$C_{OX}$ (%)	
A	100.1±1.2	2.7±0.10	7.06±0.02	5.88±0.05	1.62±0.01	
B	119.1±0.4	3.5±0.2	8.16±0.03	7.21±0.01	1.79±0.01	
	$\rho_s$ (g cm <sup>-3</sup> )	$\rho_D$ (g cm <sup>-3</sup> )	P (%)	Sand (%)	Silt (%)	Clay (%)
A	2.58±0.01	1.43±0.06	46.2±0.02	69.0	19.2	11.8
B	2.52±0.01	1.39±0.05	47.4±0.02	5.4	58.1	36.5

which is an antifolate antibacterial agent. SUL is highly mobile in the soil-water environment, because its sorption on soil constituents is low (i.e., low Freundlich  $K_F$  coefficients in Table 1). Its stability in soils is also relatively low (i.e., low dissipation half-life,  $DT_{50}$  in Table 1). Its dissipation in soils is mainly due to biodegradation under aerobic conditions and can be significantly affected by its initial concentration in soils (Shen et al., 2018; Srinivasan and Sarmah, 2014). This means that there is a strong interaction between SUL and microbial community that should largely affect  $CO_2$  effluxes from soils. SUL was purchased from BDL Czech Republic Ltd. (Turnov, Czech Republic), and has 98% analytical grade purity. Compound (2 mg) was dissolved in fresh water (2 L). The actual concentrations in the applied solution were analyzed using the normal injection LC-MS/MS method, described by Golovko et al. (2016). The intended concentration was 0.1 μg mL<sup>-1</sup> and measured concentration was 0.097 μg mL<sup>-1</sup>.

### Study sites, soil sampling and basic soil properties

The study was performed on the soil samples collected from two experimental research stations of the Czech University of Life Sciences Prague in the Czech Republic. The research station A is in Prague-Troja, (50.122°N, 14.399°E) and B is in Prague-Suchdol (50.128°N, 14.374°E). The soil type in the area of the Prague-Troja research station was defined as the Haplic Fluvisol developed on sediments of river Vltava and soil type in Prague-Suchdol was described as the Haplic Chernozem on loess (WRB, 2015). The soil samples (10 kg of disturbed soil from each location) were taken in March 2018 from the depth of 0–8 cm of the bare soils at 3 spots and transported within one day to the laboratory. Parts of the grab soil samples, which were next used to determine basic soil properties, were air-dried

and sieved through a 2-mm mesh. The basic chemical and physical properties (Table 2) were determined using standardized laboratory techniques: active soil reaction ( $pH_{H_2O}$ ) and potential soil reaction ( $pH_{KCl}$ ) (ISO 10390, 2005), salinity (EC) (Rhoades, 1996), oxidizable organic carbon content ( $C_{OX}$ ) (Skjemstad and Baldock, 2008), particle size distribution (Gee and Or, 2002) and particle density ( $\rho_s$ ) (Flint and Flint, 2002). Additional information about soil properties of studied soils were published by Pavlů et al. (2021) for A location and by Kodešová et al. (2015, 2016, 2019a, b, 2020) and Klement et al. (2020) for B location.

Parts of soil samples intended for the laboratory measurement of the net  $CO_2$  and water ( $H_2O$ ) effluxes from soils were also air-dried. The soil was homogenised and aggregates with a diameter of larger than 1 cm were extracted using a 10-mm mesh. This treatment of the material preserved the natural aggregation of the soil and at the same time it was possible to pack the material into the 665 cm<sup>3</sup> steel cylinders so that the bulk density of the naturally consolidated soil was achieved. The bulk densities and porosities of the naturally consolidated soils (Table 2) were measured on the 100 cm<sup>3</sup> undisturbed soil cores (Dane and Topp, 2002), which were taken in four replicates on the both experimental plots.

### Experimental setup for measuring net $CO_2$ and $H_2O$ effluxes from the soil sample surface

Two experiments were performed for each soil. The first set of experiments (A1 and B1) was carried out with fresh water and the second set of experiments was carried out with SUL solution (SUL dissolved in fresh water). The experiment for each soil and treatment lasted 6 days. At the beginning of each experiment the air-dried soil (989 and 855 g for A and B, re-

spectively) was packed into the 665 cm<sup>3</sup> steel cylinder (diameter of 11 cm and height of 7 cm) and then the net CO<sub>2</sub> and net H<sub>2</sub>O effluxes were measured in one minute interval for 20 hours using the LCI-SD portable photosynthesis system with a Soil Respiration Chamber (that is described below). Next, the soil was spread into the tray, wetted using the sprayer, mixed and packed back into the cylinder, and measurements of the net CO<sub>2</sub> and net H<sub>2</sub>O efflux were repeated again for 20 hours. This procedure was recurred several times as long as it was possible to treat the soil without destroying its structure. Five wetting steps were set for both soils. The intended volumetric soil water ( $\theta$ ) contents for A samples were 0.02 (air-dried soils), 0.06, 0.11, 0.15, 0.19 and 0.24 cm<sup>3</sup> cm<sup>-3</sup>, and for B samples were 0.02 (air-dried soils), 0.07, 0.11, 0.14, 0.17 and 0.21 cm<sup>3</sup> cm<sup>-3</sup>. The actual volumetric soil water content was checked gravimetrically.

The net CO<sub>2</sub> and net H<sub>2</sub>O efflux were measured using the LCI-SD portable photosynthesis system with a Soil Respiration Chamber, according to Instruction Manual to Soil Respiration Hood V2 (ADC BioScientific, 2011). Two main components of soil respiration were measured: the net CO<sub>2</sub> efflux (NCER) and the net H<sub>2</sub>O efflux ( $W_{flux}$ ). Soil CO<sub>2</sub> emission (net molar flow of CO<sub>2</sub> in/out of the soil ( $p$  mol s<sup>-1</sup>) is characterized as

$$C = u(-\Delta c) \quad (1)$$

where  $u$  is molar air flow in mol s<sup>-1</sup>;  $\Delta c$  is the difference in CO<sub>2</sub> concentration through the soil chamber, ( $\mu\text{mol mol}^{-1}$ )

$$\Delta c = C_{ref} - C_{an} \quad (2)$$

where  $C_{ref}$  is the CO<sub>2</sub> flowing into the soil chamber ( $\mu\text{mol mol}^{-1}$ ),  $C_{an}$  is CO<sub>2</sub> flowing out from the soil chamber ( $\mu\text{mol mol}^{-1}$ ).

The net CO<sub>2</sub> efflux ( $C_e$  per unit area) symbol  $NCER$  ( $\mu\text{mol s}^{-1} \text{m}^{-2}$ ) is described as:

$$NCER = u_s(-\Delta c) \quad (3)$$

where  $u_s$  is the molar flow of air per square metre of soil, mol m<sup>-2</sup> s<sup>-1</sup>;  $\Delta c$  is the difference in CO<sub>2</sub> concentration through soil hood,  $\mu\text{mol mol}^{-1}$ .

The net H<sub>2</sub>O flux (water flux)  $W_{flux}$  (mmol s<sup>-1</sup> m<sup>-2</sup>) is characterized as:

$$W_{flux} = \Delta e u_s / p \quad (4)$$

where  $u_s$  is the molar flow of air per square metre of soil, mol m<sup>-2</sup> s<sup>-1</sup>;  $\Delta e$  is the differential water vapour concentration, m Bar; and  $p$  is the atmospheric pressure, mBar.

To avoid the influence of variable solar radiation (e.g., Fér et al., 2018a) and temperature (Schaufler et al., 2010; Yueste et al., 2007) on the measured values, the net CO<sub>2</sub> and net H<sub>2</sub>O effluxes were measured in the dark and at 20°C in a growth chamber (KBF 240, Binder, Germany). The air humidity varied between 30 and 40%.

Next, the soil CO<sub>2</sub> efflux data was analyzed with the R software (R Development Core Team, 2015) to eliminate error measurements. This procedure, which was in detailed described by Fér et al. (2018a), includes the smoothing using the Savitzky-Golay filter to reduce the most urgent misleading records caused by the repeated disruption of the measurement conditions and the reconstruction of the potential unaffected course of the measurement by computing its continuum.

## Data evaluation

Since the main aim of this study was the evaluation of the coupled impact of the antibiotic SUL and soil water content on the CO<sub>2</sub> emission from the soils, the analyses mainly focused on the net CO<sub>2</sub> efflux data. The initial, maximal and final values of the net CO<sub>2</sub> efflux were expressed for each treatment and related to the water content steps. The cumulative net CO<sub>2</sub> efflux and the total net CO<sub>2</sub> efflux for 20 hours were evaluated. The values of the total net CO<sub>2</sub> efflux for the water treatment were related to the soil water contents. To assess an influence of the SUL content in soils on the CO<sub>2</sub> emission, the ratios between the values of the total net CO<sub>2</sub> efflux for the SUL solution treatment were divided by the values of the total net CO<sub>2</sub> efflux for the water treatment only at the same soil water content. These ratios were next related to the SUL concentrations in soils expressed as follows:

$$s_i = \sum_{i=0}^N (V_i c) / m \quad (5)$$

where  $s_i$  is the concentration of SUL in soil ( $\mu\text{g g}^{-1}$ ),  $V_i$  is the volume of the applied solution (mL),  $c$  is the concentration of SUL in the solution ( $\mu\text{g mL}^{-1}$ ),  $m$  is the dry mass of the soil column (g), and  $N$  is the number of wetting steps.

The net H<sub>2</sub>O efflux depended on the actual soil water content, but no influence of SUL on the net H<sub>2</sub>O efflux was observed. This data is not further discussed in this paper.

## RESULTS AND DISCUSSION

The trends of the net CO<sub>2</sub> effluxes for particular soil water contents considerably differed for different treatments (i.e., for fresh water and SUL solution). In the case of fresh water and A1 soil sample (Haplic Fluvisol), the initially high net CO<sub>2</sub> efflux exponentially decreased in time for all soil water contents (Fig 1a). The similar trends in the net CO<sub>2</sub> effluxes were observed for B1 soil samples (Haplic Chernozem) of soil water contents of 0.07 and 0.21 cm<sup>3</sup> cm<sup>-3</sup> (Fig 1c). For other soil water contents, the net CO<sub>2</sub> efflux initially increased (rise time varied between 250 and 300 min) and then declined. The range of the net CO<sub>2</sub> efflux was similar (0–2  $\mu\text{mol s}^{-1} \text{m}^{-2}$ ) for both soil sample (A1 and B1). The very high soil respiration in the beginning after rewetting and then decrease in soil respiration is called the respiration pulse or the Birch effect (Birch, 1958), which was also find in our previous study where undisturbed soil samples were wetted by a capillary rise from the bottom of the soil samples (Fér et al., 2018a). The similar results were obtained by Iovieno and Bååth (2008), who demonstrated almost no respiration on the air-dried soil samples and exponential decrease of soil respiration after rewetting to 60% of water holding capacity (WHC). The exponential decrease in soil respiration was observed after rewetting (50% of WHC) soil samples after 4 days of air-drying by Meisner et al. (2013; 2015).

In the case of SUL solution, the net CO<sub>2</sub> effluxes measured on the A2 and B2 samples of soil water contents of 0.02 (A2 and B2), 0.06 (A2) and 0.07 (B2) cm<sup>3</sup> cm<sup>-3</sup> (Figure 1b and 1d) were similar to those measured for A1 and B1 samples of the same soil water contents (Figure 1a and 1c). This similarity can be explained by relatively low SUL amounts in soil samples (i.e., low concentrations of SUL in soils, expensed as weight of SUL per unit weight of dry soil) and thus likely a low influence on a microbial community. On the other hand, the trends in the

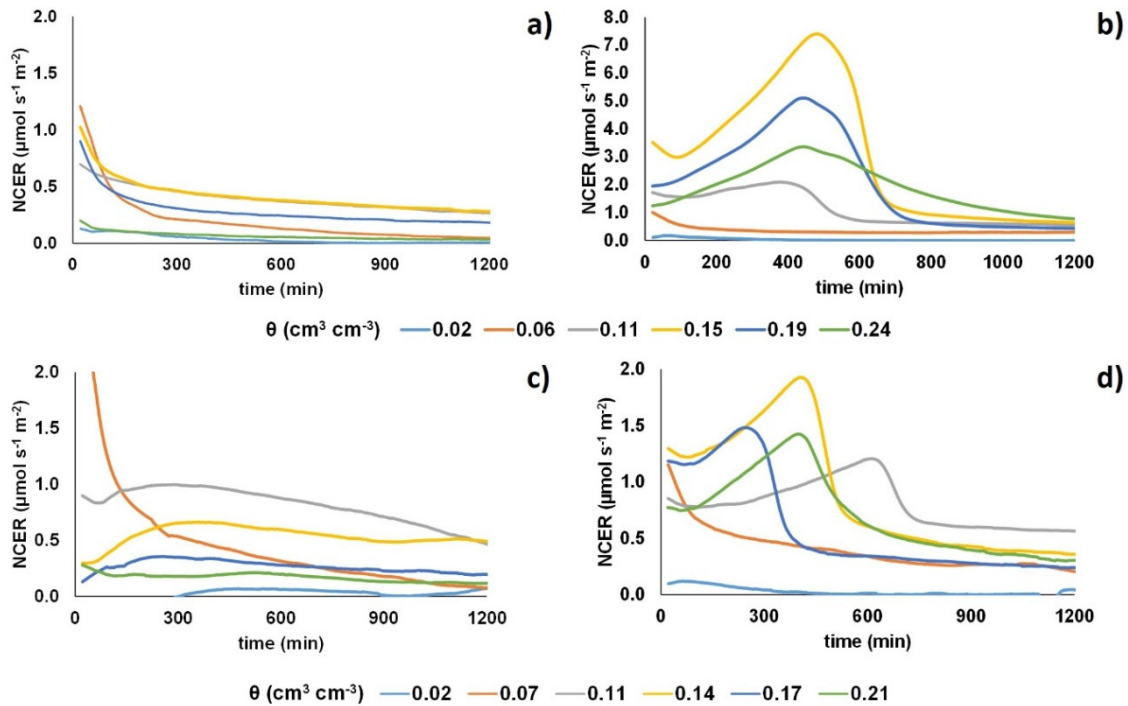


**Fig. 1.** Recorded net CO<sub>2</sub> effluxes (NCER) for 20 hours: (a) and (b) are A1 and A2 soil samples from the Haplic Fluvisol wetted with fresh water and SUL solution, respectively, and (c) and (d) are B1 and B2 soil samples from the Haplic Chernozem wetted with fresh water and SUL solution, respectively.

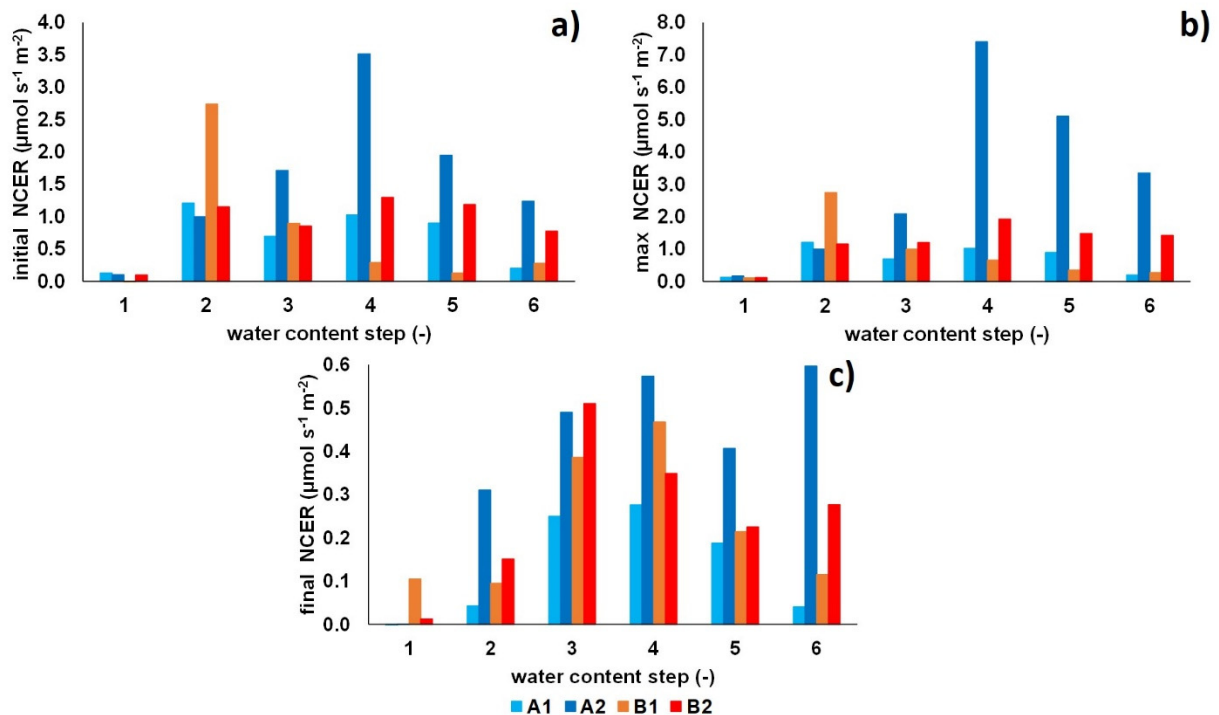


**Fig. 2.** Initial (a), maximal (b) and final (c) values of the net CO<sub>2</sub> effluxes (NCER): A1 is the soil sample from the Haplic Fluvisol wetted with fresh water, A2 is the soil sample from the Haplic Fluvisol wetted with SUL solution, B1 is the soil sample from the Haplic Chernozem wetted with fresh water and B2 is the soil sample from the Haplic Chernozem wetted with SUL solution.

net CO<sub>2</sub> effluxes for higher soil water contents and therefore also higher SUL concentrations in both soil samples (A2 and B2) completely differed from those wetted with fresh water (A1 and B1). The net CO<sub>2</sub> efflux increased during the first 450 minutes for A2 and 250–650 minutes for B2 (when the maximal net CO<sub>2</sub> efflux was reached) and next decreased (Fig. 1b and 1d). The trends in the initial and maximal values of the net

CO<sub>2</sub> effluxes evaluated for particular soil samples were similar (Figure 2a and 2b). Values mostly initially increased with wetting and then declined. The final values of the net CO<sub>2</sub> effluxes for A1 and B1 also initially increased and then decreased with increasing wetting. However, in the case of A2 and B2, the final values initially increased and then values varied between (0.4–0.6 and 0.25–0.35 µmol s<sup>-1</sup> m<sup>-2</sup>, for A2 and B2, respectively).

The cumulative net CO<sub>2</sub> effluxes from the soil samples (Figure 3a and 3c) even better showed the effect of an increasing soil water content on the net CO<sub>2</sub> efflux. The total net CO<sub>2</sub> efflux (Figure 3a) increased up to the soil water content of 0.15 cm<sup>3</sup> cm<sup>-3</sup> (A1) and 0.11 cm<sup>3</sup> cm<sup>-3</sup> (B1) and then decreased. The results confirm the fact, that with an increasing soil water content the net CO<sub>2</sub> efflux is also increasing (Fér et al., 2018a; Moayano et al., 2018) due to improving conditions for aerobic microbes. During a further soil wetting, the soil pores are gradually filled with water, which aggravates conditions for aerobic microbes, and thus the flow of soil gas (i.e., also CO<sub>2</sub>) is reduced (Fér et al., 2018a). Later on, the net CO<sub>2</sub> efflux is restricted even more due to anaerobic conditions that suppress the aerobic microbial activity (Moayano et al., 2012 or Xu et al., 2004). The similar soil water contents (0.09–0.17 cm<sup>3</sup> cm<sup>-3</sup>) related to the highest net CO<sub>2</sub> efflux were presented in our previous study (Fér et al., 2018a), in which the net CO<sub>2</sub> efflux from the undisturbed soil samples collected from loess derived soils was measured using the same device. The higher soil water contents (0.20 and 0.18 cm<sup>3</sup> cm<sup>-3</sup>) related to the highest net CO<sub>2</sub> efflux were documented by Yueste et al. (2007) and Jiang et al. (2015) for a Chromic Cambisol and Haplic Kastanozem, respectively. One of the reasons could be that a different equipment was used to measure the CO<sub>2</sub> efflux and/or both experiments were performed in the field conditions with undisturbed soils.

The cumulative net CO<sub>2</sub> effluxes from the soil samples wetted with SUL solution (Figure 3b and 3d) showed much steeper initial increases. The values of the total CO<sub>2</sub> effluxes from the soil samples wetted with SUL solution are considerably and slightly higher than those for samples wetted with fresh water (Figure 3a and 3c) for the Haplic Fluvisol and Haplic Chernozem, respectively. The reason of a higher influence of SUL on the net CO<sub>2</sub> effluxes from the Haplic Fluvisol than that from the

Haplic Chernozem could be a different influence of SUL on the soil microbial community. For instance, Frková et al. (2020) showed that SUL had a short-term stress effect on a microbial community in an Arenosol Epieutric (sandy soil that is the most similar to the Haplic Fluvisol) and the same Haplic Chernozem, which resulted in an increase in a basal respiration. This affect was more pronounced in the Arenosol Epieutric than in the Haplic Chernozem. However, the cumulative net CO<sub>2</sub> effluxes resulted from both treatments (Figure 4a) showed similar trends and the highest total net CO<sub>2</sub> efflux was measured at the 4<sup>th</sup> water content step for both soils (soil-water content of 0.15 cm<sup>3</sup> cm<sup>-3</sup> and 0.14 cm<sup>3</sup> cm<sup>-3</sup> respectively).

Calculated ratios between the total net CO<sub>2</sub> effluxes for samples wetted with SUL solution (A2 and B2) and fresh water (A1 and B1) exponentially increased with the increasing wetting (Figure 4b). This means that despite the soil water content largely controlled and at high values considerably restricted the net CO<sub>2</sub> efflux, the increasing SUL concentration in soils gradually increases the net CO<sub>2</sub> efflux.

The data points given by the water contents and the related total net CO<sub>2</sub> efflux for water treatments (A1 and B1) were fitted with the polynomial functions (Figure 4c). The intercepts of these two functions with x-axis were 0.0189 and 0.0183 cm<sup>3</sup> cm<sup>-3</sup> for A1 and B1, respectively, which can be assumed as bottom limits of the soil-water contents, for which and below these values no CO<sub>2</sub> efflux would be measured.

The data points given by the SUL concentrations in soils and ratios between the total net CO<sub>2</sub> effluxes for the samples wetted with SUL solution (A2 and B2) and fresh water (A1 and B1) were fitted with the exponential functions (Figure 4d). These equations expressed the impact of the SUL concentrations in soils under the setup experimental conditions. The calculated values of the ratios can be further considered as the multiplication coefficients with the help of which it would be

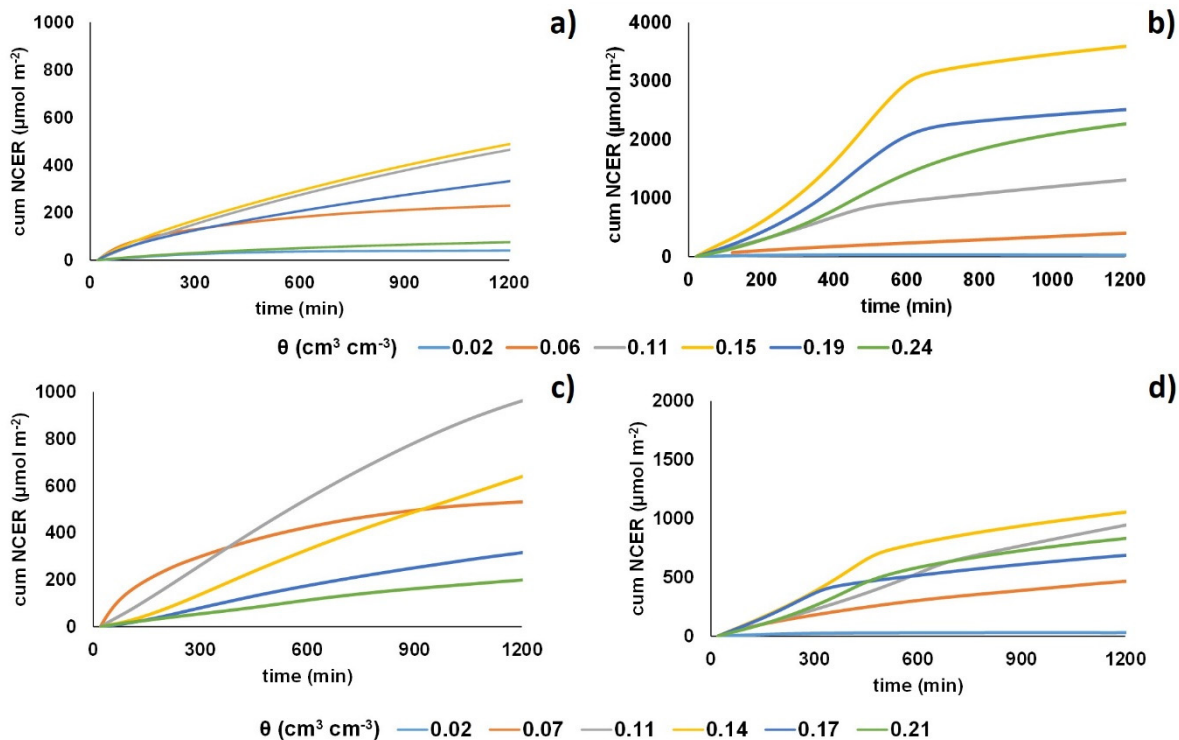


**Fig. 3.** Cumulative net soil CO<sub>2</sub> efflux (cum NCER) recorded for 20 hours: (a) and (b) are A1 and A2 soil samples from the Haplic Fluvisol wetted with fresh water and SUL solution, respectively, and (c) and (d) are B1 and B2 soil sample from the Haplic Chernozem wetted with fresh water and SUL solution, respectively.

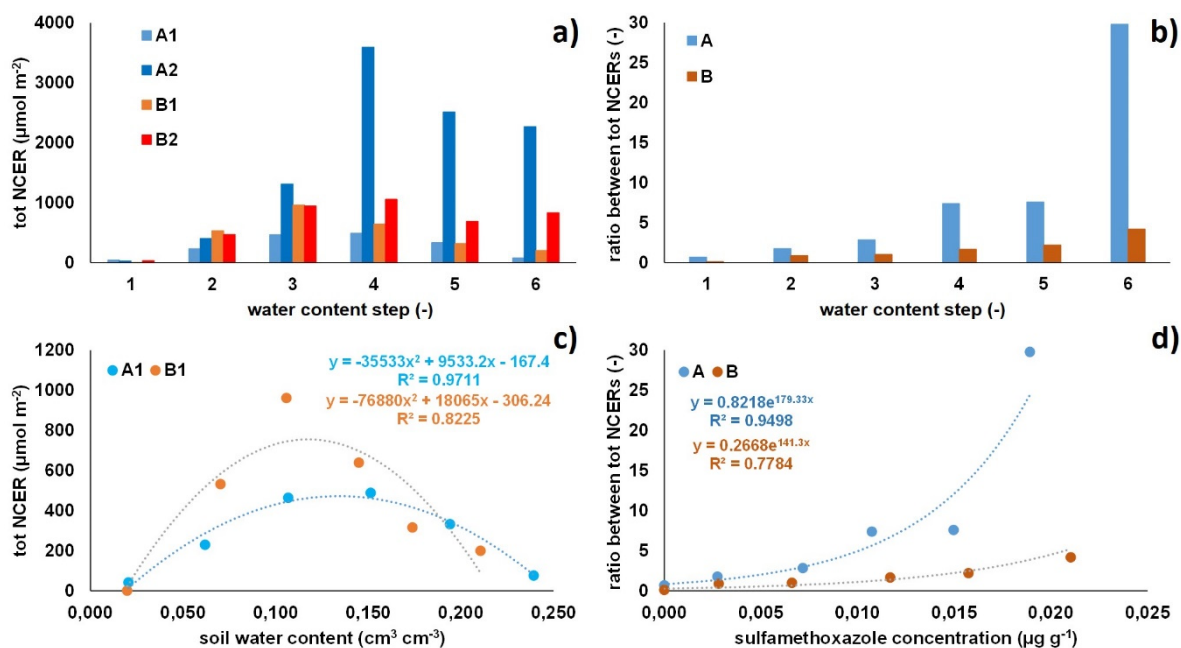


**Fig. 4.** The total net CO<sub>2</sub> efflux (tot NCER) measured for 20 hours (a), the ratio between the total net CO<sub>2</sub> effluxes for the SUL solution treatment and the water treatment (b), the relationship between the total net CO<sub>2</sub> effluxes (tot NCER) and the soil water contents (c), the relationship between the ratio of total net CO<sub>2</sub> effluxes and the SUL concentrations in soils, which was calculated using Eq. 5 (d): A1 is the sample from the Haplic Fluvisol wetted with water, A2 is the soil sample from the Haplic Fluvisol wetted with SUL solution, B1 is the soil sample from the Haplic Chernozem wetted with water and B2 is the soil sample from the Haplic Chernozem wetted with SUL solution.

possible to predict the values of the total net CO<sub>2</sub> effluxes for certain SUL concentrations from the values of the total net CO<sub>2</sub> effluxes evaluated for the water treatment. However, at this moment results cannot be generalized for different solution concentrations. One of the reasons is that the SUL concentration in soil at each wetting step was calculated as a sum of volumes of solution that were cumulatively applied into soil multiplied by the SUL concentration in solution divided by the mass of soil, and no SUL dissipation in soil was assumed. The average dissipation half-life (Table 1) indicates a relatively high dissipation rate in soils. The first order kinetic equations and reaction constant derived from the DT<sub>50</sub> values could be used to calculate a possible decrease of SUL in each dose. Values in Table 1 were obtained at the same temperature (20°C) but at the optimal soil water contents that corresponded to the field water capacities. Dissipation of SUL under dry conditions would be much slower. In addition, there could be some SUL losses during the treatments. For a better definition of soil conditions, the actual SUL concentrations in soils should be determined at each wetting step. Another reason is that experiments were carried out with solution of one SUL concentration. Similar sets of experiments should be carried out with wider range of concentrations and a possibility to generalize this empirical model for variable soil water contents and actual concentrations in soils should be investigated.

## CONCLUSION

Results of this study showed that under the established experimental conditions the relationships between the total net CO<sub>2</sub> effluxes from two soils recorded for 20 hours and the soil-water content could be approximately described using the second order polynomial functions. The antibiotic SUL considerably increased the net CO<sub>2</sub> efflux from soils. The values of the total net CO<sub>2</sub> efflux measured for the SUL solution treatment

were several times higher than those for the water treatment and this impact increased with the increasing SUL concentrations in soils. Further studies are needed to test the proposed empirical exponential model for estimating the multiplication coefficient from the SUL concentrations in soils for wider range of SUL concentrations in applied solutions. Nevertheless, results indicated a very progressive positive impact of SUL amount in soils on undesirable CO<sub>2</sub> emissions from the soil environment.

*Acknowledgement.* Authors acknowledge the financial support from the Czech Science Foundation (project No. 17-08937S) and the European Regional Development Fund-Project Centre for the investigation of synthesis and transformation of nutritional substances in the food chain in interaction with potentially harmful substances of anthropogenic origin: comprehensive assessment of soil contamination risks for the quality of agricultural products (No. CZ.02.1.01/0.0/0.0/16\_019/0000845). Authors also thank to Radim Vašát for data treatment using R code and colleagues from University of South Bohemia in České Budějovice (Faculty of Fisheries and Protection of Waters) for measurement of SUL concentration in applied solution.

## REFERENCES

- ADC BioScientific, 2011. User manual LCi-SD Leaf Chamber/Soil Respiration Analysis System. Hertfordshire.
- Al-Khazrajy, O.S.A., Bergstrom, E., Boxall, A.B.A., 2018. Factors affecting the dissipation of pharmaceuticals in freshwater sediments. *Environ. Toxicol. Chem.*, 37, 3, 829–838.
- Anderson, T.H., Domsch, K.H., 1985. Determination of ecophysiological maintenance carbon requirements of soil microorganisms in a dormant state. *Biol. Fert. Soils.*, 1, 81–89.
- Bahn, M., Reichstein, M., Davidson, E.A., Grünzweig, J., Jung, M., Carbone, M. S., Epron, D., Misson, L., Nouvellon, Y., Rouspard, O., Savage, K., Trumbore, S. E., Gimeno, C.,

- Curriel Yuste, J., Tang, J., Vargas, R., and Janssens, I. A., 2010. Soil respiration at mean annual temperature predicts annual total across vegetation types and biomes. *Biogeosciences*, 7, 2147–2157.
- Balogh, J., Pintér, K., Fóti, S., Cserhalmi, D., Papp, M., Nagy, Z., 2011. Dependence of soil respiration on soil moisture, clay content, soil organic matter and CO<sub>2</sub> uptake in dry grasslands. *Soil Biol. Biochem.*, 43, 1006–1013.
- Biel-Maeso, M., González-González, C., Lara-Martín, P.A., Corada-Fernández, C., 2019. Sorption and degradation of contaminants of emerging concern in soils under aerobic and anaerobic conditions. *Sci. Total Environ.*, 666, 662–671.
- Birch, H., 1958. The effect of soil drying on humus decomposition and nitrogen availability. *Plant Soil*, 10, 9–31.
- Buchmann, N., 2000. Biotic and abiotic factors controlling soil respiration rates in *Picea abies* stands. *Soil Biol. Biochem.*, 32, 1625–1635.
- Caracciolo, A.B., Topp, E., Grenni, P., 2015. Pharmaceuticals in the environment: biodegradation and effects on natural microbial communities. A review. *J. Pharmaceut. Biomed.*, 106, 25–36.
- Charuau, L., Jardem E., Jaffrezic, A., Thomas, M.F., Le Bot, B., 2019. Veterinary pharmaceutical residues from natural water to tap water: Sales, occurrence and fate. *J. Hazard. Mater.*, 361, 169–186.
- Chen, J., Xie, S., 2018. Overview of sulfonamide biodegradation and relevant pathways and microorganisms. *Sci. Total Environ.*, 640–641, 1465–1477.
- Davidson, E.A., Janssens, I., 2006. Temperature sensitivity of soil carbon decomposition and feedbacks to climate change. *Nature*, 440, 165–173.
- Dane, J.H., Topp, C.T. (Eds), 2002. *Methods of Soil Analysis. Part 4 – Physical Methods*. Soil Science Society of America, Inc. Madison, USA.
- Davidson, E.A., Belk, E., Boone, R., 1998. Soil water content and temperature as independent or confounded factors controlling soil respiration in a temperate mixed hardwood forest. *Glob. Change Biol.*, 4, 217–227.
- Fér, M., Kodešová, R., Klement, A., 2014. CO<sub>2</sub> emission from erosion affected soils. In: 14th International Multidisciplinary Scientific Geoconference and EXPO, SGEM 2014. Albena. Bulgaria; 17 June 2014 through 26 June 2014, 2, 3, 37–44.
- Fér, M., Kodešová, R., Nikodem, A., Jelenová, K., Klement, A., 2018a. Influence of soil–water content on CO<sub>2</sub> efflux within the elevation transect heavily impacted by erosion. *Ecohydrology*, 2018; e1989.
- Fér, M., Kodešová, R., Golovko, O., Schmidtová, Z., Klement, A., Kočárek, M., Grabic, R., 2018b. Sorption of atenolol, sulfamethoxazole and carbamazepine onto soil aggregates from the illuvial horizon of the Haplic Luvisol on loess. *Soil Water Res.*, 13, 3, 177–183.
- Flint A.L., Flint L.E., 2002. Particle density, in: J.H. Dane, G.C. Topp (Eds.), *Methods of Soil Analysis. Part 4. Physical Methods*, Soil Science Society of America, Inc., Madison, USA, pp. 229–240.
- Frková, Z., Vystavna, Y., Koubová, A., Kotas, P., Grabicová, K., Grabic, R., Kodešová, R., Chroňáková, A., 2020. Microbial responses to selected pharmaceuticals 1 in agricultural soils: Microcosm study on the roles of soil, treatment and time. *Soil Biol. Biochem.*, 149, 107924.
- Gee, G.W., Or, D., 2002. Particle-size analysis, in: J.H. Dane, G.C. Topp (Eds.), *Methods of Soil Analysis. Part 4. Physical Methods*, Soil Science Society of America, Inc., Madison, USA, pp. 255–294.
- Golovko, O., Koba, O., Kodešová, R., Fedorova, G., Kumar, V., Grabic, R., 2016. Development of fast and robust multiresidual LC-MS/MS method for determination of pharmaceuticals in soils. *Environ. Sci. Pollut. R.*, 23, 14, 14068–14077.
- Grenni, P., Ancona, V., Caracciolo, A.B., 2018. Ecological effects of antibiotics on natural ecosystems: A review. *Microch. J.*, 136, 25–39.
- Hurtado, C., Montano-Chávez, Y.N., Domínguez, C., Bayona, J.M., 2017. Degradation of emerging organic contaminants in an agricultural soil: Decoupling biotic and abiotic processes. *Water Air Soil Poll.*, 228, 243.
- Iovieno, P., Băăth, E., 2008. Effect of drying and rewetting on bacterial rates in soil. *FEMS Microbiol. Ecol.*, 65, 400–407.
- ISO 10390, 2005. Soil quality-determination of pH. International Organization for Standardization, Geneva.
- Ivanová, L., Mackuľak, T., Grabic, R., Golovko, O., Koba, O., Vojs Staňová, A., Szabová, P., Grenčíková, A., Bodík, I., 2018. Pharmaceuticals and illicit drugs – a new threat to the application of sewage sludge in agriculture. *Sci. Total Environ.*, 634, 606–615.
- Jiang, J., Guo, S., Zhang, Y., Liu, Q., Wang, R., Wang, Z., Li, N., Li, R., 2015. Changes in temperature sensitivity of soil respiration in the phase of a three-year crop rotation system. *Soil Till. Res.*, 150, 139–146.
- Klement, A., Kodešová, R., Bauerová, M., Golovko, O., Kočárek, M., Fér, M., Koba, O., Nikodem, A., Grabic, R., 2018. Sorption of citalopram, irbesartan and fexofenadine in soils: estimation of sorption coefficients from soil properties. *Chemosphere*, 195, 615–623.
- Klement, A., Kodešová, R., Golovko, O., Fér, M., Nikodem, A., Kočárek, M., Grabic, R., 2020. Uptake, translocation and transformation of three pharmaceuticals in green pea plants. *J. Hydrol. Hydromech.*, 68, 1, 1–11.
- Kočárek, M., Kodešová, R., Vondráčková, L., Golovko, O., Fér, M., Klement, A., Nikodem, A., Jakšík, O., Grabic, R., 2016. Simultaneous sorption of four ionizable pharmaceuticals in different horizons of three soil types. *Environ. Pollut.*, 218, 563–573.
- Kodešová, R., Grabic, R., Kočárek, M., Klement, A., Golovko, O., Fér, M., Nikodem, A., Jakšík, O., 2015. Pharmaceuticals' sorptions relative to properties of thirteen different soils. *Sci. Total Environ.*, 511, 435–443.
- Kodešová, R., Kočárek, M., Klement, A., Golovko, O., Koba, O., Fér, M., Nikodem, A., Vondráčková, L., Jakšík, O., Grabic, R., 2016. An analysis of the dissipation of pharmaceuticals under thirteen different soil conditions. *Sci. Total Environ.*, 544, 369–381.
- Kodešová, R., Klement, A., Golovko, O., Fér, M., Nikodem, A., Kočárek, M., Grabic, R., 2019a. Root uptake of atenolol, sulfamethoxazole and carbamazepine, and their transformation in three soils and four plants. *Environ. Sci. Pollut. Res.*, 26, 10, 9876–9891.
- Kodešová, R., Klement, A., Golovko, O., Fér, M., Kočárek, M., Nikodem, A., Grabic, R., 2019b. Soil influences on uptake and transfer of pharmaceuticals from sewage sludge amended soils to spinach. *J. Environ. Manage.*, 250, 109407.
- Kodešová, R., Chroňáková, A., Grabicová, K., Kočárek, M., Schmidtová, Z., Frková, Z., Vojs-Staňová, A., Nikodem, A., Klement, A., Fér, M., Grabic, R., 2020. How microbial community composition, sorption and simultaneous application of six pharmaceuticals affect their dissipation in soils. *Sci. Total Environ.*, 746, 141134.
- Kuzyakov, Y., 2006. Sources of CO<sub>2</sub> efflux from soil and review of partitioning methods. *Soil Biol. Biochem.*, 38, 425–448.

- Meisner, A., Bååth, E., Rousk, J., 2013. Microbial growth responses upon rewetting soil dried for four days or one year. *Soil Biol. Biochem.*, 66, 188–192.
- Meisner, A., Rousk, J., Bååth, E., 2015. Prolonged drought changes the bacterial growth response to rewetting. *Soil Biol. Biochem.*, 88, 314–322.
- Molaei, A., Lakzian, A., Haghnia, G., Astaraei, A., Rasouli-Sadaghiani, M., Teresa Ceccherini M., Datta, R., 2017. Assessment of some cultural experimental methods to study the effects of antibiotics on microbial activities in a soil: An incubation study. *PLoS ONE*, 12, 7, e0180663.
- Moyano, F.E., Vasilyeva, N., Bouckaert, L., Cook, F., Craine, J., Curiel Yuste, J., Don, D., Epron, D., Formanek, P., Franzluebbers, A., Ilstedt, U., Kätterer, K., Orchard, V., Reichstein, M., Rey, A., Ruamps, L., Subke, J.-A., Thomsen, I.K., Chenu, C., 2012. The moisture response of soil heterotrophic respiration: interaction with soil properties. *Biogeosciences*, 9, 1173–1182.
- Moyano, F.E., Vasilyeva, N., Lorenzo, M., 2018. Diffusion limitations and Michaelis–Menten kinetics as drivers of combined temperature and moisture effects on carbon fluxes of mineral soils. *Biogeosciences*, 15, 5031–5045.
- OECD, 2002. Test No. 307: aerobic and anaerobic transformation in soil. In: *OECD Guidelines for the Testing of Chemicals, Section 3: Degradation and Accumulation*. OECD, ISBN: 9789264070509, 17 p.
- Pavlu, L., Kodešová, R., Fér, M., Nikodem, A., Němec, F., Prokeš, R., 2021. The impact of various mulch types on soil properties controlling water regime of the Haplic Fluvisol. *Soil Till. Res.*, 205, 104748.
- R Development Core Team, 2015. R: a language and environment for statistical computing. R foundation for Statistical Computing. (<http://www.R-project.org>).
- Rhoades, J.D., 1996. Salinity, electrical conductivity and total dissolved solids. In: Sparks, D.L., Page, A.L., Helmke, P.A., Loeppert, R.H., Soltanpour, P.N., Tabatabai, M.A., Johnston, C.T., Sumner, M.E. (Eds): *Methods of Soil Analysis. Part 3. Chemical Methods*. Soil Science Society of America, Inc., Madison, pp. 417–435.
- Schaffer, M., Licha, T., 2015. A framework for assessing the retardation of organic molecules in groundwater: implications of the species distribution for the sorption influenced transport. *Sci. Total Environ.*, 524–525, 187–194.
- Schaufler, G., Kitzler, B., Schindlbacher, A., Skiba, U., Sutton, M.A., Zechmeister-Boltenstern, S., 2010. Greenhouse gas emissions from European soils under different land use: effects of soil moisture and temperature. *Eur. J. Soil Sci.*, 61, 683–696.
- Schmidtová, Z., Kodešová, R., Grabicová, K., Kočárek, M., Fér, M., Švecová, H., Klement, A., Nikodem, A., Grabic, R., 2020. Competitive and synergic sorption of carbamazepine, citalopram, clindamycin, fexofenadine, irbesartan and sulfamethoxazole in seven soils. *J. Contam. Hydrol.*, 234, 103680.
- Shen, G., Zhang, Y., Hu, S., Zhang, H., Yuan, Z., Zhang, W., 2018. Adsorption and degradation of sulfadiazine and sulfamethoxazole in an agricultural soil system under an anaerobic condition: Kinetics and environmental risks. *Chemosphere*, 194, 266–274.
- Skjemstad, J., Baldock, J.A., 2008. Total and organic carbon. In: Carter, M. (Ed): *Soil Sampling and Methods of Analysis, (2nd Edition)*, Boca Raton, FL, USA. Soil Science Society of Canada, CRC Press, pp. 225–238.
- Srinivasan, P., Sarmah, A.K., 2014. Dissipation of sulfamethoxazole in pasture soils as affected by soil and environmental factors. *Sci. Total Environ.*, 479–480, 284–291.
- Thelusmond, J.R., Strathmann, T.J., Cupples, A.M., 2019. Carbamazepine, triclocarban and triclosan biodegradation and the phylotypes and functional genes associated with xenobiotic degradation in four agricultural soils. *Sci. Total Environ.*, 657, 1138–1149.
- WRB, 2015. World Reference Base for Soil Resources 2014, update 2015 International soil classification system for naming soils and creating legends for soil maps. World Soil Resources Reports No. 106. FAO, Rome.
- Xu, L., Baldocchi, D.D., Tang, J., 2004. How soil moisture, rain pulses, and growth alter the response of ecosystem respiration to temperature. *Global Biogeochem. Cy.*, 18, GB4002.
- Yuste, J.C., Baldocchi, D.D., Gershenson, A., Goldstein, A., 2007. Microbial soil respiration and its dependency on carbon inputs, soil temperature and moisture. *Glob. Change Biol.*, 13, 1–18.
- Verlicchi, P., Zambello, E., 2015. Pharmaceuticals and personal care products in untreated and treated sewage sludge: occurrence and environmental risk in the case of application on soil - a critical review. *Sci. Total Environ.*, 538, 750–767.
- Zhang, Y., Hu, S., Zhang, H., Shen, G., Yuan, Z., Zhang, W., 2017. Degradation kinetics and mechanism of sulfadiazine and sulfamethoxazole in an agricultural soil system with manure application. *Sci. Total Environ.*, 607–608, 1348–1356.
- Zhi, D., Yang, D., Zheng, Y., Yang, Y., He, Y., Luo, L., Zhou, Y., 2019. Current progress in the adsorption, transport and biodegradation of antibiotics in soil. *J. Environ. Manage.*, 251, 109598.
- Zhong, Y., Yan, W., Zong, Y., Shangguan, Z., 2016. Biotic and abiotic controls on the diel and seasonal variations in soil respiration and its components in a wheat field under long-term nitrogen fertilization. *Field Crop. Res.*, 199, 1–9.

Received 22 June 2020

Accepted 20 July 2020

# Atmospheric humidity is unlikely to serve as an important water source for crustose soil lichens in the Tabernas Desert

Giora J. Kidron<sup>1\*</sup>, Rafael Kronenfeld<sup>2</sup>

<sup>1</sup> Institute of Earth Sciences, The Hebrew University, Givat Ram Campus, Jerusalem 91904, Israel.

<sup>2</sup> Meteorological unit, Israel Meteorological Service, Kibbutz Sede Boqer 84993, Israel.

\* Corresponding author. Tel.: + 972-544-967-271. Fax: +972-2-566-2581. E-mail: kidron@mail.huji.ac.il

**Abstract:** Dew is commonly regarded as an important water source for lichens. This is also the case for crustose lichens that are attached to the substrate, whether rocks or soil. While being verified during ample research on rock-dwelling lichens in the Negev, the findings from soil-dwelling lichens (lichen biocrusts) are not conclusive. In the Tabernas Desert, the soil surface is characterized by a lush cover of crustose lichens. These soil biocrusts (biological soil crusts) were reported to use dew for photosynthesis while, at the same time, it was also observed that these crustose chlorolichens are relatively non-wettable. In an attempt to explore the apparent controversy, two year-long meteorological data (minimum air temperature and relative humidity, RH), during which chlorolichens were thought to utilize dew for photosynthesis (2006–2007) were analyzed. The analysis includes a comparison to the meteorological conditions that prevailed in the Negev during 135 days of manual dew measurements. As found for the Negev, net photosynthesis by the chlorolichens is expected once the RH, as measured at the meteorological station, is  $\geq 90\%$  while vapor condensation (dew) is expected once RH is  $\geq 95\%$ . RH in the Negev was substantially higher than the average RH of 75.0–87.2% registered during the rainless days of 2006–2007 in the Tabernas, implying that RH in the Tabernas is too low to facilitate frequent dew formation and net photosynthesis by the lichens. Photosynthesis in the Tabernas is mainly confined to rainy periods, taking place either due to direct wetting by rain, or following vapor condensation from the subsurface (distillation). Our findings do not support the view that dew is an important water source for the establishment and growth of crustose soil lichens in the Tabernas. Moreover, the low RH in the Tabernas may also imply that dew may only have a very limited role in providing water to lithobionts in this ecosystem.

**Keywords:** Biocrust; Cyanobacteria; Distillation; Lithobionts; Respiration; Negev Desert.

## 1 INTRODUCTION

Covering large areas in arid and semiarid regions, biocrusts (known also as biological soil crusts or microbiotic crusts) play an important role in shaping the ecosystem. They were reported to play an important role in surface stabilization (Jia et al., 2008; Kidron et al., 2017), runoff generation and subsequently water redistribution (Kidron and Yair, 1997; Lázaro et al., 2015), evaporation (Harper and Marble, 1988; Kidron and Tal, 2012; Wang et al., 2007), and organic carbon and nitrogen fixation (Elbert et al., 2012). They were also reported to affect seedling germination (Huang and Gutterman, 1998; Prasse and Bornkamm, 2000) and the growth of vascular plants (Kidron, 2019). Precisely due to their diverse functions, knowledge regarding their water source and growth conditions is of prime importance.

Two possible water sources may be utilized by biocrusts for photosynthesis: meteoric water (rain which either directly wets the biocrusts or indirectly via distillation, i.e., vapor stemming from the wet ground, which the lichens can use either as vapor or upon condensation as liquid water) and atmospheric humidity, i.e., vapor, dew and fog, known also as non-rainfall water (NRW). In addition to rain, dew and fog has long since been considered important water sources for biocrusts, whether cyanobacteria, cyanolichens (lichens with cyanobacteria as photobionts), chlorolichens (lichens with green algae as photobionts) or mosses (Jia et al., 2014; Rodríguez-Caballero et al., 2013; Thomas et al., 2011; Veste et al., 2001; Zhang et al., 2015). This conclusion partly stems from detailed measurements that were principally conducted in the Negev Desert,

Israel, during which high photosynthetic activity was registered for rock-dwelling (lithic) lichens.

In an attempt to observe good utilization of dew and fog by lithic lichens in the Negev, CO<sub>2</sub> exchange was measured within a closed chamber in which the interior conditions were controlled in accordance with the exterior (field) conditions (Kappen et al., 1979; Lange et al., 1970a, b). Thus for instance, during 355 days of continuous measurements of the lichen *Ramalina maciformis* (1972/73), 29 days (8.2%) were rainy and as expected resulted in a positive C balance. While the carbon balance was either zero or negative during 88 days (24.7%) of the remaining days, the lichen showed a net positive carbon balance during 53.3% of the days: during 172 dewy and foggy days (48.5%) and during additional 17 days (4.8%) during which the relative humidity was sufficiently high (Kappen et al., 1979). Accordingly, while the net photosynthetic yield may have reached 10 mg CO<sub>2</sub> g<sup>-1</sup> d<sup>-1</sup> on rainy days (attributed to daytime long activity and relatively low losses of carbon following respiration under the cool nocturnal conditions), it was up to 3 CO<sub>2</sub> g<sup>-1</sup> d<sup>-1</sup> during the winter dewy days, and 1–2 CO<sub>2</sub> g<sup>-1</sup> d<sup>-1</sup> during the warm late summer and fall dewy days. Being frequent, dew was thus regarded as a main water source for the lithic lichens in the Negev, leading many scholars to assume that dew and fog play an important role in the establishment and growth for many arid and semiarid soil biocrusts. This was also the case for the Tabernas Desert.

The Tabernas Desert is located in the semiarid SE Spain, approximately 20–25 km from the Mediterranean Sea (Fig. 1a), and inhabited by a lush cover of soil lichens (Fig. 1b). Dew formation was frequently reported as taking place in the

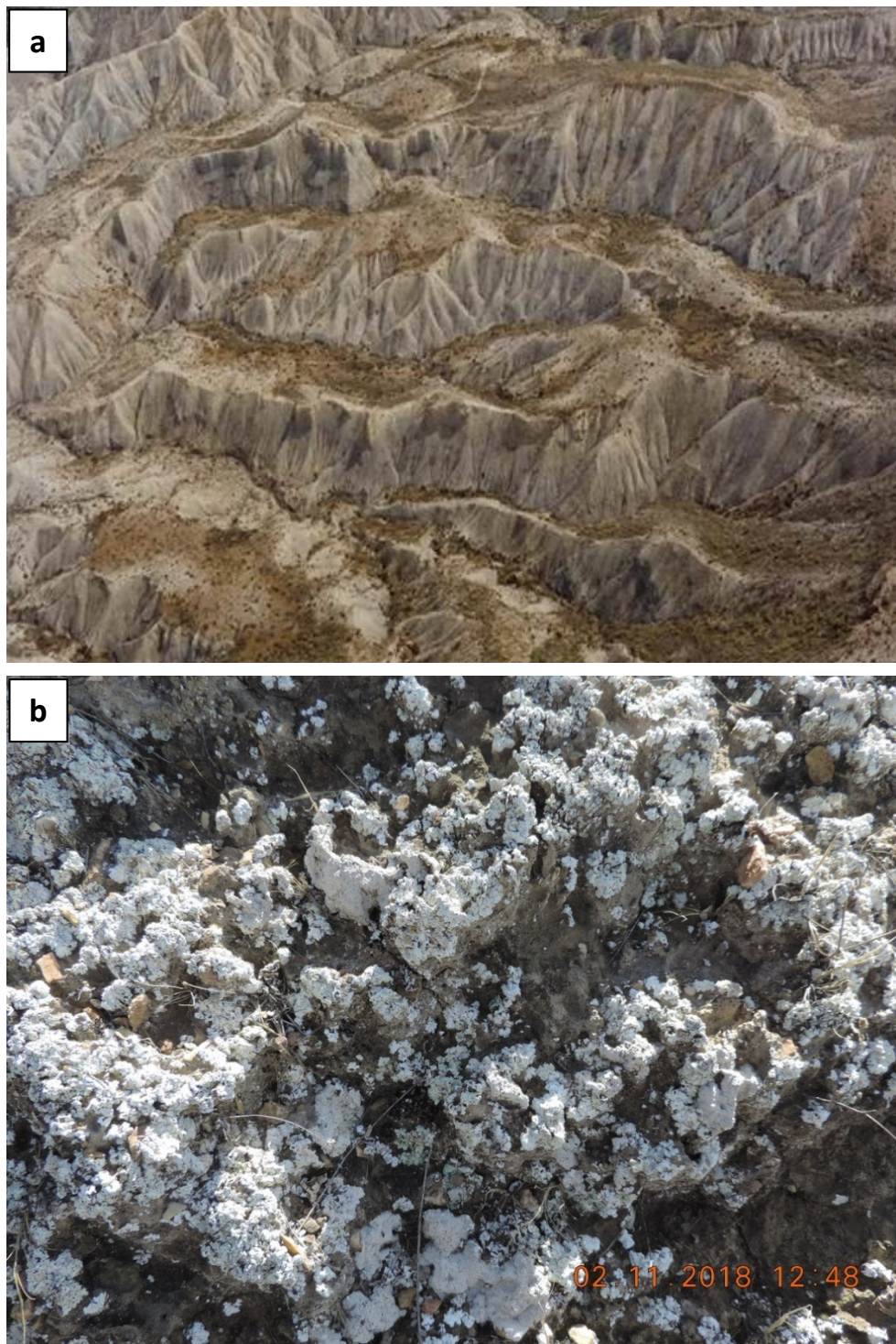


**Fig. 1.** General view (a) and a close look at the lichen biocrust (mostly *Diploschistes diacapsis*) at the Tabernas (b). Photographs courtesy of R. Lázaro.

Tabernas and its vicinity (Moro et al., 2007; Uclés et al., 2013, 2016). Although, as recently substantiated, the occurrence of dew in the Tabernas is actually infrequent as compared to the Negev Desert and therefore the Tabernas cannot be considered a dew desert (Kidron and Lázaro, 2020), many reports concluded that dew formation may play an important role as a water provider for this ecosystem. It was therefore assumed that dew will facilitate the survival and growth of many organisms, such as crustose soil lichens (Moro et al., 2007; Pintado et al., 2010), and will facilitate organism survival also during the harsh dry season (Uclés et al., 2016).

Nevertheless, there were also contradictory accounts, which do not comply with the assumption that surface moistening takes place following dew. For instance, Lázaro et al. (2008, p. 263) observe that during dewy mornings, the crustose lichens appear "waterproof", which is in agreement with detailed dew measurements that were conducted in the Negev biocrusts (Kidron and Kronenfeld, 2020a). While biocrust organisms that protrude above the soil surface, such as mosses, were found to utilize dew in the Negev, the contribution of dew to cyanobacteria or crustose lichens was found to be negligible (Kidron et al., 2002). It was postulated that either the amount is insuffi-

cient to allow for photosynthesis or that daytime photosynthesis is too short to compensate for the nocturnal carbon loss during nocturnal respiration, subsequently resulting in a negative carbon balance (Kidron and Starinsky, 2019; Kidron and Kronenfeld, 2020a).

The current research explores the absence of photosynthesis during certain summer months in the Tabernas (Pintado et al., 2010), and the apparent overestimation of the dew values reported by Uclés et al. (2013, 2016) from the Tabernas and/or its vicinity. According to Kidron and Kronenfeld (2017, 2020b), microlysimeters (MLs), used by Uclés et al. (2013, 2016) tend to overestimate the amount of dew and may therefore be unreliable in the assessment of the dew regime. It was argued that the air gap in between the two walls of the ML enhances nocturnal cooling (similarly to a loose cobble undergoing enhanced cooling in comparison to bedrock), subsequently overestimating the actual dew amounts formed on the soil surface. This implies that the amounts of dew capable of forming on the thalli of the crustose lichen may not be as high as reported, and may subsequently result in insufficient moisture to allow for lichen activation.

We propose that previously published values by Pintado et al. (2010) during 2006 and 2007 may have been erroneously attributed to dew, and that the published values of photosynthesis mainly reflect meteoric (rain) water (direct wetting by rain or distillation) rather than dew. In order to determine whether these values from the Tabernas reflect dew or rain we analyzed the meteorological data from 2006 and 2007 and undertook a comparison between this data from the Tabernas and the dew regime in a typical dew desert, the Negev Desert.

## 2 METHODOLOGY

### 2.1 The research site and previous measurements

The Tabernas Desert lies within the Rioja-Tabernas basin (~200–800 m above msl). It is formed by a series of parallel catchments on deeply dissected Toronian mudstone of marine origin, surrounded by high mountains, ~1400–2000 m above msl (Fig. 1a). The parent material is mainly composed of >60% silt-size gypsum-calcareous and siliceous particles, 20–35% of fine sand, and 5–10% of clay (for detailed account see Alexander et al., 2008). Average annual precipitation is 235 mm (Lázaro et al., 2001), with rain falling principally in fall and winter (40–50 rainy days, with an average of 36 rain events of >1 mm). Average annual temperature is 18°C; daily average maximum temperatures during the hottest and coldest months are 34.5°C and 17.5°C, respectively, whereas the average of daily minimums are 19.5°C and 4°C for the hottest and coldest month, respectively (Lázaro et al., 2000, 2001, 2004).

Biocrusts cover two thirds of the surface, mostly in between low-density (10–30%) shrubs and perennial grass, with the remaining surface exhibiting intense erosion (Cantón et al., 2004; Lázaro et al., 2001). Lichen and cyanobacterial crusts abound. Cyanobacterial biocrusts (dominated by *Microcoleus* sp.), accompanied by crustose lichens such as *Collema* spp., *Endocarpon pusillum*, and *Fulgensia* spp., mainly occupy the sun-exposed habitats (Miralles et al., 2012). A dark-coloured chlorolichen biocrust, dominated by *Psora decipiens*, also occupies the relatively sun-exposed habitats (gently sloping north-facing slopes). A whitish-coloured chlorolichen dominated biocrust with *Squamarina lentigera* and *Diploschistes diacapsis* (sometimes accompanied by *Buellia zoharyi*) predominates (Fig. 1b). This crust, mainly confined to the stable north-facing slopes, represents the late-successional stage of biocrusts at the site (Lázaro et al., 2008). Cyanolichens, such as *Collema* sp., are also present, but less abundant than chlorolichens.

Measurements of photosynthesis that were conducted in the Tabernas during 2006 and 2007 by Pintado et al. (2010) are used for the current analysis. These measurements were conducted on the predominant 1–3 mm thick crustose lichen in the Tabernas, *Diploschistes diacapsis*. Measurements included the maximum fluorescence emitted by the lichens using a pulse amplitude modulated fluorometer (Minipam, Walz, Germany), with the fiber-optic probe permanently fixed to the ground pointing at the sample lichen. A modulated inciting low red light was used to measure Ft fluorescence followed by saturating pulse (8000  $\mu\text{mol photon m}^{-2} \text{s}^{-1}$ ) that allow for the determination of the maximal fluorescence, Fm'. The effective PSII quantum yield was then calculated as  $\Delta F/\text{Fm}'$ , where  $\Delta F = \text{Fm}' - \text{Ft}$  (Schreiber, 2004). The values (referred hereafter as photosynthesis) were automatically recorded (at 0.5 h interval) and stored in a data logger. A positive PSII indicated that the lichen is active and hydrated.

The published results showed high variability. Figure 2a, 2b and 2c show the amount of rainy days, the amount of rain, and the monthly number of hours of daylight photosynthetic activity for the 2006–2007 respectively. Figure 3a, 3b, and 3c show the relationships between the amount of rainy days, the rain amount, and the average monthly RH and the monthly number of hours of daylight photosynthetic activity of the lichens, respectively. Whereas no daylight photosynthetic activity was recorded for a total of four months (July and August 2006 and June and July 2007), small or even negligible activity (< 50 h) was recorded for some of the months (March, April, June, September, October and December, 2006 and March, May, August, September and November, 2007). Long activity (> 100 h) was recorded during a few months (January and November, 2006 and January and October, 2007), with the remaining months showing intermediate values.

### 2.2 Methods

We conducted an analysis of the meteorological data from the Tabernas during January 2006 until December 2007 from a near-by meteorological station (8 km northeast of the town of Tabernas, 37°05'28"N; 02°18'08"W, operated by the Andalusian official meteorological unit). The data included the daily rain amount, the relative humidity (RH), and air temperatures (Ta). Our calculations were based on the minimum air temperatures during which the likelihood for vapor condensation is the highest. Td was calculated in accordance with the equation proposed by Lawrence (2005):

$$T_d = T_a - (100 - \text{RH})/5 \quad (1)$$

where Td = dew point temperature (°C); Ta = air temperature (°C) and RH = relative humidity (%).

Additionally, and for the sake of comparison, we analyzed dew measurements from Sede Boqer, the Negev Highlands (Israel), and compared them to the relevant meteorological data (RH, Ta, Td) from a nearby meteorological station, 150 m south of the Sede Boqer site (30°56'N; 34°23'E, operated by the Israel Meteorological Service). Assuming that the conditions determining vapor condensation and dew formation are universal (Beysens, 1995; Monteith, 1957), we infer from the climatological condition conducive to dew formation in the Negev that similar conditions might be conducive to dew formation in the Tabernas. Data collected in the Negev Desert is assumed to be reliable also due to the proximity between the meteorological station and the research site where manual dew measurements took place.

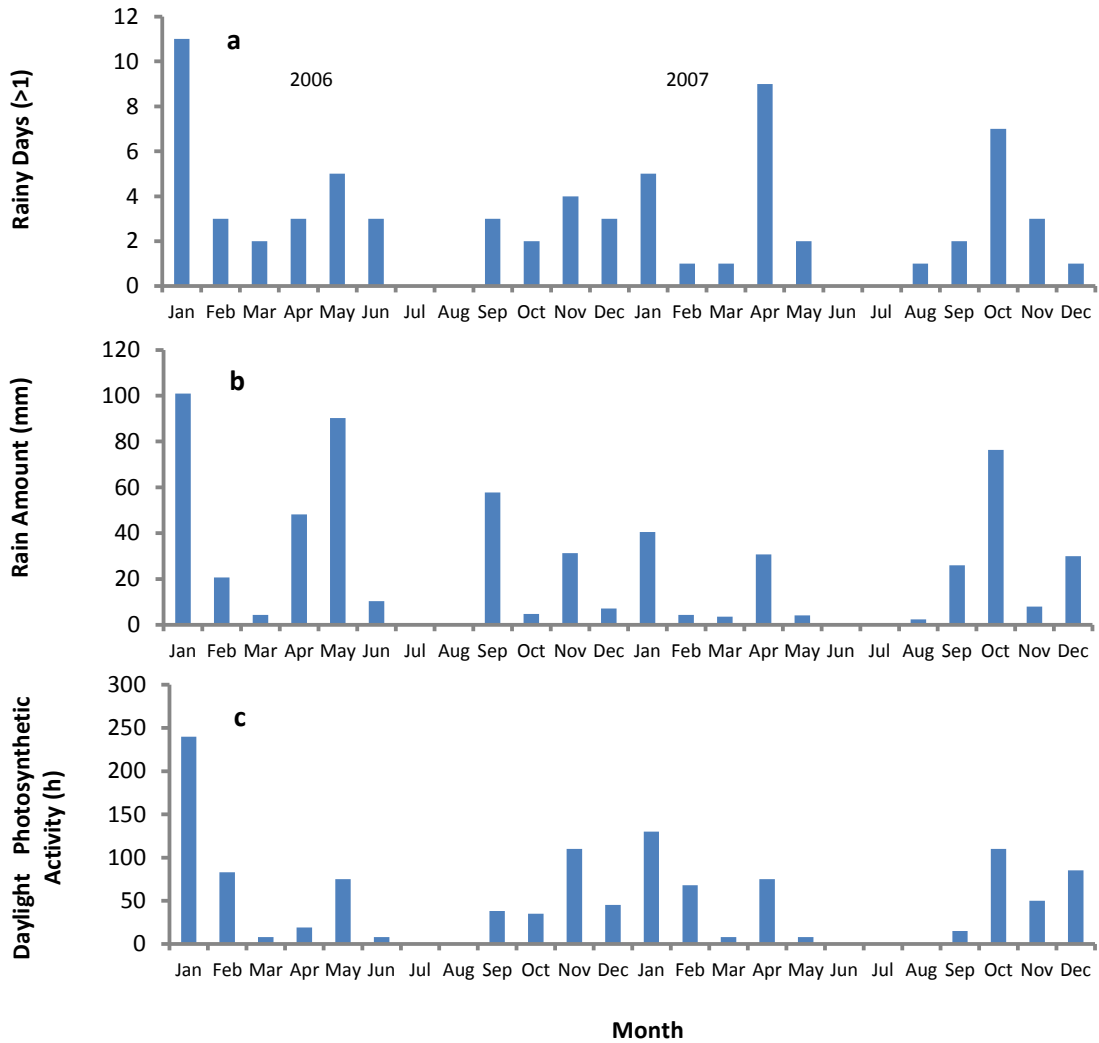


**Fig. 2.** Monthly amounts of rainy days >1 mm (a), rain amount (b) and daylight photosynthetic activity (c) as recorded during 2006 and 2007 (after Pintado et al., 2010).

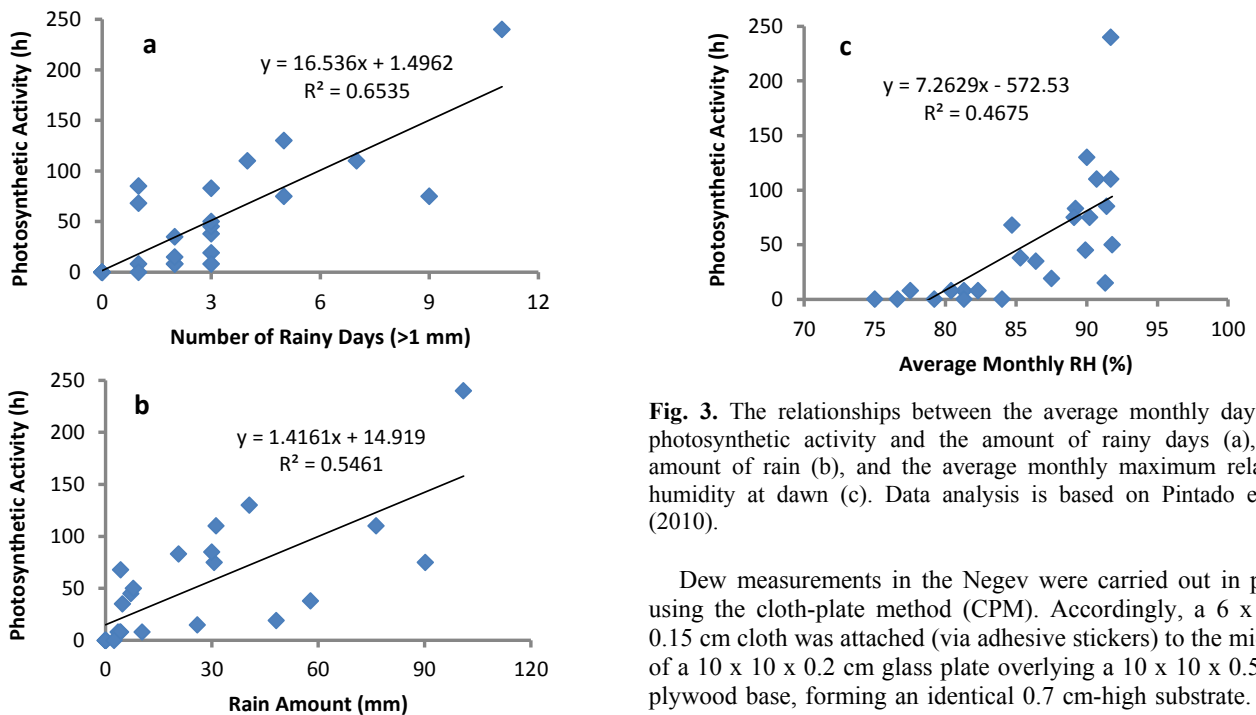


**Fig. 3.** The relationships between the average monthly daylight photosynthetic activity and the amount of rainy days (a), the amount of rain (b), and the average monthly maximum relative humidity at dawn (c). Data analysis is based on Pintado et al. (2010).

Dew measurements in the Negev were carried out in pairs using the cloth-plate method (CPM). Accordingly, a 6 x 6 x 0.15 cm cloth was attached (via adhesive stickers) to the middle of a 10 x 10 x 0.2 cm glass plate overlying a 10 x 10 x 0.5 cm plywood base, forming an identical 0.7 cm-high substrate. The cloths were attached in the late afternoon and collected during

the early morning of the following day. They were placed into separate flasks, weighed, oven-dried at 70°C until completely dried out and reweighed. A total of 135 days of dew measurements were carried out, facilitating a comparison between the dew amounts and the meteorological variables of the adjacent meteorological station.

In addition, measurements that were conducted with cloths directly attached to the soil during the fall of 2009 (using pins) were compared to adjacent cloths attached to the glass plates (CPM). All cloths were concomitantly attached to the surface during the afternoons and concomitantly collected during the following morning as described above.

We are aware of the fact that due to the screen effect of the meteorological station, the RH and Ta, as measured by the station, may underestimate the values recorded in an unsheltered space outdoors (see also below). Similarly, the actual Td in the field may be slightly lower than that calculated for the meteorological station. Nevertheless, by comparing the outdoor dew values with the data recorded by the meteorological station in the Negev, the relevant threshold for dew formation in the field may be assessed.

### 3 RESULTS AND DISCUSSION

Determining the variable role of different water sources – the role of meteoric water or atmospheric humidity – may be difficult. This is all the more so in the Tabernas Desert, where manual measurements are not available and where the rainless period is relatively short, and thus, both water sources may concomitantly play a role in providing water for lichen photosynthesis. A distinction is however possible once the apparent role played by atmospheric humidity is examined during rainless periods.

The data published by Pintado et al. (2010) do not allow for daily analysis, therefore requiring a more crude (monthly) analysis. Accordingly, and once excluding a few days with very low precipitation (June 6<sup>th</sup> and 14<sup>th</sup>, 2006 with 1.4 and 2.6 mm, respectively, and August 22<sup>nd</sup>, 2007 with 1.7 mm), two rainless periods are noted during the 2006–2007 measurement periods: from June 3<sup>rd</sup> to September 11<sup>th</sup>, 2006 and from June 1<sup>st</sup> to September 10<sup>th</sup>, 2007 (Fig. 2a, b). In order to evaluate the possible role played by atmospheric humidity (for simplicity, all NRW will be referred hereafter as dew), we focused on the analysis of these periods. These periods (and especially August and September) have relatively clear skies and long nights conducive to dew formation (Veste and Littmann, 2006; Zangvil, 1996), and as such should provide relatively higher dew amounts, as found indeed in many parts of the world (Monteith, 1957; Baier, 1966; Tuller and Chilton, 1973; Zhang et al., 2015), including southeast Spain (Uclés et al., 2015).

Analysis can be undertaken by using the meteorological variables measured at the meteorological station in the Tabernas. Figure 4a shows the distribution of RH during the months of June, July, August and the first third of September, as monitored at the meteorological station. As can be noted, a slight increase is apparent from June to September. Yet, the monthly average RH values (75.0–87.2%) were lower than the values recorded 3–5 days following eight >10 mm rain events, which ranged between 75.3–94.5% (Fig. 4b).

In order to better evaluate the atmospheric conditions conducive for dew formation in the Tabernas, we took advantage of the large amounts of data available from the Negev. In the Negev, dew measurements were principally conducted using the cloth-plate method (CPM). Subsequent measurements were also conducted aiming to study the relationship between the

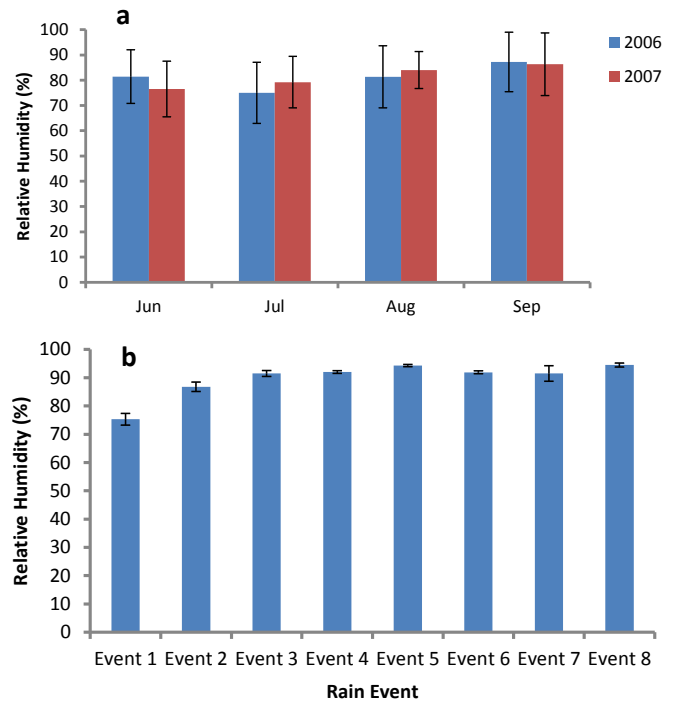


**Fig. 4.** Average dawn values of RH during the summer rainless period of June 3<sup>rd</sup> to September 11<sup>th</sup>, 2006, and June 1<sup>st</sup> to September 10<sup>th</sup> of 2007 (a), and during 3–5 days following 8 rainstorms with  $\geq 10$  mm during 2006 and 2007 (b). Bars represent one SE. Event 1 = 45 mm during 12–14.9.06; event 2 = 13 mm during 23.9.06; event 3 = 10 mm during 3.11.06; event 4 = 18 mm during 7–8.10.06; event 5 = 20 mm during 21.9.07; event 6 = 10 mm during 3.10.07; event 7 = 53 mm during 16–19.10.07; event 8 = 28 mm during 26.12.07.

dew formed on the cloths attached to the glass plates to those directly attached to the soil surface. Our analysis was in line with the detailed measurements of dew and lichen photosynthesis in the Negev (Kappen et al., 1979; Lange et al., 1986, 1992) and calculations of the corresponding dew amounts required for net photosynthesis. Accordingly, minimum amounts of 0.05 and 0.1 mm of dew were found as the thresholds for net photosynthesis of the chlorolichens, and the cyanolichens (or cyanobacteria), respectively (Kidron and Starinsky, 2019).

Figure 5 presents data from long-term periodical measurements in the Negev Highlands (during 2009, 2010, 2014, 2015, 2016, 2018), which include dew values, as measured during 135 days, and the correspondent relative humidity as measured at the adjacent ( $\leq 1.5$  km) Sede Boqer meteorological station. An important conclusion emerges from Figure 5: the relative humidity at the meteorological station which is required to reach the 0.05 and the 0.1 mm thresholds in the field are  $\sim 90\%$  and  $\sim 95\%$ , respectively. In other words, the amount of vapor that accumulated on the cloths attached to the glass plates reaches 0.05 mm only once the RH, as measured at the meteorological station, reaches  $\sim 90\%$ . Notably, the amounts condensed on the glass plates can be relevant for lithobionts, i.e., cobble-dwelling lichens, as the amounts condensed on the glass plates are similar to those condensed on 10 cm-high lichen-inhabited cobbles (Kidron, 2000).

The close link between the amounts accumulating on cloths and the lichen thalli (Kidron et al., 2014) implies that under the same conditions during which the cloths and the lichen thalli are attached on the same substrate, the same amount will also accumulate on the lichen thalli. It follows that both substrates (cloths, thalli) reach the same threshold (0.05 mm) concomitantly.

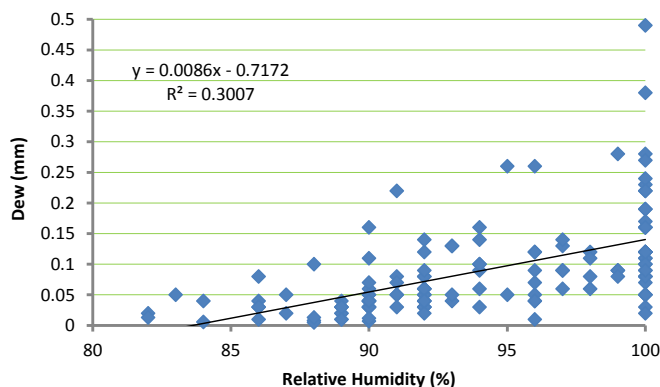


**Fig. 5.** Long-term relationship ( $N = 135$  days) between relative humidity (as measured by a meteorological station) and dew amount (as measured by the CPM) in the Negev Highlands (Sede Boqer). The measurements were carried out periodically during the late summer and fall of 2009, 2010, 2014, 2015, 2016, and 2018.

The threshold for dew formation of 0.1 mm will be reached only when RH at the meteorological station is  $\geq 95\%$ . Since water condensation requires RH of 100%, it implies that once the RH recorded at the meteorological station reaches 95%, it reaches 100% on the outdoor glass plate. The lower RH at the meteorological station reflects the slightly warmer conditions within the shielded screen of the meteorological station.

Indeed, following inversion and the lower near-surface wind velocity, minimum air temperatures under outdoor open conditions are lower than that of the meteorological station, entailing that the dew temperature is reached sooner under outdoor conditions. This is shown in Figure 6a in which two-month temperature values (July and August, 2018) that were conducted at and adjacently to a standard 2 m-high meteorological station (Beer Sheva, Israel,  $32^{\circ}00'N$ ;  $34^{\circ}90'E$ .) are presented. These measurements are part of the data collected by the Israel Meteorological Service. On average, near surface minimum temperatures (at 10 cm-height) were 1.2 K lower (with a range of 0.2–2.5 K) than that at the meteorological station. Notably, in comparison to variable heights above surface (0.7, 20, 30, 40, 50 cm), 10 cm-height glass plates yielded the higher dew amounts (Kidron, 1998). The higher amounts at 10 cm-height above ground in comparison to 0.7 cm-height above ground were explained by the cooler temperatures at this height, which are less impacted by the heat flux emitted from the soil. The higher amounts at 10 cm-height above ground in comparison to 20–50 cm-height above ground were explained by the higher wind velocities at height, which negatively affect the inversion conditions (Kidron, 1998; Kidron et al., 2000).

Concomitant dew measurements conducted during 17 dewy days on cloths attached to glass plates (CPM) and on cloths directly attached (via pins) to the soil surface (CoS) and therefore mimicking crustose soil lichens are shown in Figure 6b. Substantially higher amounts (by a factor of 3.38) were recorded on the glass plates, which reflect the thermal properties of the glass substrate, the isolating effect of the 10 x 10 cm plate from the heat flux emitted by the underlying soil, and the higher height (0.7 cm above ground) of the glass plate (Kidron, 1998).

The above data facilitate an analysis of the dew measurements in the Negev Highlands during which dew amounts and dew duration (as determined by half a dozen adjacently placed plates, and the continuous collection of the cloths in 0.5–1 h intervals during the morning hours) were measured. Figure 7a shows the relationship between dew amount ( $> 0.05$  mm) and duration (calculated for the CoS by dividing the CPM data by

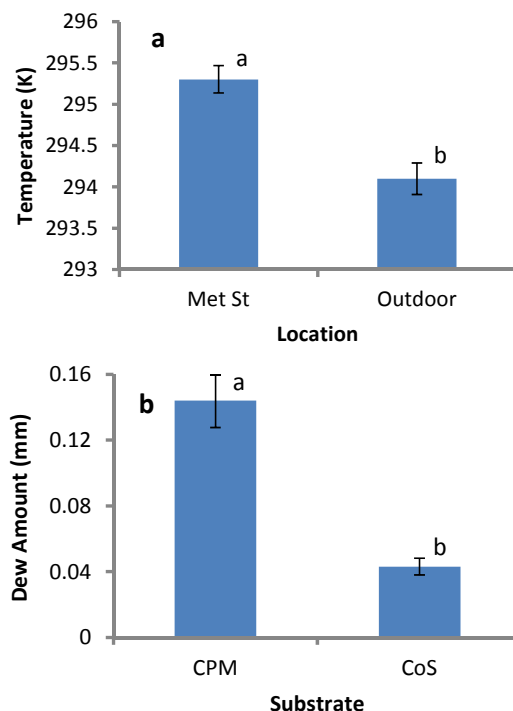


**Fig. 6.** Concomitant temperature values as measured by the Israeli Meteorological Service within and outdoors at 10 cm-height of the meteorological (Met) station of Beer Sheva during July and August, 2018 (a), and the amount of dew as measured concomitantly during 17 days by CPM (cloths attached to glass plates) and on cloths directly attached to the soil (CoS) in Sede Boqer, Negev Highlands (b). Bars represent one SE. Different letters represent significant differences (paired-*t*-test;  $P < 0.05$ ).

3.38) in the Negev (Sede Boqer). Substantially higher amounts and longer duration characterized the CPM, in agreement with previous findings that showed a high correlation between dew amount and duration (Kidron et al., 2000).

Figure 7b and 7c show the relationships between RH (as measured during these measurement days at the meteorological station) and the calculated dew amount and duration, respectively. As expected, while a relative humidity of  $\geq 95\%$ , as measured at the meteorological station, yielded dew amounts of 0.15–0.2 mm on the glass plates and lasted for  $\sim 2.5$  h, it corresponded to only  $< 0.05$  mm of dew lasting for  $< 1$  h on cloths attached to the soil surface.

The above analysis can be useful for studying the potential conditions for dew formation in the Tabernas. As already indicated above, a relatively low RH was recorded during the rainless periods in the Tabernas (Fig. 4a). Only once RH  $> 95\%$  was recorded (95.5% during July 11<sup>th</sup>, 2007). Similar findings were also found for the rainless months of June, July, August, and September of 2003–2012 in the Tabernas, during which RH  $> 95\%$  occurred on average for only 0.9–1.1 days a month (Kidron and Lázaro, 2020). These values imply that dew formation is relatively infrequent.

This conclusion is also supported by calculation of the dew-point temperatures. According to Beysens (2018), nights during which the differences between the air temperature ( $T_a$ ) and the dew-point temperature ( $T_d$ ), i.e.,  $T_a - T_d$  are minor have greater likelihood to form dew. In comparison to the Negev during which the differences between  $T_a$  and  $T_d$  were minor (1.4, 0.9 and 0.55 K for dewy days with 0.05, 0.06–0.09 and  $\geq 0.10$  mm, respectively), the differences between  $T_a$  and  $T_d$  for the rainless period of 2006 and 2007 in the Tabernas were 4.0 and 3.9 K, respectively.

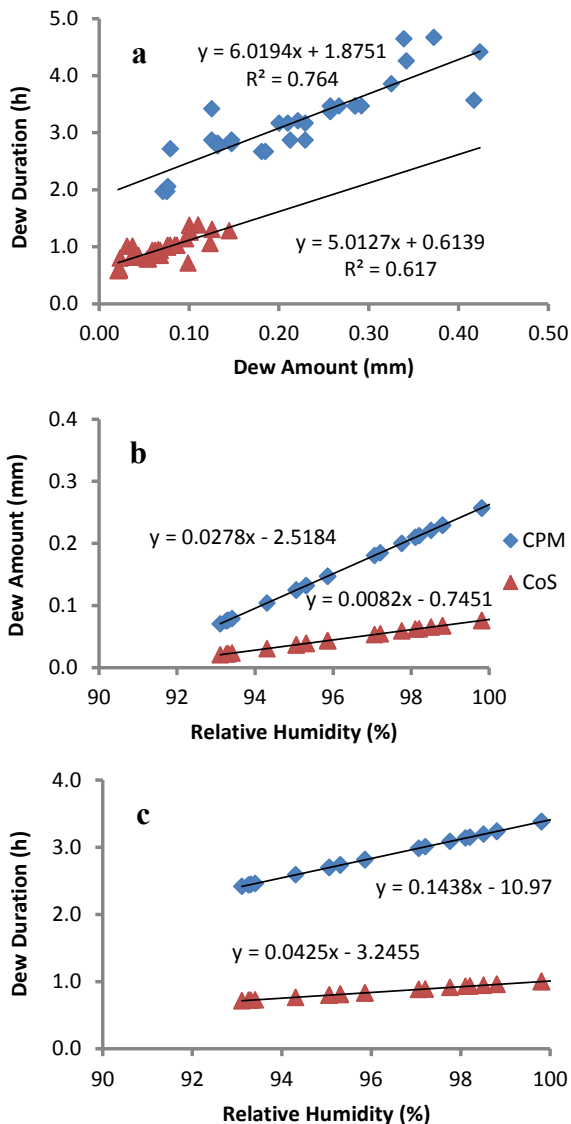


**Fig. 7.** The relationships between dew amount and duration as measured on the glass plates and calculated for cloths attached to the soil surface (a), and the calculated relationships between the relative humidity and (b) dew amount and (c) duration for cloths attached to the glass plates and the soil surface.

The substantially higher values calculated for the Tabernas may suggest that the likelihood for vapor condensation for the rainless period in the Tabernas is rather low.

With 1.5 mm-thick cloths potentially mimicking 1.5 mm-thick thalli, the analysis presented above may be relevant for lichens. Even for thicker (3 mm-thick) thalli (which corresponds to the maximal thickness of *Diploschistes diacapsis*), the values will be extremely low. According to Kidron et al. (2002), the dew amount at 3 mm-height is 1.35 times higher than that of the 1.5 mm-height, implying that at RH of 95% at the meteorological station, dew at 3 mm-above ground will only reach 0.05 mm (Fig. 7b), which may only last for ~1 h (Fig. 7c). Not only does dew amount marginally suffice to activate 3 mm-thick lichens, but activation may not necessarily result in net photosynthesis.

This was verified during detailed photosynthesis measurements. According to Tuba et al. (1996) and Csintalan et al. (2000), the time duration during which dew is available is of paramount importance for the carbon balance. According to

these authors, >2 h of carbon gain by photosynthesis is required in order to compensate for carbon loss during nocturnal respiration. According to the current calculations, the threshold of > 2 h of dew duration during the summer months and early fall may only rarely be reached in the Tabernas, implying that the input of atmospheric moisture in the Tabernas is below the necessary threshold required by the lichens to achieve net photosynthesis. And thus, even when occasionally moistened by dew, water availability may not last long enough to allow for a positive carbon balance.

The current analysis supports the *data* obtained by Pintado et al. (2010) that did not show photosynthetic activity during the rainless months of June, July, August and the first third of September. Yet, it raises doubts regarding the *conclusions* reached by these authors which considered dew an important water source for lichen photosynthesis during the remaining months. While it is not suggested herein that dew will never result in net photosynthesis, it is argued that it is uncommon and may mainly take place during the rainy season and therefore will not play an important ecological role in the survival of lichens during the rainless season.

The current analysis points therefore to the possibility that meteoric water, rather than dew, may be overwhelmingly responsible for net photosynthesis of the crustose soil lichens in the Tabernas. Thus, the extensive activity of the lichens, as reported by Pintado et al. (2010) during the early morning hours of the rainy season may largely stem from distillation, which mainly takes place due to rain-induced wet ground during the cool morning hours (Monteith, 1957). This conclusion is also supported by the high RH values recorded after rain (Fig. 4b), and the higher correlation obtained between the amount of rainy days and the monthly photosynthesis of the Tabernas lichens (Fig. 3a).

In this regard it is worth noting that no net photosynthesis was yet reported for crustose soil lichens in the Negev. Photosynthesis by crustose lichens was recorded only once (March 10<sup>th</sup>, 1999) during a rainless morning in the western Negev (Veste et al., 2001). Nevertheless, as indicated by the authors, the time duration was very short, too short to assume net photosynthesis. Similar results were obtained by Wilske et al. (2008) following photosynthetic measurements of crustose lichens in the northern Negev. While net photosynthesis, which characterized the lichens during wet winter days was partially attributed also to dew, no attempt was made to distinguish between dew and distillation, and the results could have reflected distillation, as one may conclude from the negative carbon balance that was obtained during the relatively rainless months of the winter (Wilske et al., 2008). Specifically, as noted by Wilske et al. (2008), no net photosynthesis was recorded even following light rains, a phenomenon attributed to the short duration during which sufficient moisture is present on the soil surface. This was in agreement with the findings reported by Kidron et al. (2002) following >50 days of dew measurements in the Negev. These authors reported of only one occasion during which limited moistness following dew took place on the ground, concluding that crustose biocrusts were only rarely wetted by dew.

Our findings do not support the view that dew is an important water source for the establishment and growth of crustose soil lichens in the Tabernas. The data also point to the possibility that the low RH values in the Tabernas may not even suffice to play an important role for rock or cobble dwelling lichens (lithobionts). The lush cover of the soil lichens in the Tabernas may therefore principally stem from rain precipitation (Lázaro, 2004).

#### 4 CONCLUSIONS

By comparing the climatological conditions (air temperatures and relative humidity, RH) during the years 2006 and 2007 in the Tabernas to published data on photosynthetic activity of soil lichens during the same period, it is concluded that dew formation on the crustose soil lichens is relatively unlikely. As found for the Negev Desert during 135 days of manual dew measurements, vapor condensation under unsheltered field conditions requires  $RH \geq 95\%$  at the meteorological station, while net photosynthesis by the chlorolichens require  $RH \geq 90\%$ . The average RH values recorded during the rainless months of 2006 and 2007 in the Tabernas were however substantially lower (75.0–87.2%), with only a single night during which  $RH > 95\%$  was recorded. The lower RH values at the Tabernas, coupled with the fact that positive carbon balance is contingent upon the persistence of dew on the ground for  $\geq 2$  h under daylight conditions, leads us to conclude that the use of dew by crustose soil lichens for growth in the Tabernas is relatively unlikely. Contrary to previous assumptions, dew (atmospheric humidity) cannot be seen as an important water source for the crustose soil lichens in the Tabernas, which therefore principally rely on rain (meteoric water) for growth.

*Acknowledgements.* This study was facilitated thanks to Roberto Lázaro, who provided the meteorological data and useful suggestions, and substantially improved the manuscript. His help is greatly acknowledged. The editing by Carol A. Kidron and valuable comments of two anonymous reviewers are highly appreciated.

#### REFERENCES

- Alexander, R.W., Calvo-Cases, A., Arnau-Rosalén, E., Mather, A.E., Lázaro-Suau, R., 2008. Erosion and stabilization sequences in relation to base level changes in the El Cautivo badlands, SE Spain. *Geomorphology*, 100, 83–90.
- Baier, W., 1966. Studies on dew formation under semi-arid conditions. *Agric. Forest Meteorol.*, 3, 103–112.
- Beysens, D., 1995. The formation of dew. *Atmos. Res.*, 39, 215–237.
- Beysens, D., 2018. *Dew Water*. River Publishers, Gistrup, Denmark, 305 p.
- Cantón, Y., Del Barrio, G., Solé-Benrt, A., Lázaro, R., 2004. Topographic controls on the spatial distribution of ground cover in the Tabernas badlands of SE Spain. *Catena*, 55, 341–365.
- Csintalan, Z., Takács, Z., Proctor, M.C.F., Nagy, Z., Tuba, Z., 2000. Early morning photosynthesis of the moss *Tortula ruralis* following summer dew fall in a Hungarian temperate dry sandy grassland. *Plant Ecol.*, 151, 51–54.
- Elbert, W., Weber, B., Burrows, S., Steinkamp, J., Büdel, B., Andrea, M.O., Pöschl, U., 2012. Contribution of cryptogamic covers to the global cycles of carbon and nitrogen. *Nat. Geosci.*, 5, 459–462.
- Harper, K.T., Marble, J.R., 1988. A role for nonvascular plants in management of arid and semiarid rangelands. In: Tuller, P.T. (Ed.): *Applications of Plant Sciences to Rangeland Management and Inventory*. Kluwer, Amsterdam, pp. 135–169.
- Huang, Z., Gutterman, Y., 1998. *Artemisia monosperma* achene germination in sand: effects of sand depth, sand water content, cyanobacterial sand crust and temperature. *J. Arid Environ.*, 38, 27–43.
- Jia, R.L., Li, X.R., Liu, L.C., Gao, Y.H., Li, X.J., 2008. Responses of biological soil crusts to sand burial in revegetated area of the Tengger Desert, Northern China. *Soil Biol. Biochem.*, 40, 2827–2834.
- Jia, R.L., Li, X.R., Liu, L.C., Pan, Y.X., Gao, Y.H., Wei, Y.P., 2014. Effects of sand burial on dew deposition on moss soil crust in a revegetated area of the Tengger Desert, Northern China. *J. Hydrol.*, 519, 2341–2349.
- Kappen, L., Lange, O.L., Schulze, E.-D., Evenari, M., Buschbom, V., 1979. Ecophysiological investigations on lichens of the Negev Desert, IV: Annual course of the photosynthetic production of *Ramalina maciformis* (Del.) Bory. *Flora*, 168, 85–105.
- Kidron, G.J., 1998. A simple weighing method for dew and fog measurements. *Weather*, 53, 428–433.
- Kidron, G.J., 2000. Dew moisture regime of endolithic and epilithic lichens inhabiting calcareous cobbles and rock outcrops, Negev Desert, Israel. *Flora*, 195, 146–153.
- Kidron, G.J., 2019. The dual effect of sand-covered biocrusts on annual plants: increasing cover but reducing individual plant biomass and fecundity. *Catena*, 182, 104120.
- Kidron, G.J., Kronenfeld, R., 2017. Assessing the effect of micro-lysimeters on NRWI: Do micro-lysimeters adequately represent the water input of natural soil? *J. Hydrol.*, 548, 382–390.
- Kidron, G.J., Kronenfeld, R., 2020a. Assessing the likelihood of the soil surface to condense vapor: The Negev experience. *Ecohydrology*, 2020; e2200.
- Kidron, G.J., Kronenfeld, R., 2020b. Microlysimeters overestimate the amount of non-rainfall water – An experimental approach. *Catena*, 194, 104691.
- Kidron G.J., Lázaro, R., 2020. Are coastal deserts necessarily dew deserts? An example from the Tabernas Desert. *J. Hydrol. Hydromech.*, 68, 19–27.
- Kidron, G.J., Tal, S.Y., 2012. The effect of biocrusts on evaporation from sand dunes in the Negev Desert. *Geoderma*, 179–180, 104–112.
- Kidron, G.J., Starinsky, A., 2019. Measurements and ecological implications of non-rainfall water in desert ecosystems – a review. *Ecohydrology*. 2019; e2121.
- Kidron, G.J., Yair, A., 1997. Rainfall-runoff relationships over encrusted dune surfaces, Nizzana, Western Negev, Israel. *Earth Surf. Process. Landf.*, 22, 1169–1184.
- Kidron, G.J., Herrnstadt, I., Barzilay, E., 2002. The role of dew as a moisture source for sand microbiotic crusts in the Negev Desert, Israel. *J. Arid Environ.*, 52, 517–533.
- Kidron, G.J., Starinsky, A., Yaalon, D.H., 2014. Dewless habitat within a dew desert: Implications for weathering and terrestrial evolution. *J. Hydrol.*, 519, 3606–3614.
- Kidron, G.J. Yair, A., Danin, A., 2000. Dew variability within a small arid drainage basin in the Negev highlands, Israel. *Quart. J. Royal Meteorol. Soc.*, 126, 63–80.
- Kidron, G.J., Ying, W., Starinsky, A., Herzberg, M., 2017. Drought effect on biocrust resilience: High-speed winds result in crust burial and crust rupture and flaking. *Sci. Total Environ.*, 579, 848–859.
- Lange, O.L., Schulze, E.D., Koch, W., 1970a. Ecophysiological investigations on lichens of the Negev Desert, II: CO<sub>2</sub> gas exchange and water conservation of *Ramalina maciformis* (Del.) Bory in its natural habitat during the summer dry period. *Flora*, 159, 38–62.
- Lange, O.L., Schulze, E.D., Koch, W., 1970b. Ecophysiological investigations on lichens of the Negev Desert, III: CO<sub>2</sub> gas exchange and water metabolism of crustose and foliose li-

- chens in their natural habitat during the summer dry period. *Flora*, 159, 525–538.
- Lange, O.L., Kilian, E., Ziegler, H., 1986. Water vapor uptake and photosynthesis of lichens: performance differences in species with green and blue-green algae as phycobionts. *Oecologia*, 71, 104–110.
- Lange, O.L., Kidron, G.J., Büdel, B., Meyer, A., Kilian, E., Abeliovitch, A., 1992. Taxonomic composition and photosynthetic characteristics of the biological soil crusts covering sand dunes in the Western Negev Desert. *Func. Ecol.*, 6, 519–527.
- Lawrence, M.G., 2005. The relationship between relative humidity and the dewpoint temperature in moist air. *Bull. Am. Meteorol. Soc.*, 86, 225–233.
- Lázaro, R., 2004. Implications of precipitation on vegetation of water-limited lands. In: Pandalai, S.G. (Ed): *Recent Research Development in Environmental Biology*, Vol. I. Research Signpost, Kerala (India), pp. 553–591.
- Lázaro, R., Alexander, R.W., Puigdefábregas, J., 2000. Cover distribution patterns of lichens, annuals and shrubs in the Tabernas Desert, Almería, Spain. In: Alexander, R.W., Millington, A.C. (Eds.): *Vegetation Mapping: from Patch to Planet*. Wiley, Chichester, pp. 19–40.
- Lázaro, R., Rodríguez-Tamayo, M.L., Ordiales, R., Puigdefábregas, J., 2004. El Clima. In: Mota, J., Cabello, J., Cerrillo, M.I., Rodríguez-Tamayo, M.L. (Eds.): *Subdesiertos de Almería: naturaleza de cine*. Consejería de Medio Ambiente, Junta de Andalucía. Almería, pp. 63–79.
- Lázaro, R., Calvo-Cases, A., Lázaro, A., Molina, I., 2015. Effective run-off flow length over biological soil crusts on silty loam soils in drylands. *Hydrol. Process.*, 29, 2534–2544.
- Lázaro, R., Rodrigo, F.S., Gutiérrez, L., Domingo, F., Puigdegabregas, J., 2001. Analysis of 30-year rainfall record (1967–1997) in semi-arid SE Spain for implications on vegetation. *J. Arid Environ.*, 48, 373–395.
- Lázaro, R., Cantón, Y., Solé-Benet, A., Bevan, J., Alexander, R., Sancho, L.G., Puigdefábregas, J., 2008. The influence of competition between lichen colonization and erosion on the evolution of soil surfaces in the Tabernas badlands (SE Spain) and its landscape effects. *Geomorphology*, 102, 252–266.
- Miralles, I., Domingo, F., Cantón, Y., Trasar-Cepeda, C., Leirós, M.C., Gil-Sotres, F., 2012. Hydrolas enzyme activities in a successional gradient of biological soil crusts in arid and semi-arid zones. *Soil Biol. Biochem.*, 53, 124–132.
- Monteith, J.L., 1957. Dew. *Quart. J. Royal Meteorol. Soc.*, 83, 322–341.
- Moro, M.J., Were, A., Villagarcía, L., Cantón, Y., Domingo, F., 2007. Dew measurements by Eddy covariance and wetness sensor in a semiarid ecosystem of SE Spain. *J. Hydrol.*, 335, 295–302.
- Pintado, A., Sancho, L.G., Blanquer, J.M., Green, T.G.A., Lázaro, R., 2010. Microclimatic factors and photosynthetic activity of crustose lichens from the semiarid southeast of Spain: long-term measurements for *Diploschistes diacapsis*. *Bibliotheca Lichenologica*, 105, 211–224.
- Prasse, R., Bornkamm, R., 2000. Effect of microbiotic soil surface crusts of emergence of vascular plants. *Plant Ecol.*, 150, 65–75.
- Rodríguez-Caballero, E., Cantón, Y., Chamizo, S., Lázaro, R., Escudero, A., 2013. Soil loss and runoff in semiarid ecosystems: A complex interaction between biological soil crusts, micro-topography, and hydrological drivers. *Ecosystems*, 16, 529–546.
- Schreiber, U., 2004. Pulse-amplitude (PAM) fluorometry saturation pulse method. In: Papageorgiou, G., Govindjee, S. (Eds.): *Chlorophyll fluorescence: a signature of photosynthesis*. Kluwer Academic Publishers, Dordrecht, The Netherlands, pp. 279–319.
- Thomas, A.D., Hoon, S.R., Dougill, A.J., 2011. Soil respiration at five sites along the Kalahari Transect: Effects of temperatures, precipitation pulses and biological soil crust cover. *Geoderma*, 167–168, 284–294.
- Tuba, Z., Csintalan, Z., Proctor, M.C.F., 1996. Photosynthetic responses of a moss, *Tortula ruralis*, ssp. *ruralis*, and the lichens *Cladonia convoluta* and *C. furcata* to water deficit and short periods of desiccation, and their ecophysiological significance: a baseline study at present-day CO<sub>2</sub> concentration. *New Phytol.*, 133, 353–361.
- Tuller, S.T., Chilton, R., 1973. The role of dew in the seasonal moisture balance of a summer-dry climate. *Agric. Meteorol.*, 11, 135–142.
- Uclés, O., Villagarcía, L., Cantón, Y., Domingo, F., 2013. Microlysimeter station for long term non-rainfall water input and evaporation studies. *Agric. Forest Meteorol.*, 182–183, 13–20.
- Uclés, O., Villagarcía, L., Cantón, Y., Lázaro, R., Domingo, F., 2015. Non-rainfall water inputs are controlled by aspect in a semiarid ecosystem. *J. Arid Environ.*, 113, 43–50.
- Uclés, O., Villagarcía, L., Cantón, Y., Domingo, F., 2016. Partitioning of non rainfall water input regulated by soil cover type. *Catena*, 139, 265–270.
- Veste, M., Littmann, T., 2006. Dewfall and its geo-ecological implication for biological surface crusts in desert sand dunes (north-western Negev, Israel). *J. Arid Land Studies*, 16, 139–147.
- Veste, M., Littmann, T., Friedrich, H., Breckle, S.-W., 2001. Microclimatic boundary conditions for activity of soil lichen crusts in sand dunes of the north-western Negev desert, Israel. *Flora*, 196, 465–474.
- Wang, X.P., Li, X.R., Xiao, H.L., Berndtsson, R., Pan, Y.X., 2007. Effects of surface characteristics on infiltration patterns in an arid shrub desert. *Hydrol. Process.*, 21, 72–79.
- Wilske, B., Burgheimer, J., Karnieli, A., Zaady, E., Andreae, M.O., Yakir, D., Kesselmeir, J., 2008. The CO<sub>2</sub> exchange of biological soil crusts in a semiarid grass-shrubland at the northern transition zone of the Negev Desert, Israel. *Biogeosci. Discuss.*, 5, 1969–2001.
- Zangvil, A., 1996. Six years of dew observation in the Negev Desert, Israel. *J. Arid Environ.*, 32, 361–372.
- Zhang, O., Wang, S., Yang, F.L., Yue, P., Yao, T., Wang, W.Y., 2015. Characteristics of dew formation and distribution, and its contribution to the surface water budget in a semi-arid region in China. *Boundary-Layer Meteorol.*, 154, 317–331.

Received 31 January 2020

Accepted 24 July 2020

## Interspecific variation in growth and tree water status of conifers under water-limited conditions

Adriana Leštianska<sup>1\*</sup>, Peter Fleischer Jr.<sup>1,2</sup>, Peter Fleischer<sup>1</sup>, Katarína Merganičová<sup>1,3</sup>, Katarína Strělcová<sup>1</sup>

<sup>1</sup> Technical University in Zvolen, Faculty of Forestry, T.G. Masaryka 24, 960 01 Zvolen, Slovakia.

<sup>2</sup> Institute of Forest Ecology, Slovak Academy of Sciences, Department of Plant Ecophysiology, Štúrova 2, 960 53 Zvolen, Slovakia.

<sup>3</sup> Czech University of Life Sciences Prague, Faculty of Forestry and Wood Sciences, Kamýčká 129, 16500 Praha 6 – Suchbát, Czech Republic.

\* Corresponding author. Tel.: +421 45 52 06 268. E-mail: adriana.lestianska@tuzvo.sk

**Abstract:** We monitored seasonal dynamics of stem water status of four coniferous species (*Abies alba*, *Larix decidua*, *Picea abies* and *Pinus sylvestris*) planted at the Borová hora Arboretum (300 m a.s.l., Zvolen valley, Central Slovakia) beyond their ecological and production optima, in the region with warmer and drier climate compared to the sites of their origin. Species-specific stem water deficit and maximum daily shrinkage were extracted from diurnal band dendrometer records of stem circumference recorded by digital band dendrometers DRL26 installed on five trees per species, and correlations with environmental variables were analysed. The seasonal stem circumference increment of all tree species was higher in 2017 than in the drier and hotter year of 2018. The greatest seasonal stem circumference increment in the observed periods of 2017 and 2018 was observed for *A. alba* and *P. sylvestris*, respectively. The highest and lowest values of daily and seasonal stem water deficit were observed for *L. decidua* and *A. alba*, respectively. The analysis of trees' short-term response to extreme climate events seems to be the promising and suitable method for detecting tree species tolerance towards drought.

**Keywords:** Dendrometer; Circumference changes; Stem water deficit; Drought; Stem shrinkage; Wavelet analysis.

### INTRODUCTION

Projections of near future climate indicate increases in temperature and climate variability (IPCC, 2013), which are associated with increases in the frequency, severity and duration of climatic extremes in Europe (Will et al., 2013). These climatic extremes, i.e. storms, heat waves and severe drought periods, have become important drivers of forest ecosystem dynamics (Allen et al., 2015; IPCC, 2014). Due to the wide span of the provided and expected ecosystem services, mountainous and submontane forests have long been a subject of increased public interest. In the past, mountainous forests were considered stable because of their higher level of naturalness, long-term adaptation to extreme climate conditions, and high genetic and structural diversity. It is very probable that under changing climatic conditions, forest ecosystems will be more disturbed and ecosystem services will be provided at a level below their natural potential (Hlásny et al., 2011). Due to climate change, abiotic environmental factors create serious threats to ecological stability and forest production, and can cause change of tree species composition in forest ecosystems (Teskey et al., 2015). Tree response to climate depends on tree species, age, competition, site conditions and provenances (Spiecker, 2002). The strong need to adapt many forests to future climate conditions through changes in tree species composition is frequently in stark contrast to the dearth of information about the suitability of individual species and their provenances for projected future conditions (IPCC, 2014; McDowell and Allen, 2015). Given recent climatic trends, it is crucial to understand the plasticity and adaptiveness of forest trees in order to evaluate their current and future responses to changing climatic conditions. Hence, substitute species that are able to fulfil the current socio-economic requirements of forests must be considered, in

particular at the current boundaries of tree species distribution (Bolte et al., 2009).

Temperature increase along with unchanged precipitation leads to significantly lower forest growth and production, particularly at lower elevations. Soil water availability and weather conditions have been repeatedly identified essential for tree growth and seasonal stem circumference changes (Ježík et al., 2016; Oberhuber et al., 2014). Daily stem circumference variation results from a combination of water- and growth-induced radial changes that provide us with complex information on seasonal environmental changes. The close lateral linkage of water conducting xylem with phloem translates changes in tree water status directly to shrinking and swelling of non-lignified tissues in bark and phloem (Zweifel and Häslar, 2001). These two opposite processes result from the changing water potential gradient in the plant (Zweifel et al., 2001). Depending on the species, variation in stem radius can additionally be attributed to the elastic behaviour of wood tissues (Perämäki et al., 2001), particularly xylem (Zweifel et al., 2014). Xylem elasticity is a function of wood density (Scholz et al., 2008) and/or specific tissue elasticity (Zweifel et al., 2014). Drought affects tree water status and impairs radial stem growth, because cell division and cell enlargement require adequate cell turgor (Zweifel et al., 2006). Automated band dendrometers are used for non-destructive continuous monitoring of circumference variation dynamics and small changes in stem water content with high temporal resolution. Stem water deficit has been shown to correlate with stem water potential and leaf water potential in trees (Ehrenberger et al., 2012; Offenthaler et al., 2001). Chan et al. (2016) reported that radial changes are approximately linearly proportional to changes in stem water potential. For transpiration trees first use water stored in crowns, and after their depletion the water from stem tissues is utilised (Čermák et al., 2007; Zweifel et al., 2001). Hence, stem water deficit

does not necessarily represent the ‘real’ water deficit in trees, but is a valuable indirect measure for detecting physiological responses to water deficits (Oberhuber et al., 2015; Zweifel et al., 2005).

Norway spruce (*Picea abies* (L.) Karst.) has been extensively grown in a wide spectrum of climatic conditions (Caudullo et al., 2016). Nowadays, it is well known that spruce is sensitive to extreme drought events that affect its growth rate and overall vitality (Vitali et al., 2017). Silver fir (*Abies alba* Mill.) is a coniferous species native to Europe, with a geographical distribution largely limited to the Alpine and the Carpathian ranges. Until recently, silver fir was considered a species that prefers cold and moist climate (Ellenberger, 2009). There are indications that silver fir might be more suitable for future European climate as it grew well under warmer-than-present conditions during the mid-Holocene (Ruosh et al., 2016). On the other hand, Aussenac (2002) and Battipaglia et al. (2009) reported that silver fir is highly sensitive to drought and is a species typically affected by drought-induced decline at its southern and lower altitude margins. Scots pine (*Pinus sylvestris* L.) is known as a drought-tolerant species. However, according to Bouriaud and Popa (2009), *P. sylvestris* will respond very strongly to climate fluctuations. Its productivity could decline at localities exposed to water deficit as pine is already encountered on dry sites. European larch (*Larix decidua* Mill.) is typical for mountainous regions (Geburek, 2010). At lower altitudes, it is considered to be a non-native species and studies on larch growing at lower altitudes are less common. As the text above indicates, our study focuses on four tree species with different demands on environment and sensitivity to drought and climatic extremes. Our aim was to assess the behaviour of these species outside their ecological and growth optima. From band dendrometer records (BDR) we determined stem circumference variation, tree water status (maximum daily shrinkage (MDS) and stem water deficit ( $\Delta W$ )) of selected coniferous species (*Abies alba*, *Picea abies*, *Larix decidua* and *Pinus sylvestris*) growing at the same site located in warmer and drier conditions than their natural habitats, and: i) analysed their growth responses to environmental conditions; ii) compared seasonal development of tree water status characteristics (MDS and  $\Delta W$ ) of coniferous tree species exposed to drier and hotter conditions than in their natural habitats. Following Oberhuber et al. (2015), we assume that drier and hotter conditions will cause greater sensitivity of tree species manifested by the occurrence of periodic phenomena on the daily basis.

## MATERIAL AND METHODS

### Study area

Our research was performed in Borová hora Arboretum (19°08'12.30" E, 48°35'44.22" N, ca. 350 m a.s.l.) situated in Zvolen valley (Central Slovakia). Borová hora Arboretum is located on mild 5–10% slopes with south-west aspect. The soil type is cambisol. From the climatic point of view, this area is situated in the temperate climatic zone with temperate Central-European climate. The area belongs to a warm and a slightly warm region with cold winter. Average annual air temperature is 7.9°C and annual precipitation total is 651 mm. Average temperature and precipitation total during a vegetation season (April–September) is 14.7°C and 377 mm, respectively. Long-term averages representing the period 1961–1990 were provided by the Slovak Hydrometeorological Institute from a nearby meteorological station of Sliach (313 m a.s.l.). *Querceto-Fagetum* community represents potential forest vegetation at the site (<https://geo.enviroportal.sk/atlassr>).

The provenances of the studied species (*Picea abies*, *Abies alba*, *Pinus sylvestris* and *Larix decidua*) were planted at four homogeneous research plots within the arboretum, each representing single species. At each plot, five adult trees of similar age and size (Table 1) were selected for the purpose of this study. The selected provenances originate from Slovakia and similar altitudes. In the arboretum, they grow beyond their ecological and production optima, in the region with warmer and drier climate than their original natural habitats (Table 1).

### Dendrometers

Stem circumference variations were recorded using high-resolution automatic band dendrometers DRL 26 (EMS Brno, CZ). Dendrometers were installed on 20 sample trees (5 trees per species). Circumference measurements were recorded in 20-min intervals.

### Environmental data

Meteorological data were recorded with an automatic meteorological station (EMS Brno, CZ) installed at an open area near study plots (80–150 m from their centres). The meteorological station recorded global radiation (GR,  $W \cdot m^{-2}$ ), air temperature (AT, °C), relative air humidity (RH, %) and precipitation (P, mm). Vapour pressure deficit (VPD, Pa) was calculated from air temperature and relative humidity. At each study plot, soil water potential (SWP, Pa) was measured under forest canopy at 15, 30 and 50 cm soil depths (gypsum blocks and MicroLog SP3, EMS Brno, CZ). From these values, average values of SWP from all depths were calculated per plot.

### Tree water status

Stem water deficit ( $\Delta W$ , mm) was quantified from dendrometer records de-trended for growth according to Ehrenberger et al. (2012). A ‘growth line’ was constructed by drawing lines between the daily maximum stem circumference values and the next equal stem circumference value, thus ignoring periods of incomplete stem circumference recovery due to stem shrinkage induced by water shortage. In the phases where the stem circumference values exceeded the previous maxima, the growth line followed the increasing values of stem circumference. In the following, stem water deficit was determined as a difference in stem size measured by dendrometers under low water availability conditions relative to the stem size under fully hydrated conditions ( $\Delta W = 0$ ) (Oberhuber et al., 2015) (Figure 1). Hence, increasingly negative values of  $\Delta W$  indicate increasing dehydration of water storage pools.

Maximum daily shrinkage (MDS, mm) is a difference between the morning maximum and afternoon minimum at a particular day (diurnal amplitude). MDS reflects the daily cycle of water uptake and loss (Figure 1). Both stem water deficit and maximum daily shrinkage were calculated using special routines in “DendrometerR” package (van der Maaten et al., 2016).

### BDR and environmental variables

The Spearman rank-correlation coefficients were calculated to explore the relationship between daily environmental variables (global radiation, precipitation, relative air humidity, vapour pressure deficit, air temperature and soil water potential) and water status characteristics extracted from BDR ( $\Delta W$  and MDS). Temporal variability of correlations of  $\Delta W$  and MDS to environmental variables was evaluated with

**Table 1.** Basic site characteristics of the original location of the selected tree species provenances and stem diameter measured at 1.3 m breast height (DBH) at the beginning of 2017. (E - elevation, T - long-term average of air temperature, P - long-term average of precipitation; long-term averages of the original location represent the period 1961–1990).

Species	Orographic unit	Locality	E (m a.s.l.)	T (°C)	P (mm)	Age (2017) (years)	d <sub>1.3</sub> ± std (2017) (cm)
<i>L. decidua</i>	Spišsko-gemerský kras	Voniaca valley	900	4.8	831	50	31.8±3.9
<i>A. alba</i>	Kremnica mountains	Flochovský back	950	5.8	786	46	33.4±5.0
<i>P. abies</i>	Podtatranská kotlina	Tatr. Lomnica	800	5.3	833	49	25.3±3.5
<i>P. sylvestris</i>	Spišsko-gemerský kras	Veľká Hudrová	950	4.8	831	37	30.7±3.5

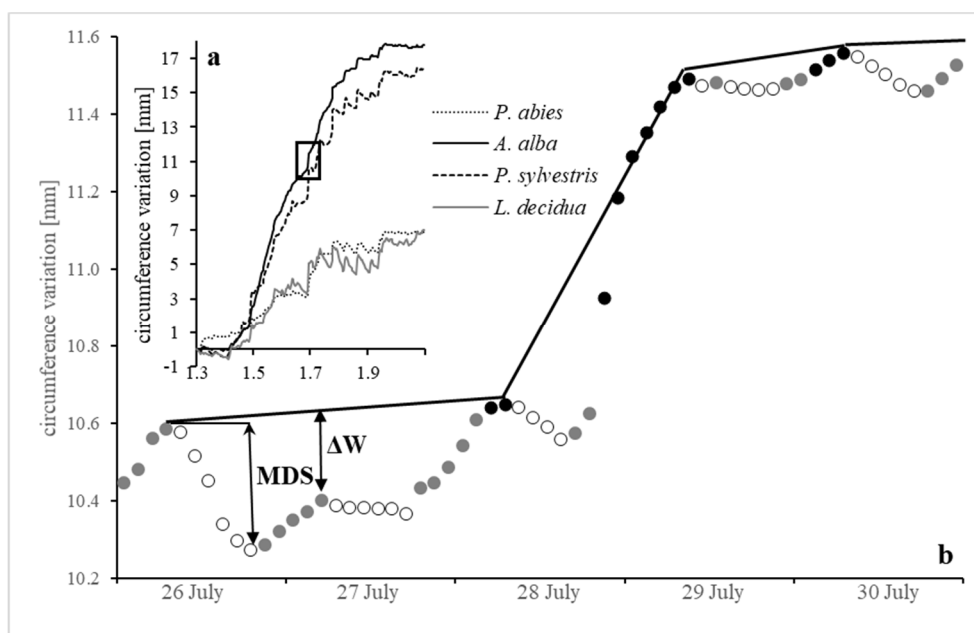


**Fig. 1.** Seasonal curves of band dendrometer records (BDR) of *Abies alba* (solid black line), *P. sylvestris* (dashed black line), *P. abies* (dotted black line) and *L. decidua* (solid grey line). Each line represents an average from 5 trees of the same species (a); growth-trend lines (solid black line) and daily stem circumference increase showing distinct phases of a daily stem cycle: contraction (open white circles), expansion (grey circles) and increment (black circles) phase (b).

a moving correlation analysis (MCA), which is based on a progressively shifting period of a fixed number of days across time to compute correlation coefficients (Oberhuber et al., 2015). To provide robust measures of association between environmental variables and  $\Delta W$  and MDS, the length of the calibration window was set to 30 days. Confidence intervals for MCA were analyzed according to Kokfelt and Muscheler (2012).

### Periodicity of BDR

Significant periodicities in the seasonal course of BDR ranging from hours to weeks was identified with a wavelet analysis (Percival and Walden, 2000; Torrence and Compo, 1998). We used the Morlet transformation, which is a sine wave modulated by a classical Gaussian function, establishing a clear distinction between random fluctuations and periodic regions (Torrence and Compo, 1998). Morlet analysis in our study is based on average BDR per species. The generated wavelet spectrum is a time-scale plot, where the x- and y axes represent the position along time and periodicity scale, respectively, and the colour contour at each x/y point represents the magnitude of the wavelet coefficient at that point. Wavelet analysis was performed using WaveletComp R package (Rösch and Schmidbauer, 2018). We applied a Weibull growth function to BDR series using Statistica 12 (Statsoft). Residuals between the Weibull

growth function and BDR were used for periodicity estimation. In Morlet analysis, the lower period was set to 20 min intervals, while the upper one to 4,600 min intervals (i.e. 2 months). Shorter periods allow detecting small cycles, while long periods long lasting cycles. To compare and outline diurnal Morlet spectra of different tree species we selected the region from 0.0 to 0.1 to display.

## RESULTS AND DISCUSSION

### Environmental characteristics of the studied periods in 2017 and 2018

Both study periods from March to October in 2017 and 2018 were characterised by average air temperatures above the long-term normal (1961–1990), while 2018 was the warmer study period with the air temperature by +2.9°C above the long-term average versus +2.0°C in 2017. Monthly mean air temperatures were in all but one month (March 2018) above their respective long-term normals. The study period in 2018 with the precipitation total of 365 mm was drier compared to the long-term precipitation normal of 460 mm, while the precipitation total of 533 mm recorded for the study period in 2017 exceeded the long-term normal by 15%. The precipitation was differently distributed during the study periods. Daily precipitation totals were higher in 2017, while in the year 2018 we recorded a higher number of days without precipitation or with low precip-

itation (Figures 2c, d). Higher air temperatures and lower precipitation totals in 2018 resulted in higher values of vapour pressure deficit in comparison with 2017 (Figures 2c, d). Overall, variation of vapour pressure deficit was smooth, and the range of 2017 values was slightly greater than of 2018. This was also reflected in the temporal course of soil water potential at all plots (Figures 6, 7). At the beginning of both studied periods, soil was sufficiently saturated with water. In May, SWP began to decrease, while in 2018 the reduction in SWP was observed already at the beginning of May in comparison to 2017, when it occurred only in the second half of May. Similarly, the lowest values of  $-1.5$  MPa were recorded earlier in 2018 than in 2017 (at the end of May versus the beginning of June). Afterwards, SWP values substantially fluctuated depending on the precipitation occurrence, while in 2018 SWP was on average below SWP in 2017 (Figures 6, 7).

### Seasonal development of stem growth and tree water status

Seasonal development of stem circumference records and tree species specific water status characteristics (stem water deficit and maximum daily shrinkage) derived from BDR showed pronounced differences between species and between two monitored periods of the years 2017 and 2018 (Figure 3).

In both years, stem circumference increments of *A. alba* ( $17.8 \pm 5.3$  mm and  $11.2 \pm 4.2$  mm, in 2017 and 2018) and *P. sylvestris* ( $16.3 \pm 3.7$  mm and  $13.8 \pm 3.1$  mm) were more than twice times greater than of *P. abies* ( $6.9 \pm 3.5$  mm and  $5.3 \pm 2.4$  mm) and *L. decidua* ( $7.0 \pm 2.1$  mm and  $5.2 \pm 1.4$  mm). The observed differences in seasonal tree circumference growth result from the existence of species-specific temperature and/or photoperiod thresholds of cambial activity (Begum et al., 2013; Körner and Basler, 2010). Due to more limiting water conditions in 2018 (Figures 2, 7), seasonal radial growth of all tree species in 2018 was reduced in comparison to 2017, while *P. sylvestris* reduced its growth only by 16% in comparison to other tree species with more than 20% reduction compared to 2017 (Figures 3a, b). This suggests greater tolerance of *P. sylvestris* to drought (Irvine et al., 1998; Oberhuber et al., 1998). Consistent reduction of radial increment after drought has been observed for multiple species in previous studies (e.g. Camarero et al., 2015).

While in 2017 fir radial increment was the highest, in the subsequent year *P. sylvestris* overtook *A. alba* in radial growth in the second half of July 2018 (Figure 3 b). We assume that this may be caused by the differences in SWP between the plots that were apparent particularly in the second half of 2018 season (Figure 7). While after rainy events in the second half of July, soil at *P. sylvestris* became saturated with water

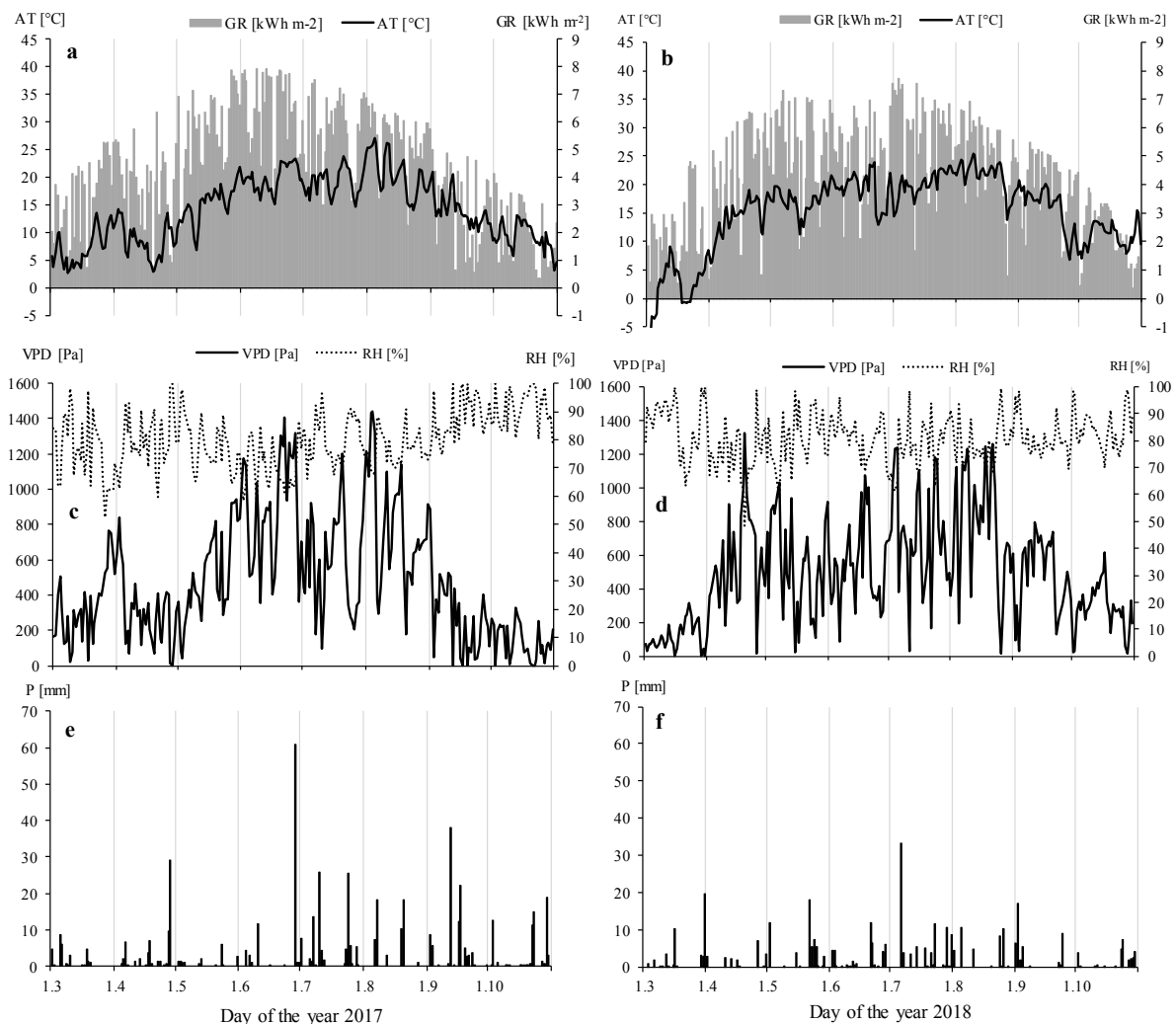


**Fig. 2.** Courses of daily mean air temperature (AT) and daily totals of global radiation (GR) (a, b), daily mean vapour pressure deficit (VPD) and relative air humidity (RH) (b, d) and daily precipitation totals (P) (e, f) recorded during the study periods (March–October) in 2017 and 2018.

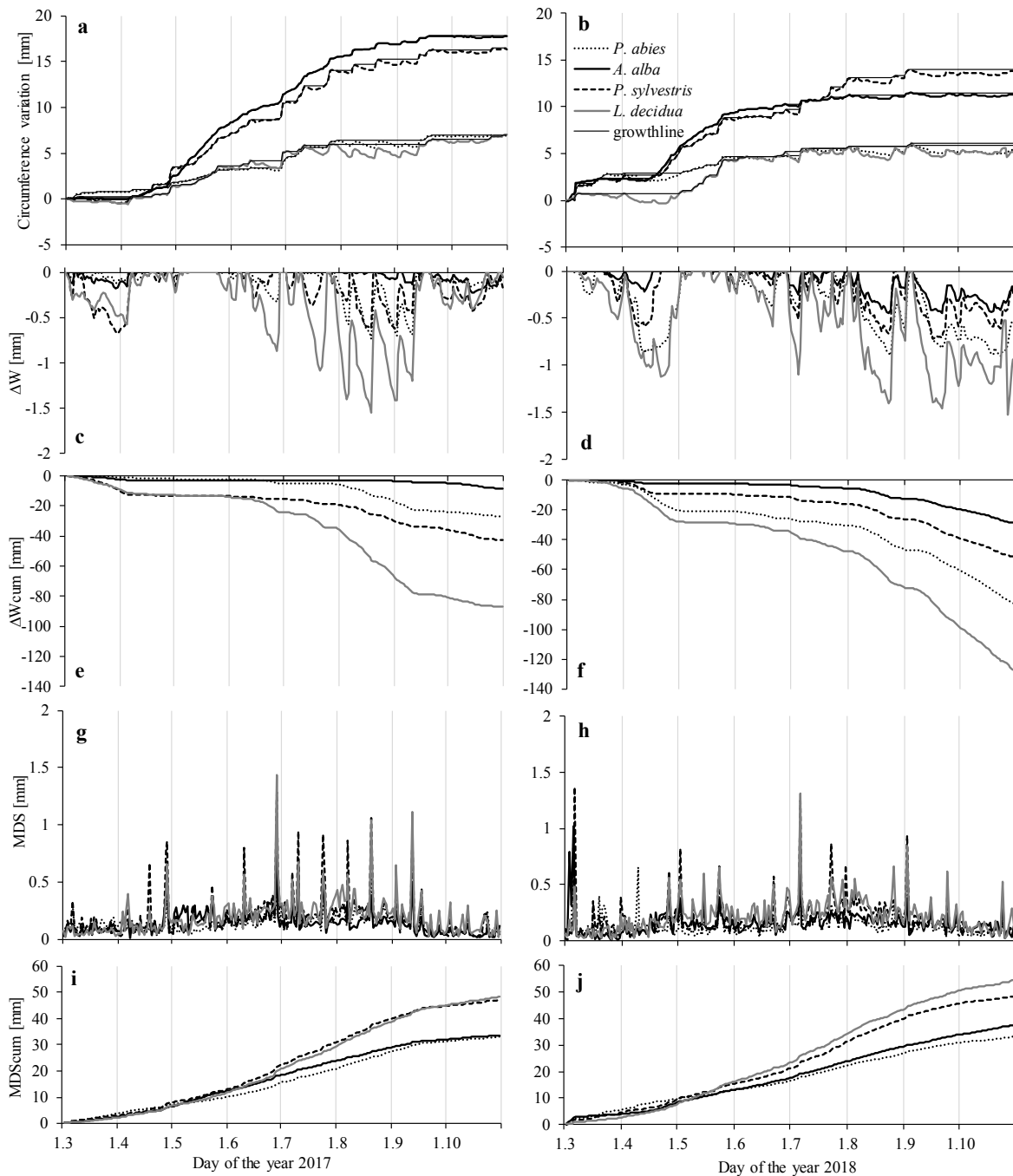


**Fig. 3.** Growth line (solid thin line) and band dendrometer records (BDR) of stem circumference over bark (a, b), mean daily stem water deficit ( $\Delta W$ ) (c, d) and cumulative stem water deficit ( $\Delta W_{cum}$ ) (e, f), maximum daily shrinkage (MDS) (g, h) and cumulative maximum daily shrinkage ( $MDS_{cum}$ ) (i, j).

(SWP = 0.0 MPa), SWP values at other plots were reduced to -0.5 MPa already at the end of April or beginning of May 2018 and remained below this threshold until the end of the observation period (Figure 7). Soil water conditions at *A. alba* plot were most limiting, due to which the radial growth of this species stagnated (Figure 3b). BDR of all species showed temporal fluctuations in stem circumference with plateaus representing stagnation periods. The largest fluctuations in BDR were recorded for *L. decidua* due to its anisohydric strategy (Bréda et al., 2006). Notable stagnation of radial growth occurred in periods with low precipitation and soil water deficit (Figures 2, 6 and 7). Stem circumference increase was clearly observed after precipitation events, which indicates re-hydration of “water storage cells” (Vieira et al., 2013; Zweifel et al., 2005).

Indirect measures of tree water status (MDS and  $\Delta W$ ) are very valuable for detecting physiological responses to water deficits (Oberhuber et al., 2015; Zweifel et al., 2005). Extracted water deficit values indicate limited water storage relative to fully hydrated stem conditions. Increasingly negative values mean more pronounced water shortage. Over the examined periods, stem water deficit gradually decreased in all species, although with different magnitudes (Figures 3c, d). This trend was occasionally disrupted by precipitation events, after which  $\Delta W$  reached values close to zero (Figure 2, Figures 3c, d). Calculated  $\Delta W$  and MDS of all species showed synchronous fluctuations in both years (Figures 3c–f). *L. decidua* showed greatest cumulative stem water deficit ( $-86.9 \pm 47.6$  mm in 2017, and  $-128.4 \pm 48.1$  mm) and seasonal daily  $\Delta W$  throughout

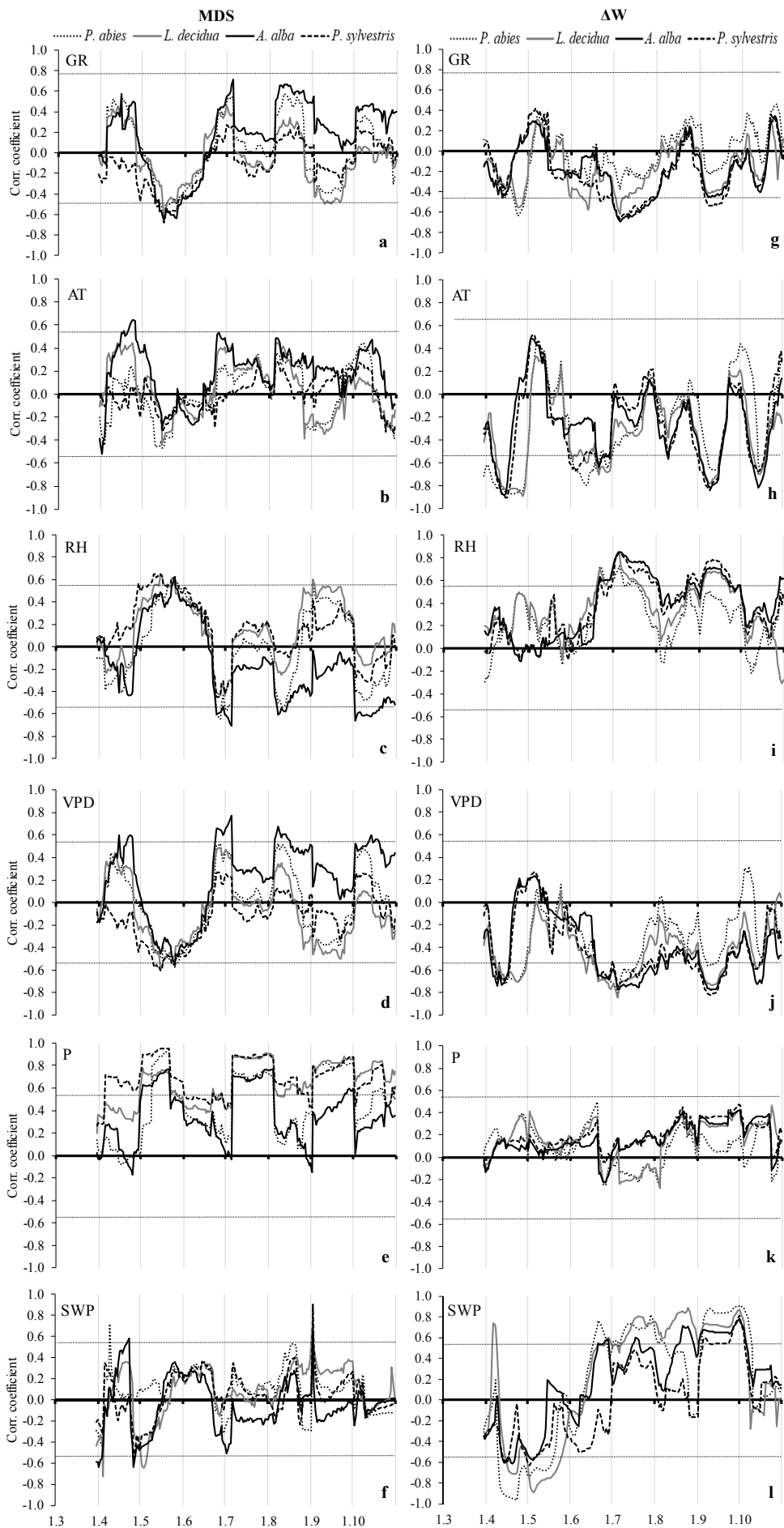


**Fig. 4.** Species-specific moving correlations (windows of 30 days) between environmental variables: global radiation (GR), air temperature (AT), relative air humidity (RH), vapour pressure deficit (VPD), precipitation (P) and soil water potential (SWP) and tree water status characteristics: maximum daily stem shrinkage (MDS) (a–f) and tree water deficit ( $\Delta W$ ) (g–l) of four tree species: *A. alba* (solid black line), *P. abies* (dotted black line), *P. sylvestris* (dashed black line) and *L. decidua* (solid grey line) during the study period of the year 2017.

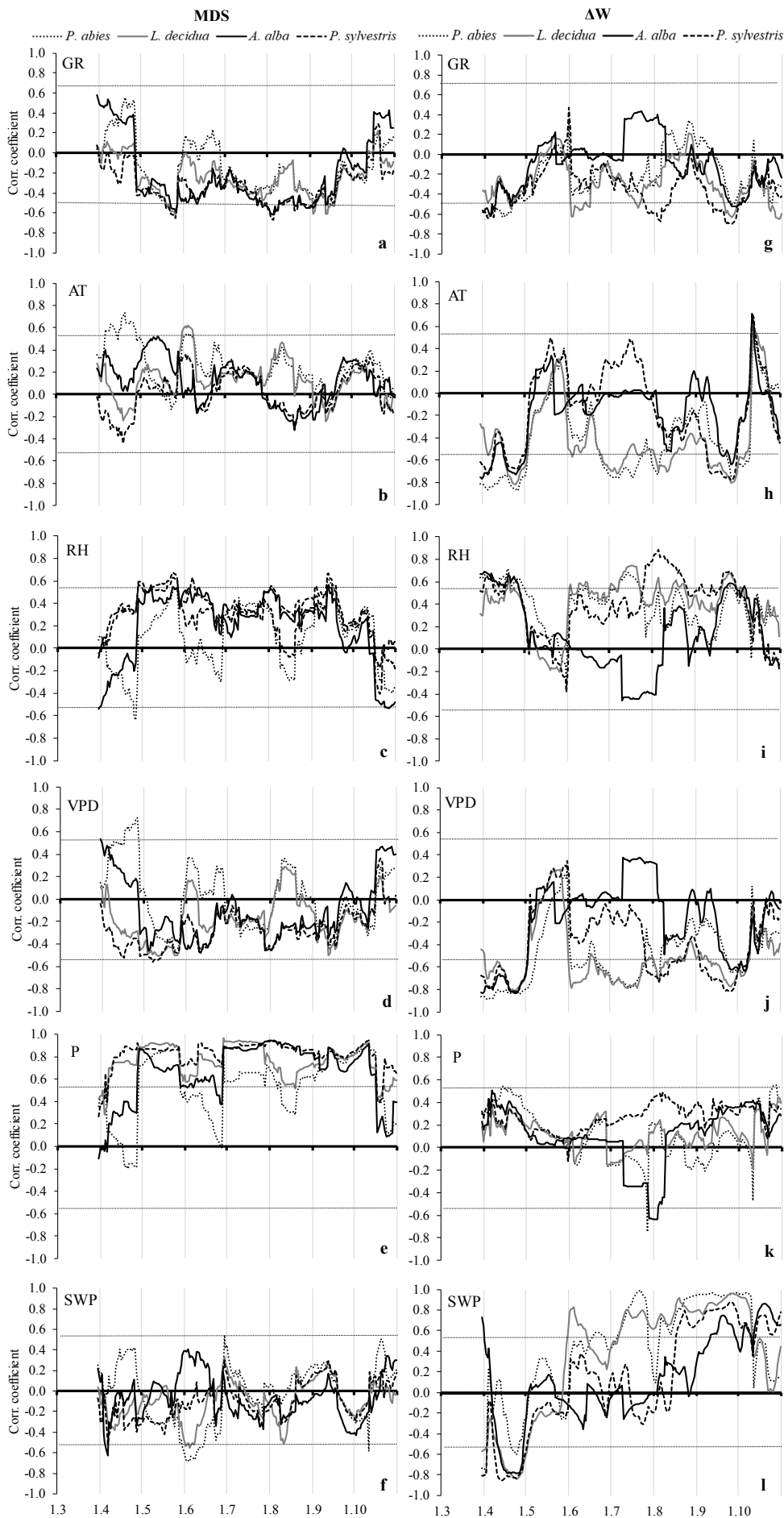


**Fig. 5.** Species-specific moving correlations (windows of 30 days) between environmental variables: global radiation (GR), air temperature (AT), relative air humidity (RH), vapour pressure deficit (VPD), precipitation (P) and soil water potential (SWP) and tree water status characteristics: maximum daily stem shrinkage (MDS) (a–f) and tree water deficit ( $\Delta W$ ) (g–l) of four tree species: *A. alba* (solid black line), *P. abies* (dotted black line), *P. sylvestris* (dashed black line) and *L. decidua* (solid grey line) during the study period of the year 2018.

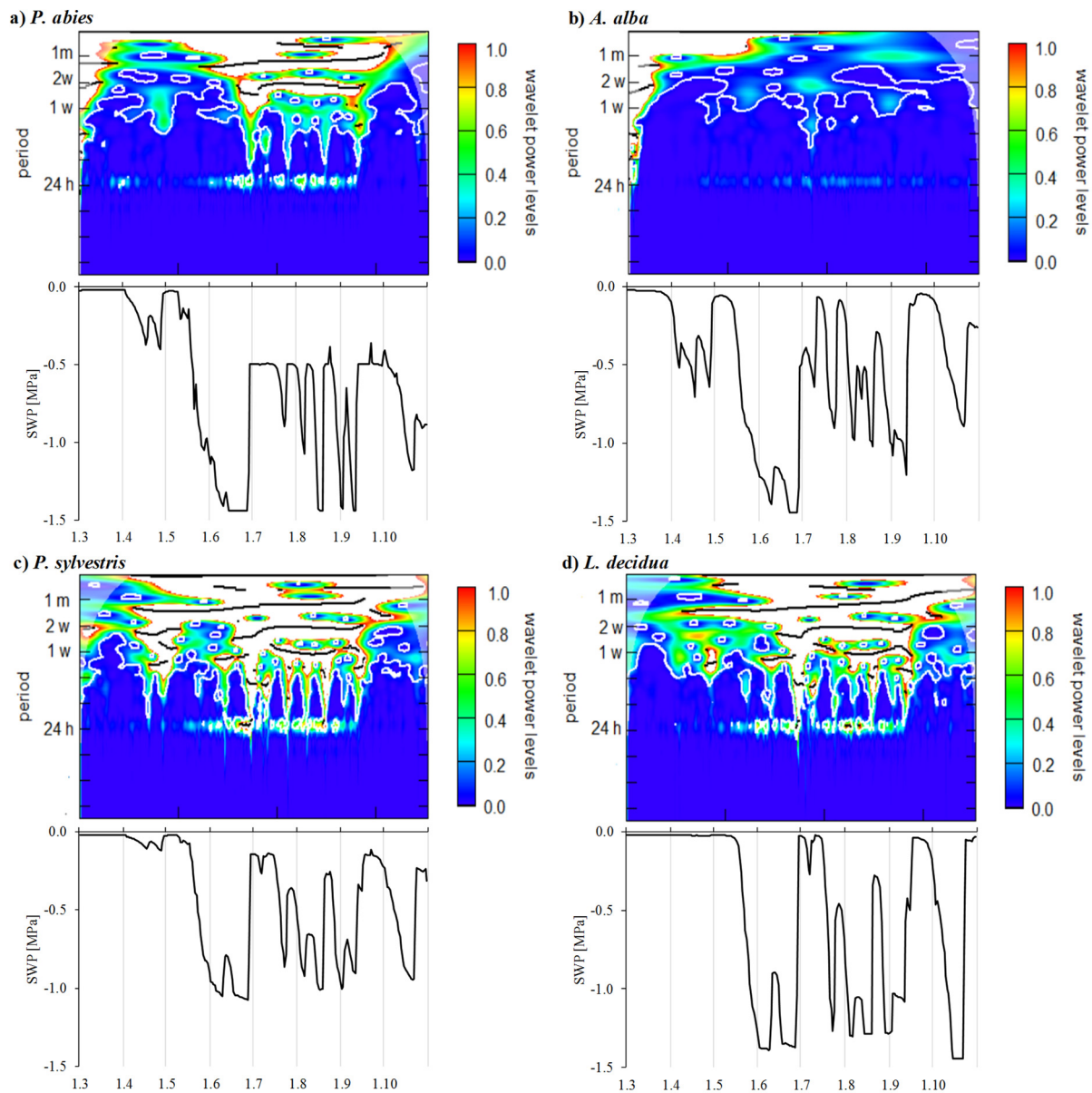


**Fig. 6.** Morlet wavelet spectra of 20-min measured records of stem circumference and soil water potential for the studied tree species: *P. abies* (a), *A. alba* (b), *P. sylvestris* (c) and *L. decidua* (d) in the study period (March–October) of the year 2017. Dark red and white colours are assigned to the highest wavelet power spectra, whereas a dark blue colour is assigned to the lowest values. Wavelet power levels were set from 0.0 to  $1.10^{-1}$ .

both study years because, unlike the other three investigated species, larch maintains high transpiration rates even under dry conditions (Bréda et al., 2006). On the contrary, the smallest values of cumulative and daily  $\Delta W$  were determined for *A. alba* throughout both study years, since this species is known for its strong regulation of transpiration (Nourtier et al., 2014).

However, when we examined relative changes in stem water deficit of the same species between the years, we found that cumulative  $\Delta W$  of *A. alba* in 2018 was 3.31 times greater than in 2017 ( $-28.8 \pm 16.6$  mm versus  $-8.7 \pm 2.0$  mm). Although this relative increase was the largest from all investigated species, cumulative  $\Delta W$  of *A. alba* remained the lowest of all species (Figures 3e, f). Similar threefold increase in cumulative stem water deficit was observed for *P. abies* ( $-27.2 \pm 11.3$  mm in 2017 versus  $-83.2 \pm 31.2$  mm in 2018). In 2017, cumulative  $\Delta W$  of *P. abies* was lower in comparison to *P. sylvestris*, while in 2018 it was the other way round, because *P. sylvestris* increased its cumulative stem water deficit only by 20% ( $-42.8 \pm 19.5$  mm

in 2017 and  $-51.5 \pm 15.3$  mm in 2018). Similar increase of smaller magnitude in cumulative  $\Delta W$  by less than 50% was observed for *L. decidua* in 2018. We assume that the lower inter-annual changes in cumulative  $\Delta W$  of *P. sylvestris* and *L. decidua* result from lower elasticity of their tissues due to their higher wood density (Požgaj et al., 1993; Zeidler et al., 2018).

González-Rodríguez et al. (2017) have shown that stem diameter shrinkage is mainly determined by sap flow changes. Variations in stem diameter act in response to a tree daily water intake and loss of moisture (Irvine and Grace, 1997). In both studied years, species specific maximum daily shrinkage and seasonal cumulative shrinkage were greater for *L. decidua* and *P. sylvestris* than for *P. abies* and *A. alba* (Figures 3i, j). This indicates species specific water status regulation driven by bark thickness (Mencuccini et al., 2013). Oberhuber et al. (2014) showed that the fraction of reversible stem swelling and shrinkage caused by diurnal changes in atmospheric conditions is higher when trees are growing slowly as is *L. decidua*. The

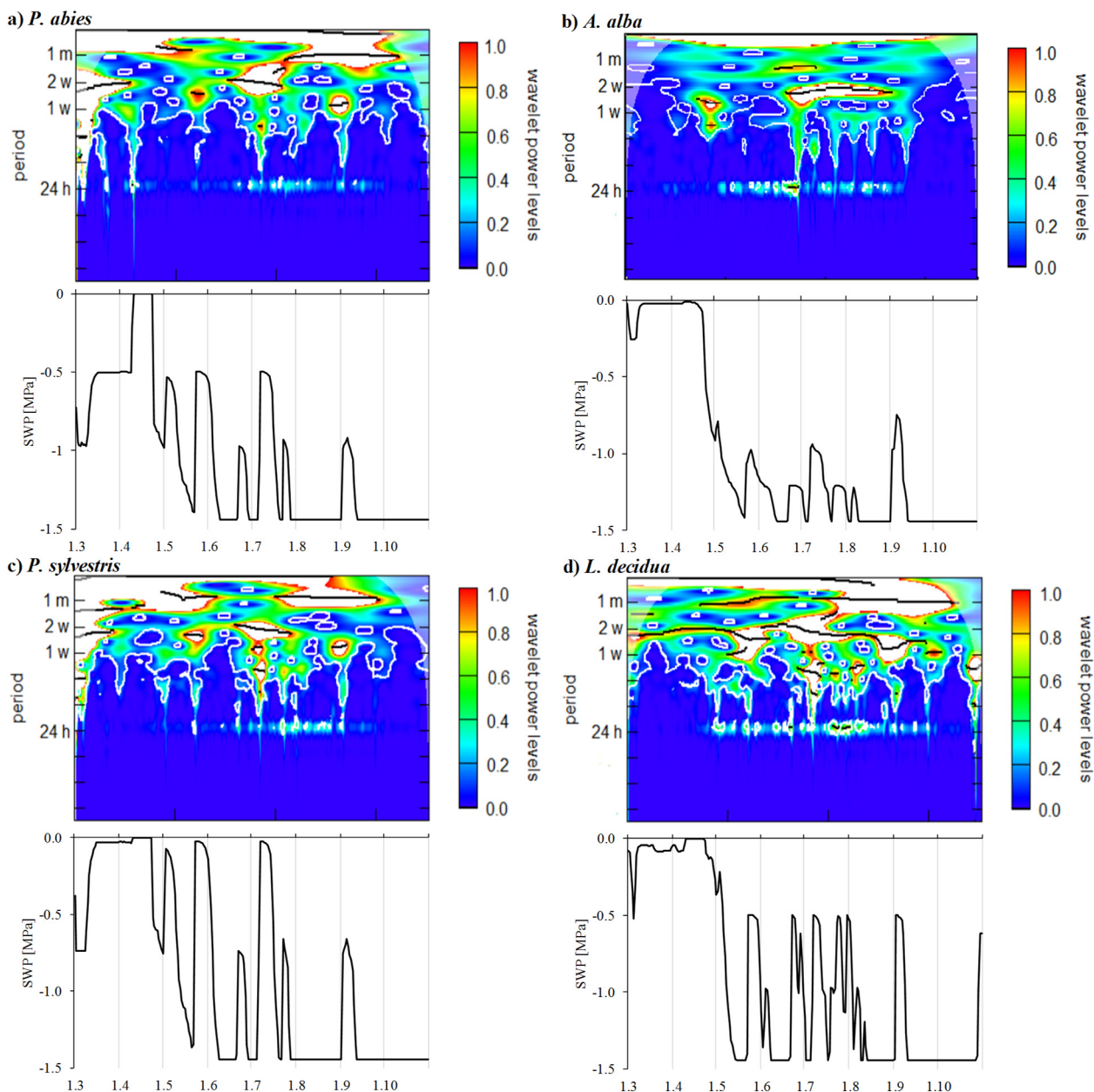


**Fig. 7.** Morlet wavelet spectra of 20-min measured records of stem circumference and soil water potential for the studied tree species: *P. abies* (a), *A. alba* (b), *P. sylvestris* (c) and *L. decidua* (d) in the study period (March–October) of the year 2018. Dark red and white colours are assigned to the highest wavelet power spectra, whereas a dark blue colour is assigned to the lowest values. Wavelet power levels were set from 0.0 to  $1.10^{-1}$ .

seasonal cumulative shrinkage of the species in the years 2017 and 2018 increased in the following order: *P. abies* ( $35.1 \pm 14.7$  mm,  $34.9 \pm 12.8$  mm), *A. alba* ( $35.0 \pm 11.8$  mm,  $39.2 \pm 13.3$  mm), *P. sylvestris* ( $45.7 \pm 6.3$  mm,  $51.1 \pm 7.9$  mm) and *L. decidua* ( $49.6 \pm 14.6$  mm,  $56.8 \pm 12.7$  mm). MDS has been shown to gradually decline when trees are experiencing poor water supply for extended periods of time (Dietrich et al., 2018). Declining MDS with declining soil water supply is caused by insufficient tissue rehydration during night time, due to which the stem undergoes a constant shrinkage (on a daily cadence) during dry periods. Since MDS is proportional to the volume of daily used storage water (Zweifel et al., 2000), poor night-time rehydration, and, therefore, declining storage water, will have a decreasing effect on MDS during dry periods (Dietrich et al., 2018).

#### Environmental conditions and tree water status

Tree growth and water status are controlled by a vast array of conditions. Several authors (e.g. Köcher et al., 2013, Oberhuber et al., 2015) reported that  $\Delta W$  and MDS are closely related to drought stress and are mainly determined by a combination of atmospheric and soil conditions. The close lateral linkage of water conducting xylem with phloem translates changes in tree water status directly to shrinking and swelling of non-lignified tissues in the bark and phloem (Zweifel and Häslér, 2001). Spearman rank-correlations between tree water status characteristics (MDS and  $\Delta W$ ) and environmental variables (Table 2) revealed that all monitored environmental characteristics were highly significantly correlated with MDS irrespective of species. Closest positive correlations of MDS were found

with GR and AT of all species. Significant negative relationships were observed with RH and SWP. Hence, close correlations found between daily radial change and VPD, which reflects RH and air temperature and influences transpiration rate besides wind and radiation, can be attributed to changes in leaf transpiration. Transpiration, in turn, will directly cause water depletion of the bark storage compartments and, thus, stem shrinkage. Further, stomatal regulation strongly determines tree water relations and thus has a distinct impact on  $\Delta W$  (Zweifel et al., 2001). SWP affected MDS of *P. sylvestris* and *L. decidua* more strongly than  $\Delta W$  of *P. abies*. This result most likely indicates that in the short term the use of water stored in the living stem tissues makes *P. abies* less dependent on the current water availability in the soil. Strongest relationships were found between MDS and air temperature ( $P < 0.001$ ) with the highest correlation coefficient for *L. decidua* ( $r = 0.676$ ), while  $\Delta W$  was most strongly correlated to SWP (Table 2). Closer correlations between MDS and atmospheric conditions than with soil water status indicate that trees utilise water stored in stem reservoirs for transpiration, which is driven by climate variables (Ehrenberger et al., 2012; Zweifel et al., 2005), on a daily basis. In contrast to MDS,  $\Delta W$  allows accounting for accumulated water deficits also over extended periods (few days to months) of drought. Differences between these two variables only become apparent during longer periods of stem shrinkage. Hence, elastic tissue reservoirs contribute to the avoidance of the early stomatal regulation under increasing soil drought (Čermák et al., 2007). Soil moisture, influenced by changing precipitation, is a slowly changing factor, the effects of which can only be seen over longer time scales. Atmospheric moisture, on the other hand, changes on a daily scale, and through its effect on transpiration it hereby directly influences stem diameter variation. Because a close coupling of transpiration with xylem sap flow was reported by Steppe et al. (2006), missing significant relationships between SWP and tree water parameters extracted from BDR of all species imply that transpiration draws upon water stored in the stem rather than soil water (Betsch et al., 2011; Čermák et al., 2007). This reasoning is supported by Zweifel et al. (2005), who found that transpired water is more strongly withdrawn from internal storage tissues at dry sites than at moist sites. Replenishment of these water reservoirs strongly depends on available water in soil (Turcotte et al., 2011), due to which tree water deficit is more affected by SWP. Our results contradict to Oberhuber et al. (2015), who found that  $\Delta W$  was controlled more by air temperature. We assume that this is because their study dealt with drier soil conditions than our study, under which atmospheric conditions may become more prevailing influential factors, since soil water is already limiting (Hinckley et al., 1978; Pataki et al., 1998). All species had the highest significant linear negative relationships between soil water potential and MDS and high positive relationships of SWP with  $\Delta W$ . The highest positive value of correlation coefficient between soil water potential and  $\Delta W$  was found for *P. abies* ( $r = 0.505$ ) and the lowest value was found for *P. sylvestris* ( $r = 0.216$ ). Lower although significant values of correlation coefficients were found between tree water status characteristics and relative air humidity and precipitation in all species. Global radiation and  $\Delta W$  positively significantly correlated only in the case of shade tolerant *A. alba* ( $r = 0.243$ ) (Table 2). Its lowest correlation coefficients between  $\Delta W$  and AT, RH, and VPD from all investigated species confirm its high capability to regulate transpiration (Aussenac, 2002).

Moving correlation analysis with 30-day windows showed the closest positive correlations of MDS with precipitation (Figures 4, 5e) in all monitored species in both years. Trees

undergo daily cycles of circumference fluctuation that are usually consistent with expectations based on known physiological mechanisms (Steppe et al. 2015), and they commonly exhibit circumference changes in response to precipitation events (Figures 3, 4e, 5e).  $\Delta W$  showed significant negative correlations with soil water potential in April and significant positive correlations with SWP from June to October. In both study periods, *L. decidua* and *P. abies* reached the highest values of correlation coefficients between  $\Delta W$  and SWP (Figures 5, 6l). High significant negative correlations between AT, VPD and  $\Delta W$  of *L. decidua* and *P. abies* were observed in July and September in the year 2017. Correlations revealed close negative relationships between  $\Delta W$  and AT in April, June and in September and October and between  $\Delta W$  and VPD in April, June, July and September in the year 2018 irrespective of species. The results did not reveal any significant correlations between  $\Delta W$  and precipitation in either of the study periods (Figures 4, 5k). As depicted in Figures 4 and 5, MDS and  $\Delta W$  of all species showed more synchronous response to environmental factors in the year 2018 in comparison with 2017. Between the beginning of June and September in the year 2017 we observed asynchronous reactions of species  $\Delta W$  to environmental factors (Figures 4, 5g–l). MDS was most frequently significantly correlated with precipitation, while greater fluctuations were observed in 2018 (Figures 4d and 5d). Higher correlations of MDS with precipitation were found for *P. sylvestris* and *L. decidua* due to greater thickness of bark. High temperatures stimulate evaporation rates, due to which water availability, characterised by soil water potential, becomes further constrained. This agrees with other studies from temperate forests at low elevations that reported that above average temperatures induce negative growth responses (Battipaglia et al., 2009; Schuster and Oberhuber, 2013). High sensitivity of stem water status to VPD and soil moisture was reported in several experimental studies (e.g. Turcotte et al., 2011; Will et al., 2013).

Our results support reports presenting *A. alba* more resilient to climate change than other conifers of temperate forests (Bouriaud and Popa, 2009; Latreille et al., 2017) and an adaptive species to changing conditions (Bošela et al., 2018) including adverse events such as drought (Vitali, 2017). Since its productivity does not seem to be affected by increasing temperature (Bošela et al., 2018; Usoltsev et al., 2019), *A. alba* is often considered as a prospective species under climate change (Lindner et al., 2008). In another study of the 2003 drought event, *P. abies* cell production stopped in August to September of the drought year, while *A. alba* was active until October (Gričar and Čufar, 2008). At similar elevations in Slovenian forests, *A. alba* had a significantly longer wood formation period than spruce, with the beginning in early April and the end in late October (Gričar and Čufar, 2008). It appears that longer periods of wood formation in *A. alba* allow this species to partially compensate for drought periods during which cell formation ceases. This may be achieved through early or late growth during dry years, and through replenishing resources to support growth in the following year, resulting in its higher resistance and resilience. The fact that *P. sylvestris* was a less responsive species than *P. abies* and *L. decidua* was expected because this species is known to be drought-resistant maintaining a tight control over its transpiration (Oberhuber et al., 1998) already in early stages of drought (Irvine et al., 1998). Pronounced stomatal control generally allows high drought avoidance capacity (Aubin et al., 2016). Moreover, *P. sylvestris* is known to be well protected against drought due to its imbedded stomata and pronounced waxy layer on the epidermis (Krakau et al., 2013). Limited radial growth of *L. decidua* at the studied

**Table 2.** Species-specific Spearman rank-correlation coefficients ( $r$ ) for the relationships between daily environmental variables: global radiation (GR), air temperature (AT), relative air humidity (RH), precipitation (P), vapour pressure deficit (VPD) and soil water potential (SWP), and tree water status characteristics: maximum daily shrinkage (MDS) and tree water deficit ( $\Delta W$ ) in the study periods of the years 2017 and 2018.

		GR	AT	RH	P	VPD	SWP
<i>P. abies</i>	MDS	0.334***	0.418***	-0.269***	0.090*	0.366***	-0.073
	$\Delta W$	0.069	-0.183***	0.132**	0.150***	-0.220***	0.505***
<i>P. sylvestris</i>	MDS	0.397***	0.611***	-0.157***	0.219***	0.394***	-0.256***
	$\Delta W$	0.059	-0.026	0.210***	0.261***	-0.195***	0.216***
<i>L. decidua</i>	MDS	0.432***	0.676***	-0.092*	0.220***	0.408***	-0.345***
	$\Delta W$	-0.052	-0.254***	0.268***	0.221***	-0.351***	0.401***
<i>A. alba</i>	MDS	0.446***	0.543***	-0.273***	0.073	0.470***	-0.408***
	$\Delta W$	0.243***	0.099*	0.042	0.176***	-0.002	0.298***

site (Figures 3a, b) is a consequence of its sensitivity to soil water conditions (Eilmann and Rigling, 2012), especially during summer months. Its weak adjustability to drought results from its deciduous habit and/or anisohydric strategy resulting in high transpiration rates under drought, and finally causing impairment of tree water status (Bréda et al., 2006; Oberhuber et al., 2015). Isohydric species such as *P. abies*, *P. sylvestris* or *A. alba* suffer more but recover quicker under short drought events, while anisohydric species such as larch reduce their growth less but may suffer during longer lasting drought events (Hartmann, 2011; McDowell et al., 2008).

Morlet wavelet analysis of the detrended BDR of four coniferous species confirmed the occurrence of periodicity in BDR with various frequency ranging from days to weeks in both studied years. Significant daily cycles ( $p < 0.05$ ) were found during substantial parts of both years 2017 and 2018, except for *A. alba* in the year 2017. The daily cycle was notably more pronounced during the rainless periods (Figures 6, 7, Figures 3 e, f) reflecting the changing plant hydric status during a day (Ježik et al., 2016; Zweifel et al., 2006). Pronounced occurrence of daily cycles in the wavelet spectrum of *P. abies*, *L. decidua* and *A. alba* in our study in the warmer and drier year 2018 (Figure 2) is connected with plant water reservoir depletion under more stressing conditions (Oberhuber et al., 2015). *P. sylvestris* exhibited the presence of diurnal cycles in more favourable conditions of the year 2017. This result can be explained by *P. sylvestris* elasticity of bark affected by atmospheric conditions (Oberhuber et al., 2020). In the year 2017 characterised with greater short-term fluctuations of soil water conditions (Figure 6), both *A. alba* and *P. sylvestris* grew in a cascade-like manner, while in the year 2018 they adapted to limited soil water conditions due to which the daily cycle was not so pronounced (Figure 7). Since the presented hypothesis is based only on two study periods, a more extensive study is required for its verification. To our knowledge, the literature about species specific wavelet spectra response to hydric conditions is rather scarce.

Morlet wavelet analysis offered us an opportunity to present tree water status from a different point of view that stem water status indicators (MDS and  $\Delta W$ ) usually provide. Relations between the diurnal water status indicator (MDS) and environmental predictors (SWP) were relatively low. We speculate this was due to more frequent low MDS amplitudes in rainless periods when compared with MDS peaks just after rain events resulting in low Spearman correlation values. Since Morlet analysis incorporates also low MDS amplitudes in resulting power spectra, Morlet spectra showed synchronous courses with SWP (Figures 6, 7) despite the low correlation between SWP and MDS (Figures 4, 5).

The advantage of Morlet analysis is that it visualizes also BDR cycles of other than of a diurnal length (Oberhuber et al., 2015) driven by underlying processes such as cell division and enlargement, phenology, etc. (Rathgeber et al., 2016). No BDR cycles appeared at a sub-diurnal scale (Figures 6 and 7). However, we revealed evident occurrence of significant 1–2 week-long cycles corresponding to highly negative SWP values. A thorough analysis of these long-lasting cycles is beyond the scope of this paper since it requires additional data on e.g. phenological development and respective statistical testing.

## CONCLUSIONS

Knowledge on the relationships between climate and growth is essential for assessing the future performance of conifers exposed to drought and air temperature anomalies. Detailed information on climate-growth relationships can be obtained via dendroecological analyses. Fine-scale stem circumference dynamics recorded by dendrometers reflect tree water status and hold some potential for characterising forest ecophysiology. This is one of the few studies that compared tree growth responses of economically important coniferous species of Central Europe (*P. sylvestris*, *P. abies*, *A. alba* and *L. decidua*) growing at the same site characterised by warmer and drier environmental conditions in comparison to their natural habitats. Thus, the settings of the study gave us an opportunity to examine tree species response to projected future climate.

Monitored species exhibited remarkably different growth patterns over two climatically different periods in 2017 and 2018. The differences in drought responses between the species may be explained by their intrinsic differences in morphology and physiology. *L. decidua* and *P. abies* were more sensitive species to environmental conditions than *A. alba* and *P. sylvestris* that was reflected in their radial stem growth. *A. alba* exhibited smooth radial growth during the growing season unaffected by the changes in environmental conditions including periodical droughts. Climate-growth relationships revealed competitive advantage of drought adapted *P. sylvestris* compared to *P. abies* and *L. decidua*. During the drought in 2018, *P. sylvestris* overtook *A. alba* in stem radial growth, which indicates that although *A. alba* can withstand slight temperature increase, it becomes less resistant than *P. sylvestris* if higher temperature is combined with water deficit. Although our study did not examine population-level responses, it clearly indicates that Silver fir is more resistant and resilient to drought events, and therefore, it is a suitable alternative to *P. abies* or *L. decidua*.

The examined tree water status parameters, namely stem water deficit and maximum daily shrinkage, were proved suitable for the comparison of different tree species water status. Tree

water status parameters ( $\Delta W$  and MDS) should be used for the inter-species comparison of water status with regard to different bark thickness of tree species and its corresponding elasticity, which can significantly affect the derived water status signal. Moving correlation analysis showed that stem water deficit of *L. decidua* and *P. abies* was more sensitive to air temperature and VPD than *A. alba* and *P. sylvestris*. During summer months, precipitation deficits, heat waves and consequently decreased soil water potential significantly affected stem circumference increase and tree water deficit, mainly of *L. decidua* and *P. abies*, also given that the studied species are not situated in an area of their optimal species growth.

**Acknowledgements.** The study was supported by research grants of the Slovak Research and Development Agency APVV-16-0325, APVV-16-0306, APVV-17-0644, APVV-15-0265, APVV-18-0390 and the Scientific Grant Agency of the Ministry of Education, Science, Research and Sport of the Slovak Republic under contracts VEGA 2/0049/18. This work was also supported by the grant "EVA4.0", No. CZ.02.1.01/0.0/0.0/16\_019/0000803 financed by the OP RDE.

## REFERENCES

- Allen, C.D., Breshears, D.D., McDowell, N.G., 2015. On underestimation of global vulnerability to tree mortality and forest die-off from hotter drought in the Anthropocene. *Ecosphere*, 6, 8, Article Number 129.
- Aubin, I., Munson, A.D., Cardou, F., Burton, P.J., Isabel, N., Pedlar, J.H., et al., 2016. Traits to stay, traits to move: are view of functional traits to assess sensitivity and adaptive capacity of temperature and boreal trees to climate change. *Environ. Rev.*, 24, 164–186.
- Aussenac, G., 2002. Ecology and ecophysiology of circum-mediterranean firs in the context of climate change. *Ann. For. Sci.*, 59, 823–832.
- Battipaglia, G., Saurer, M., Cherubini, P., Siegwolf, R.T.W., Cotrufo, M.F., 2009. Tree rings indicate different drought resistance of a native (*Abies alba* Mill.) and a non-native (*Picea abies* (L.) Karst.) species co-occurring at a dry site in Southern Italy. *For. Ecol. Manag.*, 257, 820–828.
- Begum, S., Nakaba, S., Yamagishi, Y., Oribe, Y., Funada, R., 2013. Regulation of cambial activity in relation to environmental conditions: understanding the role of temperature in wood formation of trees. *Physiol. Plant.*, 147, 46–54.
- Betsch, P., Bonal, D., Breda, N., Montpied, P., Peiffer, M., Tuzet, A., Granier, A., 2011. Drought effects on water relations in beech: the contribution of exchangeable water reservoirs. *Agric. For. Meteorol.*, 151, 531–543.
- Bole, A., Ammer, C., Löf, M., Nabuurs, G.J., Schall, P., Spathelf, P., Rock, J., 2009. Adaptive forest management in central Europe: climate change impacts, strategies and integrative concept. *Scand. J. For. Res.*, 24, 473–482.
- Bošela, M., Lukáč, M., Castagneri, D., Sedmák, R., Biber, P., Carrer, P. et al., 2018. Contrasting effects of environmental change on the radial growth of cooccurring beech and fir trees across Europe. *Sci. Total Environ.*, 615, 1460–1469.
- Bouriaud, O., Popa, I., 2009. Comparative dendroclimatic study of Scots pine, Norway spruce, and silver fir in the Vrancea Range, Eastern Carpathian Mountains. *Trees*, 23, 1, 95–106.
- Bréda, N., Huc, R., Granier, A., Dreyer, E., 2006. Temperate forest trees and stands under severe drought: a review of ecophysiological responses, adaptation processes and long-term consequences. *Ann. For. Sci.*, 63, 625–544.
- Camarero, J.J., Gazol, A., Sangüesa-Barreda, G., Oliva, J., Vicente-Serrano, S.M., 2015. To die or not to die: early warnings of tree dieback in response to a severe drought. *J. Ecol.*, 103, 44–57.
- Caudullo, G., Tinner, W., de Rigo, D., 2016. *Picea abies* in Europe: distribution, habitat, usage and threats. In: San-Miguel-Ayanz, J., de Rigo, D., Caudullo, G., Houston Durrant, T., Mauri, A. (Eds.): *European Atlas of Forest Tree Species*. European Commission, pp. 114–116.
- Čermák, J., Kučera, J., Bauerle, W.L., Phillips, N., Hinckley, T.M., 2007. Tree water storage and its diurnal dynamics related to sap flow and changes in stem volume in old-growth Douglas-fir trees. *Tree Physiol.*, 27, 181–198.
- Chan, T., Holttä, T., Berninger, F., Mäkinen, H., Nojd, P., Mencuccini, M., Nikinmaa, E., 2016. Separating water-potential induced swelling and shrinking from measured radial stem variations reveals a cambial growth and osmotic concentration signal. *Plant Cell Environ.*, 39, 233–244.
- Dietrich, L., Zweifel, R., Kahmen, A., 2018. Daily stem diameter variations can predict the canopy water status of mature temperate trees. *Tree Physiol.*, 38, 7, 941–952.
- Eilmann, B., Rigling, A., 2012. Tree-growth analyses to estimate tree species' drought tolerance. *Tree Physiol.*, 32, 178–187.
- Ehrenberger, W., Rüger, S., Fitzke, R., Vollenweider, P., Günthardt-Goerg, M.S., Kuster, T., Zimmermann, U., Arend, M., 2012. Concomitant dendrometer and leaf patch pressure probe measurements reveal the effect of microclimate and soil moisture on diurnal stem water and leaf turgor variations in young oak trees. *Funct. Plant Biol.*, 39, 297–305.
- Ellenberger, H., 2009. *Vegetation Ecology of Central Europe*. Fourth edition. Cambridge University Press, Cambridge, UK.
- Geburek, T., 2010. *Larix decidua* Miller, 1768. In: Roloff, A., Weissgerber, H., Lang, U., Stimm, B. (Eds.): *Bäume Mitteleuropas*. Wiley, Weinheim, pp. 431–450.
- González-Rodríguez, Á.M., Brito, P., Lorenzo, J.R., Gruber, A., Oberhuber, W., Wieser, G., 2017. Seasonal cycles of sap flow and stem radius variation of *Spartocytisus supranubius* in the alpine zone of Tenerife, Canary Islands. *Alp. Bot.*, 127, 97–108.
- Gričar, J., Čufar, K., 2008. Seasonal dynamics of phloem and xylem formation in silver fir and Norway spruce as affected by drought. *Russ. J. Plant Physiol.*, 55, 538–543.
- Hartmann, H., 2011. Will a 385 million year-struggle for light become a struggle for water and for carbon? - How trees may cope with more frequent climate change-type drought events. *Glob. Change Biol.*, 17, 642–655.
- Hinckley, T.M., Lassoie, J.P., Running, S.W., 1978. Temporal and spatial variations in water status of forest trees. *For. Sci. Monogr.*, 20, 1–72.
- Hlásny, T., Barcza, Z., Fabrika, M., Balázs, B., Chirkina, G., Pajtk, J., Sedmák, R., Turčáni, M., 2011. Climate change impacts on growth and carbon balance of forests in Central Europe. *Clim. Res.*, 47, 219–236.
- IPCC, 2013. Stocker, T.F., Qin, D., Plattner, G.-K., Tignor, M., Allen, S.K., Boschung, J., Nauels, A., Xia, Y., Bex, V., Midgley, P.M. (Eds.): *Climate Change 2013: The Physical Science Basis*. Contribution of Working Group I to the Fifth Assessment Report of the Intergovernmental Panel on Climate Change. Cambridge University Press, Cambridge, UK.
- IPCC, 2014. *Climate Change 2014: Impacts, Adaptation, and Vulnerability*. Part A: Global and Sectoral Aspects. Contribution of Working Group II to the Fifth Assessment Report of the Intergovernmental Panel on Climate Change. Cambridge University Press, Cambridge, United Kingdom and New York, NY, USA.

- Irvine, J., Grace, J., 1997. Continuous measurement of water tensions in the xylem of trees based on the elastic properties of wood. *Planta*, 202, 455–461.
- Irvine, J., Perks, M.P., Magnani, F., Grace, J., 1998. The response of *Pinus sylvestris* to drought: stomatal control of transpiration and hydraulic conductance. *Tree Physiol.*, 18, 393–402.
- Ježík, M., Blaženc, M., Kučera, J., Střelcová, K., Ditmarová, K., 2016. The response of intra-annual stem circumference increase of young European beech provenances to 2012–2014 weather variability. *iForest – Biogeosciences and Forestry*, 9, 6, 960–969.
- Kokfelt, U., Muscheler, R., 2012. Solar forcing of climate during the last millennium recorded in lake sediments from northern Sweden. *Holocene*, 2, 447–452.
- Köcher, P., Horna, V., Leuschner, C., 2013. Stem water storage in five coexisting temperate broad-leaved tree species: significance, temporal dynamics and dependence on tree functional traits. *Tree Physiol.*, 33, 817–832.
- Körner, C., Basler, D., 2010. Phenology under global warming. *Science*, 327, 5972, 1461–1462.
- Krakau, U.K., Liesebach, M., Aronen, T., Lelu-Walter, M.-A., Schneck, V., 2013. Scots Pine (*Pinus sylvestris* L.). In: Pâques, L.E. (Ed.): *Forest Tree Breeding in Europe. Current State-of-the-Art and Perspectives*. Springer, Dordrecht, New York.
- Latreille, A., Davi, H., Huard, F., Pichot, Ch., 2017. Variability of the climate-radial growth relationship among *Abies alba* trees and populations along altitudinal gradients. *For. Ecol. Manag.*, 396, 150–159.
- Lindner, M., Garcia-Gonzalo, J., Kolstrom, M., Green, T., Reguera, R., Maroschek, M. et al., 2008. Impacts of Climate Change on European Forests and Options for Adaptation. European Forestry Institute, Joensuu, 173 p.
- McDowell, N.G., Allen, C.D., 2015. Darcy's law predicts widespread forest mortality under climate warming. *Nat. Clim. Change*, 5, 669–672.
- McDowell, N., Pockman, W.T., Allen, C.D., Breshears, D.D., Cobb, N., Kolb, T., et al., 2008. Mechanisms of plant survival and mortality during drought: why do some plants survive while others succumb to drought? *New Phytol.*, 178, 719–739.
- Mencuccini, M., Hölttä, T., Sevanto, S., Nikinmaa, E., 2013. Concurrent measurements of change in the bark and xylem diameters of trees reveal a phloem-generated turgor signal. *New Phytol.*, 198, 1143–1154.
- Nourtier, M., Chanzy, A., Cailleret, M., Yingge, X., Huc R., Davi, H., 2014. Transpiration of silver Fir (*Abies alba* mill.) during and after drought in relation to soil properties in a Mediterranean mountain area. *Ann. For. Sci.*, 71, 683–695.
- Oberhuber, W., Stumböck, M., Kofler, W., 1998. Climate-tree-growth relationships of Scots pine stands (*Pinus sylvestris* L.) exposed to soil dryness. *Trees*, 13, 19–27.
- Oberhuber, W., Gruber, A., Kofler, W., Swidrak, I., 2014. Radial stem growth in response to microclimate and soil moisture in a drought-prone mixed coniferous forest at an inner Alpine site. *Eur. J. Forest Res.*, 133, 3, 467–479.
- Oberhuber, W., Hammerle, A., Kofler, W., 2015. Tree water status and growth of saplings and mature Norway spruce (*Picea abies*) at a dry distribution limit. *Front. Plant Sci.*, 6, 703.
- Oberhuber, W., Sehr, M., Kitz, F., 2020. Hygroscopic properties of thin dead outer bark layer strongly influence stem diameter variations on short and long time scales in Scots pine (*Pinus sylvestris* L.). *Agric. For. Meteorol.*, 290, Article Number 108026. DOI: 10.1016/j.agrformet.2020.108026
- Offenthaler, I., Hietz, P., Richter, H., 2001. Wood diameter indicates diurnal and long-term patterns of xylem water potential in Norway spruce. *Trees*, 15, 215–221.
- Pataki, D.E., Oren, R., Katul, G., Sigmon, J., 1998. Canopy conductance of *Pinus taeda*, *Liquidambar styraciflua* and *Quercus phellos* under varying atmospheric and soil water conditions. *Tree Physiol.*, 18, 307–315.
- Perämäki, M., Nikinmaa, E., Sevanto, S., Ilvesniemi, H., Siivola, S., Hari, P., Vesala, T., 2001. Tree stem diameter variations and transpiration in Scots pine: an analysis using a dynamic sap flow model. *Tree Physiol.*, 21, 12–13, 889–897.
- Percival, D.B., Walden, A.T., 2000. *Wavelet Methods for Time Series Analysis*. Cambridge University Press, Cambridge UK.
- Požgaj, A., Kurjatko, S., Chovanec, D., Babiak, M., 1993. *Štruktúra a vlastnosti dreva*. 1<sup>st</sup> Ed. Príroda, Bratislava, 483 p.
- Rathgeber, C.B.K., Cuny, H.E., Fonti, P., 2016. Biological basis of tree ring formation a crash course. *Front. Plant Sci.*, 7, 734.
- Rösch, A., Schmidbauer, H., 2018. *WaveletComp1.1: A guided tour through the R package*. 58 p.
- Ruosch, M., Spahni, R., Joos, F., Henne, P.D., van der Knaap, W.O., Tinner, W., 2016. Past and future evolution of *Abies alba* forests in Europe - comparison of a dynamic vegetation model with palaeo data and observations. *Glob. Chang. Biol.*, 22, 727–740.
- Scholz, F.C., Bucci, S.J., Goldstein, G., Meinzer, F.C., Franco, A.C., Miralles-Wilhelm, F., 2008. Temporal dynamics of stem expansion and contraction in savanna trees: withdrawal and recharge of stored water. *Tree Physiol.*, 28, 469–480.
- Schuster, R., Oberhuber, W., 2013. Age-dependent climate-growth relationships and regeneration of *Picea abies* in a drought-prone mixed coniferous forest in the Alps. *Can. J. For. Res.*, 43, 609–618.
- Spiecker, H., 2002. Tree rings and forest management in Europe. *Dendrochronologia*, 20, 1, 191–202.
- Steppe, K., De Pauw, D.J.W., Lemeur, R., Vanrolleghem, P.A., 2006. A mathematical model linking tree sap flow dynamics to daily stem diameter fluctuations and radial stem growth. *Tree Physiol.*, 26, 257–273.
- Steppe, K., Sterck, F., Deslauriers, A., 2015. Diel growth dynamics in tree stems: linking anatomy and ecophysiology. *Trends Plant Sci.*, 20, 335–343.
- Teskey, R., Wertin, T., Bauweraerts, I., Ameye, M., McGuire, M.A., Steppe, K., 2015. Responses of tree species to heat waves and extreme heat events. *Plant Cell Environ.*, 38, 9, 1699–1712.
- Torrence, C., Compo, G.P., 1998. A practical guide to wavelet analysis. *Bulletin of the American Meteorological Society*, 79, 1, 61–78.
- Turcotte, A., Rossi, S., Deslauriers, A., Krause, C., Morin, H., 2011. Dynamics of depletion and replenishment of water storage in stem and roots of black spruce measured by dendrometers. *Front. Plant Sci.*, 2, Article Number 21.
- Usoltsev, V., Merganičová, K., Konôpka, B., Osmirko, A.A., Tsepordey, I.S., Chasovskikh, V.P., 2019. Fir (*Abies* spp.) stand biomass additive model for Eurasia sensitive to winter temperature and annual precipitation. *Cent. Eur. For. J.*, 65, 166–172.
- van der Maaten, E., van der Maaten-Theunissen, M., Smiljanić, M., Rossi, S., Simard, S., Wilmking, M., Deslauriers, A., Fonti, P., von Arx, G., Bouriaud, O., 2016. dendrometeR: Analyzing the pulse of tree in R. *Dendrochronologia*, 40, 12–16.

- van der Maaten, E., van der Maaten-Theunissen, M., Smiljanić, M., Rossi, S., Simard, S., Wilmking, M., Deslauriers, A., Fonti, P., von Arx, G., Bouriaud, O., 2016. DendrometeR: Analyzing the pulse of tree in R. *Dendrochronologia*, 40, 12–16.
- Vieira, J., Rossi, S., Campelo, F., Freitas, H., Nabais, C., 2013. Seasonal and daily cycles of stem radial variation of *Pinus pinaster* in a drought-prone environment. *Agric. For. Meteorol.*, 180, 173–181.
- Vitali, V., Büntgen, U., Bauhus, J., 2017. Silver fir and Douglas fir are more tolerant to extreme droughts than Norway spruce in south-western Germany. *Glob. Chang. Biol.*, 23, 5108–5119.
- Will, R.E., Wilson, S.M., Zou, C.B., Hennessey, T.C., 2013. Increased vapour pressure deficit due to higher temperature leads to greater transpiration and faster mortality during drought for tree seedlings common to the forest–grassland ecotone. *New Phytol.*, 200, 366–374.
- Zeidler, A., Borůvka, V., Schönfelder, O., 2018. Comparison of wood quality of douglas fir and spruce from afforested agricultural land and permanent forest land in the Czech Republic. *Forests*, 9, 1. DOI: 10.3390/f9010013
- Zweifel, R., 2006. Intra-annual radial growth and water relations of trees: implications towards a growth mechanism. *J. Exp. Bot.*, 57, 6, 1445–1459.
- Zweifel, R., Häsler, R., 2001. Dynamics of water storage in mature subalpine *Picea abies*: temporal and spatial patterns of change in stem radius. *Tree Physiol.*, 21, 561–569.
- Zweifel, R., Item, H., Hasler, R., 2000. Stem radius changes and their relation to stored water in stems of young Norway spruce trees. *Trees*, 15, 50–57.
- Zweifel, R., Item, H., Häsler, R., 2001. Link between diurnal stem radius changes and tree water relations. *Tree Physiol.*, 21, 869–877.
- Zweifel, R., Zimmermann, L., Newbery, D.M., 2005. Modelling tree water deficit from microclimate: an approach to quantifying drought stress. *Tree Physiol.*, 25, 147–156.
- Zweifel, R., Zimmermann, L., Zeugin, F., Newberry, D.M., 2006. Intra-annual radial growth and water relations of trees: implications towards a growth mechanism. *J. Exp. Bot.*, 57, 1445–1459.
- Zweifel, R., Drew, D.M., Schweingruber, F., Downes, G.M., 2014. Xylem as the main origin of stem radius changes in *Eucalyptus*. *Funct. Plant Biol.*, 41, 520–534.

Received 4 December 2019

Accepted 7 July 2020

# Water repellency in eucalyptus and pine plantation forest soils and its relation to groundwater levels estimated with multi-temporal modeling

H.I.G.S. Piyaruwan<sup>1</sup>, P.K.S.C. Jayasinghe<sup>2</sup>, D.A.L. Leelamanie<sup>1\*</sup>

<sup>1</sup> Department of Soil Science, Faculty of Agriculture, University of Ruhuna, Mapalana, Kamburupitiya 81100, Sri Lanka.

<sup>2</sup> Department of Information and Communication Technology, Faculty of Technology, University of Ruhuna, Karagoda-Uyangoda, Kamburupitiya 81100, Sri Lanka.

\* Corresponding author. Tel.: +94-71-861-4380. Fax: +94-41-2292384. E-mails: leelamanie@soil.ruh.ac.lk; leelamanie@yahoo.co.uk

**Abstract:** Water repellency makes soils capable of resisting to the penetration of water applied on the surface and inflict various influences on groundwater. The objectives of the present study were to identify the water repellency under pine and eucalyptus plantations, to determine social impacts of water level changes, to find possible changes in groundwater levels in the surrounding areas during the past four decades, and to relate water repellent characteristics of soils with the groundwater level changes. The study was conducted in eucalyptus (*Eucalyptus grandis*) and pine (*Pinus caribaea*) plantation forests located in Upcountry intermediate zone, Sri Lanka. Each land was separated into three blocks (B1, B2, B3) based on the slope. Water repellency was measured with water drop penetration time (WDPT) and contact angle. The water entry value was estimated with the pressure head method. Interconnected social impacts was examined using a questionnaire based survey. Groundwater levels from 1980 to present were modeled with remotely sensed information. Both eucalyptus and pine forest soils showed water repellency, which decreased with increasing soil depth. Eucalyptus soils showed highly hydrophobic conditions on the surface (WDPT>7200 s). Ponding depths required for entry of water into the soil in eucalyptus soils was 4.6–5.3 cm, whereas that of pine soils was 1.5–4.0 cm, although achieving these levels would be difficult considering the steep slopes. Contact angle showed positive logarithmic correlation with water entry value. The people living in the surrounding areas expressed less water availability for their domestic purposes, decreased water level in household wells, and drying up of natural water resources at present compared with 1980s. Modelling with remotely sensed thematic maps confirmed that the groundwater levels in both areas has decreased over the time. It indicated that the eucalyptus and pine vegetation have created unfavorable conditions in regard with water entry and groundwater recharge. Proper attention from the responsible authorities will be essential to prevent the adverse impacts of on groundwater resources.

**Keywords:** *Eucalyptus grandis*; Groundwater modeling; *Pinus caribaea*; Water repellency; Water entry value.

## INTRODUCTION

Soil water repellency (SWR) is a phenomenon that make soils capable of resisting to the penetration of water applied on the surface. It is caused by organic compounds containing hydrophobic properties that are coating individual soil particles, or present in soil as interstitial matter. These hydrophobic molecules are released at natural conditions, during fires from plants, organisms, and decomposing organic matter in soils. Water repellent coatings also can restrict the interactions between pores inside and outside of the soil aggregates (Fér et al., 2016). SWR lessens the affinity of soils towards water to different degrees, resisting the wetting for durations that may range from a few seconds to hours or days (Doerr and Thomas, 2000). It influences important hydrological and geomorphological consequences such as lowered infiltration rates, upsurge of the overland flow, uneven wetting, development of preferential fingerlike and bypass flows (Imeson et al., 1992; Kobayashi and Shimizu, 2007). SWR decreases the capacity of infiltration in soil and enhances runoff events specially in steep slope lands during the early stages of rainfall (Contreras et al., 2008; Siteur et al., 2016). In addition, organic-clay coatings on soil aggregates in some soils may influence water and solute transport into soil aggregates (Fér and Kodešová, 2012; Gerke and Köhne, 2002).

Occurrence of SWR has been reported in diverse natural climatic and weather conditions, soil types and vegetation cover

of large trees to small turf grasses. Forests with water repellent conditions have been recognized to alter the hydraulic properties of soils (Kajiura et al., 2012; Kobayashi and Shimizu, 2007; Leelamanie and Nishiwaki, 2019; Lichner et al., 2013; Wahl et al., 2003). Various kinds of impacts of SWR on the soil water systems have been characterized by several studies under different land uses, climatic conditions, and regions. Water repellency is frequently found in soils covered by tree species such as Eucalyptus (*Eucalyptus globulus*), Cluster pine (*Pinus pinaster*), Scots pine (*Pinus sylvestris*), Cypress (*Chamaecyparis obtusa*), Japanese cedar (*Cryptomeria japonica*), and Casuarina (*Casuarina equisetifolia*) (Alagna et al., 2017; Benito et al., 2019; Iovino et al., 2018; Kobayashi and Shimizu, 2007; Leelamanie, 2016; Leelamanie and Nishiwaki, 2019; Lichner et al., 2013). The SWR observed in conifer forests is considered to be a natural characteristic rather than being induced by external factors such as forest fires (Doerr et al., 2009). Water repellency is known to influence groundwater in different ways. It induces preferential flow paths that provide shortened and faster routes for the transport of water and solutes, accelerating the driving of solutes to the groundwater increasing the risk of groundwater pollution (Bauters et al., 1998; Ziogas et al., 2005). Eucalyptus and pine plantations in Sri Lanka, which show water repellent conditions (Leelamanie et al., 2016), are getting increasing attention at present due to the social uneasiness on lowering the availability of water resources related to the establishment of these exotic species.

Groundwater is one of the most important natural resources on the earth that supports the ecological diversity and human health (Rao et al., 2001). Falling of groundwater tables are reported at remarkable rates in most parts of the world (Giordano, 2009). Decline of groundwater level causes numerous eco-environmental problems such as oasis degeneration, drying up of wetlands, disappearance of streams and artesian wells, and salt water intrusions etc. The recharge of groundwater depends mainly on several factors such as infiltration capacity and permeability, stochastic characteristics of rainfall, and other climatic factors. In arid regions, recharge of groundwater occurs mainly through ephemeral streams. In semiarid regions, the recharge of groundwater is mostly irregular and occurs in the periods of heavy rainfall (Şen, 2015). With above 1800 mm of average annual rainfall (Zubair and Ropelewski, 2006) the main natural groundwater recharge in Sri Lanka is by the precipitation as rainfall. In general, upland areas are considered to be the sources for groundwater recharge or replenishment, and lowland areas are considered to be the points of discharge. In recent decades, the natural systems of groundwater recharge and discharge in many regions of the world are found to be critically altered by various human activities (Giordano, 2009). Groundwater table diminishes when the rate of recharge is lower than the rate of withdrawal (Senanayake et al., 2016). It is clear that low rates of replenishment or high rates of withdrawal may lead to depletion of groundwater table, leading to dropped water level in groundwater wells as well as in surface water resources such as lakes and streams.

Remote sensing and Geographical Information System (GIS) play an important role in the management of water and land resources. GIS technique can be used as an efficient tool in identification of groundwater levels in different locations. Remote sensing can be effectively used to acquire surface feature information related to groundwater such as land use, land forms, and drainage and to handle widespread data for modeling (Brunner et al., 2007). Standardizing the low reflectance in red band and higher reflectance in infrared band, it is possible to measure various vegetation-related features using normalized difference vegetation index (NDVI) (Pan et al., 2008). Modeling techniques use remotely sensed data with surface reflectance to relate surface soil moisture to the shallow groundwater level. The relationship of the surface reflectance and the depth to the groundwater level can be assessed with the observation of groundwater wells (Pan et al., 2008).

Only limited reports are available to understand the influence of repellency-induced changes to the groundwater levels. Adane et al. (2017) recently reported that the presence of water repellent conditions reduced groundwater recharge, which is caused by the combinations of increased extraction of water by plants and the declined infiltration rates due to water repellent surface layer. Still, the hydrological alterations caused by soil water repellent conditions and their multi-temporal consequences on groundwater dynamics have received comparatively a less attention. Present study was planned with the four main purposes: to identify the SWR under pine and eucalyptus plantations; to determine the social impacts of water level changes using a questionnaire based survey; to find the possible changes in groundwater levels in the surrounding areas of pine and eucalyptus plantations during the past four decades; and to relate the water repellent characteristics of the soils with the groundwater level changes of the areas.

## MATERIALS AND METHODS

### Study sites and soil sampling

The experimental site one (S1) was a eucalyptus (*Eucalyptus grandis*) plantation forest in Diyathalawa with an area of around 100 ha, located in the Upcountry intermediate zone (IU3c agro ecological region) of Sri Lanka (National Atlas of Sri Lanka, 2007). The mean annual rainfall is above 1700 mm. The second experimental site (S2) was a pine (*Pinus caribaea*) plantation forest in Haputale with an area of around 5 ha, which was also located in the Upcountry intermediate zone. The area belongs to the IU3a and IU3b agro ecological regions with annual precipitation of 1700–1900 mm. The road distance between the two study sites is around 11 km (the areal distance ~5–6 km). In the both sites, the largest rainfall events are in between December to February and the mean annual temperature is in the range of 20–22.5°C. The soils of the two sites are of a sandy loam texture and classified as red yellow podzolic soils under local classification and Hapludults under USDA classification (Soil Survey Staff, 2014).

Three sampling blocks (B1, B2, and B3) were selected from each site based on the slope of the experimental site, where B3 was selected to be on the top of the hill in both sites. The distances between the blocks were kept around 100–150 m. Table 1 shows the coordinates of the three soil blocks and slopes of the two sites. Core samples (undisturbed: for measurement of bulk density) and the bulk samples (disturbed) were collected from the blocks at the depths of 0–5, 5–10, and 10–15 cm in three replicates for each depth, in years of 2017 and 2018, in wet season (November to February). The collected samples were transported to the laboratory in labeled and sealed polythene containers.

**Table 1.** Sampling locations and land slopes in eucalyptus and pine plantation forests.

Soil Block	N	E	Slope (°)
Eucalyptus			
B1	06° 47' 42"	080° 57' 57"	10.4
B2	06° 47' 45"	080° 57' 58"	20.3
B3	06° 47' 56"	080° 57' 43"	34.4
Pine			
B1	06°46'15"	080°55'50"	11.4
B2	06°46'13"	080°55'52"	24.8
B3	06°46'13"	080°55'50"	41.5

### Laboratory measurements

The samples were air dried at room temperature (27±3°C), and 75±5% relative humidity, for 3 days. Samples were passed through a 2 mm mesh to eliminate the coarse particles before the soil testing. The persistence and the degree of water repellency was measured using the water drop penetration time (WDPT) and soil-water contact angle, respectively. The critical point of water-entry into the soil was measured using the water entry value (Wang et al., 2000) of the samples. Bulk density (Undisturbed core method; Blake and Hartge, 1986a), particle density (Pycnometer method; Blake and Hartge, 1986b), Porosity (numerical method), Texture (Hydrometer method; Bouyoucos, 1962) and OM% (Loss on ignition method; Schumacher, 2002) were determined all soil depths for both sites. The measurements were conducted in three replicates, in the laboratory with air-dried samples.

### The WDPT test

Soil samples were placed in porcelain containers with a sample thickness of >5 mm to avoid interferences of drops reaching the bottom of the containers. A burette was filled with distilled water and one drop (50±1µl) of distilled water was carefully placed on the soil surface from a height of about 10 mm to minimize the collision impacts by the falling drops. The volume of the droplet was set to 50 µl to represent the average size of a raindrop. Containers were covered with lids to minimize the evaporation during the experimental period. The time taken for water drop to complete the penetration was measured using a stop watch (Leelamanie et al., 2008). Penetration times shorter than 0.5 s were considered as 0 s, because the actual measurement could not be taken accurately corresponding to the instantaneous penetration. The measurement of penetration time was terminated after 7200 s and all WDPTs exceeding 7200s were assigned to be 7200 s. The WDPT values were determined in six replicates for each soil depth in the three blocks in both sites.

### Soil-water contact angle

The Soil-water contact angle was measured using the modified sessile drop method (SDM) (Bachmann et al., 2000), in six replicates, using a digital microscopic camera (FS-3100-PC, Fujikoden Co. Ltd., Japan). Monolayers of soil samples was prepared by sprinkling the air dried and sieved soil samples on a double-sided adhesive tape (1.5 cm × 1.5 cm) fixed on smooth glass slides. Sprinkled soil was pressed to the tape using a 100 g weight for 10 s and the surplus soil was removed by gently tapping the glass slide. To ensure the stabilization of a soil monolayer on the adhesive tape, the same procedure was repeated twice. The slides with soil monolayers were placed on the stage of the digital microscopic camera. A drop of distilled water (10 µL) was placed on the soil surface using a micro pipette (Nichipet EX II J15615241, Nichiriyo, Japan). Digital micro-photograph of the horizontal view of the water drop was taken within 1 s. Contact angle of each sample was determined using the micro-photographs of the horizontal view of the drop on the soil monolayer (Leelamanie et al., 2008; Leelamanie, 2016), using the both points of contacts of the water to the soil layer in the two-dimensional photograph of the drop.

### Water entry value

Low hydraulic pressures at the soil surface is not sufficient to make water infiltrate into water repellent soils. The critical pressure head that requires to the breakdown repellency and start the infiltration can be determined using the water entry value. The water entry values of the samples were tested for soils collected from the surface (0–5 cm) using the pressure head method (Wang et al., 2000). Air-dried 50-g soil samples were placed on the porous plate of a Buchner funnel, which was covered with a membrane filter mounted filter paper, and the funnel was connected to a burette by a flexible tube. A hydraulic pressure was applied to the soil by raising the burette level, starting from a negative pressure head to avoid initial wetting of the soil (Wang et al., 2000). The pressure was carefully increased by 5 min time intervals up to the point where the water enters the soil matrix. At the point of water entry, the height of the water column was measured with respect to the reference level considering the soil as the water entry values of the samples (Liyanage and Leelamanie, 2016).

### Groundwater modeling with remotely sensed information

This method was used to determine the relations of the irregularities in recharge of groundwater in water repellent soils to the groundwater levels of the areas surrounding the study sites. The method depends on the fact that the soil moisture on the surface is related with the shallow groundwater level. As the reflectance of the land surface related to normalized difference vegetation index (NDVI) obtained from the remote sensing images varies with the surface soil moisture, a relationship between the reflectance obtained from the remote sensing images and groundwater level depth using the method by Pan et al. (2008).

The NDVI is related to the surface vegetation coverage, in regard with the quality or the density. The higher the density of vegetation, the larger the value of NDVI.

$$NDVI = (R_{S2} - R_{S1}) / (R_{S2} + R_{S1}) \quad (1)$$

where  $R_{S1}$  and  $R_{S2}$  are respectively the radiance of the band 1 (near infrared) and band 2 (red) in Landsat images (wave lengths: 0.63–0.67 µm and 0.77–0.90 µm for band 1 and 2 respectively). The temperature surface can be determined using the split window technique with thermal infrared band data.

$$T_s = R_{S10} + a(R_{S10} - R_{S11}) + c \quad (2)$$

$T_s$  denotes the surface temperature (Land surface temperature, LST),  $R_{S10}$ ,  $R_{S11}$  are the radiance of thermal bands 10 and 11, respectively in Landsat images (wavelengths: 10.6–11.19 µm and 11.5–12.51 µm for band 10 and 11, respectively),  $a$  denotes the model parameter, and  $c$  denotes the split window coefficient. The soil moisture on the surface is described by using the LST and NDVI.

$$MC_s = f(T_s, NDVI) \quad (3)$$

where  $MC_s$  is surface soil moisture content.

The depth level of shallow groundwater is related to the surface soil moisture, where the relationship between the groundwater level depth and the soil moisture is stated as follows

$$MC_s = \alpha_0 + C_1 \exp(D_w) \quad (4)$$

$D_w$  is the depth of groundwater level. By combining Eq. (3) and (4), a mathematical model can be developed for the depth of groundwater level (Pan et al., 2008);

$$D_w = k \times \ln(NDVI \times T_s) + b \quad (5)$$

where  $k$  and  $b$  are the coefficients that can be achieved by curve fitting using the groundwater levels obtained by the observation of water levels of groundwater wells in the field. The field data on the water levels of groundwater wells situated surrounding both study areas (3 wells per study area) were gathered for consecutive period of six months to represent (Pan et al., 2008). The  $NDVI$  and  $T_s$  parameters were estimated through remote sensing images of the areas in same time period. Surface temperature and  $NDVI$  thematic maps for eucalyptus and pine plantation forest areas in 2018 are presented in Fig. 1 and Fig. 2. Then the  $D_w$  values were plotted against the  $\ln(NDVI \times T_s)$  to obtain a linear correlations and the  $k$  and  $b$  values were determined for the linear curves. Finally, these  $k$  and  $b$  coefficients can be used in the Eq. (5) with  $NDVI$  and  $T_s$  parameters estimated through remote sensing images in the areas in the

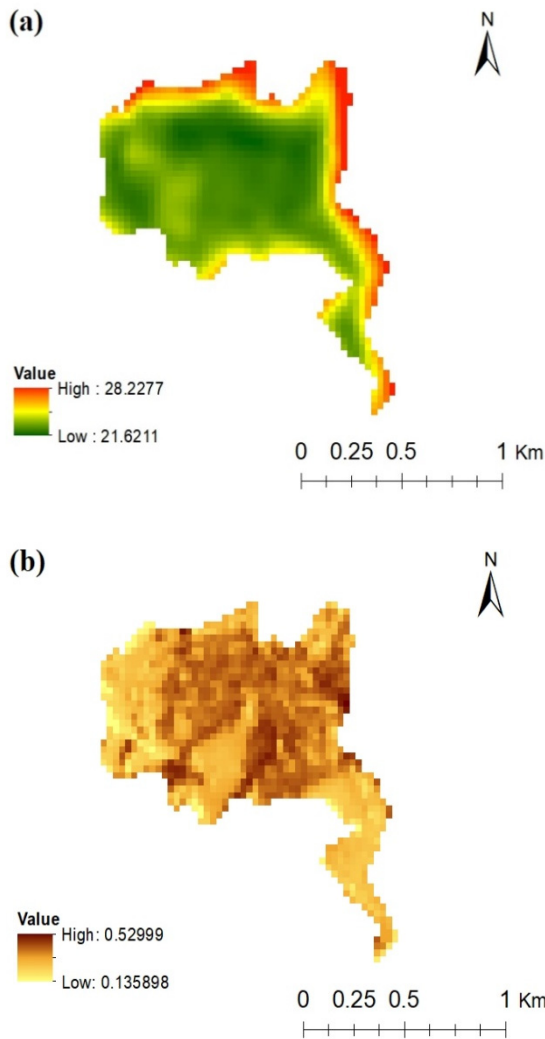


**Fig. 1.** Thematic maps of the land surface temperature (LST) and normalized difference vegetation index (NDVI) for eucalyptus plantation forest area in 2018.

past. These estimated  $k$  and  $b$  values were used with  $NDVI$  and  $T_s$  parameter for the years of 1980, 1990, 2000, 2010 and 2018, to estimate depth to the groundwater level from surface in both Haputale (pine) and Diyathalawa (eucalyptus) areas.

Remote sensing images were obtained from satellite sensors for 1980 (Landsat 5), 1990 (Landsat 5), 2000 (Landsat 7), 2010 (Landsat 7), and 2018 (Landsat 8). Pre-processing functions were performed for the satellite images before analyzing. Google earth application was used to extract the maps of the study areas (eucalyptus and pine plantation forests). These maps were used to subset the study areas from Landsat images. Thermal bands of the Landsat images were used to estimate the LST and NDVI through the raster image calculator in ArcMap tool (ESRI, 2017).

### Social impacts of SWR

Questionnaire based survey was conducted in Haputale and Diyathalawa areas to relate onsite SWR of the studied sites to the hydrological consequences and interconnected social impacts. Forty persons from each area were selected randomly among the people living near (within a distance of 5km to each site) to the respective pine and eucalyptus plantations for this

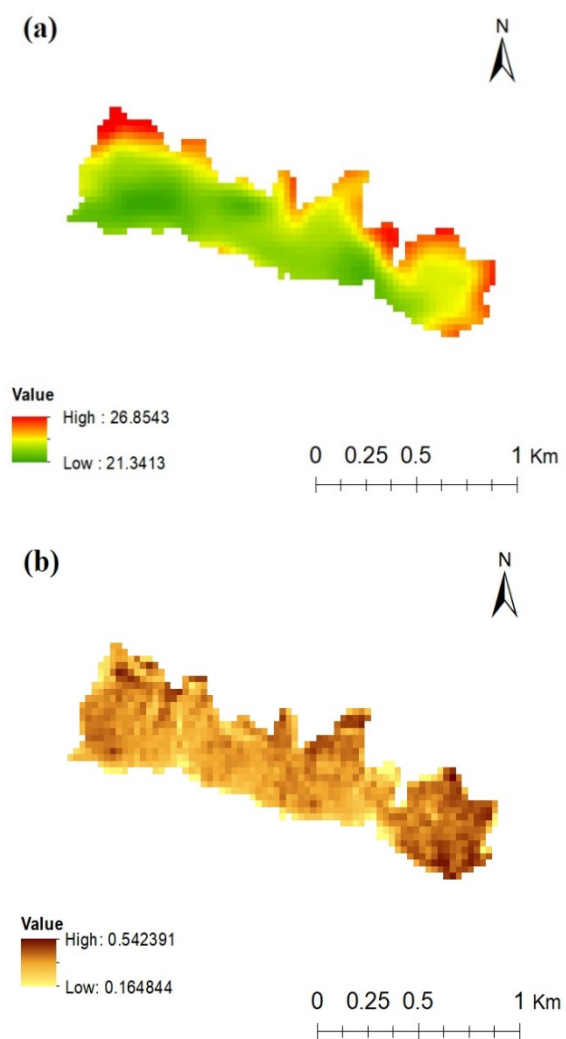


**Fig. 2.** Thematic maps of the land surface temperature (LST) and normalized difference vegetation index (NDVI) for pine plantation forest area in 2018.

survey. Questions were mainly focused to determine the impressions and opinion of the people in relation to the hydrological consequences, basically the water scarcity conditions comparing the past and present conditions. For the statistical analysis, the responses of people on the availability of water for their domestic purposes were separated into three categories as 'better', 'worse', and 'no change' and assigned 2, -2, and 0, respectively. The responses on the changes in water level in their household groundwater wells were also separated into three categories as 'increase', 'decrease', and 'no change' and assigned 2, -2, and 0, respectively. The responses of the people living in the Diyathalawa and Haputale areas on the drying up of proximate artesian wells and water resources were separated into two categories as 'yes' and 'no'.

### Data analysis

The data were statistically analyzed with analysis of variance (ANOVA), regression analysis and correlation, at 0.05 probability level using Microsoft Excel 2013 data analysis tool pack. Results from questionnaire based survey was analyzed using non-parametric statistics with Wilcoxon sign rank test, where Minitab 17 software was used for the analysis.

**RESULTS AND DISCUSSION**

**Basic properties of soils**

Both soils showed comparatively high bulk densities (mostly > 1 g cm<sup>-3</sup>). The texture of soils in both sites in all the soil depths were sandy loam. Organic matter decreased with increasing depth of the soil profile in all three blocks in both study sites. Table 2 presents the information on the basic properties of the soils in the two study sites (three blocks, three depths) in detail.

**Presence of water repellency**

The persistence of water repellency in eucalyptus and pine plantation forest soils as measured by WDPT (log WDPT) is given in Fig. 3. In all the soil, the highest WDPT was found in the top soil layer (0–5 cm), decreased with the increasing soil depth. Surface soils in all three blocks of the eucalyptus forest were extremely water repellent with WDPT exceeding 7200 s (Fig. 3a). Pine forest soils showed lower repellency compared with that of eucalyptus except in the B3, which showed WDPT > 7200 (Fig. 3b). Surface soils in B1 showed slight water repellency (10 s <WDPT < 60 s) and those of B2 showed severe water repellency (600 s <WDPT < 3600 s).

The degree of water repellency in eucalyptus and pine plantation forest soils as measured by soil-water contact angle is given in Fig. 4. Similar to the WDPT results, surface soils of both eucalyptus and pine forests showed the highest contact angle and decreased with increasing soil depth. Eucalyptus forest soils showed highly hydrophobic nature on the surface with soil-water contact angles in all the blocks exceeding 90° (Fig. 4a). Pine forest soils showed comparatively low contact angles (83–84°) on the surface in B1 and B2, and similar to the WDPT results, very high contact angle in B3 (100°) (Fig. 4b).

Several contradictory reports are available to show the water repellency to be existing from the top down to the weathered horizon as well as to be increased with increasing soil depth (eg. Doerr et al., 1996; Santos et al., 2016). However, weakening of water repellency with increasing soil depth is more commonly reported in casuarina, pine, eucalyptus, and oak forest soils in most continents (Badia-Villas et al., 2014; Flores-Mangual et al., 2013; Leelamanie, 2016; Lichner et al., 2007; Rodriguez-Alleres et al., 2007). It was clear that the highest repellency of both eucalyptus and pine soils tested in this study

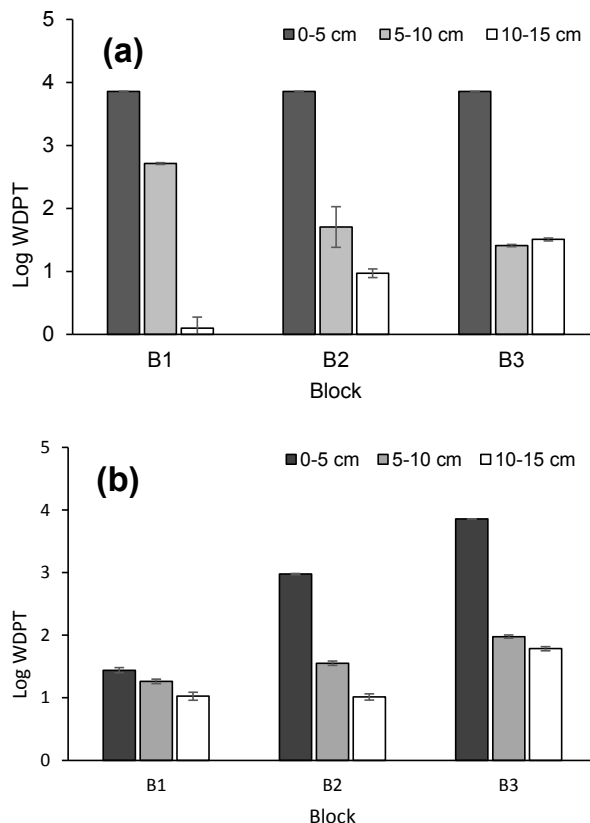


**Fig. 3.** The persistence of water repellency in eucalyptus and pine plantation forest soils as measured by WDPT (log WDPT).

confined to the surface layer revealing a diminishing water repellency with increasing depth of soil. According to numerous reports, soil water repellency is influenced by the content and the composition of organic matter. Mostly reported correlations between the organic matter content and SWR are positive, where the reductions in the SWR soil depth are generally attributed to the diminishing organic matter content (McKissock et al., 1998; Rodriguez-Alleres et al., 2007; Vogelmann et al., 2010; Wallis et al., 1990; Woche et al., 2005). Accordingly, the lowering of SWR towards deeper soil layers in the present study can be considered related to the declining of organic matter content.

**Table 2.** The basic properties of eucalyptus and pine plantation forest soils.

Soil property	Block 01			Block 02			Block 03		
	0–5 cm	5–10 cm	10–15 cm	0–5 cm	5–10 cm	10–15 cm	0–5 cm	5–10 cm	10–15 cm
<b>Eucalyptus</b>									
Bulk density (g cm <sup>-3</sup> )	1.03 ± 0.10	1.11 ± 0.04	1.20 ± 0.01	0.98 ± 0.08	1.04 ± 0.11	1.19 ± 0.08	1.02 ± 0.06	1.04 ± 0.09	1.04 ± 0.04
Porosity (%)	53.5 ± 7.1	50.1 ± 4.6	48.8 ± 2.9	57.37 ± 6.5	58.6 ± 2.3	51.3 ± 5.4	57.0 ± 2.7	55.5 ± 5.7	55.0 ± 3.6
Sand %	80.3 ± 1.5	74.4 ± 0.1	79.5 ± 0.1	82.1 ± 0.1	79.4 ± 0.1	76.7 ± 0.2	79.4 ± 0	71.6 ± 0.1	81.9 ± 0.1
Silt %	6.9 ± 1.5	6.8 ± 1.5	4.3 ± 1.5	5.1 ± 0	6.9 ± 1.5	10.3 ± 0.1	3.4 ± 1.5	7.7 ± 0	2.6 ± 0
Clay %	12.9 ± 0	18.8 ± 1.4	16.2 ± 1.4	12.8 ± 0	13.7 ± 1.5	12.9 ± 0.1	17.1 ± 1.5	20.6 ± 0.1	15.5 ± 0
Organic matter (%)	9.93 ± 0.12	7.04 ± 0.05	6.88 ± 0.04	11.6 ± 0.30	7.71 ± 0.08	6.33 ± 0.02	9.19 ± 0.17	7.83 ± 0.12	6.75 ± 0.03
<b>Pine</b>									
Bulk density (g cm <sup>-3</sup> )	0.93 ± 0.05	1.03 ± 0.08	1.03 ± 0.18	0.82 ± 0.01	1.04 ± 0.08	1.11 ± 0.09	1.13 ± 0.07	1.15 ± 0.06	1.22 ± 0.05
Porosity (%)	63.4 ± 0.9	59.6 ± 2.8	60.5 ± 6.2	67.6 ± 0.6	60.9 ± 1.0	58.7 ± 4.6	56.5 ± 4.4	59.5 ± 1.0	51.1 ± 2.2
Sand %	76.12 ± 7.32	74.17 ± 4.16	73.84 ± 1.57	69.16 ± 2.26	69.89 ± 2.73	72.88 ± 3.51	75.76 ± 2.90	73.62 ± 1.32	71.11 ± 1.58
Silt %	9.76 ± 6.21	7.37 ± 5.74	9.02 ± 1.56	10.6 ± 2.86	7.07 ± 1.45	7.89 ± 0.14	10.79 ± 2.80	10.02 ± 1.63	10.82 ± 2.64
Clay %	14.12 ± 1.66	18.46 ± 1.63	17.14 ± 1.57	20.23 ± 1.31	23.03 ± 1.32	23.53 ± 10.92	13.46 ± 2.67	16.37 ± 2.60	18.07 ± 3.24
Organic matter (%)	19.08 ± 1.6	15.47 ± 1.11	12.4 ± 0.39	16.12 ± 1.1	11.81 ± 2.99	10.4 ± 0.8	11.09 ± 0.38	10.03 ± 0.29	9.12 ± 0.42

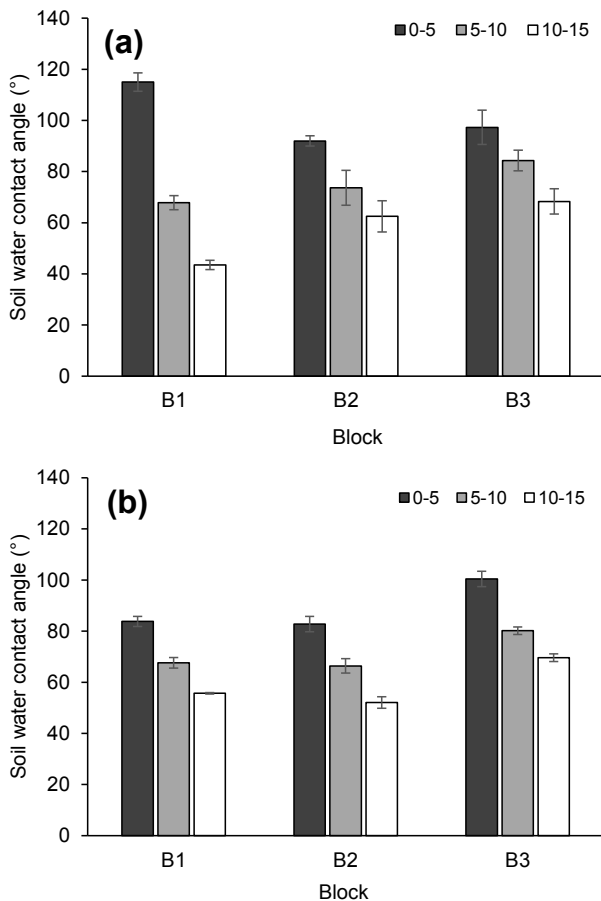


**Fig. 4.** The degree of water repellency in eucalyptus and pine plantation forest soils as measured by soil-water contact angle.

#### Water entry value

Fig. 5 presents the water entry values of the eucalyptus and pine forest soils. The water entry values of eucalyptus forest soils showed significantly high values than those of pine forest, except in B3 soils. It was clear that the water entry values of all the soils can be closely related to the water repellent conditions on the surface soils. As presented in Fig. 6, soil-water contact angle showed positive logarithmic correlation ( $R^2 = 0.66$ ) to the water entry values. Liyanage and Leelamanie (2016) observed similar results in soils treated with hydrophobic casuarina leaf litter. Lee et al. (2015) observed similar results, and reported that water entry pressure increased with increasing water repellency in an artificially-prepared water-repellent silty soil. The increasing hydrophobicity of soil tend to increase the air encapsulation within the soil during the intake of water, which is known to reduce the rates of water intake by increasing the pressure required for the water entry of the repellent soils (Liyanage and Leelamanie, 2016; Sullivan, 1990). As explained by Letey et al. (2000), the water entry pressure is a function of both soil-water contact angle and the pore radius. Theoretically, a need of positive pressure arises to force water entry into the soil when the soil-water contact angles exceed  $90^\circ$ . This justifies the positive correlation between the water entry values and the soil-water contact angle (Bauters et al., 2000). With positive water entry values in water repellent soils, a ponding depth would be required to induce water entry into soils (Letey, 2001; Wang et al., 2000). High water entry values predict the potential risks of soil erosion, where building up of required ponding depths for water intake is difficult due to various reasons such

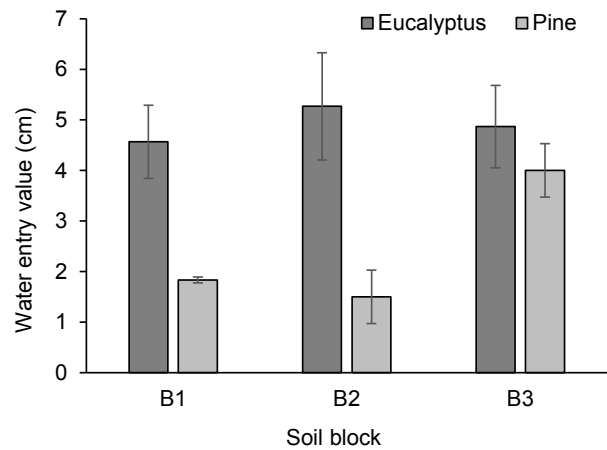


**Fig. 5.** Water entry values of the eucalyptus and pine forest soils.

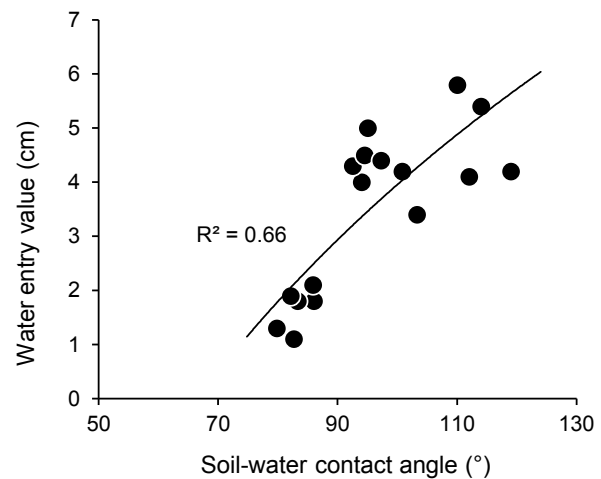


**Fig. 6.** Relation of soil-water contact angle to the water entry values of the eucalyptus and pine forest soils.

as high steepness of the slopes, which is characteristic in the study-sites of the present research.

#### Social impacts as revealed by questionnaire based survey

The responses of the people living in the surrounding areas of the two plantation forests on the availability of water for their domestic purposes, changes in water level in their household wells, and experience in drying up of artesian wells and water resources at present condition when compared with the situation in 1980–1990 are presented in Fig. 7. Results showed that about 90% the selected people living in both Diyathalawa and Haputale areas neighboring the eucalyptus and pine plantation forests, expressed that availability of water for domestic purposes at present is poor (response: ‘worse’) compared with the situation in 1990 (Fig. 7a), and 10% expressed no difference (response: ‘no change’) in the availability of water. Considering the response of the people, Wilcoxon sign rank test revealed a statistically significant ( $p < 0.05$ ) level of water scarcity conditions compared to the past in both areas.

About 85% of the interviewed people in Diyathalawa area (neighboring eucalyptus forest) and 88% in Haputale area (neighboring pine forest), claimed that they have experienced decreases in water levels in their groundwater wells compared with the past (Fig. 7b). Wilcoxon sign rank test revealed

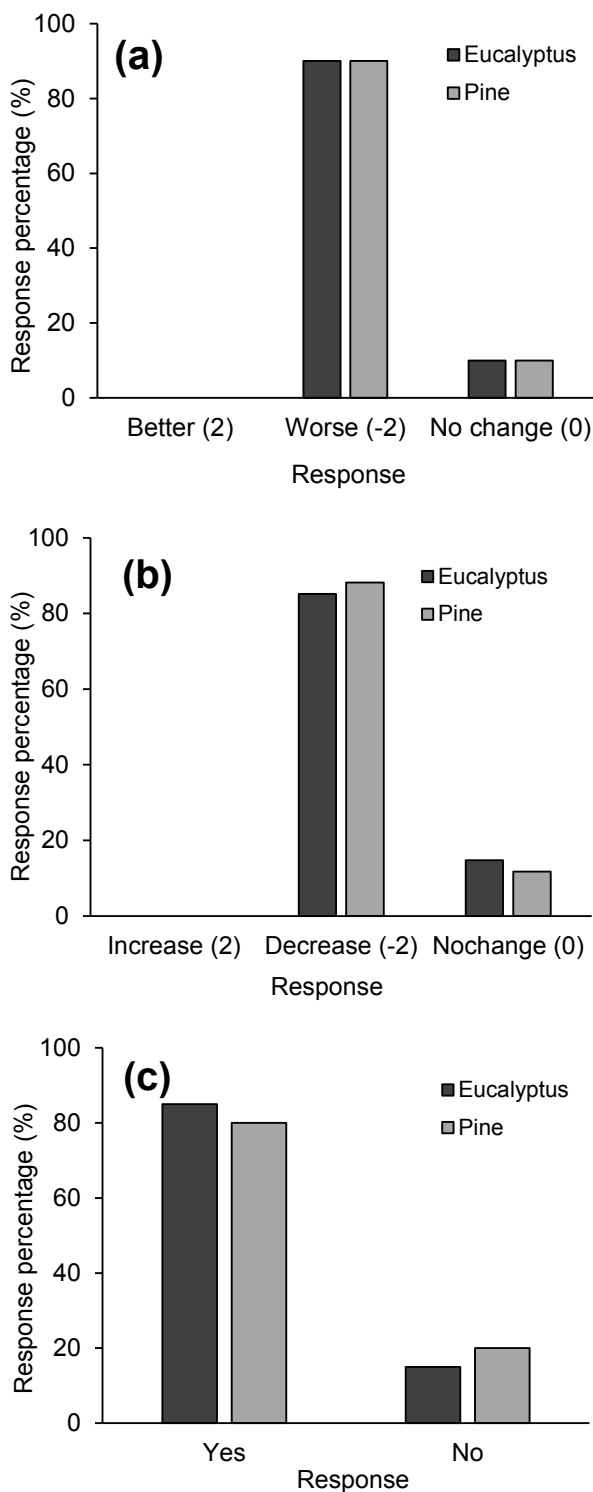


**Fig. 7.** The responses of the people living in the surrounding areas of the two plantation forests on (a) the availability of water for their domestic purposes, (b) changes in water level in their household wells, and (c) experience in drying up of fountains and water resources at present compared with the past (1980–1990).

significant decreases in groundwater levels in both Diyathalawa and Haputale areas.

Based on the results, 85% of the people living in the Diyathalawa area, 80% of the people living in the Haputale area have experienced drying up of artesian wells and water resources, which they have used in the past (Fig. 7c).

Results of the questionnaire based survey revealed that the people living in the surrounding areas of eucalyptus and pine forests have experiences in lowering groundwater levels and water scarcity conditions compared with the past. The groundwater level and natural water resources are highly important parameters for the people living in both areas as the people are accustomed to the use of groundwater wells as well as artesian wells and other natural water resources for their domestic purposes. The survey further revealed that the majority of the people are considering the introducing of these exotic species as the cause of initiating the water scarcity conditions. However, no person living in the area had any knowledge on water repellent conditions. People believed that the deep root systems in these exotic species withdraw water from deeper layers resulting in water scarcity conditions.

**Groundwater levels through modeling**

Changes in depth to the groundwater level from the surface in Diyathalawa and Haputale areas, respectively related with eucalyptus and pine plantation forests, from 1980 to 2018 as estimated through modelling using LST and NDVI thematic maps are presented in Fig. 8. The depth to the water level in groundwater wells in both Diyathalawa and Haputale areas showed exponential increases during the period from 1980 to 2018, revealing a gradual decrease in the groundwater levels. The standard deviations of the curves for eucalyptus was 1.227 (m) and that of pine was 1.356 (m).

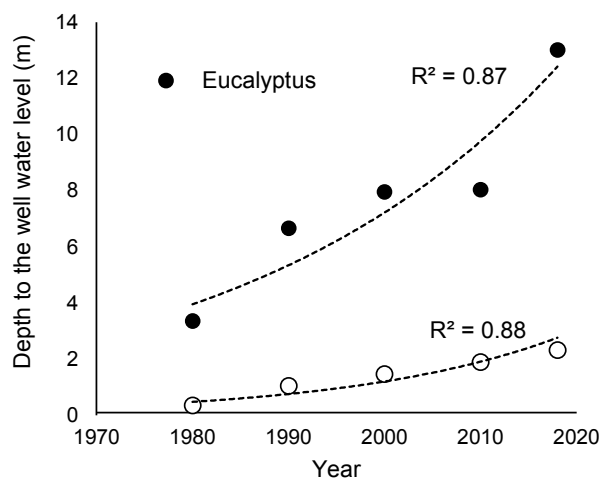


**Fig. 8.** Changes in depth to the groundwater level from the surface in Haputale and Diyathalawa areas from 1980 to 2018.

The reduction of groundwater level was apparently low in the Haputale area, where the pine plantation is located, compared to the Diyathalawa area where eucalyptus plantation is located. In addition, dense and extremely water-repellent litter cover under these plantations might play an important role in assisting the overland flow, reducing the groundwater recharge. The results further revealed that the changes in groundwater level were very low in 1980s. The exponential trend of lowering the groundwater table hints on more pronounced water scarcity conditions in the future. The results of the present study revealed lowered water movements in the soil matrix as well as uneven distribution of water in the profile related to extreme water-repellent conditions observed on the soil surfaces of both pine and eucalyptus plantation forest soils.

## Relation of water repellency to groundwater levels

Results clearly revealed that soils of both lands covered by eucalyptus and pine plantation forests are showing water repellent conditions. Water repellent condition as well as the water entry values are significantly high compared with eucalyptus soils (Figs. 3, 4, 5). Water entry values revealed that for the entry of water from the surface, eucalyptus soils would require a ponding depth of 4.6–5.3 cm, whereas the pine soils would require a ponding depth of 1.5–4.0 cm. Considering the topography, especially the slopes, of the study sites, it was clear that achieving these ponding depths would be difficult. For eucalyptus forest, attaining a ponding depth of above 4.5 cm would be almost impossible.

Modelling results revealed that the groundwater levels in the area of the eucalyptus forest diminished more dramatically, whereas the decline in the area of the pine forest was comparatively low. It was clear from the results that the groundwater recharge in the eucalyptus land was in a worse state compared with that in the pine forest land, suggesting endangered groundwater recharge in the highly hydrophobic eucalyptus land. Even with water repellent nature on the surface soils, presence of preferential flow paths in pine soils considered to be a possible process that supported groundwater recharging process.

## CONCLUSIONS

The tested eucalyptus and pine forest soils showed very high water repellent levels on the surface. From the two soils, eucalyptus soils showed highly hydrophobic conditions. Considering the sloping landscape of the both areas, the surface runoff can be expected to become excessive. This would be the reason for the abundance of evidence of topsoil erosion in the area, which was more prominent in steeper slopes. Furthermore, achieving high ponding depths required for water entry would be difficult in these forested areas, more specifically in eucalyptus soils.

The modelling with remotely sensed thematic maps confirms that the groundwater levels in both areas, where the pine and eucalyptus plantations were located, has decreased exponentially over the time. Decline in the groundwater levels in the pine forest area was comparatively low, suggesting the presence of a successful process of groundwater recharge. Presence of preferential flow paths is considered to be a possible process for the groundwater recharge.

It was clear that the eucalyptus and pine vegetation have created unfavorable circumstances in regard with water entry and groundwater recharge. Proper attention from the responsible authorities will be essential to prevent the adverse impacts of on groundwater resource that can be considered as caused by introducing the exotic plant species, although the initial objective of introducing these plant species was to protect lands from degradation.

*Acknowledgements.* This work was financially supported by the University Grants Commission (UGC) Block grant for strengthening research [RU/PG-R/16/01].

## Conflicts of interest

As the authors of the manuscript, herewith we confirm that the study has not received any funds from interested parties, except for the UGC Block grant [RU/PG-R/16/01] and that there are no conflicts of interest in any manner.

## REFERENCES

- Adane, Z., Nasta, P., Gates, J.B., 2017. Links between soil hydrophobicity and groundwater recharge under plantations in a sandy grassland setting, Nebraska Sand Hills, USA. *Forest Science*, 63, 4, 388–401. <https://doi.org/10.5849/FS-2016-137>
- Alagna, V., Iovino, M., Bagarello, V., Mataix-Solera, J., Licher, L., 2017. Application of minidisk infiltrometer to estimate water repellency in Mediterranean pine forest soils. *Journal of Hydrology and Hydromechanics*, 65, 3, 254–263. <https://doi.org/10.1515/johh-2017-0009>
- Bachmann, J., Ellies, A., Hartge, K.H., 2000. Development and application of a new sessile drop contact angle method to assess soil water repellency. *Journal of Hydrology*, 231, 66–75. [https://doi.org/10.1016/S0022-1694\(00\)00184-0](https://doi.org/10.1016/S0022-1694(00)00184-0)
- Badia-Villas, D., González-Pérez, J.A., Aznar, J.M., Arjona-Gracia, B., Martí-Dalmau, C., 2014. Changes in water repellency, aggregation and organic matter of a mollic horizon burned in laboratory: soil depth affected by fire. *Geoderma*, 213, 400–407. <https://doi.org/10.1016/j.geoderma.2013.08.038>
- Bauters, T.W., Steenhuis, T.S., Parlange, J.Y., DiCarlo, D.A., 1998. Preferential flow in water-repellent sands. *Soil Science Society of America Journal*, 62, 5, 1185–1190. <https://doi.org/10.2136/sssaj1998.03615995006200050005x>
- Bauters, T.W.J., Steenhuis, T.S., DiCarlo, D.A., Nieber, J.L., Dekker, L.W., Ritsema, C.J., Parlange, J.Y., Haverkamp, R., 2000. Physics of water repellent soils. *Journal of Hydrology*, 231, 233–243. [https://doi.org/10.1016/S0022-1694\(00\)00197-9](https://doi.org/10.1016/S0022-1694(00)00197-9)
- Benito, E., Varela, E., Rodríguez-Alleres, M., 2019. Persistence of water repellency in coarse-textured soils under various types of forests in NW Spain. *Journal of Hydrology and Hydromechanics*, 67, 2, 129–134. <https://doi.org/10.2478/johh-2018-0038>
- Blake, G.R., Hartge, K.H., 1986a. Bulk density. In: Klute, A. (Ed.): *Methods of Soil Analysis. Part 1: Physical and Mineralogical Methods*. 2nd Ed. Soil Science Society of America: Madison, WI, pp. 363–375. <https://doi.org/10.2136/sssabookser5.1.2ed.c13>
- Blake, G.R., Hartge, K.H., 1986b. Particle Density. In: Klute, A. (Ed.): *Methods of Soil Analysis. Part 1: Physical and Mineralogical Methods*. 2nd Ed. Soil Science Society of America: Madison, WI, pp. 377–382. <https://doi.org/10.2136/sssabookser5.1.2ed.c14>
- Bouyoucos, G.J., 1962. Hydrometer method improved for making particle size analyses of soils 1. *Agronomy Journal*, 54, 5, 464–465. <https://doi.org/10.2134/agronj1962.00021962005400050028x>
- Brunner, P., Franssen, H.J.H., Kgotlhang, L., Bauer-Gottwein, P., Kinzelbach, W., 2007. How can remote sensing contribute in groundwater modeling? *Hydrogeology journal*, 15, 1, 5–18. <https://doi.org/10.1007/s10040-006-0127-z>
- Contreras, S., Cantón, Y., Solé-Benet, A., 2008. Sieving crusts and macrofaunal activity control soil water repellency in semiarid environments: evidences from SE Spain. *Geoderma*, 145, 3–4, 252–258. <https://doi.org/10.1016/j.geoderma.2008.03.019>
- Doerr, S.H., Shakesby, R.A., Walsh, R.P., 1996. Soil hydrophobicity variations with depth and particle size fraction in burned and unburned Eucalyptus globulus and Pinus pinaster forest terrain in the Agueda Basin, Portugal. *Catena*, 27, 1, 25–47. [https://doi.org/10.1016/0341-8162\(96\)00007-0](https://doi.org/10.1016/0341-8162(96)00007-0)
- Doerr, S.H., Thomas, A.D., 2000. The role of soil moisture in controlling water repellency: new evidence from forest soils

- in Portugal. *Journal of Hydrology*, 231, 134–147. [https://doi.org/10.1016/S0022-1694\(00\)00190-6](https://doi.org/10.1016/S0022-1694(00)00190-6)
- Doerr, S.H., Woods, S.W., Martin, D.A., Casimiro, M., 2009. ‘Natural background’ soil water repellency in conifer forests of the north-western USA: its prediction and relationship to wildfire occurrence. *Journal of Hydrology*, 371, 1–4, 12–21. <https://doi.org/10.1016/j.jhydrol.2009.03.011>
- ESRI, 2017. ArcGIS-Desktop ArcMap: Release 10.4.1. Redlands, CA: Environmental Systems Research Institute.
- Fér, M., Kodešová, R., 2012. Estimating hydraulic conductivities of the soil aggregates and their clay-organic coatings using numerical inversion of capillary rise data. *Journal of Hydrology*, 468, 229–240. <https://doi.org/10.1016/j.jhydrol.2012.08.037>
- Fér, M., Leue, M., Kodešová, R., Gerke, H.H., Ellerbrock, R.H., 2016. Droplet infiltration dynamics and soil wettability related to soil organic matter of soil aggregate coatings and interiors. *Journal of Hydrology and Hydromechanics*, 64, 2, 111–120. <https://doi.org/10.1515/johh-2016-0021>
- Flores-Mangual, M.L., Lowery, B., Bockheim, J.G., Pagliari, P.H., Scharenbroch, B., 2013. Hydrophobicity of Sparta sand under different vegetation types in the Lower Wisconsin River Valley. *Soil Science Society of America Journal*, 77, 5, 1506–1516. <https://doi.org/10.2136/sssaj2012.0343>
- Gerke, H.H., Köhne, J.M., 2002. Estimating hydraulic properties of soil aggregate skins from sorptivity and water retention. *Soil Science Society of America Journal*, 66(1), 26–36. <https://doi.org/10.2136/sssaj2002.2600>
- Giordano, M., 2009. Global groundwater? Issues and solutions. *Annual Review of Environment and Resources*, 34, 153–178. <https://doi.org/10.1146/annurev.enviro.030308.100251>
- Imeson, A.C., Verstraten, J.M., Van Mulligen, E.J., Sevink, J., 1992. The effects of fire and water repellency on infiltration and runoff under Mediterranean type forest. *Catena*, 19(3–4), 345–361. [https://doi.org/10.1016/0341-8162\(92\)90008-Y](https://doi.org/10.1016/0341-8162(92)90008-Y)
- Iovino, M., Pekárová, P., Hallett, P.D., Pekár, J., Lichner, E., Mataix-Solera, J., Alagna, V., Walsh, R., Raffan, A., Schacht, K., Rodný, M., 2018. Extent and persistence of soil water repellency induced by pines in different geographic regions. *Journal of Hydrology and Hydromechanics*, 66, 4, 360–368. <https://doi.org/10.2478/johh-2018-0024>
- Kajiura, M., Etori, Y., Tange, T., 2012. Water condition control of in situ soil water repellency: an observational study from a hillslope in a Japanese humid-temperate forest. *Hydrological Processes*, 26, 20, 3070–3078. <https://doi.org/10.1002/hyp.8310>
- Kobayashi, M., Shimizu, T., 2007. Soil water repellency in a Japanese cypress plantation restricts increases in soil water storage during rainfall events. *Hydrological Processes: An International Journal*, 21, 17, 2356–2364. <https://doi.org/10.1002/hyp.6754>
- Lee, C., Yang, H.J., Yun, T.S., Choi, Y., Yang, S., 2015. Water-entry pressure and friction angle in an artificially synthesized water-repellent silty soil. *Vadose Zone Journal*, 14, 4. <https://doi.org/10.2136/vzj2014.08.0106>
- Leelamanie, D.A.L., 2016. Occurrence and distribution of water repellency in size fractionated coastal dune sand in Sri Lanka under Casuarina shelterbelt. *Catena*, 142, 206–212. <https://doi.org/10.1016/j.catena.2016.03.026>
- Leelamanie, D.A.L., Karube, J., Yoshida, A., 2008. Characterizing water repellency indices: Contact angle and water drop penetration time of hydrophobized sand. *Soil Science & Plant Nutrition*, 54, 2, 179–187. <https://doi.org/10.1111/j.1747-0765.2007.00232.x>
- Leelamanie, D.A.L., Liyanage, T.D.P., Piyaarwan, H.I.G.S., 2016. Occurrence and Distribution of Water Repellency in soils under Exotic Plantation Forests in Sri Lanka. 13th Academic Sessions, University of Ruhuna, March 02, 2016. ISSN: 2362-0412
- Leelamanie, D.A.L., Nishiwaki, J., 2019. Water repellency in Japanese coniferous forest soils as affected by drying temperature and moisture. *Biologia*, 74, 2, 127–137. <https://doi.org/10.2478/s11756-018-0157-8>
- Letey, J., 2001. Causes and consequences of fire-induced soil water repellency. *Hydrological Processes* 15, 15, 2867–2875. <https://doi.org/10.1002/hyp.378>
- Letey, J., Carrillo, M.L.K., Pang, X.P., 2000. Approaches to characterize the degree of water repellency. *Journal of Hydrology*, 231, 61–65. [https://doi.org/10.1016/S00221694\(00\)00183-9](https://doi.org/10.1016/S00221694(00)00183-9)
- Lichner, L.U., Hallett, P.D., Feeney, D.S., Ďugová, O., Šír, M., Tesář, M., 2007. Field measurement of soil water repellency and its impact on water flow under different vegetation. *Biologia*, 62, 5, 537–541. <https://doi.org/10.2478/s11756-007-0106-4>
- Lichner, E., Capuliak, J., Zhukova, N., Holko, L., Czachor, H., Kollár, J., 2013. Pines influence hydrophysical parameters and water flow in a sandy soil. *Biologia*, 68, 6, 1104–1108. <https://doi.org/10.2478/s11756-013-0254-7>
- Liyanage, T.D.P., Leelamanie, D.A.L., 2016. Influence of organic manure amendments on water repellency, water entry value, and water retention of soil samples from a tropical Ultisol. *Journal of Hydrology and Hydromechanics*, 64, 2, 160–166. <https://doi.org/10.1515/johh-2016-0025>
- McKissock, I., Gilkes, R.J., Harper, R.J., Carter, D.J., 1998. Relationships of water repellency to soil properties for different spatial scales of study. *Soil Research*. 36, 3, 495–508. <https://doi.org/10.1071/S97071>
- National Atlas of Sri Lanka, 2007. Second Edition, Survey Department of Sri Lanka. Colombo, Sri Lanka.
- Pan, S.B., Wang, Z., Su, Q., Sun, T., Zhang, Y., 2008. Groundwater level monitoring model using multi-temporal images in arid region of northwest China. *The International Archives of the Photogrammetry, Remote Sensing and Spatial Information Sciences*, 37, 745–750.
- Rao, N.S., Chakradhar, G.K.J., Srinivas, V., 2001. Identification of groundwater potential zones using remote sensing techniques in and around Guntur town, Andhra Pradesh, India. *Journal of the Indian Society of Remote Sensing*, 29, 69–78. <https://doi.org/10.1007/BF02989916>
- Rodríguez-Alleres, M., Benito, E., de Blas, E., 2007. Extent and persistence of water repellency in north-western Spanish soils. *Hydrological Processes: An International Journal*, 21, 17, 2291–2299. <https://doi.org/10.1002/hyp.6761>
- Santos, J.M., Verheijen, F.G., Tavares Wahren, F., Wahren, A., Feger, K.H., Bernard-Jannin, L., Rial-Rivas, M.E., Keizer, J.J., Nunes, J.P., 2016. Soil water repellency dynamics in pine and eucalypt plantations in Portugal—a high-resolution time series. *Land Degradation & Development*, 27, 5, 1334–1343. <https://doi.org/10.1002/ldr.2251>
- Schumacher, B.A., 2002. Methods for the determination of total organic carbon (TOC) in soils and sediments. *Ecological Risk Assessment Support Center Office of Research and Development US. Environmental Protection Agency*, 25 p.
- Şen, Z., 2015. Applied Drought Modeling, Prediction, and Mitigation. Chapter 6: Climate change, droughts, and water resources. Elsevier, pp. 321–391. <https://doi.org/10.1016/B978-0-12-802176-7.00006-7>

- Senanayake, I.P., Dissanayake, D.M.D.O.K., Mayadunna, B.B., Weerasekera, W.L., 2016. An approach to delineate groundwater recharge potential sites in Ambalantota, Sri Lanka using GIS techniques. *Geoscience Frontiers*, 7, 115–124. <https://doi.org/10.1016/j.gsf.2015.03.002>
- Siteur, K., Mao, J., Nierop, K.G., Rietkerk, M., Dekker, S.C., Eppinga, M.B., 2016. Soil water repellency: a potential driver of vegetation dynamics in coastal dunes. *Ecosystems*, 19, 7, 1210–1224. <https://doi.org/10.1007/s10021-016-9995-9>
- Soil Survey Staff, 2014. *Keys to Soil Taxonomy*. 12th ed. USDA-Natural Resources Conservation Service, Washington, DC.
- Sullivan, L.A., 1990. Soil organic matter, air encapsulation and water-stable aggregation. *Journal of Soil Science* 41, 3, 529–534. <https://doi.org/10.1111/j.1365-2389.1990.tb00084.x>
- Vogelmann, E.S., Reichert, J.M., Reinert, D.J., Mentges, M.I., Vieira, D.A., de Barros, C.A.P., Fasinmirin, J.T., 2010. Water repellency in soils of humid subtropical climate of Rio Grande do Sul, Brazil. *Soil and Tillage Research*, 110, 1, 126–133. <https://doi.org/10.1016/j.still.2010.07.006>
- Wahl, N.A., Bens, O., Schäfer, B., Hüttl, R.F., 2003. Impact of changes in land-use management on soil hydraulic properties: hydraulic conductivity, water repellency and water retention. *Physics and Chemistry of the Earth, Parts A/B/C*, 28, 33–36, 1377–1387. <https://doi.org/10.1016/j.pce.2003.09.012>
- Wallis, M.G., Horne, D.J., McAuliffe, K.W., 1990. A study of water repellency and its amelioration in a yellow-brown sand: 1. Severity of water repellency and the effects of wetting and abrasion. *New Zealand Journal of Agricultural Research*, 33, 1, 139–144. <https://doi.org/10.1080/00288233.1990.10430670>
- Wang, Z., Wu, L., Wu, Q.J., 2000. Water-entry value as an alternative indicator of soil water-repellency and wettability. *Journal of Hydrology*, 231, 76–83. [https://doi.org/10.1016/S0022-1694\(00\)00185-2](https://doi.org/10.1016/S0022-1694(00)00185-2)
- Woche, S.K., Goebel, M.-O., Kirkham, M.B., Horton, R., Van der Ploeg, R.R., Bachmann, J., 2005. Contact angle of soils as affected by depth, texture, and land management. *European Journal of Soil Science*, 56, 2, 239–251. <https://doi.org/10.1111/j.1365-2389.2004.00664.x>
- Ziogas, A.K., Dekker, L.W., Oostindie, K., Ritsema, C.J., 2005. Soil water repellency in north-eastern Greece with adverse effects of drying on the persistence. *Soil Research*, 43, 3, 281–289. <https://doi.org/10.1071/SR04087>
- Zubair, L., Ropelewski, C.F., 2006. The strengthening relationship between ENSO and northeast monsoon rainfall over Sri Lanka and southern India. *Journal of Climate*, 19, 8, 1567–1575. <https://doi.org/10.1175/JCLI3670.1>

Received 19 April 2020

Accepted 17 July 2020

# Development of a universal microinfiltrometer to estimate extent and persistence of soil water repellency as a function of capillary pressure and interface chemical composition

Nasrollah Sepehrnia\*, Susanne K. Woche, Marc-O. Goebel, Jörg Bachmann

Institute of Soil Science, Leibniz Universität Hannover, Herrenhäuser Str. 2, D-30419 Hannover, Germany.

\* Corresponding author. Tel.: +4951176119250. Fax: +49511762-5559. E-mail: sepehrnia@ifbk.uni-hannover.de

**Abstract:** Microinfiltrometers to assess soil water repellency (SWR) are limited to small tension ranges and have different technical setups, hindering a comparison between results from different laboratories. Hence, a microinfiltrometer which considers various aspects like extent and persistence of SWR is needed. The technical update suggested here uses glass tubes (e.g., 3 mm inner diameter), a fabric of mesh size 15  $\mu\text{m}$  around the tip to enable good contact between soil surface and tip, ultrapure degassed water, and an evaporation protection for tip and reservoir during long-term infiltration. The adjustment of a continuous range of pressures and tensions (i.e., +0.5 to  $-40$  cm) was done using glass tubes of various lengths connected to the tip. Three soil samples with initial contact angles, CA, of 18°, 62°, and 91° after 25°C treatment were additionally treated at 80°C to increase SWR persistence and CA. The soil particle interface chemical composition was determined by X-ray photoelectron spectroscopy (XPS). The hydrophysical properties evaluated included water and ethanol sorptivity as well as very important aspects of SWR, i.e. water drop penetration time, water repellency cessation time, repellency index, and modified repellency index. The results derived from the technically modified microinfiltrometer setup showed consistent differences between initial wettability and the water repellency cessation time as a parameter describing the development of SWR with time. The interface O/C ratio as derived from XPS data was negatively correlated with CA ( $p < 0.05$ ), thus proving the close relationship between interface chemistry and wettability. Our findings illustrated a strong positive correlation ( $R^2 = 0.99$ ,  $p < 0.05$ ) between sorptivity and O/C ratio under  $-2$  cm tension which can be considered as the universal tension for different aspects of SWR.

**Keywords:** Ethanol; Infiltration; Interface chemistry; Sorptivity; Thermal treatment; X-ray photoelectron spectroscopy.

## INTRODUCTION

Soil exhibits different levels of water repellency due to the complex nature and the spatial arrangement of hydrophobic moieties at the soil particle interfaces (Beatty and Smith, 2014). More frequent and intensive droughts due to global warming may increase the occurrence of water repellency in soil, which may last for weeks (Dekker et al., 2005; Goebel et al., 2011). Hydrophobic organic compounds in soils are exudates of plant roots, components produced by microbes (Hallett et al., 2003; Lichner et al., 2018) or various hydrophobic humic substances (Tschapek, 1984).

Soil water repellency (SWR), as a transient property of soil particle interfaces, often has high temporal and spatial variability that makes water infiltration measurements and predictions of hydrological processes complex (Bauters et al., 2000; Cosentino et al., 2010; Dekker et al., 2001, 2005; Sepehrnia et al., 2017). An accurate prediction of soil hydraulic properties is difficult as SWR changes over the time of infiltration (Bachmann et al., 2007; Clothier et al., 2000). To get spatial resolution, microinfiltrometers are widely used to estimate SWR on small soil samples such as soil aggregates to reveal small-scale variability of hydraulic and hydrophysical properties of soil in the lab. They began by adopting a design developed by Leeds-Harrison et al. (1994) and have developed into different designs (Johnson et al., 2005), including an automated setup (Gordon and Hallett, 2014). A limitation of the original infiltrometer (Leeds-Harrison et al., 1994), which was subsequently adopted to measure SWR (Hallett and Young, 1999) was the use of a sponge tip. This had the advantage of providing good contact

with a rough soil surface, but its packing into the infiltrometer tip and variability between manufacturers could affect flow rate and produce erroneous results (personal communication Paul Hallett). Another challenge was the use of varying tip sizes, originally between 1.45 and 2.5 mm radius (Hallett and Young, 1999; Leeds-Harrison et al., 1994), and then subsequently decreased to 0.4 mm radius to allow measurements at the root-soil interface (Hallett et al., 2003). The latter was also modified by Orfánus et al. (2014) and Lichner et al. (2013), and later used by Sepehrnia et al. (2016). The automated microinfiltrometer developed by Gordon and Hallett (2014) had a tip of 2.9 mm in radius to measure SWR with less experimental effort during operation. All proposed microinfiltrometers obey the same physical principle to establish a hydraulic gradient for infiltration (Fig. 1) but support water and ethanol infiltration only over a narrow range of tensions; i.e., 0 to  $-7$  cm.

Microinfiltrometers currently used for routine measurements do not yet reach tensions greater than  $-7$  cm, due to the pore size of tip materials and probably air bubble formation due to degassing of water (Hallett et al., 2003; Lichner et al., 2013). Most testing by previous researchers has focused on early time infiltration (e.g., 3 min) and small infiltrometer tensions, so that mostly hydrophilic or only the largest pores will conduct water at a hydrophilic or a moderate water repellent state. A narrow range of infiltrometer tensions has two limitations: effects of water conducting pores and their development with time cannot be explored, and hydraulic conductivity estimations from infiltration data at multiple tensions are limited. With the rapid measurement approach deployed in most research, SWR is often assumed to be a transient soil property that disappears

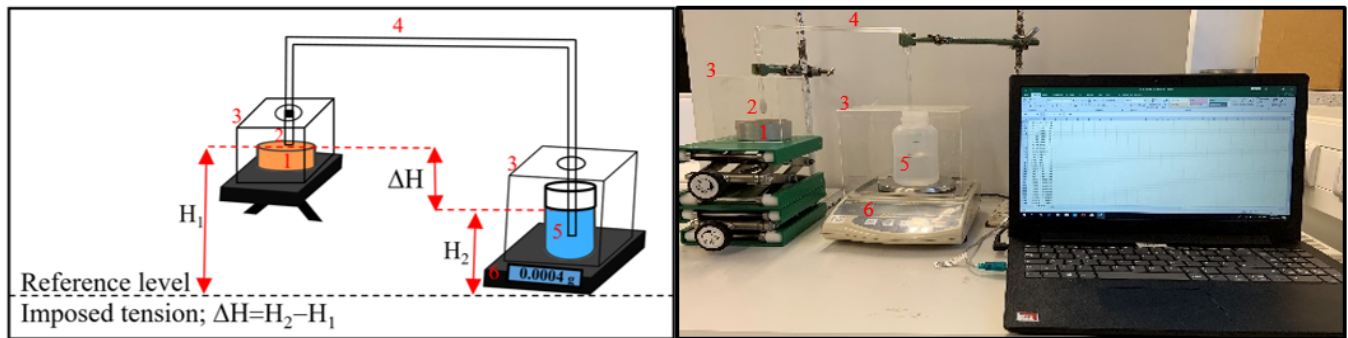


**Fig. 1.** Microinfiltrometer apparatuses widely used to measure ethanol and water infiltration to estimate the repellency index with updates used in this study. 1 – Steel core with soil sample, 2 – Tip enclosed in fabric (mesh size 0.15  $\mu\text{m}$ ), enabling good contact between soil surface and tip. 3 – Plexiglas hood to prevent evaporation during long-term measurement, 4 – Glass tube with inner diameter of 3 mm, 5 – Water or ethanol reservoir, 6 – Four-digit balance.  $H_1$  and  $H_2$  show the hydraulic potentials of the microinfiltrometer tip and the liquid level, respectively, with respect to the reference level.

after initial infiltration and filling of pores in the contact zone. From the research of Clothier et al. (2000), SWR can take several hours or days to breakdown.

In this study we keep the general microinfiltrometer setup, but we modified some very important technical aspects to allow long-term measurements with either water or ethanol (e.g., 24 h) at a wider range of hydraulic gradients, i.e., from +0.5 to –40 cm. This modified approach addresses longer-term SWR breakdown (Clothier et al., 2000) and more realistic hydraulic conditions regarding capillary pressure in unsaturated soil. It offers to compare common parameters that are used to assess the degree of water repellency under standard conditions (i.e., tension  $> -7$  cm), such as the repellency index under extended infiltration time. In addition, to provide a modified testing apparatus that can be standardized across laboratories, we also provide a standard sample preparation approach. Wetting properties of the soil samples were initially evaluated after drying at 25°C (room temperature) and categorized into three groups according to their contact angle as determined by the sessile drop method (Goebel et al., 2013). In this study, soil materials also received thermal treatment at 80°C. This produced samples with the same texture and carbon content, but increased SWR (i.e., increased CA; Gaj et al., 2019). Such conditions may also be found in natural soils, e.g., in the contact zone of wildfires. The main objectives of this study were i) to update the microinfiltrometer approach technically for a more comprehensive estimation of SWR, ii) to compare repellency indices under an extended range of hydraulic conditions, and iii) to link chemical composition of the interface with micro-hydraulic properties like extent and persistence of SWR. The last step should give the relation between chemical composition of the interface layer and soil hydraulic behaviour. To achieve these objectives, the new infiltrometer was tested against conventional infiltrometers, encompassing a broader range of tensions than could be previously obtained. With the new infiltrometer, tests were conducted over extended periods of time to assess water repellency breakdown. The chemical composition of solid interfaces was used to unravel soil properties that drive SWR behaviour.

## MATERIALS AND METHODS

### Soil samples and studied area

Soil samples were taken from the beech forest research site Grunderwald (52°49.834'N 10°18.967'E), located in Lower

Saxony, Germany. Three samples were taken from a soil profile from three depths corresponding to different SWR levels, i.e., water-repellent (0–5 cm), subcritically water-repellent (10–20 cm), and wettable (20–40 cm). Initial SWR was quantified by CA measurement using the sessile drop method (Bachmann et al., 2003; Goebel et al., 2013). To provide homogeneous samples to allow for repetitive tests, samples were air-dried, sieved  $< 2$ -mm and divided into two portions. One portion of the air-dried materials was treated at 25°C in a climate-controlled chamber and the other portion was treated at 80°C for 24 hours in an oven to emulate a higher level of SWR in conjunction with stronger persistence of SWR (Gaj et al., 2019). The 25°C-treated material served as reference. Some chemical, physical, and hydrophysical properties of the soil samples are presented in Tables 1 and 2.

## Methods

### Microinfiltrometer

The microinfiltrometer follows similar previous designs with a tip that transmits water to the soil that is attached via a tube to a liquid reservoir on a logging balance (Fig. 1). Soil samples are placed on a lab lift to bring the surface into contact with the infiltrometer tip. Key differences to previous designs are the use of mesh fabric at the tip that increases the tension range, a Plexiglas cover for the sample and reservoir to decrease evaporation, and the use of rigid glass tubes to minimize measurement errors. The connecting tube consisted of a 3-mm inner diameter glass U-bend with exchangeable ends for the infiltrometer tip so that tension from +0.5 cm to –40 cm could be applied. The mesh fabric is commercially used in tension infiltrometers (Product code: 09.09, Eijkelkamp Soil & Water, The Netherlands) and has a 15  $\mu\text{m}$  mesh size with a bubble point of 32 cm  $\text{H}_2\text{O}$ . The hydraulic conductivity of the tip membrane was 11  $\text{cm min}^{-1}$ , which is considerably faster than the infiltration rates of most soils. A more detailed description of the different properties of the nylon mesh is listed in the caption of Fig. 1. Preliminary results showed that it is suggested to replace the nylon mesh at the tip after five measurement cycles or clean it using compressed air, because fine soil material could block the mesh.

Ultrapure degassed water was used to reduce air bubble formation in the system and to enable long-time measurements (i.e.,  $> 24$  h) under higher tensions (i.e., –20 and –40 cm) of the testing liquids; a very important difference to previous approaches (Hallett et al., 2003; Sepehrnia et al., 2016, 2017; Tillman et al., 1989).

**Table 1.** Chemical and physical properties of the studied soils presented as mean  $\pm$  standard deviation (WS: wettable soil, SRS: subcritically water-repellent soil, RS: water-repellent soil).

Soil	Depth (cm)	OC (%)	Clay (%)	Silt (%)	Sand (%)
WS	20–40	0.04 ( $\pm 0.03$ )	1.9 ( $\pm 0.3$ )	38.9 ( $\pm 0.3$ )	59.1 ( $\pm 0.61$ )
SRS	10–20	2.52 ( $\pm 0.15$ )	4.5 ( $\pm 0.2$ )	34.1 ( $\pm 0.1$ )	61.4 ( $\pm 0.29$ )
RS	0–5	10.10 ( $\pm 0.58$ )	6.4 ( $\pm 0.4$ )	21.6 ( $\pm 3.12$ )	72.0 ( $\pm 2.7$ )

OC = organic carbon content.

**Table 2.** The results of water sorptivity ( $S_w$ ) and unsaturated hydraulic conductivity ( $K_h$ ), presented as mean  $\pm$  standard deviation, measured using a standard infiltrometer (diameter: 31.8 mm, tension:  $-0.5$  cm, Decagon, USA) to validate the developed microinfiltrometer. Tested were soils (WS: wettable soil, SRS: subcritically water-repellent soil, RS: water-repellent soil) treated at 25°C and at 80°C.

Treatment temperature	$S_w$ (cm s <sup>-0.5</sup> )			$K_h$ (m day <sup>-1</sup> )		
	WS	SRS	RS	WS	SRS	RS
25°C	0.140 ( $\pm 0.023$ )	0.440 ( $\pm 0.01$ )	0.047 ( $\pm 0.041$ )	1.10 ( $\pm 0.06$ )	3.84 ( $\pm 0.93$ )	0.734 ( $\pm 0.104$ )
80°C	0.143 ( $\pm 0.015$ )	0.110 ( $\pm 0.02$ )	0.036 ( $\pm 0.01$ )	1.10 ( $\pm 0.28$ )	2.05 ( $\pm 0.63$ )	0.261 ( $\pm 0.01$ )

Water and ethanol (Normapur, 96 vol-%, VWR Chemicals, France) infiltration tests were performed under different slight pressures (+0.5 and 0 cm) as well as under different tensions ( $-2$ ,  $-5$ ,  $-20$ ,  $-40$  cm) on soil cores repacked to their field bulk density. All experiments were conducted in triplicate. The respective time of each infiltration experiment varied as it depended on soil wetting properties, liquid type, and imposed hydraulic conditions (Table 2). Disturbed soil material was chosen to reduce the natural soil heterogeneity for this evaluation, as the present study focuses on the technical capabilities of the new infiltrometer.

#### Repellency index

To estimate the extent of SWR under different tensions, we compared the conventional repellency index  $RI$  approach (Eq. (1)) of Tillman et al. (1989), to the modified SWR index defined by Sepehri et al. (2016),  $RI_m$  (Eq. (2)):

$$RI = S_e(h_0) / S_w(h_0) \quad (1)$$

$$RI_m = S_{ww}(h_0) / S_{wh}(h_0) \quad (2)$$

In Eqs. (1) and (2)  $S_e$  and  $S_w$  are ethanol and water sorptivities and  $S_{ww}$  and  $S_{wh}$  are water sorptivities for hydrophilic and hydrophobic wettability states of the respective samples during the infiltration process. Eq. (2) considers also infiltration under hydraulic pressure ( $h_0$ ; +0.5 and 0 cm) or tension ( $-2$ ,  $-5$ ,  $-20$ , and  $-40$  cm) conditions. Only tensions close to zero (i.e.,  $-2$  and  $-7$  cm) have been considered in most previous studies (Alagna et al., 2019; Lichner et al., 2013; Tillman et al., 1989).

When the initial SWR in dry soil is not stable and decreases with infiltration time, the conventional procedure (Eq. (1)) gives information on the initial stage of water repellency. Corresponding estimates may overestimate the general water repellency state during the infiltration process after the initial contact with water (Alagna et al., 2019). The  $RI_m$  (Eq. (2)) overcomes this limitation because it can be used to estimate the water repellency cessation time, WRCT, as an additional and very important characteristic feature of SWR. The WRCT is estimated from the point of intersection of two straight lines, representing the  $I = f(\sqrt{t})$  relationship, where  $I$  and  $t$  are cumulative infiltration and time, for transient water repellency changing to a state of wettability (Lichner et al., 2013; Sepehri et

al. 2016). The water sorptivity  $S_{wh}(h_0)$  for hydrophobic states was estimated from the slope of the “hockey-stick-like” relationship  $I = f(\sqrt{t})$ , measured under tension or positive pressure ( $h_0$  and  $P_0$ ) after the beginning of the infiltration, represented by a straight line showing the less steep part of the hockey stick. If a steeper part of the infiltration characteristics  $I = f(\sqrt{t})$  is observed after a longer time, the corresponding WRCT can be determined. This potentially steeper branch of the water sorptivity graph provides an estimate of the  $S_{ww}(h_0)$  (Lichner et al., 2013; Sepehri et al., 2016).

#### Water drop penetration time and sessile drop method

Water drop penetration time, WDPT, was used to evaluate the persistence of water repellency of the studied samples (Dekker and Ritsema, 1994; Letey et al., 2000). It tests the stability of hydrophobic soil conditions with time. The WDPT method consists of placing a drop of water on the soil surface and recording the time required for its complete penetration. Penetration is assumed to start when the solid-liquid CA is  $< 90^\circ$ . We placed ten drops of ultrapure water ( $35 \pm 5$   $\mu$ L) onto the horizontal soil surface from a standard height (10 mm) above the surface, and the time required for infiltration of each drop was recorded (Dekker and Ritsema, 1994; Lichner et al., 2013).

Air-liquid-solid CAs of the studied soils were directly measured by the sessile drop method using a CCD-equipped CA microscope (OCA 15, DataPhysics, Filderstadt, Germany; Goebel et al., 2013). CA of untreated and heat-treated samples was measured by placing water drops (drop volume 1  $\mu$ L) onto a dense one-grain layer fixed with a double-sided adhesive tape on a microscope slide. CA was measured almost instantaneously after the drop had stabilized (initial CA) and again after 5 seconds (Bachmann et al., 2003; Goebel et al., 2013). This measurement was also conducted after infiltration at the applied pressures/tensions ( $CA_{infil}$ ). A small sample was taken at the wetted tip area ( $\sim 1 \times 1$  cm<sup>2</sup>) from a depth of 0–1.5 cm. The samples were shock-frozen by dipping polyethylene containers with the sample material for 10 seconds in liquid nitrogen ( $-196^\circ$ C), followed by freeze-drying to preserve the orientation of hydrophilic and hydrophobic functional groups of the particle interfaces during infiltration (Mao et al., 2019; Thieme et al., 2016).

### Microinfiltrometer validation

Independent water infiltration tests were conducted under  $-0.5$  cm tension using a standard infiltrometer (Decagon, 2007) with a bigger contact area ( $7.92$  cm<sup>2</sup>) to compare with our new microinfiltrometer. The first-term of the Philip infiltration equation (Philip, 1957) was fitted to the cumulative infiltration data:

$$I = C_1 t^{1/2} + C_2 t + C_3 t^{3/2} + C_4 t^2 + \dots + C_m t^{m/2} + \dots \quad (3)$$

where  $t$  is time and  $C_1, C_2, C_3, C_4, \dots,$  and  $C_m$  are coefficients of the series expansion. This enables the calculation of unsaturated hydraulic conductivity ( $K_h$ ) (Eq. (5)) and the estimation of water sorptivity of the studied soils (Eq. (6)) under  $-0.5$  cm tension as proposed by Zhang (1997) with regard to the two-term form of Philip's equation:

$$I = C_1(h_0) t^{1/2} + C_2(h_0) t \quad (4)$$

$$k(h_0) = C_2(h_0)/A_2 \quad (5)$$

and

$$S(h_0) = C_1(h_0)/A_1 \quad (6)$$

where  $A_1$  and  $A_2$  are dimensionless coefficients which are considered to be 5.3 for the standard infiltrometer (Decagon, 2007) according to Zhang (1997).

### Evaluation of interface chemical composition

Interface chemical composition of selected samples was determined by X-ray photoelectron spectroscopy, XPS, using an Axis Ultra DLD device (Kratos Analytical, Manchester, UK; monochromated Al  $K_{\alpha}$  radiation at 20 mA and 12 kV). Recorded were survey spectra and C 1s detail scans. Quantification of the survey scans (Vision 2, Kratos Analytical, Manchester, UK) gave the interface chemical composition in atomic-% (at.-%). C speciation was performed in two ways by either fitting the survey C 1s peak in a basic procedure with two peaks (polar,  $C_p$ , and non-polar,  $C_{np}$ , C species; Woche et al. 2017) or fitting the C 1s detail scan with four sub-peaks, representing O = C–O; O = C–N at 289.3 eV ( $C_1$ , polar bond), C = O; O–C–O at 287.8 eV ( $C_2$ , polar bond), C–O; C–N at 286.4 eV ( $C_3$ , partly polar bond), and C–C; C–H at 284.8 eV ( $C_4$ , nonpolar bond) (Gerin et al., 2003). The selection of samples tested by XPS allowed to compare interface chemical composition before and after thermal treatment (air-dry samples) and after wetting during infiltration (shock-frozen and freeze-dried samples) in conjunction with CA and water sorptivity. For each sample, spectra were recorded at three different spots, comprising an area of  $0.21$  mm<sup>2</sup> each.

### Data analysis

The experiment was performed using a complete randomized design with three replications for all variables. The independent variables were the wetting properties (wetable, subcritically water-repellent, and water-repellent), the thermal treatments ( $25^\circ\text{C}$  and  $80^\circ\text{C}$ ) of the soil, and applied pressures/tensions ( $+0.5, 0, -2, -5, -20,$  and  $-40$  cm) of the infiltrating water from the infiltrometer. The dependent parameters included CA,  $RI, RI_m, S_w, S_e, WRCT,$  and interface chemical composition (O/C ratio, the amount of non-polar C compounds  $C_{np}$ , and the interface C/N ratio). Statistical analyses were done using two-way ANOVA (R Core Team, 2013) and the post-hoc mean comparisons were performed by the LSD test ( $p < 0.05$ ).

## RESULTS AND DISCUSSION

### Technical features of the microinfiltrometer

A few preliminary remarks outline some features of the new system in comparison to existing microinfiltrometers. Early tests showed that due to very small water flow rates, infiltration measurements are not advisable for very coarse sand textures in combination with tensions  $< -20$  cm within a reasonable time span. It was assumed that insufficient hydraulic contact between the tip and soil caused a disruption of water films at the soil-tip contact zone (data not shown). Corresponding disconnected water films in partly saturated water repellent media have been visualized by Muehl et al. (2012). Capillary barrier effects were also evident at the interface between the tip and soil, a well-known effect that occurs in layered wettable media, e.g., a fine-textured layer above a coarse textured soil layer (Li et al., 2014). However, regardless of the water repellency status and applied tensions, our experiments proved that infiltration into the sandy loam worked well (Table 3).

The values of  $K_h$  measured by the infiltrometer were  $1.90$  m day<sup>-1</sup> for the wettable soil (at  $25^\circ\text{C}$ ) under zero tension, using Zhang (1997)'s method, which was in agreement with Leeds-Harrison and Youngs (1997) who measured a soil with similar texture. Independent tests using the minidisk infiltrometer (Decagon, 2007) with a significantly bigger contact area ( $7.92$  vs.  $0.071$  cm<sup>2</sup>) at tension of  $-0.5$  cm also found good agreement with our new microinfiltrometer design (Table 3). The results of water sorptivity and  $K_h$  under zero tension were also comparable with observations from Leeds-Harrison et al. (1994) and Leeds-Harrison and Youngs (1997) who used a microinfiltrometer with a  $2.9$  mm diameter tip. Their results for a fine sand under zero tension were  $S_w = 0.255$  cm s<sup>-0.5</sup> and  $K_h = 3.76$  m day<sup>-1</sup>, which are comparable to  $S_w = 0.220$  cm s<sup>-0.5</sup> and  $K_h = 1.30$  m day<sup>-1</sup> that we measured for the wettable Grindewald soil treated at  $25^\circ\text{C}$  (sand content =  $59.1 \pm 0.6\%$ , CA =  $18^\circ$ ).

**Table 3.** The time (min), presented as mean  $\pm$  standard deviation, when water begins to infiltrate into the studied soils (WS: wettable soil, SRS: subcritically water-repellent soil, RS: water-repellent soil).

Treatment temperature Pressure/tension (cm)	WS		SRS		RS	
	25°C	80°C	25°C	80°C	25°C	80°C
+0.5	0.08 ( $\pm 0.00$ )	0.08 ( $\pm 0.00$ )	0.08 ( $\pm 0.00$ )	0.17 ( $\pm 0.00$ )	0.17 ( $\pm 0.00$ )	–
0	0.08 ( $\pm 0.00$ )	0.08 ( $\pm 0.00$ )	0.08 ( $\pm 0.00$ )	0.17 ( $\pm 0.00$ )	0.14 ( $\pm 0.05$ )	158.0 ( $\pm 93.00$ )
-2	0.08 ( $\pm 0.00$ )	0.08 ( $\pm 0.00$ )	0.08 ( $\pm 0.00$ )	0.22 ( $\pm 0.05$ )	0.33 ( $\pm 0.32$ )	398.50 ( $\pm 231.10$ )
-5	0.08 ( $\pm 0.00$ )	0.08 ( $\pm 0.00$ )	0.11 ( $\pm 0.05$ )	0.22 ( $\pm 0.05$ )	3.20 ( $\pm 4.82$ )	–
-20	0.14 ( $\pm 0.05$ )	0.19 ( $\pm 0.05$ )	0.36 ( $\pm 0.05$ )	2.30 ( $\pm 1.10$ )	1.61 ( $\pm 1.14$ )	–
-40	0.11 ( $\pm 0.05$ )	0.22 ( $\pm 0.05$ )	50.30 ( $\pm 43.10$ )	26.10 ( $\pm 28.50$ )	21.36 ( $\pm 26.80$ )	–

A significant difference to existing infiltrometer devices, technically realized by using the membrane at the tip and degassed ultrapure water, was the ability to extend the range of applied tensions beyond the limitation of  $-10$  cm of previous microinfiltrometer studies (Hallett et al., 2003; Lichner et al., 2013; Sepehrnia et al., 2016). However, the use of tensions more negative than  $-60$  cm was not possible for long-term experiments, particularly for the water-repellent soil (data not shown). Capillarity was likely disrupted from evaporation and instability and it is possible that the surface tension of the infiltrating liquid decreased due to dissolved organic compounds, thus leading to air entry points of the porous membrane at less capillary pressure (closer to zero). Moreover, slow flow rates may have caused the tip to dry, due to evaporation, leading to air invasion.

Rigid tubes for the entire microinfiltrometer setup improved earlier designs where components were connected with flexible tubes (Hallett et al., 2003; Lichner et al., 2013). When using flexible tubes, fluctuations in recorded data of water infiltration at different tensions occurred within a day, possibly caused by slight mechanical disturbances transferred to the elastic properties of the flexible tube (data not shown). By using a Plexiglas hood to protect the tip and water/ethanol reservoir, losses due to evaporation became insignificant, which was particularly important for tensions more negative than  $-5$  cm with the accompanying longer measurement times.

The microinfiltrometer was also robust for ethanol infiltration for all tested pressures and tensions because a big advantage of glass tubes is the avoidance of chemical reactions with the flexible tube material (discoloration) or Plexiglas (cracking) (Evonik, 2000).

### Water and ethanol sorptivity

The values of  $S_w$  ranged from  $0.0041 (\pm 0.007)$  to  $0.275 (\pm 0.0091) \text{ cm s}^{-0.5}$  and  $S_e$  ranged from  $0.019 (\pm 0.003)$  to  $0.383 (\pm 0.0091) \text{ cm s}^{-0.5}$  (Fig. 3). These values agree with the ranges reported by Lichner et al. (2013) for pure sand ( $S_w$ :  $0.293\text{--}1.17 \text{ cm s}^{-0.5}$ ,  $S_e$ :  $0.099\text{--}0.398 \text{ cm s}^{-0.5}$ ).  $S_w$  and  $S_e$  differed between soils ( $p < 0.05$ ), and were influenced by pressures/tensions ( $p < 0.001$ ). Thermal treatments affected  $S_w$  ( $p < 0.05$ ), particu-

larly at higher tensions ( $< -5$  cm, Fig. 2), but  $S_e$  did not vary. Greater soil organic carbon (OC) affected  $S_w$  and  $S_e$  (Fig. 2), with subcritically water-repellent soil with the greater OC content having a higher sorptivity compared to the wettable soil at  $25^\circ\text{C}$ . In turn, the water-repellent soil with greater OC content and greater CA showed slightly reduced  $S_w$  compared to the subcritically water-repellent soil. This behaviour, likely driven by the quality and quantity of OC, was clearly observed in the  $S_e$  data (Table 1, Fig. 2) as ethanol wets soil regardless of wettability.  $S_e$  could possibly be affected by slight modifications of the particle surfaces (e.g. swelling due to reaction of ethanol and organic particle coating compounds), but these impacts are small compared to the impacts of SWR on  $S_w$ . Therefore, the changes of  $S_e$  were mainly affected by soil pore size and applied pressures/tensions if variables are compared in Fig. 2.

### Persistence, extent, and water repellency cessation time (WRCT)

The SWR parameters including persistence, extent, and WRCT are presented in Figs. 3, 4, and 5, respectively.

There was no significant change in the persistence of SWR (WDPT  $< 1$  s) of wettable soil after  $80^\circ\text{C}$ -treatment, while  $80^\circ\text{C}$ -treatment increased WDPT distinctly for the subcritically water-repellent and the water-repellent soils (Fig. 3). This was consistent with CA analysis that indicated no change in CA for the wettable soil and a distinct CA increase for the subcritically water-repellent and the water-repellent soils after  $80^\circ\text{C}$ -treatment (Fig. 3). At the same time, CA stability increased after  $80^\circ\text{C}$ -treatment, with  $\text{CA} > 125^\circ$  for the water-repellent soil and  $70^\circ$  for the subcritically water-repellent soil after five seconds, compared to  $58^\circ$  and  $17^\circ$  after  $25^\circ\text{C}$ -treatment, respectively. The wettable soil, however, showed no effect. This behaviour fitted well with the observed increase in WDPT (Fig. 3). Bachmann et al. (2003) found WDPT to be sensitive only within a narrow CA range around  $90^\circ$ . Leelamanie et al. (2008) also examined wettable to extremely water-repellent fine sand and reported that the WDPT was  $< 1$  s for CAs ranging from  $11^\circ$  to  $69^\circ$ , between 1s and 3600 s for CA from  $69^\circ$  to  $93^\circ$ , and then exceeded 3600 s for larger CAs. Leelamanie

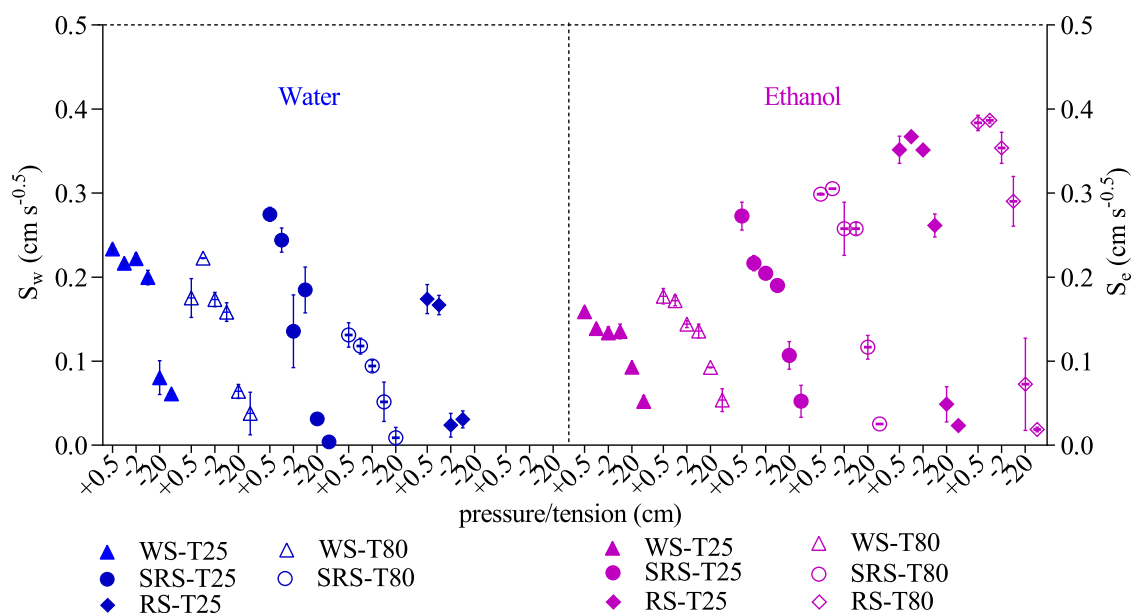


**Fig. 2.** Water and ethanol sorptivities ( $S_w$  and  $S_e$ , respectively) during infiltration for  $25^\circ\text{C}$ - and  $80^\circ\text{C}$ -treated soils (WS: wettable soil, SRS: subcritically water-repellent soil, RS: water-repellent soil) under different imposed pressures/tensions.

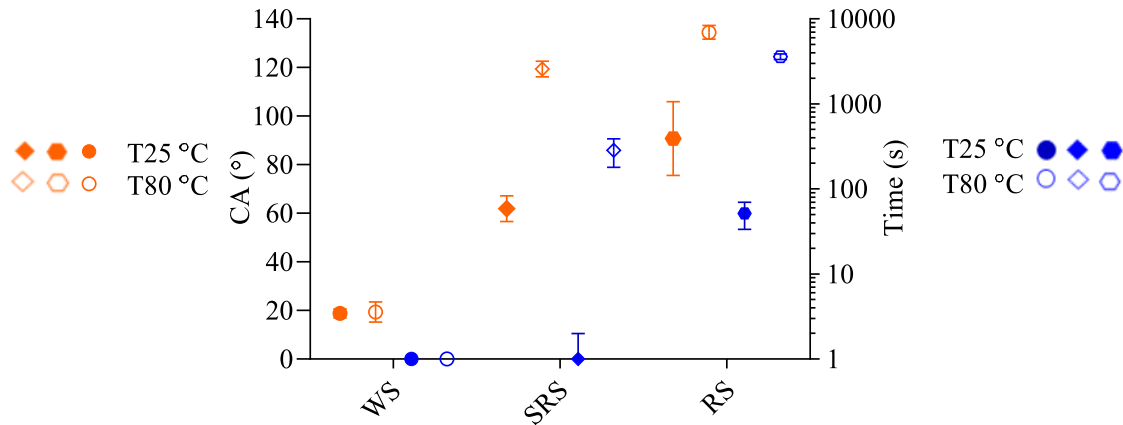


**Fig. 3.** SWR persistence of the studied soils, quantified by the contact angle, CA (left) and the water drop penetration time, WDPT (right), for 25°C- and 80°C-treated soils (WS: wettable soil, SRS: subcritically water-repellent soil, RS: water-repellent soil).

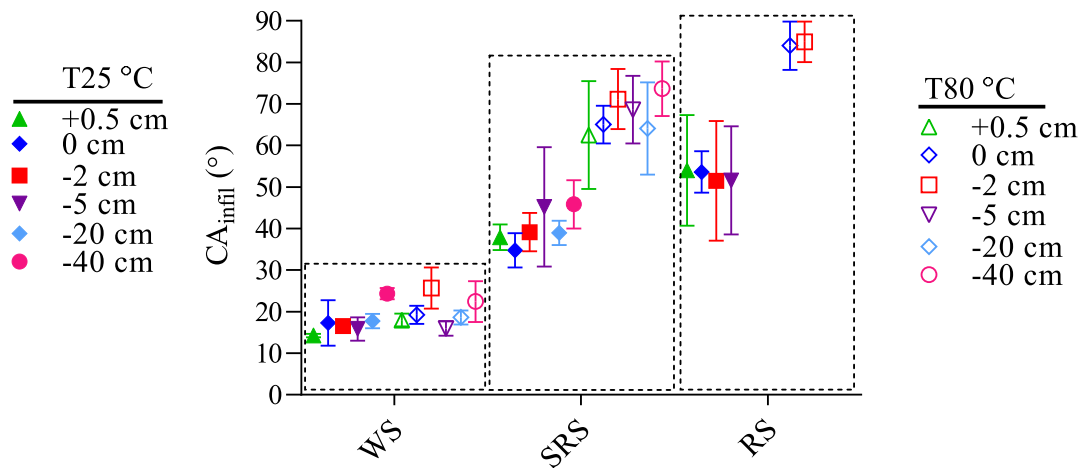


**Fig. 4.** Contact angle after water infiltration,  $CA_{infil}$ , for 25°C- and 80°C-treated soils under different imposed hydraulic pressures/tensions. The soils are wettable soil (WS), subcritically water-repellent soil (SRS) and water-repellent soil (RS).

et al. (2008) found that the WDPT was most sensitive for CA within the range of 88–93°. Therefore, the evaluation of the persistence of SWR proved that as water repellency appears in soil, exposure to moderately increased temperatures will increase initial water repellency (revealed by CA measurement; Goebel et al., 2011), as well as persistence, as indicated by both, CA and WDPT in our study (Fig. 3). This is especially evident for the subcritically water-repellent soil that showed a high potential for increased persistence in conjunction with the greatest CA increase among the studied forest soil samples.

The  $CA_{infil}$  of all three soils were  $< 90^\circ$  after water infiltration, but the subcritically water-repellent and the water-repellent soil still showed the effect of thermal treatment at 80°C (Fig. 4), with  $CA \geq 60^\circ$ . The data also illustrated the impact of imposed tensions, however the CA differences became small if subcritically water-repellent soil or water-repellent soil was considered separately for thermal treatments. This demonstrates the amphiphilic character of soil organic matter (i.e., coexistence of hydrophilic and hydrophobic functional groups, Goebel et al., 2011) and the orientation of the amphiphilic compounds with respect to pore space under dry and wet conditions (Doerr et al., 2000; Figs. 3 and 4). At the same time, persistence of SWR was observed for the water-

repellent soil, because the  $CA_{infil}$  remained between 75° to 90° after infiltration, even for applied pressures of +0.5 and 0 cm as outlined below.

The  $RI$  values of the soils under the applied pressures/tensions for the 25°C- and 80°C-treatments are shown in Fig. 5a. The wettable soil showed no significant increase of the  $RI$ , after 80°C-treatment, similar to the results shown in Figs. 3 and 4 for CA and WDPT. Also, in agreement with observed WDPT and CA (Figs. 3 and 4),  $RI$  values given in Fig. 5a were larger for water-repellent soil, while the differences between soils treated at 25 and 80°C increased with increasing tensions. Interestingly, infiltration was not possible at –20 cm for the subcritically water-repellent soil treated at 80°C. This demonstrates the high sensitivity of the microinfiltrometer to detect non-linear and steeply increasing infiltration resistance for soils at intermediate water repellency under hydraulic tensions greater than a certain value. Fig. 5a suggests further that the  $RI$  values for the water-repellent soil with a CA of about 90° were smaller at slightly positive (+0.5 cm) or zero pressure compared to the values of the subcritically water-repellent soil (with a CA of about 62°) at –20 and –40 cm. This result outlines that differences in the degree of repellency increase with increasing tension of the infiltrating water. This confirms quantitatively in

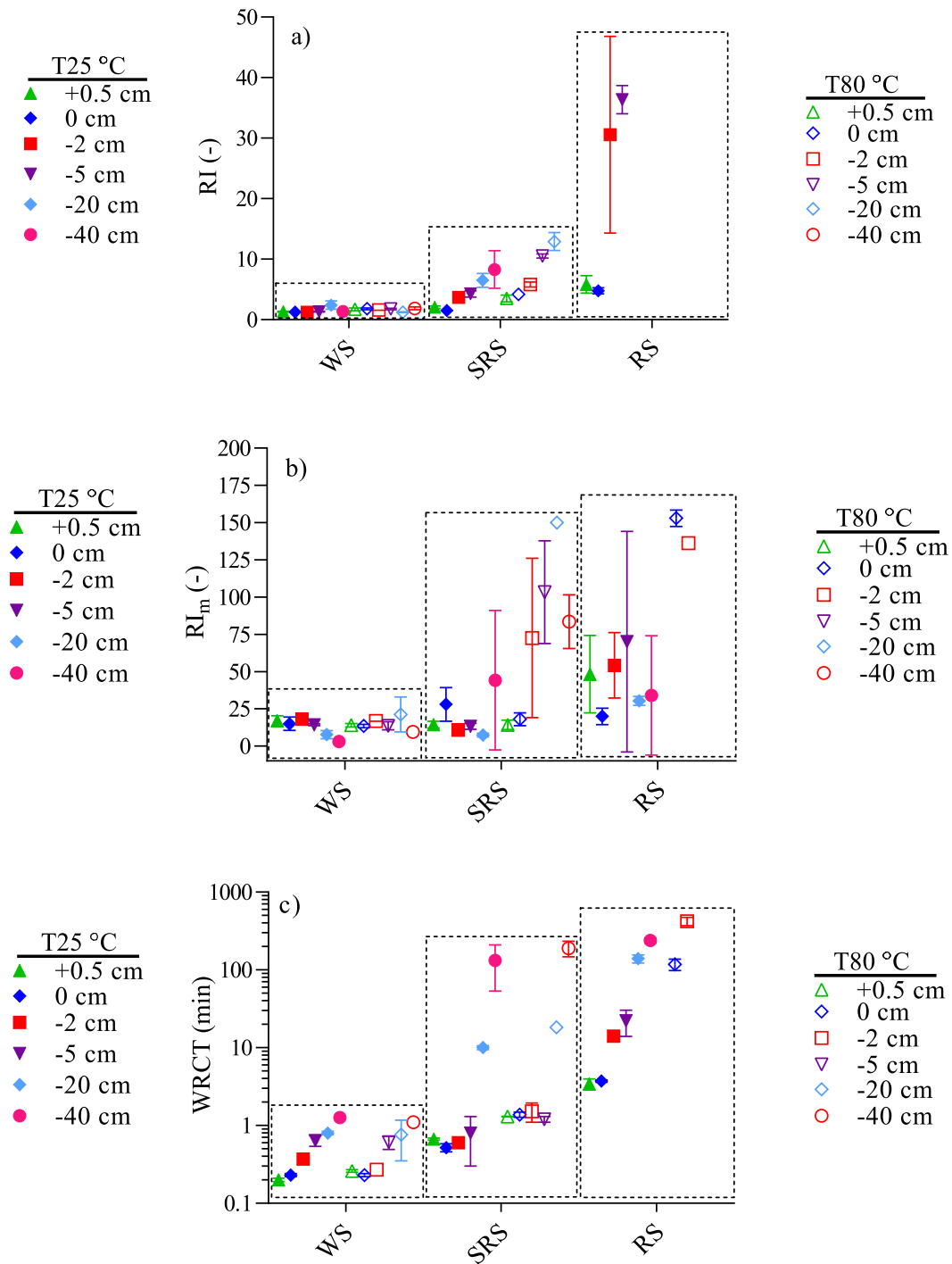


**Fig. 5.** Extent of SWR of studied soils (WS: wettable soil, SRS: subcritically water-repellent soil, RS: water-repellent soil) quantified by the repellency index,  $RI$ , (a), modified repellency index,  $RI_m$ , (b), and extent and persistence of SWR of studied soils using the water repellency cessation time, WRCT, for 25°C- and 80°C- treatment (c) under different imposed hydraulic pressures/tensions.

the lab the reason for moisture patterns with sharp moisture content boundaries, which may exist in natural soil profiles over weeks and months (Deurer and Bachmann, 2007). A specific roughness (i.e., texture and/or particle microrelief) at the moisture wetting fronts can impede water flow and infiltration through reduced capillary forces and trapping of air in the cavities of the pores when the material itself is hydrophobic (i.e., CA measured at a flat surface of the same material is  $\geq 90^\circ$ ), which may lead from partially to fully impregnated states (Jonas et al., 2020).

The results of  $RI$  measurements for different extents of SWR (Fig. 5a) were consistent with the  $RI$  thresholds proposed by Iovino et al. (2018). These results imply that the proposed modifications in the microinfiltrometer construction are promising for its usability within a broad range of hydraulic tensions and different states of SWR. However, we observed some minor under- and overestimations at the applied tensions if  $RI$  was considered. For the wettable soil, slight repellency is indicated at -20 cm and for the subcritically water-repellent soil, wettability is indicated at 0 cm tension. Finally, it should be noted

here that for the water-repellent soil treated at 80°C, infiltration measurements were not possible at any tension, similar to the 25°C-treatment variant at -20 and -40 cm, which explains missing data in Fig. 5a.

An alternative method to assess SWR is the characterization through single water infiltration experiments, expressed by the  $RI_m$  index. These data are shown in Fig. 5b. In comparison, the  $RI_m$  data showed less regular trends as a function of applied tensions if compared with the  $RI$  data (Fig. 5a). This could be due to the insensitivity to define hydrophilic sorptivity, as the reference value based only on water infiltration ( $S_w$ ) data could be at a different stage of infiltration compared to ethanol ( $S_e$ ) as the reference state. The latter result might be considered as a disadvantage of the  $RI_m$  concept so that a representative hydrophilic sorptivity may not be found for soils with a high extent and persistence of water repellency. In general, the trend of data showed the difference in water repellency extent between the studied soils and the applied tensions. However, there is still no classification reference for  $RI_m$  values to illustrate whether the predictions fit in their own water repellency thresholds or not. This suggests the need for the definition of thresholds as well as for a clear reference of  $RI_m$  as suggested by Sepehrnia et al. (2016). Alagna et al. (2019) and Sepehrnia et al. (2016, 2017) also discussed that  $RI_m$  may not be an appropriate index to capture SWR across all possible states because both the WRCT and the  $RI_m$  are obtained from the  $I$  versus  $\sqrt{t}$  plot of cumulative water infiltration, with the drawbacks discussed above. Furthermore, the WRCT may also be an effect of the volume of water already infiltrated and/or flowing into the soil, hence the wetting bulb size. Additionally, the size and volume of the conducting pores could be different with regards to time and applied pressures/tensions (Beatty and Smith, 2014). Notwithstanding, in comparison to  $RI$ , the  $RI_m$  showed slightly greater flexibility in describing the repellency state of water-repellent soil for all applied tensions at 25°C, as well as 0 and -2 cm at 80°C after 24 h. Altogether, the results imply that  $RI_m$  can be a promising parameter to predict the water repellency status of non-repellent ( $CA = 0^\circ$ ) and subcritically water-repellent ( $0^\circ < CA < 90^\circ$ ) soils through short (3–15 min) infiltration tests, as well water-repellent soils ( $CA \geq 90^\circ$ ) using long-term (24 h) infiltration tests.

No infiltration at pressures lower +0.5 cm for water indicates, most likely, high local water repellency persistence at the interfaces (solid-water and air-water), which would result in weak imbibition (Ruspini et al., 2017). In this case, given that water repellency may even inhibit water vapor condensation, local water vapor adsorption may even increase the level of water repellency (Goebel et al., 2004). For the water-repellent soil, infiltration was still observed at tensions of 0 cm and -2 cm, but infiltration began with a delay after 158 and 398.5 min, respectively (Table 2). When no infiltration occurred for tensions lower than -2 cm (i.e., -5, -20, and -40 cm) it showed that the effect of wettability on water infiltration was significantly affected by the tension of the invading water. This meant that the wetting front would not overcome water repellency of the interfaces in the respective pore size classes to create any laminar film or further flow pathways, especially for soils at the transition between subcritically water-repellent and water-repellent soils.

The WRCT of the studied soils, which considers the extent and persistence of SWR for the applied thermal treatments (25°C and 80°C) is presented in Fig. 5c. It can be seen that the WRCT was very sensitive to the applied tensions and was greatest for water-repellent samples (Fig. 5c). However, WRCT values of the wettable and subcritically water-repellent soils

treated at 25°C were similar to those of the 80°C-treated soils. For the 80°C-heated water-repellent soil, however, WRCT increased at low tensions (i.e., 0 and -2 cm). This may indicate a more stable modification in interface chemical composition towards greater rigidity of the arrangement of functional groups compared to the subcritically water-repellent soil.

### Extent and persistence of soil water repellency in relation to interface chemical composition

The main compounds of all interfaces were O and C, followed by Si, Al, and some Fe. Further, traces (< 0.2 at.-%) of Na, Ca, K, and Mg were detected (data not shown). Interface O/C ratio of air-dry soils increased from water-repellent to subcritically water-repellent to wettable soil (Woche et al., 2017). There was a tendency for the 80°C-treatment to have a slightly decreased O/C ratio for the water-repellent soil, while no measurable effect was observed for the subcritically water-repellent and the wettable soils (Table 4). A decrease in O/C ratio along with increasing CA after heat treatment of sandy soil (sand content > 75%) has been observed before (Bachmann et al., 2020; Diehl et al., 2014; Gaj et al., 2019). Thus, the distinctly smaller sand content of the subcritically water-repellent and the wettable material (Table 1) may explain the different behaviour. Pooling of all samples identified a tendency of O/C ratio of air-dry soils to be slightly smaller than for shock-frozen and freeze-dried soils ( $1.66 \pm 0.57$  and  $1.81 \pm 0.78$ , respectively), but the difference was not significant ( $p > 0.05$ ).

However, CA as well as  $CA_{infil}$  (measured after infiltration) and O/C ratios of all tested soils fitted very well within the general regression of O/C ratio vs. CA, derived from a broad range of different materials (Woche et al., 2017). Within the samples tested, a significant negative linear relationship between CA and O/C ratio was observed for both air-dry ( $R^2 = 0.80$ ,  $p < 0.05$ ) as well as shock-frozen and freeze-dried samples ( $R^2 = 0.72$ ,  $p < 0.05$ ; Fig. 6a). Further, the values of  $S_w$  were found to be positively related to the interface O/C ratio of shock-frozen and freeze-dried samples. This was most apparent at -2 cm and -5 cm infiltrating tensions, where a significant positive relationship was observed ( $R^2 = 0.99$ ,  $p < 0.001$  and  $R^2 = 0.86$ ,  $p < 0.05$ , respectively; Fig. 6b). Therefore, we confirmed the hypothesis that the general relation between the water repellency parameters (evaluated at -2 cm) are also valid for greater tension values.

The results revealed that the reduced infiltration at higher tensions was governed by the same wettability parameters. In other words, the reduced infiltration was caused by water repellency and not by additional effects caused by the technical setup of the proposed microinfiltrometer. This is a very important finding that can be utilized to build up hydraulic models for SWR. Along with decreasing CA from water repellent to subcritically water-repellent and wettable soils, C speciation indicated decreasing amounts of non-polar C-C and C-H species, as confirmed by decreasing  $C_{np}$  contents derived from the fit of the survey C 1s peak. For 80°C-treated water-repellent soil, the content of C-C and C-H species and  $C_{np}$  increased as CA increased (Table 3, Figs. 4 and 6). However, in agreement with observed O/C ratios, for subcritically water-repellent and wettable soils, the content of C-C and C-H species and  $C_{np}$  compounds was similar for the 25°C and 80°C treatments, despite a distinct increase in CA for the subcritically water-repellent soil (Table 3, Figs. 4 and 6).

Benito et al. (2019) evaluated persistence of SWR using WDPT. They concluded that water repellency exhibited a significant positive correlation with C content and C/N ratio,

**Table 4.** Interface O/C and C/N ratio as derived from XPS analysis for the 25°C- and the 80°C-treated soils (WS: wettable soil, SRS: subcritically water-repellent soil, RS: water-repellent soil). Further, the amounts of non-polar C–C, C–H species (derived from fit of the C 1s detail scans) and the amounts of polar ( $C_p$ ) and non-polar ( $C_{np}$ ) compounds (derived from fit of the survey C 1s peak) and their ratio ( $C_{np}/C_p$ ) are given. Data, presented as mean  $\pm$  standard deviation, refer to spectra recorded on air-dry soils.

	O/C (-)	C/N (-)	C–C, C–H (at.-%)	$C_p$ (at.-%)	$C_{np}$ (at.-%)	$C_{np}/C_p$ (-)
	25°C					
WS	2.40 ( $\pm 0.1$ )	20.30 ( $\pm 2.20$ )	9.20 ( $\pm 1.60$ )	14.60 ( $\pm 2.80$ )	8.30 ( $\pm 2.70$ )	0.60 ( $\pm 0.30$ )
SRS	1.50 ( $\pm 0.3$ )	27.10 ( $\pm 2.00$ )	14.30 ( $\pm 3.40$ )	18.10 ( $\pm 2.60$ )	14.50 ( $\pm 2.50$ )	0.80 ( $\pm 0.10$ )
RS	1.20 ( $\pm 0.1$ )	26.10 ( $\pm 1.50$ )	17.10 ( $\pm 1.80$ )	19.50 ( $\pm 0.20$ )	19.30 ( $\pm 1.00$ )	1.00 (0.00)
	80°C					
WS	2.3 ( $\pm 0.1$ )	18.80 ( $\pm 3.70$ )	10.0 ( $\pm 0.90$ )	11.10 ( $\pm 0.90$ )	13.20 ( $\pm 0.30$ )	1.20 ( $\pm 0.10$ )
SRS	1.6 ( $\pm 0.1$ )	33.40 ( $\pm 4.00$ )	15.2 ( $\pm 0.50$ )	16.40 ( $\pm 0.90$ )	15.80 ( $\pm 0.90$ )	1.0 ( $\pm 0.10$ )
RS	1.0 ( $\pm 0.3$ )	31.40 ( $\pm 3.40$ )	21.70 ( $\pm 4.80$ )	19.80 ( $\pm 3.60$ )	23.30 ( $\pm 4.30$ )	1.20 (0.00)

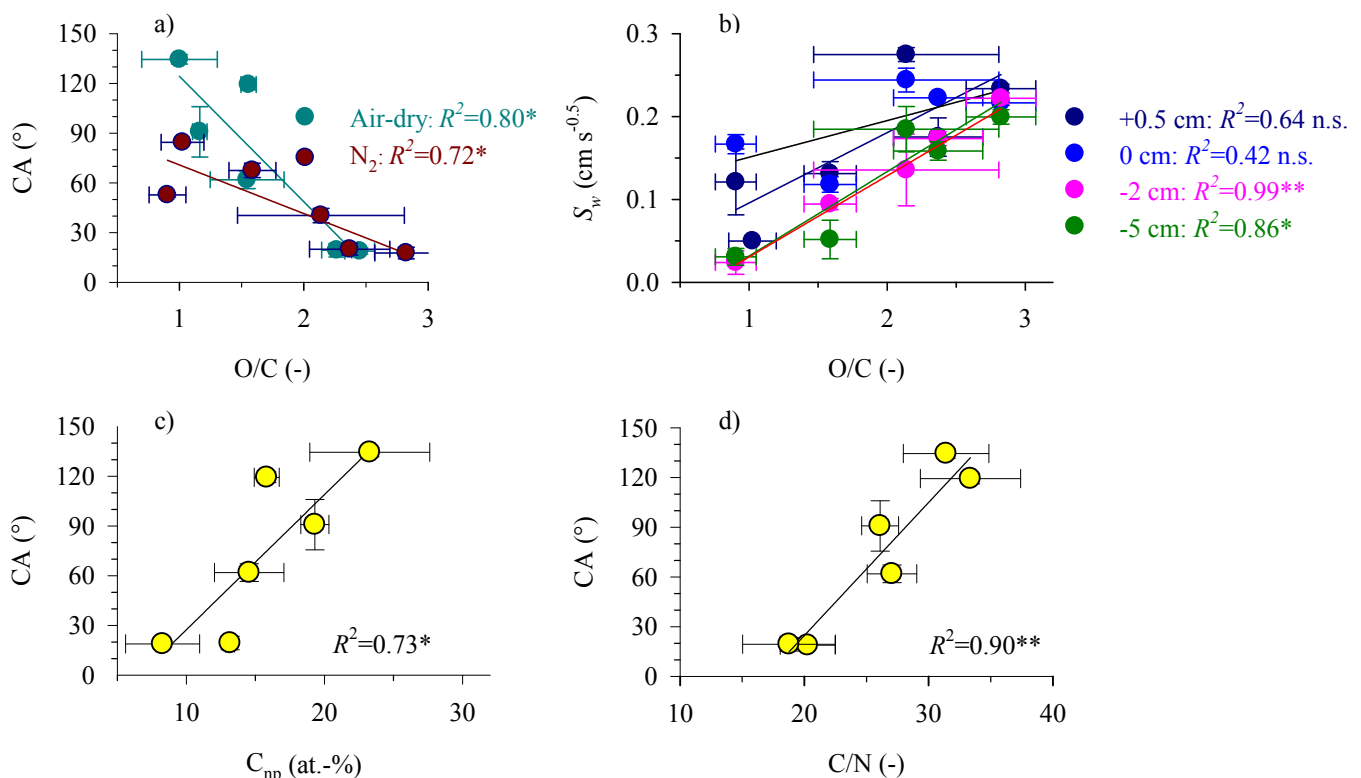


**Fig. 6.** Relationship between interface O/C ratio and contact angle (CA) for air-dry and shock-frozen and freeze-dried ( $N_2$ ) samples (a), relationship between O/C ratio of shock-frozen and freeze-dried ( $N_2$ ) samples and water sorptivity ( $S_w$ ) for pressures applied (b), relationship between CA and the amount of non-polar C compounds ( $C_{np}$ ; c), and relationship between CA and interface C/N ratio (d). The lines represent linear regression fits. Significance levels: \* $p < 0.05$ ; \*\* $p < 0.01$ .

regardless if samples were air-dried or field-moist. Bulk and interface C content showed the same trend, i.e., decreasing contents from water-repellent to subcritically water-repellent and wettable soil. Total interface C content of the 25°C and the 80°C treated soils was significantly positively correlated with CA ( $R^2 = 0.77$ ,  $p < 0.05$ ). Based on C speciation and the basic fit of the survey C 1s peaks, the content of non-polar C–C, C–H species and non-polar C compounds ( $C_{np}$ ), respectively, were indicated to determine wetting properties ( $R^2 = 0.84$ ,  $p < 0.001$ , and  $R^2 = 0.73$ ,  $p < 0.05$ , respectively). Correlations were also valid for CA determined after five seconds (C–C/C–H:  $R^2 = 0.80$ ,  $p < 0.05$ ;  $C_{np}$ :  $R^2 = 0.76$ ,  $p < 0.05$ ), supporting the relation between sessile drop CA vs. the amount of non-polar C species and  $C_{np}$  within the interface layer. In line with Benito et al. (2019), the interface C/N ratio was significantly positively correlated with CA ( $R^2 = 0.90$ ,  $p < 0.05$ ).

#### Rating of the microinfiltrometer signals

We showed that the effect of SWR on water infiltration depends on the applied hydraulic pressure/tension. As a consequence, the proposed microinfiltrometer can measure the effect of pressure/tension-dependent water repellency. It allows the relation between the infiltration behaviour of liquids in water-repellent soil and the respective penetration dynamics of several liquids (i.e., water and ethanol) to be identified, so that water repellency-based parameters can be derived. Further information can be obtained from liquid infiltration using a microinfiltrometer if the  $RI$  is compared with WDPT and sessile drop CA. Although CA and WDPT characterize soil wetting properties (Bachmann et al., 2003; Dekker and Ritsema, 1994; Hallett, 2007), neither CA nor WDPT gives information on real water flow because additional parameters like pore-size-dependent

wettability determine the infiltration process. The *RI* provides this information and could possibly be used with an adapted infiltrometer design in the field to detect small-scale variability, i.e., in and around macropores or aggregate surfaces. In addition, valuable information can be derived from cumulative infiltration with time. For example, Fig. 7a shows cumulative water infiltration under  $-2$  cm tension. From Fig. 7b, the cumulative infiltration curve for the subcritically water-repellent soil, treated at  $80^\circ\text{C}$ , consisted of three phases. These phases became more distinct as SWR increased. These phases are postulated to show SWR persistence (phase I), the transition state (phase II) which simultaneously reflects changes in the orientation of functional groups with respect to pore space and pore size switch to allow water infiltration, and the nearly stationary steady-state infiltration (phase III). The infiltration rate versus time evaluated with this microinfiltrometer could be applied to investigate wetting front propagation in soil aggregates (Leeds-Harrison, 1994, 1997; Wang et al., 2000) at the micro-scale (Hallett and Young, 1999; Hallett et al., 2001; Mao et al., 2019). This allows progress in small-scale detection of spatial variability of water repellency as suggested by Mao et al., (2019) and Rodríguez-Alleres and Benito (2011). Since the infiltration front is not infinitely small, the transition must be regarded as a complicated process of several overlaying processes (Bauters et al., 2000; Dekker and Ritsema, 2000), which

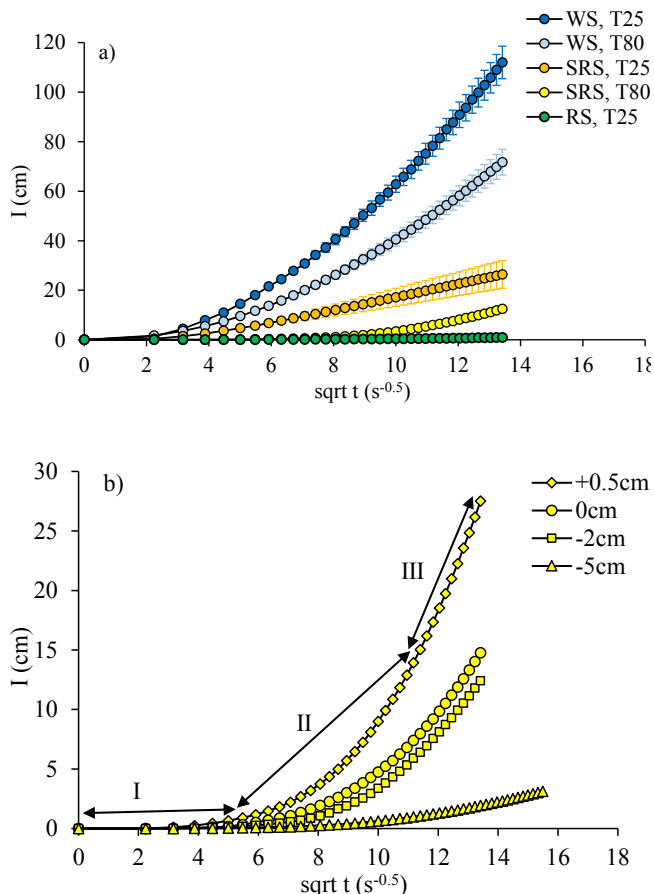


**Fig. 7.** Cumulative water infiltration at a  $-2$  cm tension for the studied soils (WS: wettable soil, SRS: subcritically water-repellent soil, RS: water-repellent soil) treated at 25 and  $80^\circ\text{C}$  (a), magnified cumulative infiltration curve of the SRS treated at  $80^\circ\text{C}$  under different hydraulic pressures/tensions (+0.5, 0,  $-2$ , and  $-5$  cm), with three different infiltration phases marked (I, II, III; b).

explains the extended transition zone of the hockey-stick behaviour between the linear infiltration rates of phase I and III. This will be evaluated in further research exploring soil CA. Generally, the microinfiltrometer signal displays the small-scale transition in the wetting zone caused by the loss of water repellency depending on several factors like aggregate size, the respective location of water repellent zones such as hydrophobic coatings under different tensions, and the energy status of the soil water (De Rooij, 2000; Deurer and Bachmann, 2007).

## CONCLUSIONS

We designed an improved microinfiltrometer to allow for long-time measurements at a broad range of tensions with a standardized tip that allowed for high rates of liquid transport for different liquids. The modified microinfiltrometer worked well in water and ethanol infiltration tests. Studies were conducted with three sandy soils with different initial wettability that were thermally treated at  $25^\circ\text{C}$  and  $80^\circ\text{C}$ . Infiltration measurements could be made for a broad range of hydraulic conditions (+0.5, 0,  $-2$ ,  $-5$ ,  $-20$ , and  $-40$  cm). The suggested microinfiltrometer modifications are i) to use a glass tube with 3 mm inner diameter to make both water and ethanol infiltrations possible at constant flow rate and prevent a noisy signal during the test, ii) to cover the microinfiltrometer with Plexiglas hoods to prevent evaporation from tip and reservoir, iii) to use degassed ultrapure water to run tensions higher than  $-5$  cm, and iv) to use a  $15\ \mu\text{m}$ -nylon mesh to enclose the tip in order to prevent air bubble formation in the system. It is thus expected that this microinfiltrometer also works for soils with finer texture. Our study led to the following conclusions:

- XPS data and the evaluated SWR indices (*RI*, *RI<sub>m</sub>*, and WRCT) demonstrated infiltration tests  $-2$  cm tension provides valuable information for different aspects of water repellency, like extent and persistence. In this respect it is possible to analyse water infiltration also for hydrophobic soils ( $\text{CA} \geq 90^\circ$ ) through long-time tests (24 h), which may allow a better characterization of sorptivity of hydrophobic soils.
- Experimental data derived from the proposed microinfiltrometer setup may support the development of micro-hydraulic models to simulate infiltration at the pore scale under different boundary conditions like the tension of the infiltration water.
- Thermal treatment effects on wetting properties and sorptivity illustrated a sufficient sensitivity of the microinfiltrometer to detect changes in water repellency caused by the chemical composition of the particle interfaces while all other factors (organic carbon content, pore shape) remained constant. This suggests that further modifications of SWR; e.g., caused by changing climatic conditions like extended droughts or slightly increasing soil temperatures, may be detected with respect to their micro-hydraulic relevance. A modified wettability of bulk soil or soil aggregates might be relevant for complex environmental issues like soil erosion, available water or /and contaminant transport.
- Interface O/C ratio and the amount of non-polar carbon compounds of the outermost soil particle interface layer explains the level of water repellency as well as the infiltration behaviour with respect to extent and persistence of SWR which was shown in this paper for the first time. Further, the positive relationship (in trend and significant, respectively) between water sorptivity and interface O/C ratio of shock-frozen and freeze-dried samples additionally proves the governing role of the interface chemical composition for all soil processes.

**Acknowledgements.** We thank the Alexander von Humboldt Foundation for financial support of this project and donating post-doctoral fellowship to first author. We acknowledge Martin Volkmann, Moritz Rahlfs, Hanna Böhme, Stephanie Günther, and Henrik Redweik for their help with soil sampling and preparing stuff. We appreciate Professor Paul Hallett for his constructive comments and direct communication about microinfiltrometer tips and improving the English language of the text. Furthermore, we appreciate the feedback of anonymous reviewers whose constructive comments improved the article.

## REFERENCES

- Alagna, V., Iovino, M., Bagarello, V., Mataix-Solera, J., Lichner, L., 2019. Alternative analysis of transient infiltration experiment to estimate soil water repellency. *Hydrol. Process.*, 33, 661–674.
- Bachmann, J., Woche, S.K., Goebel, M.-O., Kirkham, M.B., Horton, R., 2003. Extended methodology for determining wetting properties of porous media. *Water Resour. Res.*, 39, 1353.
- Bachmann, J., Deurer, M., Arye, G., 2007. Water-repellent soil: Development of a contact angle–dependent water-retention model. *Vadose Zone J.*, 6, 436–445.
- Bachmann, J., Söffker, S., Sepehrnia, N., Goebel, M.-O., Woche, S.K., 2020. The effect of temperature and wetting–drying cycles on soil wettability: Dynamic molecular restructuring processes at the solid–water–air interface. (In preparation).
- Bauters, T.W.J., Steenhuis, T.S., DiCarlo, D.A., Nieber, J.L., Dekker, L.W., Ritsema, C.J., Parlange, J.-Y., Haverkamp, R., 2000. Physics of water repellent soils. *J. Hydrol.*, 231–232, 233–243.
- Beatty, S.M., Smith, J.E., 2014. Infiltration of water and ethanol solutions in water repellent post wildfire soils. *J. Hydrol.*, 514, 233–248.
- Benito, E., Varela, E., Rodríguez-Alleres, M., 2019. Persistence of water repellency in coarse-textured soils under various types of forests in NW Spain. *J. Hydrol. Hydromech.*, 67, 129–134.
- Clothier, B.E., Vogeler, I., Magesan, G.N., 2000. The breakdown of water repellency and solute transport through a hydrophobic soil. *J. Hydrol.*, 231–232, 255–264.
- Cosentino, D., Hallett, P.D., Michel, J.C., Chenu, C., 2010. Do different methods for measuring the hydrophobicity of soil aggregates give the same trends in soil amended with residue? *Geoderma*, 159, 221–227.
- De Rooij, G.H., 2000. Modeling fingered flow of water in soils owing to wetting front instability: a review. *J. Hydrol.*, 231–232, 277–294.
- Decagon, 2007. Minidisk Infiltrometer User's Manual. Version 6. Decagon Devices, Inc., Pullman.
- Dekker, L.W., Ritsema, C.J., 1994. How water moves in a water repellent sandy soil. I. Potential and actual water repellency. *Water Resour. Res.*, 30, 2507–2517.
- Dekker, L.W., Ritsema, C.J., 2000. Wetting patterns and moisture variability in water repellent Dutch soils. *J. Hydrol.*, 231–232, 148–164.
- Dekker, L.W., Doerr, S.H., Oostindie, K., Ziogas, A.K., Ritsema, C.J., 2001. Water repellency and critical soil water content in a dune sand. *Soil Sci. Soc. Am. J.*, 65, 1667–1674.
- Dekker, L.W., Oostindie, K., Ritsema, C.J., 2005. Exponential increase of publications related to soil water repellency. *Aust. J. Soil Res.*, 43, 403–441.
- Deurer, M., Bachmann, J., 2007. Modeling water movement in heterogeneous water-repellent soil: 2. A conceptual numerical simulation. *Vadose Zone J.*, 6, 446–457.
- Diehl, D., Schneckenburger, T., Krüger, J., Goebel, M.-O., Woche, S.K., Schwarz, J., Shchegolikina, A., Lang, F., Marschner, B., Thiele-Bruhn, S., Bachmann, J., Schaumann, G.E., 2014. Effect of multivalent cations, temperature and aging on soil organic matter interfacial properties. *Environ. Chem.*, 11, 709–718.
- Doerr, S.H., Shakesby, R.A., Walsh, R.P.D., 2000. Soil water repellency: its causes characteristics and hydrogeomorphological significance. *Earth-Sci. Rev.*, 51, 33–65.
- Evonik, 2000. Stress Crack and Chemical Resistance. Darmstadt, Germany.
- Gaj, M., Lamparter, A., Woche, S.K., Bachmann, J., McDonnell, J.J., Stange, C.F., 2019. The role of matric potential, solid interfacial chemistry, and wettability on isotopic equilibrium fractionation. *Vadose Zone J.*, 18. DOI: 10.2136/vzj2018.04.0083
- Goebel, M.-O., Bachmann, J., Woche, S.K., Fischer, W.R., Horton, R., 2004. Water potential and aggregate size effects on contact angle and surface energy. *Soil Sci. Soc. Am. J.*, 68, 383–393.
- Goebel, M.-O., Bachmann, J., Reichstein, M., Janssens I.A., Guggenberger, G., 2011. Soil water repellency and its implications for organic matter decomposition – is there a link to extreme climatic events? *Glob. Change Biol.*, 17, 2640–2656.
- Goebel, M.O., Woche, S.K., Abraham, P.M., Schaumann, G.E., Bachmann, J., 2013. Water repellency enhances the deposition of negatively charged hydrophilic colloids in a water-saturated sand matrix. *Colloids Surf. A*, 431, 150–160.
- Gordon, D.C., Hallett, P.D., 2014. An automated microinfiltrometer to measure small-scale soil water infiltration properties. *J. Hydrol. Hydromech.*, 62, 248–252.
- Hallett, P.D., 2007. An introduction to soil water repellency. In: Gaskin, R.E. (Ed.): *Adjuvants for Agrochemicals*. Hand Multimedia, Christchurch, New Zealand, 9 p.
- Hallett, P.D., Young, I.M., 1999. Changes to water repellence of soil aggregates caused by substrate-induced microbial activity. *Eur. J. Soil Sci.*, 50, 35–40.
- Hallett, P.D., Baumgartl, T., Young, I.M., 2001. Subcritical water repellency of aggregates from a range of soil management practices. *Soil Sci. Soc. Am. J.*, 65, 184–190.
- Hallett, P.D., Gordon, D.C., Bengough, A.G., 2003. Plant influence on rhizosphere hydraulic properties: direct measurements using a miniaturized infiltrometer. *New Phytol.*, 157, 597–603.
- Iovino, M., Pekárová, P., Hallett, P.D., Pekár, J., Lichner, L., Mataix-Solera, J., Alagna, V., Walsh, R., Raffan, A., Schacht, K., Rodný, M., 2018. Extent and persistence of soil water repellency induced by pines in different geographic regions. *J. Hydrol. Hydromech.*, 66, 360–368.
- Johnson, M.S., Lehmann, J., Steenhuis, T.S., Oliveira, L.V., Fernandes, E.C.M., 2005. Spatial and temporal variability of soil water repellency of Amazonian pastures. *Aust. J. Soil Res.*, 43, 319–326.
- Jonas, A.M., Cai, R., Vermeyen, R., Nysten, B., Vanneste, M., Smet, D.D., Glinel, K., 2020. How roughness controls the water repellency of woven fabrics. *Mater. Des.*, 187, 108389.
- Leeds-Harrison, P.B., Youngs, E.G., 1997. Estimating the hydraulic conductivity of aggregates conditioned by different tillage treatments from sorption measurements. *Soil Till. Res.*, 41, 141–147.
- Leeds-Harrison, P.B., Youngs, E.G., Uddin, B., 1994. A device

- for determining the sorptivity of soil aggregates. *Eur. J. Soil Sci.*, 45, 269–272.
- Leelamanie, D.A.L., Karube, J., Yoshida, A., 2008. Characterizing water repellency indices: Contact angle and water drop penetration time of hydrophobized sand. *J. Soil Sci. Plant Nutr.*, 54, 179–187.
- Letey, J., Carrillo, M.L.K., Pang, X.P., 2000. Approaches to characterize the degree of water repellency. *J. Hydrol.*, 231–232, 61–65.
- Li, X., Chang, S.S.X., Salifu, K.F., 2014. Soil texture and layering effects on water and salt dynamics in the presence of a water table: a review. *Environ. Rev.*, 22, 41–50.
- Lichner, L., Hallett, P.D., Drongova, Z., Czachor, H., Kovacik, L., Mataix-Solera, J., Homolak, M., 2013. Algae influence the hydrophysical parameters of a sandy soil. *Catena*, 108, 58–68.
- Lichner, L., Felde, V.J.M.N.L., Büdel, B., Leue, M., Gerke, H.H., Ehlerbrock, R.H., Kollár, J., Rodný, M., Šurda, P., Fodor, N., Sándor, R., 2018. Effect of vegetation and its succession on water repellency in sandy soils. *Ecohydrology*, 11, e1991.
- Mao, J., Nierop, K.G.J., Dekker, S.C., Dekker, L.W., Chen, B., 2019. Understanding the mechanisms of soil water repellency from nanoscale to ecosystem scale: a review. *J. Soils Sediments*, 19, 171–185.
- Muehl, G.J.H., Ruehlmann, J., Goebel, M.-O., Bachmann, J., 2012. Application of confocal laser scanning microscopy (CLSM) to visualize the effect of porous media wettability on unsaturated pore water configuration. *J. Soils Sediments*, 2, 75–85.
- Orfánus, T., Dlapa, P., Fodor, N., Rajkai, K., Sándor, R., Nováková, K., 2014. How severe and subcritical water repellency determines the seasonal infiltration in natural and cultivated sandy soils. *Soil Till. Res.*, 135, 49–59.
- Philip, J.R., 1957. The theory of infiltration: 1. The infiltration equation and its solution. *Soil Sci.*, 83, 345–357.
- R Core Team, 2013. R: A language and environment for statistical computing. R Foundation for Statistical Computing, Vienna, Austria. URL <http://www.R-project.org/>.
- Rodríguez-Alleres, M., Benito, E., 2011. Spatial and temporal variability of surface water repellency in sandy loam soils of NW Spain under *Pinus pinaster* and *Eucalyptus globulus* plantations. *Hydrol Process.*, 25, 3649–3658.
- Ruspini, L.C., Farokhpoor, R., Øren, P.E., 2017. Pore-scale modeling of capillary trapping in water-wet porous media: A new cooperative pore-body filling model. *Adv. Water Resour.*, 108, 1–14.
- Sepehrnia, N., Hajabbasi, M.A., Afyuni, M., Lichner, L., 2016. Extent and persistence of water repellency in two Iranian soils. *Biologia*, 71, 1137–1143.
- Sepehrnia, N., Hajabbasi, M.A., Afyuni, M., Lichner, L., 2017. Soil water repellency changes with depth and relationship to physical properties within wettable and repellent soil profiles. *J. Hydrol. Hydromech.*, 65, 99–104.
- Thieme, L., Graeber, D., Kaupenjohann, M., Siemens, J., 2016. Fast-freezing with liquid nitrogen preserves bulk dissolved organic matter concentrations, but not its composition. *Bio-geosciences*, 13, 4697–4705.
- Tillman, R.W., Scotter, D.R., Wallis, M.G., Clothier, B.E., 1989. Water-repellency and its measurement by using intrinsic sorptivity. *Aust. J. Soil Res.*, 27, 637–644.
- Tschapek, M., 1984. Criteria for determining the hydrophilicity-hydrophobicity of Soils. *J. Plant Nutr. Soil Sci.*, 137–149.
- Wang, Z., Wu, Q.J., Wu, L., Ritsema, C.J., Dekker, L.W., Feyen, J., 2000. Effects of soil water repellency on infiltration rate and flow instability. *J. Hydrol.*, 231–232, 265–276.
- Wenzel, R.N., 1936. Resistance of solid surfaces to wetting by water. *Ind. Eng. Chem.*, 28, 988–994.
- Woche, S.K., Goebel, M.-O., Mikutta, R., Schurig, C., Kaestner, M., Guggenberger, G., Bachmann, J., 2017. Soil wettability can be explained by the chemical composition of particle interfaces - An XPS study. *Sci. Rep.*, 7, 42877.
- Zhang, R., 1997. Determination of soil sorptivity and hydraulic conductivity from the disk infiltrometer. *Soil Sci. Soc. Am. J.*, 61, 1024–1030.

Received 24 March 2020  
Accepted 20 August 2020

# The effect of a prototype hydromulch on soil water evaporation under controlled laboratory conditions

Antoni M.C. Verdú<sup>1</sup>, M. Teresa Mas<sup>1</sup>, Ramon Josa<sup>1</sup>, Marta Ginovart<sup>2\*</sup>

<sup>1</sup> Department of Agri-Food Engineering and Biotechnology, Universitat Politècnica de Catalunya, C/ Esteve Terradas 8, 08860-Castelldefels, Barcelona, Spain.

<sup>2</sup> Department of Mathematics, Universitat Politècnica de Catalunya, C/ Esteve Terradas 8, 08860 Castelldefels, Barcelona, Spain.

\* Corresponding author. Tel.: +34 935 521 133. Fax: +34 935 521 122. E-mail: marta.ginovart@upc.edu

**Abstract:** Organic hydromulches can be an interesting alternative for weed control in perennial crops, but can also reduce soil water evaporation. To examine the effect of a hydromulch layer on soil water content in dry conditions laboratory experiments were conducted at constant 25°C, 40% air RH. Both for small soil containers with a short time course and for larger soil columns (with two sensors at depths of 6 cm and 11 cm) with a longer time course, the presence and also the thickness of hydromulch were significant factors for the temporal evolution of soil water content. Two distinct stages of the evaporation process, the first or initial stage and the last or final stage, were identified, analysed and compared for these experiments. General linear models performed on the soil water content temporal evolutions showed significant differences for the first and last stages at the top and bottom of the soil columns with and without hydromulch. Hydromulch application delayed the evaporation process in comparison with the control. Moreover, the hydromulch layer, which was tested for mechanical resistance to punching, offered enough resistance to prevent its perforation by the sprouts of weed rhizomes.

**Keywords:** Byproducts reuse; Punching resistance; Sandy loam soil; Water conservation; Weeds.

## INTRODUCTION

It is well recognized that the main challenge facing the sustainability of water management in agriculture is to improve the efficiency of water use and its sustainability. This is an objective that is pursued worldwide. There are several management practices for increasing water use efficiency, one of them being mulching (Biswas et al., 2015). In particular, this is important in rain-fed crop cultivation (Kader et al., 2019). These authors list a series of benefits that the use of mulch in agriculture can provide, both from an edaphic environmental perspective (conservation of soil water, reduction of water evaporation, improvement of water holding capacity, soil temperature regulation, pest control, minimization of weed effects, increase in nutrient status) and from an economic one (enhancement of crop yields, increase in fruit quality, higher water use efficiency, earlier crop harvests).

Kasirajan and Ngouajio (2012) define mulching as a covering material over the soil surface. There are many types of mulching. An initial classification reflects the kind of materials employed: organic or inorganic (Kader et al., 2017; Pramanik et al., 2015).

It is evident that plastics have been the materials most commonly used as mulch in agriculture in recent decades. As Steinmetz et al. (2016) comment, this practice provides interesting economic benefits and increases water use efficiency. Kasirajan and Ngouajio (2012) summarize a very interesting history of plastic mulch. However, at present it is accepted that the use of non-degradable plastics, in particular polyethylene, represents a serious environmental problem since it poses a significant risk for the sustainability of the ecosystem in agricultural lands (Steinmetz et al., 2016).

Photodegradable and biodegradable plastics to be used as mulch have been developed since the 1960s and 1980s, respec-

tively, as an environmentally friendly alternative to synthetic mulches. Biodegradable plastics designed to be tilled into the soil after use (Bandopadhyay et al., 2018) are particularly interesting. Nevertheless, as Sintim et al. (2019) point out, there is limited information on the possible repercussions of biodegradable mulches on soil health. And in spite of a great deal of research in the area of biodegradable plastics, it is important to bear in mind that, in general, there is a serious economic limitation to using them at farm level due to the high cost of these plastics (Kasirajan and Ngouajio, 2012).

Taking into account the above, it is not surprising that the use of organic mulches has returned to the fore. Organic by-products, crop, pruning or clearing remains, woodchips and pine bark have been used as mulches for many years (Zribi et al., 2015). As Rico Hernández et al. (2016) indicate, it is extremely important to use plant waste mulch in such a way that all of its potential advantages are optimized. These authors mention, for example, that cereal straw facilitates aeration and the entry of water into the soil, but because it decomposes slowly and has low nitrogen content, adding some type of supplementary fertilizer to the soil to facilitate its subsequent mineralization is considered necessary. Shumova (2013) points out that in wet regions, evapotranspiration decreases when the soil is mulched with cereal straw, which can result in a certain disturbance of the natural structure of the hydrological cycle and possible overmoistening of soils. Not long ago the possibility of reusing paper as mulch was reconsidered (Haapala et al., 2014). This organic material was already employed before the era of plastics, although due to its characteristics it was normally used in formulations that involved paper coated with several materials (Haapala et al., 2014; Shogren, 2000).

Other possible alternative mulches are biodegradable materials applied as slurries (foam mulch, hydraulic mulches and hydromulches) (Warnick et al., 2006). In fact, the mode of

application is based on hydromulching and hydroseeding technologies, used on burned slopes to prevent soil erosion or to foster revegetation. Claramunt et al. (2020) describes some aspects of the composition of a set of hydromulches, as well as their mechanical properties from the point of view of resistance to traction and punching forces. Likewise, the mentioned authors found that some hydromulches can efficiently prevent weed seedling emergence and reduce the seed bank.

In this study we are interested in presenting a slurry product that can be sprayed on the soil surface of crop fields. This prototype of hydromulch has been developed by mixing several substances, as detailed in Claramunt et al. (2020), including paper pulp and crop residues, waste products that can be reused. Although it was initially thought of as a weed control system, it should provide possibilities from the point of view of soil protection (Rico Hernández et al., 2016). According to McMillen (2013) the use of hydromulches, as a type of organic mulches, can result in higher water use efficiency by preventing soil evaporation, increasing the soil water holding capacity due to the decomposition of the hydromulch, and reducing the undesirable impact of raindrops and water runoff and the severity of certain diseases, among others.

In many agricultural areas available water, together with soil mechanical resistance (Letey, 1985), is essential for agricultural practices. Nowadays, the principles of conservation agriculture emphasize the importance of the soil and explicitly cite the need for water conservation (Dumanski et al., 2006). Therefore, many strategies have been used to optimize soil water content, particularly in arid and semiarid lands (Jones et al., 1969), by minimizing the amount of water lost from the soils through evaporation (CTCN, 2019). On the other hand, some experiments carried out in non-agricultural lands suggest the interest in using water repellent soil materials (duff) as mulch layers in order to reduce soil water evaporation ratio in sandy and clay-loam soils of the central part of the Mediterranean area (Lichner et al., 2020).

Zribi et al. (2015) document the effectiveness of inorganic and organic mulches in preventing soil evaporation in numerous annual crops. Likewise, Martín-Closas et al. (2016) mention the advantages of mulching utilization in tree crops. Successive stages of the soil drying process were described (Balugani et al., 2018; Han et al., 2017) after a field application of mulch, according to the balance between soil water potential and atmospheric capacity. Consequently, application of mulch in field conditions can modify the water dynamics of the whole profile. But hydromulch also generates a more or less continuous layer that can harden. So, under some conditions, when hydromulch dries it could become a layer opaque enough to prevent weed seed germination and rhizome sprouting or it could become hard enough to be impenetrable for weed seedlings or sprouts.

The aim of this paper is to understand how the hydromulch affects soil water evaporation and mechanical stress in the soil-atmosphere interface. We focus on topsoil behaviour after the application of hydromulch under laboratory conditions simulating extreme dry conditions, from both a hydrological and a mechanical point of view.

## MATERIAL AND METHODS

### Environmental conditions, soil and hydromulch characteristics

All the experiments were performed in a climatic chamber (Radiber GERHR-700 ESP) at constant 25°C, 40% air RH, and 12 h light / 12 h dark daily cycle, simulating the dry extreme conditions that can occur in the western Catalonia (NE Spain)

vineyard and fruit orchard production zones towards the end of May and June (Meteocat, 2019).

Four experiments were performed to compare the loss of water by evaporation from wet soil with and without a mulch cover. A preliminary experiment was conducted, on a small scale and short in time, to observe the possible effect of mulch thickness, using 13.5 cm internal diameter x 10 cm height glass cylinders. Small samples helped us to understand the hydromulch drying process and to verify the mechanical behaviour of the hydromulch, in particular whether dry cracking would occur. The other three experiments, on a larger scale and longer in time, named experiments 1, 2 and 3, used 29.5 cm internal diameter x 25 cm height plastic columns equipped with soil moisture, water potential and temperature sensors. The soil employed in all experiments was air dried and sieved (<2 mm). It was a sandy loam (tending towards sandy clay loam; 62.5% sand, 19.3% silt, and 18.1% clay) obtained from the Ap horizon of a calcareous soil. In the experiments the bulk density of the packed soil was 1400 kg m<sup>-3</sup> (CV = 4.38%) and its porosity was 0.47 m<sup>3</sup> m<sup>-3</sup>; no mechanical forces were applied to the soil, other than gravity. Soils in the containers were irrigated with distilled water over saturation (preliminary experiment) or field capacity for the other three experiments (0.221 m<sup>3</sup> m<sup>-3</sup> according to Saxton et al. 1986). Whatever the sample size, there were two types of situations: soil, and soil + hydromulch. A ring of rubber sealing strip was placed around the inner top perimeter of both types of containers, just above the soil or the mulch, in order to avoid water evaporation through the space between the content and the container walls. The monitoring of the experiments started just after the hydromulch was applied.

The hydromulch employed was applied as a liquid heterogeneous paste. It was a mixture of four components: (i) paper pulp supplied by Saica, a paper mill in Zaragoza (Spain) that manufactures recovered waste paper and cardboard; (ii) wheat straw cut in a mill and sieved at 2 mm; (iii) powdered gypsum type B1, at less than 4.5% by weight; and (iv) kraft pulp from *Pinus radiata* D. Don supplied by Pacifico BSKP. The density of the hydromulch varied between 1030 and 1120 kg m<sup>-3</sup>, depending on the proportion of water and fibres of the paper pulp. Just after an application, around 21% of the weight of the hydromulch was lost in the form of liquid that drained down by gravity. This amount of liquid was taken into consideration to calculate the soil water content (vol/vol) of the samples having hydromulch treatment. After the mentioned rapid loss, the mean bulk density of the moist hydromulch layer was 66.9 kg m<sup>-3</sup> (CV = 13.6%). After that, during the course of the experiments, the hydromulch slowly lost its water until it became a drier, hardened solid mulch. Under the experiments' environmental conditions, it took six days for a sample of hydromulch without soil to lose as much water as in an oven at 105°C for 24 h, giving a mean bulk density value of 18.8 kg m<sup>-3</sup> (CV = 7.8%).

### Small sample experiment

During the experiment all data on water evaporation were obtained by weighing the 12 small samples, which were filled with soil from the bottom to a height of approximately 4.5 cm, and adding water until soil saturation. Two levels of hydromulch were tested, SH<sub>10</sub> and SH<sub>16</sub>, corresponding to doses of 9.9 (0.14) kg m<sup>-2</sup> and 15.8 (0.12) kg m<sup>-2</sup>, these numbers being the mean doses and their standard errors (SE, standard deviation of the mean) in parentheses. Each level of hydromulch was represented by three containers, while six containers were used as controls. The two doses of hydromulch applied became layers of approximately 10 mm and 20 mm in

thickness when wet, just after their application, but the thinner had reduced to 8.1 (SE 0.38) mm and the thicker to 15.2 (SE 0.52) mm on average by the end of the experiment.

The experiment lasted 8 days (190 hours); eight weight values were taken during the period. The relative position of the samples within the chamber was changed daily, ensuring that all of them experienced intra-chamber variability with respect to evaporative demand, because it was noted previously that, at the temperature and air RH employed, the water evaporation rate (evaporative demand) ranged between 6.4 mm day<sup>-1</sup> and 3.8 mm day<sup>-1</sup>, depending on the particular zone within the chamber; there was a gradient between the zone close to the door (drier) and the zone far from the door (wetter).

Three variables related to water evaporation were obtained and analysed: (1) accumulated water loss (weight), (2) relative water loss (vol/vol), that is, initial water content minus final content relative to initial, and (3) daily evaporation (mm/day<sup>-1</sup>), computed from the difference between the water content for the intervals of time measured.

One-way analysis of variance followed by Tukey's multiple comparison test were performed with the arcsine-transformed relative water loss values. The only source of variation was the treatment, with three levels: control, thin hydromulch, and thick hydromulch. General linear models (GLM) and variance tests (ANOVA) were used to evaluate the influence of the factor treatment on the temporal evolution of the daily evaporation.

### Column experiments

The columns employed were lined at the bottom with 3 cm thickness expanded clay covered by a non-woven geotextile for drainage. Over this layer they were filled with soil up to a thickness of 18 cm, and were equipped with two sets of temperature (ECT/RT-1, Decagon devices), soil water content (ECH20, Decagon devices) and soil water potential sensors (MPS-6, Decagon devices), one at a depth of 6 cm (top) and other at 11 cm (bottom). The sensors were installed perpendicular to the soil column; soil water content was monitored as volume/volume (vol/vol) and soil water potential was measured in kPa each 6 hours. The temperature was monitored to check its stability. In each experiment three types of columns were placed in the climatic chamber: one column was the control (soil), the second had soil and hydromulch, and the third had soil, hydromulch and three non-dormant weed rhizomes buried 1 cm under the soil surface. The position of each type of column within the chamber was set at random for each experiment to take into account the intra-chamber variability in evaporative demand. Only one dose of hydromulch was employed, 18.5 (SE 0.8) kg m<sup>-2</sup>, producing a wet mulch layer around 23 mm thick at the beginning of the experiments and 12.3 (SE 0.35) mm at the end.

Rhizomes of *Paspalum dilatatum* Poiret in Lam., tubers of *Cyperus rotundus* L., and rhizomes of *Sorghum halepense* L. (Pers.), were employed in experiments 1, 2, and 3 respectively. Their mean sizes were 41 mm length and 9 mm diameter for *P. dilatatum*, 54 mm length and 12.8 mm diameter for *C. rotundus*, and 37 mm length and 7.8 mm diameter for *S. halepense*. The ability of the rhizomes (collected and cut similarly) to sprout and to perforate by punching a wet hydromulch layer was previously tested at 25°C and 12 h light / 12 h dark daily cycle (Figure 1).

The weights of the soil columns were taken at the beginning (together with that of each of the components) and at the end of each experiment. Just after the hydromulch application the experiments began inside the chamber, and the sensors were turned on.



**Fig. 1.** Sprout of *Sorghum halepense* that had passed through a wet layer of the prototype hydromulch by punching it.

The experimental data were first analysed statistically using a set of exploratory techniques to investigate the relationship between the measured variables, the soil water potential and the soil water content with the two types of sensors. Regarding the temporal evolution of the soil water content in the columns, linear models were investigated for two different periods of time, the first days and the last, and it took into account various sets of data characterized by the measurement depth and by the treatment performed on the column. GLM and ANOVA were used to evaluate the influence of the factor under study, the presence or absence of mulch, on the temporal evolution of soil water content in these two periods of time, the first and the final stages, distinguishing the subsets of data by the recorded position of the sensor.

All data were analysed using SAS (SAS, 2013) and Minitab® Statistical Software (Minitab Inc., 2012). The probability level of significance was set at 0.05.

### Hydromulch resistance to punching

Punching tests were performed to determine the resistance (MPa) of the mulches at the end of the experiments, because this test could inform about the resistance of the hydromulch to being penetrated by the weed seedlings or sprouts. The equipment used was a Stable Micro Systems XT-plus Texture Analyser, with a probe 7.86 mm in diameter. The load cell of the analyser has a maximum capacity of 500 N and the cross head speed in the tests was 4 mm min<sup>-1</sup>. The punching test subsamples used were circular. They were obtained by cutting the hydromulch layers once, after the experiments in the chamber had finished, and they were removed from the soil surface at room temperature and humidity. Three punching tests were made with the mulch of each hydromulch layer, whether they were from the small sample experiment or from the three column experiments. The parameter resistance to punching was the maximum breaking strength or modulus of rupture, also called stress, which was obtained according to Claramunt et al. (2020).

## RESULTS AND DISCUSSION

### Experiment in small containers

Relative losses in water content over the period with respect to initial moisture showed that the hydromulch layers caused a

certain delay in the evaporation process and, at the same time, diminished the total amount of water losses by evaporation (Table 1, Figures 2–3). While the control showed a 98.3% relative loss, the treatments with hydromulch presented lower mean values, 82.9% and 68.7%, depending on the thickness of the mulch (Table 1). The one-way ANOVA test applied to the variable relative water loss showed the treatment was significant ( $p$ -value < 0.001). In addition, the three means were significantly different from each other (Tukey method), the level with the thickest hydromulch having the lowest value.

**Table 1.** Mean values and their respective standard errors (SE) of the water contents registered in the small containers at the beginning ( $WC_0$ ) and after 190 hours ( $WC_{190}$ ) at 25°C and 40% air RH. Control: soil without mulch; SH\_10: soil with a thin mulch layer; SH\_16: soil with a thick mulch layer.

Treatment	$WC_0$ (vol/vol) (SE)	$WC_{190}$ (vol/vol) (SE)
No mulch	0.422 (0.002)	0.007 (0.001)
Mulch SH_10	0.466 (0.002)	0.080 (0.009)
Mulch SH_16	0.518 (0.001)	0.162 (0.020)

Figure 2 describes the evolution of the accumulated water losses of the three treatments. The initial water applied was the same in all the small containers, but hydromulch, as a water slurry, included an additional dose of water in both SH\_10 and SH\_16 levels. Two periods in the temporal evolution of the water evaporation can be considered, one for the first three days and the other for the last three days, since the values in the initial stage were higher than those in the final stage, when a clear decrease in the evaporation took place (Figure 3). Teng et al. (2013) also consider two stages in the soil water evaporation process: a constant-rate stage, which occurs when the soil surface is at or near saturation and is controlled by atmospheric conditions; and a falling-rate stage in which the water movement is controlled by the soil water potential. In the initial stage, the linear regression model for the daily evaporation and time was non-significant (Figure 3), there was no significant effect for time in this period of the temporal evolution ( $p$ -value = 0.099) and, at the same time, there were no significant differences between constants for the three treatments ( $p$ -value = 0.154). Nevertheless, in the final stage (Figure 3) significant differences were detected between the three linear regression

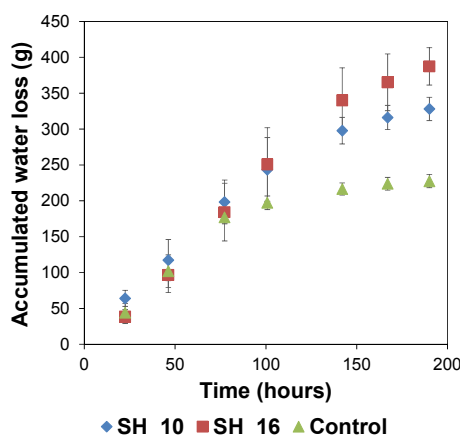


**Fig. 2.** Temporal evolution of the mean accumulated water losses in small containers in an experiment conducted under controlled conditions (25°C, 40% air RH) to study the effect of the two hydromulch levels on the drying process (SH\_10 and SH\_16). Standard deviations have been reported in the error bars.

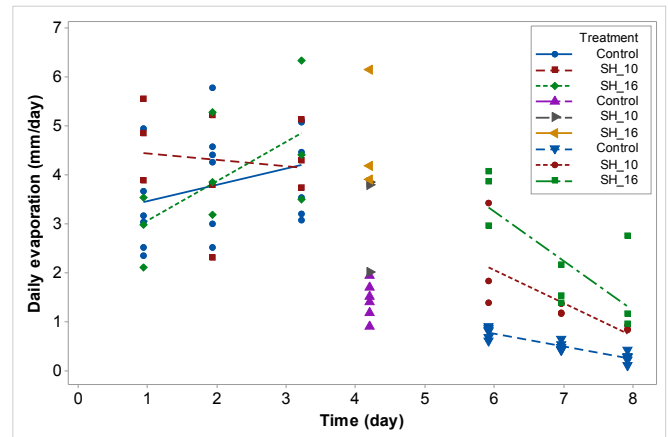


**Fig. 3.** Temporal evolution of surface evaporation and fitted regression lines obtained for each of the levels of the treatment, distinguishing the first and the last stages, in an experiment conducted in a chamber under controlled conditions (25°C, 40% air RH) to study the effect of the hydromulch.

models for the constants of the adjusted regression lines ( $p$ -value = 0.001) and for their slopes ( $p$ -value = 0.013).

Differences between daily water evaporation slopes would suggest that the water evaporation rate was reduced when hydromulch was applied. The slopes corresponding to the SH\_10 and SH\_16 mulch treatments were  $-0.68$  and  $-1.02$  respectively, whereas the slope for the control was  $-0.26$ . Thus, the hydromulch tested favoured water retention in the soil, as do most other organic mulches (Haapala et al., 2014; Rico Hernández et al., 2016; Zribi et al., 2015), but, interestingly, the water loss diminished with mulch thickness (Table 1, Figure 2), which is a trait directly linked with another important quality of the mulches: their lifetime (O'Brien et al., 2018).

## Experiments in columns

In all three experiments the weed rhizomes sprouted, but none of them was able to perforate the mulch layer. Due to the behaviour of the rhizomes, the soil water content *versus* soil water potential curves were very similar (Figure 4), because no transpiration occurred.

According to the weight values, the soil water contents at the beginning of experiment 1 were near to saturation, between 0.36 and 0.40  $\text{kg kg}^{-1}$ , while in the other two experiments (2 and 3) they were lower, between 0.24 and 0.27  $\text{kg kg}^{-1}$ . At the end, the soil water contents were, respectively, between 0.09 and 0.16  $\text{kg kg}^{-1}$  in experiment 1, and between 0.07 and 0.11  $\text{kg kg}^{-1}$  in experiments 2 and 3. They lasted 23 days, 32 days, and 29 days respectively. So, the range of soil water content in experiment 1 was greater than those of the other experiments (Figure 4). In view of these differences, added to the non-emergence of any weed sprout, the detailed comparisons of the water evaporation of the columns with and without hydromulch were performed considering only the columns of experiments 2 and 3 placed in particular chamber sites with similar evaporative demand.

The hydromulch participated in the water evaporation of the system in two ways. Soil water content did not increase noticeably at the beginning of the experiment (Figure 4). A gradual drying process of the hydromulch took place by water transfer to the underlying soil and by evaporation. The drying process of the hydromulch decreases its water content (and its water potential) until an equilibrium is reached with the controlled atmosphere of the chamber. The transition took place around

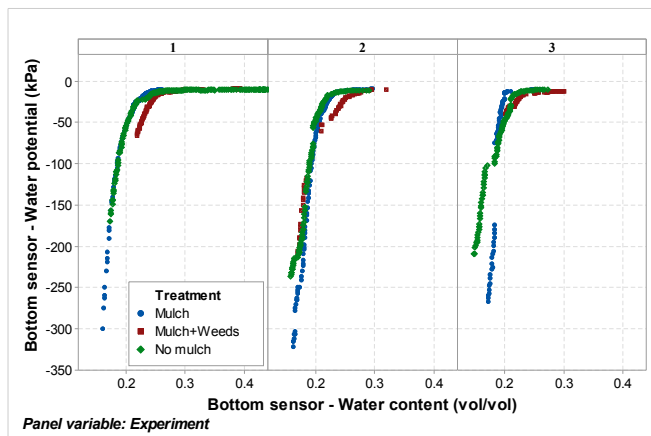
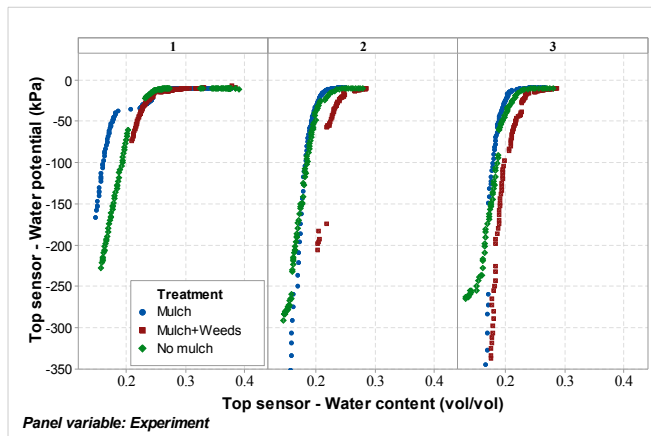


**Fig. 4.** Soil water potential versus soil water content of the top and bottom for the three levels of the factor treatment in the three experiments performed with soil columns in a chamber under controlled laboratory conditions (25°C, 40% air RH).

-25 kPa to -30 kPa, depending on the column and the soil depth. While at the top sensor of the control columns the minimum water potential measured was between -200 kPa and -300 kPa, in the columns with mulch water potential achieved values lower than -600 kPa (data not shown, Figure 4). The water loss rate was lower in the bottom zone, because during the same period of time water potential achieved values of around -300 kPa and, at the same time, those from columns with mulch and without mulch were similar (Figure 4). Although our experiment was carried out at very low air RH, there are parallels with the results obtained in field and other laboratory conditions by several authors (Balugani et al., 2018; Han and Zhou, 2013; Han et al., 2017; Qiu and Ben-Asher, 2010; Teng et al., 2013; Zhang et al., 2015; Zribi et al., 2015), who found that the evaporation process from soils can be divided into a number of stages (between two and four) depending on the evolution of water potential and soil water content. Figure 4, jointly with Figure 5 showing the temporal evolution of water content, suggests that, in our experiments, two noticeable and clear stages could straightway be considered in the columns (with and without mulch), and they can be identified as the first or initial period and the last or final period of these temporal evolutions.

Figure 5 displays the temporal evolution of the soil water content for the period of the first 18 days. Two different behaviours of the water loss ratio are observed in all cases, with transient values between them. The slopes of the first and last part of the data evolve differently depending on the treatment.

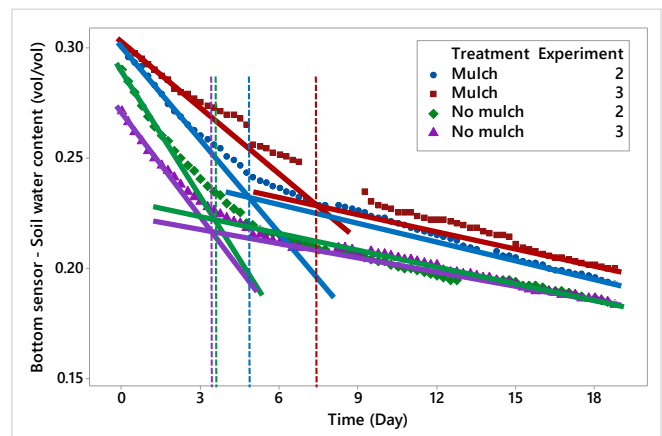
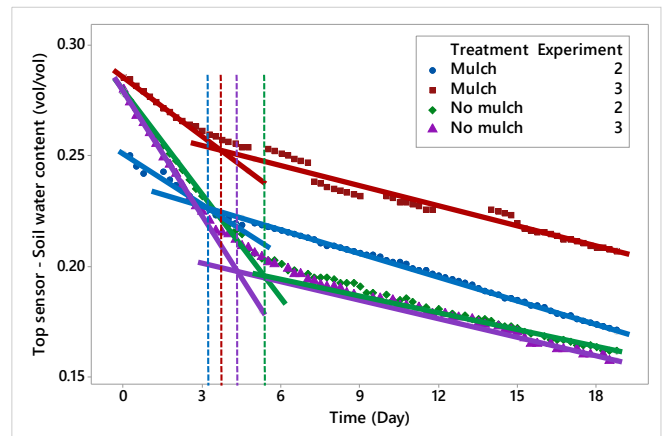


**Fig. 5.** Temporal evolution of the soil water content (vol/vol) for the period of 18 days under controlled laboratory conditions (25°C, 40% air RH) with the fitted regression lines achieved considering the subdata of the initial stage and the final stage for each part (top and bottom) of the soil columns corresponding to the two experiments (2 and 3) and the presence or absence of mulch. The intersection of the two fitted regression lines corresponding to each temporal evolution is also displayed.

The characterization of the first stage by a linear model was accomplished with the subset of chosen data having approximately constant values for the differences of consecutive soil water content measurements to ensure and guarantee a stage with a linear decrease. The linear model for the characterization of the final stage was established with a regression using the data corresponding to the last three days (16, 17 and 18) in all experiments, since it had been confirmed that all columns had already entered into the last part of the evaporation process during those days.

For each subset of data combining the sensors (bottom, top) and these two stages (initial and final), four GLMs were carried out to fit least squares models for the variable soil water content as the continuous response, with mulch as the categorical factor (yes / no) and time as the covariate, and considering the interaction between time and factor. Significant differences in each of the four ANOVA tables performed were detected in terms of the interaction of the factor mulch over time (slope of the regression line) with p-values less than 0.01, and the R<sup>2</sup> values showed that the model explained more than 99% of the variance in soil water content. The linear model fitted the data very well in all four combinations. Figure 5 shows the fitted regression equations obtained by each sensor, differentiating the cases with and without mulch for the first and last stage. For

the top of the column, the slopes of the regression lines for water content in the first stage were around  $-0.02$  in the case of non-mulch whereas in the case of mulch they were around  $-0.01$ , but in the last stage the coefficients of the slopes were much more similar and both with and without mulch were around  $-0.003$ . With respect to the bottom of the column (for the initial and final stages), the interception at the origin of the regression lines indicates that with mulch these values (around 0.30 and 0.25 respectively) are higher than without mulch (around 0.28 and 0.23 respectively). The final water content that was reached was higher in the columns with mulch, although their slopes or evaporation rates were similar. In addition, the fitted regression lines resulting from the use of the last subsets of data (days 16, 17 and 18) make it possible to display periods of time with constant evaporation, periods that differ between experiments, but which are not restricted to only the last three days like the plotted regression lines shown (Figure 5). The intersection of the two regression lines corresponding to the first and final stages represents the time when the water evaporation regime changes from fast to the slowest rate after irrigation. This interval is shorter in the top part of the two columns with hydromulch than in the columns without hydromulch. On the other hand, the water content in the bottom part of the hydromulch columns is higher than in the columns without hydromulch at this time.

So, applying hydromulch in these experimental conditions favours an early reduction of the evaporation rate from the topsoil and at the same time a higher water content in the bottom part of these columns.

In the dry zone transport of water is merely as water vapour because the continuity of the water capillarity breaks down. The hydromulch layer on top of the soil surface could contribute to increase the role of the dry surface layer, which according to Han and Zhou (2013) has a significant impact on surface energy balance. In this way, the evaporation divides the soil into two parts, with only vapour flow occurring in the profile above the evaporation zone and liquid water flows mainly occurring in the profile below. It seems that there could be a connection between hydromulch and soil at the level of their respective pores.

### Hydromulch resistance to punching

The mean resistance to punching of the mulches at the end of the experiments was 1.47 (SE 0.19) MPa. The mean force needed to perforate the mulch was 573.6 N in the columns, while those of the experiment in small samples were 264.6 N for SH\_10, and 459.5 N for SH\_16. These values, higher than those obtained by Claramunt et al. (2020), who tested several hydromulches containing also recycled paper pulp and lignocellulosic crop residues, could be considered promising, because no rhizome was able to perforate the mulch, and probably the small seeds of many weeds would not emerge if the mechanical impedance attained 0.5 MPa (Mas et al., 2017). But they are far from the 3.87 MPa achieved by some black polyethylene plastics employed as agricultural mulches (Hosseinabadi et al., 2011).

### CONCLUSIONS

In the very dry conditions tested, the mulch layer formed after hydromulch application delayed the evaporation process with respect to the control. In the experiment with small containers, the evaporation rate was lower the thicker the mulch.

Regarding water flow across the boundary between atmosphere and mulch-soil, the interest in the use of hydromulch lies in delaying the process by which the liquid water is converted into vapour and removed from the surface. Therefore, applying hydromulch could be useful both for delaying water evaporation and at the same time for controlling weeds by reducing emergence thanks to its mechanical behaviour.

*Acknowledgements.* This work was supported by the Instituto Nacional de Investigaciones Agrarias of the Spanish Government [grant numbers RTA2015-00047-C01 and RTA2015-00047-C04]. We would like to thank Dr. J. Claramunt for his assistance on mechanical tests, and S. Alcalá and M. Julià for their technical assistance. We are indebted to the companies that supplied the raw materials used to develop the prototype of the hydromulch.

### REFERENCES

- Balugani, E., Lubczynski, M.W., van der Tol, C., Metselaar, K., 2018. Testing three approaches to estimate soil evaporation through a dry soil layer in a semi-arid area. *Journal of Hydrology*, 657, 405–419.
- Bandopadhyay, S., Martin-Closas, L., Pelacho, A.M., DeBruyn, J.M., 2018. Biodegradable plastic mulch films: impacts on soil microbial communities and ecosystem functions. *Frontiers in Microbiology*, Volume 9, Article Number 819.
- Biswas, S.K., Akanda, A.R., Rahman, M.S., Hossain, M.A., 2015. Effect of drip irrigation and mulching on yield, water-use efficiency and economics of tomato. *Plant, Soil and Environment*, 61, 3, 97–102.
- Claramunt, J., Mas, M.T., Pardo, G., Cirujeda, A., Verdú, A.M.C., 2020. Mechanical characterization of blends containing recycled paper pulp and other lignocellulosic materials to develop hydromulches for weed control. *Biosystems Engineering*, 191, 35–47.
- CTCN (Climate Technology Center & Network), 2019. Connecting countries to climate technology solutions. <<https://www.ctc-n.org/technologies/soil-moisture-conservation-techniques-0>> [accessed 29 November 2019].
- Dumanski, J., Peiretti, R., Benites, J.R., McGarry, D., Pieri, C., 2006. The paradigm of conservation agriculture. In: *Proceedings of World Association of Soil and Water Conservation*. Paper No. P1: 58–64.
- Haapala, T., Palonen, P., Korpela, A., Ahokas, J., 2014. Feasibility of paper mulches in crop production: a review. *Agricultural and Food Science*, 23, 60–79.
- Han, J., Zhou, Z., 2013. Dynamics of soil water evaporation during soil drying: laboratory experiment and numerical analysis. *The Scientific World Journal*, Article ID 240280, 10 pages.
- Han, J., Lin, J., Day, Y., 2017. Numerical modeling of soil evaporation process and its stages dividing during a drying cycle. *Geofluids*, Article ID 5892867, 11 pages.
- Hosseinabadi, F., Zebarjad, S.M., Mazinani, M., 2011. Investigation on perforation mechanism of medium density polyethylene. *Materials Science Forum*, 675–677, 387–390.
- Jones, J.N., Moody, J.E., Lillard, J.H., 1969. Effects of tillage, no tillage, and mulch on soil water and plant growth. *Agronomy Journal*, 61, 719–721.
- Kader, M.A., Senge, M., Mojid, M.A., Itob, K., 2017. Recent advances in mulching materials and methods for modifying soil environment. *Soil & Tillage Research*, 168, 155–166.
- Kader, M.A., Singha, A., Begum, M.A., Jewel, A., Khan, F.H., Khan, N.I., 2019. Mulching as water-saving technique in

- dryland agriculture: review article. *Bulletin of the National Research Centre*, 43, 147.
- Kasirajan, S., Ngeouajio, M., 2012. Polyethylene and biodegradable mulches for agricultural applications: a review. *Agronomy for Sustainable Development*, 32, 501–529.
- Letey, J., 1985. Relationship between soil physical properties and crop production. In: Stewart, B.A. (Ed.): *Advances in Soil Science*, 1. Springer, New York, pp. 277–294.
- Lichner, E., Alagna, V., Iovino, M., Laudicina, V.A., Novák, V., 2020. Evaporation from soils of different texture covered by layers of water repellent and wettable soils. *Biologia*. <https://doi.org/10.2478/s11756-020-00471-5>
- Martin-Closas, L., Costa, J., Cirujeda, A., Aibar, J., Zaragoza, C., Pardo, A., Suso, M.L., Moreno, M., Moreno, C., Lahoz, I., Mácuca, J.I., Pelacho, A.M., 2016. Above-soil and in-soil degradation of oxo- and bio-degradable mulches: a qualitative approach. *Soil Research*, 54, 2, 225–236.
- Mas, M.T., Verdú, A.M.C., Ginovart, M., Josa, R., 2017. Seedling emergence through soil surface seals under laboratory conditions: effect of mechanical impedance and seal moisture. *Biologia*, 72, 862–868.
- McMillen, M., 2013. The effect of mulch type and thickness on the soil surface evaporation rate. Horticulture and Crop Science Department, California Polytechnic State University, San Luis Obispo.
- Meteocat. Servei Meteorològic de Catalunya, 2019. Normals climàtiques recents. URL <<http://www.meteo.cat/wpweb/climatologia/serveis-i-dades-climatiques/normals-climatiques-recents/>> [accessed 28 October 2019].
- Minitab Inc., 2012. Minitab Statistical Software Version 17.2.1. Minitab Inc., State College, PA. URL <<http://www.minitab.com/>> [accessed 30 October 2019].
- O'Brien, P., Acharya, U., Alghamdi, R., Niaghi, A.R., Sanyal, D., Wirtz, J., Daigh, A.L.M., DeSutter, T.M., 2018. Hydromulch application to bare soil: soil temperature dynamics and evaporative fluxes. *Agricultural & Environmental Letters*, 3, 180014. DOI: 10.2134/ael2018.03.0014
- Pramanik, P., Bandopadhyay, K.K., Bhaduri, D., Bhattacharyya, R., Aggawal, P., 2015. Effect of mulch on soil thermal regimes - a review. *International Journal of Agriculture, Environment and Biotechnology*, 8, 3, 645–658.
- Qiu, G.Y., Ben-Asher, J., 2010. Experimental determination of soil evaporation stages with soil surface temperature. *Soil Science Society of America Journal*, 74, 1, 13–22.
- Rico Hernández, J.R., Navarro Pedreño, J., Gómez Lucas, I., 2016. Evaluation of plant waste used as mulch on soil moisture retention. *Spanish Journal of Soil Science*, 6, 2, 133–144.
- SAS, 2013. *Statistical Analysis Systems, Software Version 9.4*. SAS Institute Inc., Cary, North Carolina, USA.
- Saxton, K.E., Rawls, W.J., Romberger, J.S., Papendick, R.I., 1986. Estimating generalized soil-water characteristics from texture. *Soil Science Society of America Journal*, 50, 4, 1031–1036.
- Shogren, R.L., 2000. Biodegradable mulches from renewable resources. *Journal of Sustainable Agriculture*, 16, 4, 33–47.
- Shumova, N., 2013. Evapotranspiration changes in the forest-steppe and steppe zones under soil mulching. *Journal of Hydrology and Hydromechanics*, 61, 1, 140–145.
- Sintim, H.Y., Bandopadhyay, S., English, M.E., Bary, A.I., DeBruyn, J.M., Schaeffer, S.M., Miles, C.A., Reganold, J.P., Flury, M., 2019. Impacts of biodegradable plastic mulches on soil health. *Agriculture, Ecosystems and Environment*, 273, 36–49.
- Steinmetz, Z., Wollmann, C., Schaefer, M., Buchmann, C., David, J., Tröger, J., Muñoz, K., Frör, O., Schaumann, G.E., 2016. Plastic mulching in agriculture. Trading short-term agronomic benefits for long-term soil degradation? *Science of the Total Environment*, 550, 690–705.
- Teng, J., Yasufuku, N., Liu, Q., Liu, S., 2013. Analytical solution for soil water redistribution during evaporation process. *Water Science & Technology*, 68, 12, 2545–2551.
- Warnick, J.P., Chase, C.A., Rosskopf, E.N., Simonne, E.H., Scholberg, J.M., Koenig, R.L., Roe, N.E., 2006. Weed suppression with hydramulch, a biodegradable liquid paper mulch in development. *Renewable Agriculture and Food Systems*, 21, 4, 216–223.
- Zhang, C., Li, L., Lockington, D., 2015. A physically based surface resistance model for evaporation from bare soils. *Water Resources Research*, 51, 1084–1111.
- Zribi, W., Aragüés, R., Medina, E., Faci, J.M., 2015. Efficiency of inorganic and organic mulching materials for soil evaporation control. *Soil & Tillage Research*, 148, 40–45.

Received 16 December 2019

Accepted 2 May 2020